PERFORMANCE EVALUATION OF SANDWICH COMPOSITES WITH FUNCTIONALLY GRADED CORE FOR BALLISTIC IMPACT

Thesis

Submitted in partial fulfillment of the requirements for the degree of

DOCTOR OF PHILOSOPHY

by

MOHAN KUMAR T S

DEPARTMENT OF MECHANICAL ENGINEERING

NATIONAL INSTITUTE OF TECHNOLOGY KARNATAKA, SURATHKAL, MANGALORE-575 025

OCTOBER, 2024

DECLARATION

I hereby declare that the Research Thesis titled **"PERFORMANCE EVALUATION OF SANDWICH COMPOSITES WITH FUNCTIONALLY GRADED CORE FOR BALLISTIC IMPACT,"** which is being submitted to the **National Institute of Technology Karnataka, Surathkal,** in partial fulfillment of the requirements for the award of the degree of **Doctor of Philosophy** in **Department of Mechanical Engineering** is a *bonafide report of the research work carried out by me*. The material contained in this Research Thesis has not been submitted to any other Universities or Institutes for the award of any degree.

Register Number: 2170002ME014

Name of the Research Scholar: **Mohan Kumar T S**

Signature of the Research Scholar: 

Department of Mechanical Engineering

Place: NITK-Surathkal

Date: 22-10-2024

CERTIFICATE

This is to certify that the Research Thesis titled **"PERFORMANCE EVALUATION OF SANDWICH COMPOSITES WITH FUNCTIONALLY GRADED CORE FOR BALLISTIC IMPACT"** submitted by **Mr. Mohan Kumar T S (Register Number:** 2170002ME014**)** as the record of the research work carried out by him, *is accepted as the Research Thesis submission* in partial fulfillment of the requirements for the award of the degree of **Doctor of Philosophy.**

23.10.2024

Dr. Sharnappa Joladarashi
Research Guide

Dr. S M Kulkarni
Research Guide

Chairman-DRPC
Date: 24/10/2024

राष्ट्रीय प्रौद्योगिकी संस्थान, कर्नाटक
यांत्रिकी अभियांत्रिकी विभाग
Dept. of Mechanical Engineering
National Institute of Technology Karnataka

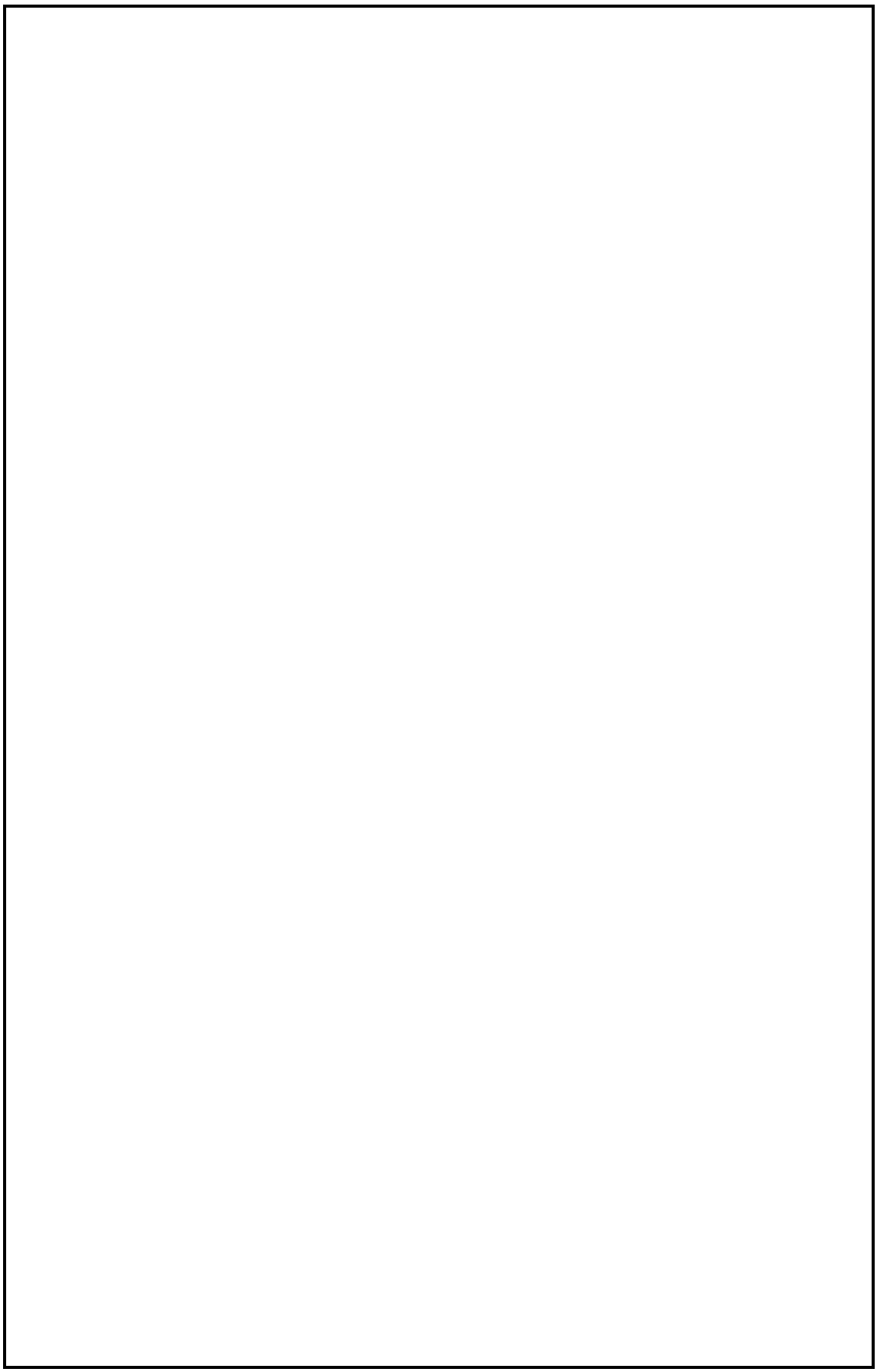

ACKNOWLEDGEMENT

It gives me immense pleasure to acknowledge everybody for their assistance, inspiration, and support during my dissertation. My sincere appreciation goes out to everyone who has given up comfort in one way or another to enable me to complete my doctoral studies. I express my sincere pranams to His Holiness, **Dr. Sri Sri Sri Shivakumara Swamigalu**, and **Sri. Siddalinga Swamigalu** for their blessings.

I would like to express my sincere gratitude and heartiest thanks to my supervisors, Dr. **Sharnappa Joladarashi**, Professor, and **Dr. S M Kulkarni**, Professor, Department of Mechanical Engineering, National Institute of Technology Karnataka (N.I.T.K), Surathkal, for considering me worthy of working under their esteemed guidance. This research outcome is a result of their excellent guidance and support throughout the work. This thesis could not have attained its present form in content and presentation without their active interest, timely support, direction, and valuable guidance. My professional ethics, problem-solving skills, and knowledge level have received a professional boost through all those days I was able to spend in their proximity. Their vast knowledge and insight into the area of composite materials have helped me to overcome the hurdles throughout my dissertation. Words are insufficient to express my deep feelings, and heartfelt thanks to my supervisors for their un hesitated guidance throughout my doctoral work. For all this, I will remain grateful to them throughout my career.

I express my sincere thanks to Director NITK Surathkal **Prof. B Ravi** and **Dr. S. M. Murigendrappa**, Professor and Head of the Department of Mechanical Engineering, for providing all academic and administrative help during the course of my work.

I would like to express my deepest appreciation to the Research Progress Assessment Committee (RPAC) members during various presentations and review meetings comprising **Dr. Ranjeet Kumar Sahu** and **Dr. Prashantha Kumar H** for their valuable remarks, critical suggestions, and technical advice throughout my research.

I wish to express my sincere gratitude **to all the faculty members** and **non-teaching staff** of the Department of Mechanical Engineering of N.I.T.K Surathkal for their unbiased appreciation and support through this research work. I take this opportunity to thank all my friends and colleagues of both N.I.T.K and S.I.T, who have supported directly or indirectly to expedite towards my goal.

I am deeply grateful to **Dr. Vishwas M** for his humble and unwavering support throughout the work. His assistance, encouragement, and friendship have been invaluable to me. I would like to express my gratitude to my lab-mates— **Dr. Saleemsab Doddamani**, **Mr. Ashish Kumar Gurjar**, and **Mrs. Uma B Baliga**—for their help and suggestions throughout our time together. Their support has significantly contributed to the development of this work.

This work is also the outcome of the blessing, guidance, love, and support of my father, Mr. **Sadashivaiah N P**, my mother, Mrs. **Mahadevamma H S**, my mother-in-law **Rathnamma N P**, my wife, Mrs. **Kavyashree J**, and my son Master **Varnav M Dodmatt** and Master **Manav M Dodmatt**. This thesis is the outcome of my family's sincere prayers and dedicated support.

Last but not least, I am very thankful to the **Director, CEO, Principal, and Management of Siddaganga Institute of Technology**, Tumakuru, who deputed me under QIP to pursue my Ph.D.

Mohan Kumar T S.

National Institute of Technology Karnataka, Surathkal

Date:

ABSTRACT

Sandwich composites with flexible skin and stiff core are appropriate for a wide range of engineering applications because of their capacity to withstand greater deformation while maintaining a high load-carrying capacity. The main objective of the current research includes material selection, fabricating, and analyzing functionally graded sandwich composite for ballistic impact applications. Statistical Six Sigma DMAIC methodology was used for material selection, incorporating qualitative and quantitative approaches, ensuring a comprehensive and accurate material selection process. Considering a careful literature review, the choice of jute and rubber for skin material paired with epoxy and sea sand for core material in the sandwich composite. Finite element (FE) studies, based on the rule of mixtures, estimated composite material properties, showing increased energy absorption and a decrease in residual velocity with higher filler composition (0% to 30%) at velocities of 10, 50, 100, and 350 m/s, and with core thickness from 10mm to 30mm at 350 m/s.

Following the initial FE studies, experimental testing was conducted on composite coupons to evaluate their physical and mechanical properties. The gradation test was performed to check the functional gradience for the core material. These tests provided insights into sea sand's spatial distribution and gradation within the core samples, emphasizing the impact of sea sand composition on the stepwise layering gradation. The void % (3.44%) in the composite coupons increases as the filler composition increases. Specific tensile strength decreases (2.41 times) with an increase in the filler composition. Hardness (12.47%), Flexural strength (27.93%), and impact strength (2.35 times) increase as the filler composition increases compared to neat epoxy. High strain rate compression strength is improved with higher strain rates.

The FE analysis for low and ballistic impact testing was conducted based on the properties obtained experimentally from the composite coupons. For low-velocity and impact testing, it is observed that a sandwich with 30% sea sand composition has superior damage resistance capabilities compared to its counterparts. Both experimental and FE analyses show that higher filler percentages lead to increased energy absorption. The sandwich composite with 30% sea sand exhibited the lowest depth of damage and minimized overall damage across all impact energies, demonstrating superior damage

resistance compared to other compositions. For ballistic impact, the similar trend that increasing the volume percentage of sea sand and core thickness improved energy absorption, with a 30 vol% sand content and 30mm core thickness performing the highest energy absorption capability compared to its counterparts. The results indicate that while thinner cores (10 mm) are inadequate for arresting projectiles, thicker cores (20 mm and 30 mm) show progressively better performance, with the 30 mm core providing the most effective ballistic impact protection. Incorporating sea sand into epoxy reduced costs by 8.9% to 32.47%, making it an economical core material for ballistic impact applications. Experimental and FE simulations for the entry area at 200 m/s showed a damage area percentage error of about 12.61%. Fractography analysis indicated face sheet damage from compression and bending, fiber breakage, rubber tearing, and core failure from sand particle crushing and matrix cracking, with a river-like pattern suggesting brittle failure.

KEYWORDS: Sandwich composite, Functionally graded Core, Flexible Skin, Finite Element Analysis, Split-Hopkinson pressure bar, Ballistic impact, Low-velocity impact

Table of Contents

LIST OF FIGURES

LIST OF TABLES

NOMENCLATURE

ABBREVIATIONS

ANOVA	:	Analysis of Variance
CoR	:	Coefficient of Restitution
DOE	:	Design of Experiments
ELP	:	Energy Loss Percentage
FE	:	Finite Element
HVI	:	High Velocity Impact
LVI	:	Low-Velocity Impact
JRJ	:	Jute/Rubber/Jute
JRJ-ES-JRJ	:	Jute/Rubber/Jute-Epoxy/Sea sand- Jute/Rubber/Jute
MADM	:	Multi-Attribute Decision Making
MCDM	:	Multi-Criteria Decision Making
NR	:	Natural Rubber
SEA	:	Specific Energy Absorption
DMAIC	:	Define, Measure, Analysis, Improve, Control
SHPB	:	Split-Hopkinson Pressure Bar
TB	:	Transmission Bar
IB	:	Incident Bar
SB	:	Striker bar
HSR	:	High Strain Rate
LSR	:	Low Strain Rate
FGPC	:	Functionally graded polymer composites
UTM		Universal Testing Machine
SEM		Scanning Electron Microscopy
TOPSIS		Technique for Order of Preference by Similarity to Ideal Solution
AHP		Analytic Hierarchy Process
PSI		Preference selection index

NOTATIONS

E_A	:	Absorbed Energy
E_I	:	Impact Energy
E_{abl}	:	Energy Absorbed at Ballistic Limit
C_0	:	Wave velocity of the bar
E_{KE}	:	Kinetic Energy of Moving Projectile
I_{KE}	:	Internal Kinetic Energy
R_{KE}	:	Residual Kinetic Energy
V_B	:	Ballistic Velocity
V_I	:	Impact/Initial Velocity
ρ	:	Density
E	:	Young's modulus
$\dot{\varepsilon}$	:	Strain rate
ε_t	:	True strain
σ_t	:	True stress
ϵ_n	:	Normal strain
A_s		c/s area of sample
A_t		c/s area of transmission bar
NF		Natural Fiber
SF		Synthetic Fiber

CHAPTER 1

1 INTRODUCTION

Humans have used for their protection various components composed of metals, wood, sandbags, etc., to shield themselves and their armor from the impact of projectiles over the decades (Mazumdar 2002). Several fabrics and laminates of conventional fibers, including linen, cotton, silk, and nylon, were employed as shielding materials against various threats, including ballistic applications (Abtew et al. 2019). At the initial stage of industrialization, and in the context of ever-increasing threats, it became necessary for even smaller armies to be fully armored. In conclusion, the need for ballistic protection was recognized (Lakshmi and Nandakumar 2016). Eventually, as defense forces advanced with innovative war techniques, there was a greater desire for lightweight, more damage-resistant, flexible, and high-energy-absorbing armor materials. Because other materials are typically expensive and difficult to handle, composite materials came into existence and replaced other materials due to their features, such as less weight and high resistance to corrosion (Morye et al. 2000; Shokrieh and Javadpour 2008).

It is essential to consider the fundamentals of the science behind the sandwich armor design to satisfy the demands of the armor industry better; although a lot of effort has been put into understanding these principles, particularly in terms of armor composites, the industries still have substantial hurdles in terms of shielding and mobility. The recent development of armor material focuses on reducing weight and enhancing strength to improve mobility. Because of their lower weight and high stiffness, sandwich composites have become more popular for ballistic applications (Alam and Khanal, 2020).

Many studies have been done on bulletproof composites from the defense sectors because of their shielding capabilities. Bulletproof materials have evolved from basic steel and alloys to better-performance fibers. Aramid, UHMWPE (Ultra-High

Molecular Weight Polyethylene Fibers), and other materials are widely used in bulletproof fibers. Most anti-ballistic fabrics used in bullet-proofing are composed of Kevlar and Dyneema fibers, which spread and absorb the energy of impact. Still, they often cause damage to critical parts of the target material. These fibers were bonded with a matrix to produce composites that can be used to develop stronger bullet-resistant composites. Susceptibility and resistance to impacts are top priorities in almost all industries. Internal damage caused by the impact of materials can substantially decrease strength properties. Composite materials must undergo ballistic impact testing before being used in defense applications. The energy absorption ability of the material and ballistic velocity limit are parameters considered for building these protective components. Projectile material properties, shape, mass, size, and velocity, as well as the geometry and material properties of the structure, determine the ballistic limit (Tan et al., 2003). The ballistic limit is often obtained by material examination, either modeling or experimentation. For ballistic analysis, the focus is on adopting eco-friendly composite materials with naturally available resources (SANGAMESH 2019a).

Composite materials offer a high-volume production focus due to the wide range of reinforcing materials available and the development of novel processing methods (Ramanathan et al., 2019). Many studies are available on how to improve the performance of composite structures. Investigators are testing several parameters for sandwich composites, integrating various materials to enhance energy-absorbing capabilities while maintaining the same weight. Other properties that can be changed to improve the sandwich composite's performance include core and skin material properties and thicknesses. A study showed that the damage caused by impact load is considered more crucial, limiting the application of FRPs (Fiber-reinforced polymers). They also examine materials, environmental conditions, geometry, and process as the main factors that cause irreversible damage to composite structures. The critical

outcome of the study is the orientation of fiber; bonding between fiber and matrix is the factor that affects the composites' strength (Andrew et al. 2019).

1.1 Composite materials and their classification

The traditional composite material is a collection of materials on a macroscopic scale consisting of two or more elements blended to get new components with superior properties to individual materials. Composite materials comprise fibers, particles, flakes, and fillers as matrix material, and they also consist of metal, non-metal, polymers, and ceramic material as reinforcing elements. These matrixes materials blend with the reinforcing elements to get the desired shape, and reinforcing elements integrate with the matrix to enhance their mechanical properties. By appropriately mixing these two, the newly formed composite material shows greater strength when compared to individual material (Mathur and Bairwa 2017). As the load moves from matrix to reinforcement, the primary objective is to withstand that load (Sanjay K 2002). Classifications of composite materials based on the reinforcing material are shown in Figure 1.1.

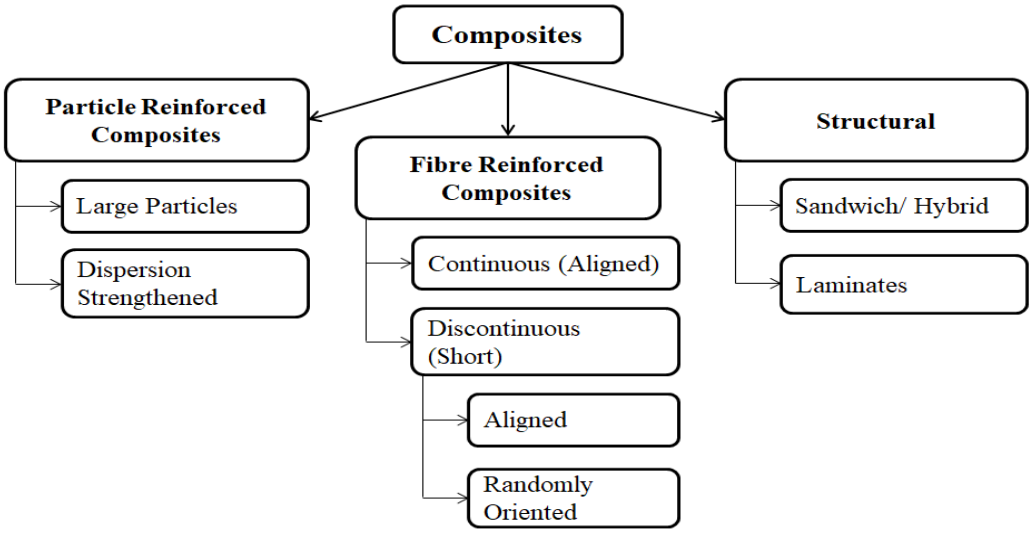

Figure 1.1 Classification (based on the reinforcement) (Otani et al. 2015)

- Particulate Composites: This type of reinforcement is particle-based and comes in various circular, cubic, tetragonal, platelet, rectangular, and irregular shapes. It enhances composites' stiffness while improving matrix material attributes such as thermal and electrical conductivity (Kumar et al. 2014).
- Fibrous Composite: A fiber is distinguished by length compared to the c/s dimension of the fiber. The reinforcement dimensions influence its ability to contribute to the composites with properties.
- Structural composites: In these types, laminates are fabricated by a pair of laminates stacked in the direction of the desired thickness. Generally, three layers are arranged in distinct manners to provide adequate bonding at the fiber-resin interface. Composite laminates can be fabricated using various techniques, including changing the sequence of stacks of the same or different materials. Another form of laminate composite is Sandwich composite. High-strength two skins (top and bottom) are bonded with less weight core material. A hybrid composite is another form of laminate, the physical combination used to fabricate composite using different fibers, matrices, and fillers (SANGAMESH 2019a).

1.2 Sandwich Composites

Sandwich composites are a subset of multi-layered composite structures consisting of skin/facing sheets at the top and the bottom. The core is embedded between them in a classic sandwich configuration. Figure 1.2 shows two skins/ facing sheets, and the core is sandwiched between them. Foam, honeycomb, corrugated cores, different bio-inspired cores, and other core designs have been used.

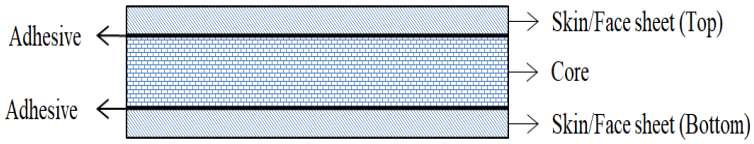

Figure 1.2 Sandwich composite panel

The facings materials are rigid, robust, and much thinner than the core, which is light and somewhat flexible. In conventional structural applications, the thickness of the facings rarely exceeds a few millimeters (mm), whereas the core can be over 50mm thick, but it is usually much thinner. There are exceptions to the dimensions mentioned here, but they rarely warrant the construction of a new theory for the study. A sandwich structure's facings and core do not have to be homogeneous. In place of a single metal layer, laminated composites are commonly used (Birman and Kardomateas 2018). Composite sandwich panels are widely employed in the automobile, aerospace, marine, and defense industries to create lightweight components. They are subjected to various loading situations during serviceability, including targeted bullet impact. Even though these structures would not be suitable for usage as defensive or shielding structures against external object ballistic impact, their mechanical properties and failure modes should be studied appropriately (Ahmadi and Liaghat 2019).

The influence of core thickness and intermediate layers on the mechanical properties of armor composites has been extensively studied. The influence of core thickness (range 10-40mm) and intermediate layers (from single to quadruple) on the mechanical properties of a polypropylene honeycomb core facing multilayer sandwich structure under three points bending were studied. The results displayed that the increase in thickness of the core and intermediate layer shows an improvement in mechanical properties (Arbaoui et al. 2014). Similarly, manufacturing techniques influence the mechanical properties of sandwich structure polymer composites. A study shows that hand lay-up, autoclave, and press methods influence mechanical properties. It is observed that pressure applied to sandwich structures affects mechanical properties like compressive, flexural, and impact strength (Krzyzak et al. 2016).

Ballistic impact behavior analysis is a complicated mechanical process largely dependent on the target strength, thickness, ductility, density, toughness, and impactor factors (Alam and Khanal, 2020). A study discusses that ballistic material performance is influenced by density, design, fabric type, etc. They also observed interconnected

factors that influence a material's ballistic penetration resistance. The study's outcome is required to understand better the dynamic deformation and failure behavior of ballistic material deep study (Abtew et al. 2019). FE (Finite element) analysis was carried out to study the ballistic response of HSPs (honeycomb sandwich panels) and observed that the capacity to resist penetration depends on factors like core, skin thickness, and density of the core; other factors showed no effect on sandwich panels (Qi et al. 2013).

1.2.1 Core materials in sandwich

The core material is placed between two face sheets in sandwich structures to provide stiffness and strength. The choice of core material depends on the application and the desired properties of the sandwich structure.

Some commonly used core materials in sandwich structures include:

1. Foam Core Materials: These materials are lightweight and have good mechanical properties such as stiffness, strength, and energy absorption. They are commonly made from polyurethane, polystyrene, polyethylene, or PVC foams.
2. Balsa Core Materials: Balsa wood is a natural, lightweight material with a high strength-to-weight ratio and excellent mechanical properties. It is often used in marine and aerospace applications due to its resistance to moisture and temperature changes.
3. Honeycomb Core Materials: Honeycomb cores are made from lightweight materials such as aluminum, fiberglass, or paper. They are commonly used in aerospace and automotive industries due to their high strength and stiffness-to-weight ratio.
4. Metal Core Materials: Metal cores such as aluminum or steel are used in sandwich structures where high strength and rigidity are required. They are commonly used in construction and transportation applications.

5. Natural Core Materials: Natural materials such as cork, wood, and bamboo can be used as core materials in sandwich structures. These materials are renewable and biodegradable, making them attractive for sustainable applications.

The core material selection depends on the application requirements, such as strength, stiffness, weight, cost, and environmental considerations. The core material is sandwiched between the face sheets using adhesive bonding techniques, and the resulting sandwich structure offers a high strength-to-weight ratio, stiffness, and durability.

1.2.2 Fiber materials used for skin

Fiber is essential in any fiber-reinforced composites because it comprises a significant volume fraction in composite and carries maximum load acting on composites. Orientations of fiber, volume fraction, geometry, and type of fiber are all factors that affect the properties of composites, like density, ultimate tensile and compressive strength, Fatigue strength, thermal and electrical properties, and cost (Sangamesh 2019a). Two types of fibers are available: natural fibers (NF) and synthetic fibers (SF). The differences between these fibers are shown in Table 1.1. The fiber's characteristics are mainly driven by cellulose, the main ingredient (Kabir et al. 2007a). Table 1.2 lists NF and SF's physical, chemical, and mechanical properties.

Table 1.1 Difference between natural and synthetic fibers.

Properties	Fiber structure	Nature	Cost	Eco-friendly	Bio-degradability	Density	Strength and Modulus
SF	Modified	Hydro-phobic	More	No	No	High	High
NF	Difficult to Modify	Hydrophilic	Less	Yes	Yes	Low	Low

Table 1.2 Natural fibers' Physical, Chemical, and Mechanical properties (Dicker et al. 2014; Mahesh et al. 2021a; Maya Jacob John 2008; Sahu and Gupta 2017; Yahaya et al. 2014).

	Physical Properties				**Chemical Properties**			**Mechanical Properties**			**Cost**
Fiber Type		% Elongation	Density (kg/m^3)	Moisture Content (Wt. %)	Cellulose (Wt. %)	Hemi-celluloses (Wt. %)	Lignin (Wt. %)	Tensile strength (MPa)	Young's Modulus (GPa)	Failure strain (%)	Price (₹/kg)
Synthetic Fiber	Carbon HS-Fiber	0	1800–1840	-	-	-	-	4400–4800	225–260	-	9000-12000
	E-Glass Fiber	1.8-4.8	2550–2600	-	-	-	-	1900–2050	72–85	-	120-250
Fruit Fiber	Coir	15-35	1150–1220	8	32–43.8	0.15–20	40–45	135–240	4–6	25-40	18-38
	Cotton	5-12	1520–1560	7.85–8.5	82.7–90	5.7	<2	350–800	7–12	7	150-320

		Physical Properties			Chemical Properties			Mechanical Properties			Cost
Bast Fiber	Flax	1.2-1.8	1420–1520	8–12	62–72	18.6–20.6	2–5	750–940	75–90	2.3	150-320
	Hemp	1.4-1.7	1470–1520	6.2–12	68–74.4	15–22.4	3.7–10	550–920	55–70	3	70-150
	Jute	1.7-2	1440–1520	12.5–13.7	59–71.5	13.6–20.4	11.8–13	400–860	35–60	2.5	25-110
	Kenaf	1.3-5.5	1435–1500	–	31–72	20.3–21.5	8–19	195–666	60–66	-	19-40
	Ramie	2-2.2	1450–1550	7.5–17	68.6–85	13–16.7	0.5–0.7	500–680	38–44	-	110-180
Leaf Fiber	Sisal	4-6	1400–1450	10–22	60–78	10–14.2	8–14	550–790	10–25	-	44-52
Grass Fiber	Bamboo	2.5-3.7	600–1100	–	26–65	30	5–30	140–800	11–32	-	37-50

The hybrid and non-hybrid forms and their usage data as Polymer matrix composite (PMC) are shown in Figure 1.3. Percentage NF and their usage data from the past 20 years as PMC for impact application are shown in Figure 1.4. Non-hybrid PMCs employ NF more than hybrid PMCs. Even though jute fiber has acceptable mechanical properties, the researchers have not completely exposed it for impact applications, as shown in Figure 1.4 (Célino et al. 2014). Very few or limited numbers of literature use jute fiber in PMC. These studies also focus more on bio-composites for use in impact applications. However, all existing studies focus on producing composites for LVI applications. The gap has been identified in producing hybrid sandwich composites for ballistic impact applications.

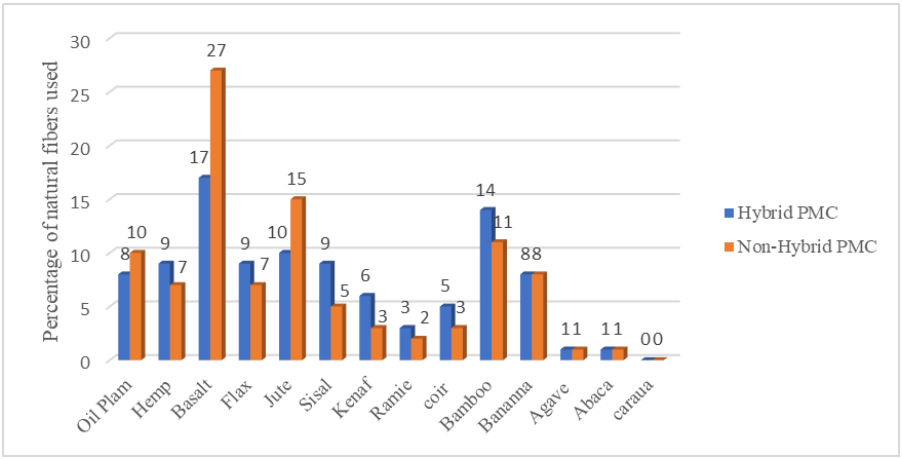

Figure 1.3 Percentage of NF used in hybrid and non-hybrid PMCs (Mahesh et al. 2021a)

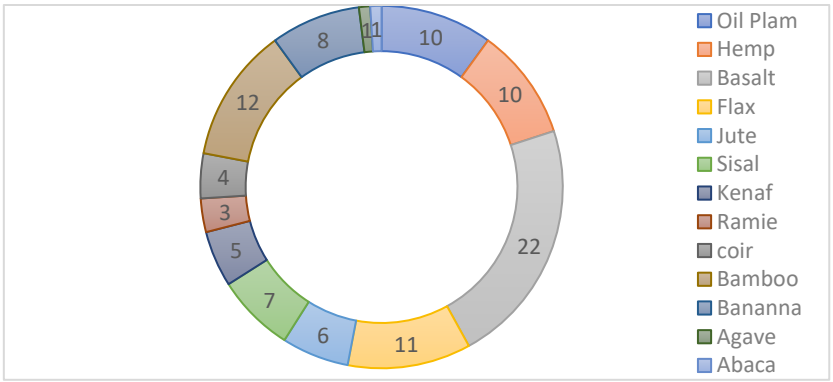

Figure 1.4 Percentage of NF used for impact application (Mahesh et al. 2021a)

1.2.3 Matrix materials are used for the skin and core.

In Greek, polymer means “many members,” so a collection of smaller molecules called monomers and a combination of these monomers are known as polymers. Some natural polymers, including natural rubber, starch, lignin, and cellulose, are chemically converted to other components like gun cotton, celluloid, and vulcanized rubber. Polymerization is defined as polymers synthesized from monomers by chemical reactions because polymerization reactions to several chemical reactions are required. A recent study indicates synthetic polymers are formed using chemical reactions to improve engineering technology for various applications (Evans 1992).

Thermoplastic and thermoset are two types of resin used in the PMC matrix materials. Matrix selection for required application is significant because the final product directly influences the matrix used for composite. Depending on the desired application, selecting an appropriate matrix system for the PMC is a considerable undertaking because the matrix utilized directly impacts the composite's final properties. (Kabir et al. 2007b). Although the longitudinal tensile property of the composite is determined by the fiber employed, other qualities such as transverse tensile property, shear, compressive strength, and heat and environmental resistance are determined by the matrix employed. Table 1.3 shows some mechanical and physical characteristics of thermoplastic and thermoset resins.

Several matrices are used to reinforce the NF to obtain PMC. Figure 1.5 shows that when NF is employed as reinforcement, epoxy is the most widely used matrix in PMC. Synthetic fibers are employed in the majority of PMCs for impact applications. Figure 1.6 shows the matrix percentage used in impact applications with natural and synthetic fibers, which indicates epoxy is the most used matrix in combination with natural and synthetic fiber for impact applications. Natural rubber and STF (shear-thickening fluids) are used for flexible composites as matrix materials for synthetic fibers. In the case of natural fibers, very few matrix materials like epoxy, PE, PP, and PU are used. Some investigators have studied the impact behavior of the PMC utilizing

a variety of polymer-based matrices. Most studies focused on determining the LVI of composites used in structural applications. Natural rubber capable of being employed in PMC exposed to ballistic impact loading (Vishwas et al. 2017, 2019) is not fully exposed in research. The matrix defines the amount of deformation in PMCs, which impacts the local strain and impact resistance. Even though there is a lot of literature on composite impact studies, it turns out that the application of hybrid sandwich composites made from naturally accessible fiber and the matrix has still not been explored. In this perspective, a hybrid sandwich composite made of jute (readily available, eco-friendly, and low cost) and natural rubber (readily available, eco-friendly, and low cost) and face and end sheet and the matrix extensively used epoxy (low cost, readily available and better mechanical properties) as core stands out as a potentially attractive candidate for testing.

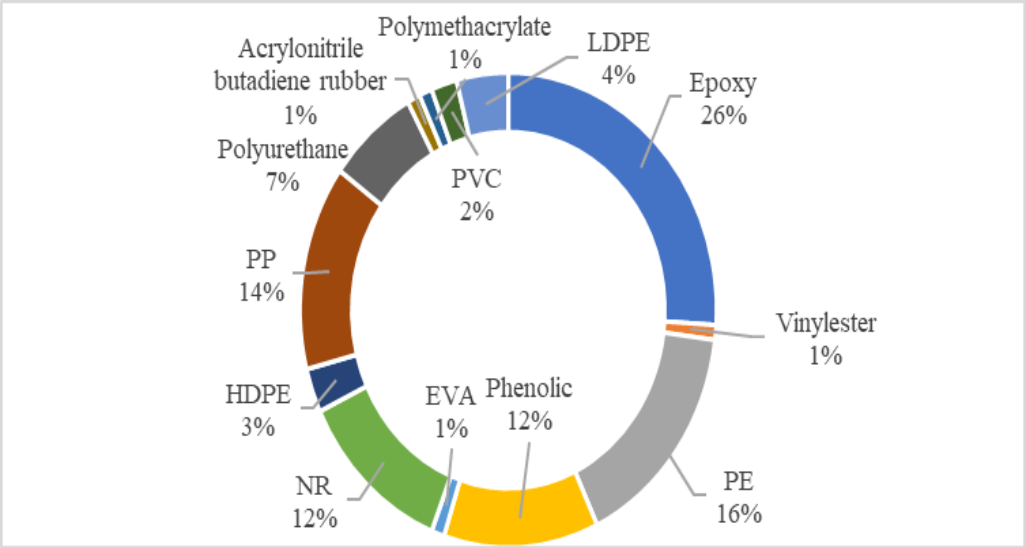

Figure 1.5 Matrix % employed with natural fibers (Mahesh et al. 2021a).

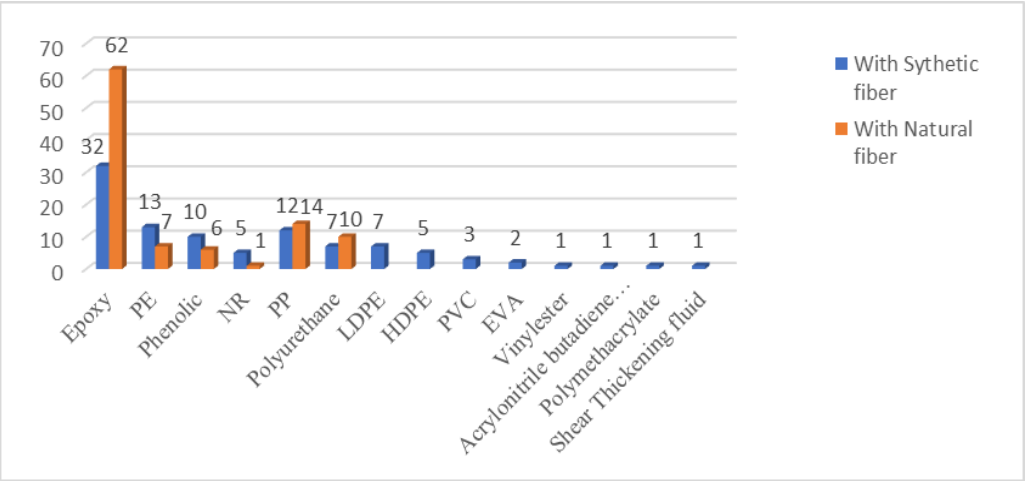

Figure 1.6 Matrix % employed with natural and synthetic fiber for impact application (Mahesh et al. 2021a).

Assessing the impact resistance of FRPs is a significant problem as most of them are subjected to impact testing, and investigators are interested in studying the impact behavior of these composites. Understanding its energy absorption mechanism is also essential to developing a component with higher resistance to impact damage. The behavior of GFRP under low and high-velocity impact was studied, and results revealed that the thickness of the fiber layers should be increased to survive higher impact velocity (Safri et al. 2014a; b, 2015). Synthetic fibers are costly and non-biodegradable; investigators are looking for PMCs with NF for impact applications. Many researchers investigated the physical and mechanical characteristics of thermoplastic and thermosets, and it was clear that thermoset shows better mechanical and physical properties. (Rout et al. 2001, Gupta et al. 2010, Silva et al. 2010). The selection matrix is significant for PMCs as the selection fiber material for impact application. Table 1.4 shows different matrices and fibers used for impact application.

Some researchers have studied different matrix types to withstand damage during impact loading(Reyes and Sharma 2010). Several studies showcased how thermoplastics can withstand damage better than thermosetting during impact loading (Nash et al. 2015).

Table 1.3 Mechanical and Physical properties of thermosetting polymers (Mahesh et al. 2021a).

Properties	TS (MPa)	Compressive strength (CS) (MPa)	Elastic modulus (EM) (GPa)	Percentage elongation (%)	(LVI) strength (Izod) (J/m)	Water absorption (24 hr @20^0C)	Density (g/cm^3)
Epoxy	40–90	90–250	2–4.5	2	0.15–3.2	0.1–0.3	1.2–1.5
Iso Polyester resin	69–83	100	3.1–3.8	4–7	2.5	0.1	1.2–1.4
Vinyl ester resin	35–100	100–200	3–6	1–6	0.3	0.1–0.4	1.1–1.4
Polypropylene	26–41.4 12.4–94	--	0.95–1.77	15–700	21.4–267	0.01–0.02	0.899–0.920
LDPE	40–78	--	0.055–0.38	90–800	>854	< 0.015	0.910–0.925

HDPE	14.5–38	--	0.4–1.5	2.0–130	26.7–1068	0.01–0.2	0.94–0.96
Polystyrene	25–69	--	4–5	1–2.5	1.1	0.03–0.10	10.4–1.06
Nylon 6	43–79	--	2.9	20–150	42.7–160	1.3–1.8	1.12–1.14

Table 1.4 Matrix and Fiber used for different velocity impact

Impact	Matrix used	Fiber used	References
Low and ballistic impact	Vinyl-ester and PU	Polyethylene	(Lee et al. 2001)
	Epoxy	Kevlar, Glass, Flax	(Reddy et al. 2015; Siegfried et al. 2014; Sreekantha Reddy et al. 2019; Sy et al. 2019)
Ballistic impact	HDPE [201]	Chonta palm wood	(Haro et al. 2018)
	Rubber [202,203]	Kevlar	(Khodadadi et al. 2019b; a)
	Epoxy, Flexible Epoxy, and PU.[190]	Dyneema	(Wang et al. 2017)
	Polypropylene [198-200]	Kevlar	(Bandaru et al. 2016)
	Shear thickening fluid [192-193]	Glass	(Sen et al. 2019; Wetzel et al. 2004)
	Soft and Stiff matrix [189]	Kevlar	(Gopinath et al. 2012)

1.2.4 Filler materials used with core

Filler materials are frequently blended with polymers to improve the strength of the material (compressive and tensile) to improve tribological properties like abrasion, toughness, structural and thermal resistance, and other attributes. Filler materials are added to the resin to enhance mechanical properties and lower the costs of the composites (BERNHARD PELZL et al., 2018). As a result, the emphasis is on using inexpensive filler to replace a portion of the more expensive polymer, lowering the cost of the final product. Filler can be made from almost any material, but the ultimate and crucial choice is mainly determined by the specifications needed for the finished product. Once the fillers are chosen to work with the matrix system, the interface compatibility, form, size, and particle packing will be determined. GCC (Ground calcium carbonate), PCC (precipitated calcium carbonate), carbon black, talc (Ceresana 2021), fly ash, nanofillers, chemosphere, sand, etc., are used. Carbon black is mainly employed in transport industries as a filler in rubbers and plastics. Carbon black is used for its economy, thermal and UV protection, electrical conductivity, and reinforcing properties. Commercial carbon blacks have average arithmetic particle sizes ranging from 10 - l00 µm and are typically generated utilizing channel, furnace, and thermal approaches. Another filler method popular among composite researchers is spherical fillers, which can be hollow or solid.

The spheroidal shape, frequently regarded as the most suitable shape to perform tasks with, is one of this category's distinguishing features. Additional benefits include minimal impact on matrix viscosity and flow and the lack of unfavorable stress concentrations due to irregularly shaped and sharp-edged particle fillers, which result in significantly lower mechanical characteristics for composited products. Organic polymeric spheres can also be used as fillers, although they do not have the excellent performance attributes of glass or carbon fillers. The suspension polymerization procedure is typically used to produce them. Due to their reduced properties, they are only used in non-engineering applications. An additional filler method uses a dispersed

phase, such as an elastomer, in a thermoset matrix system. During preparation, the dispersed phase is introduced to the epoxy, which cures to generate core-shell particles spread throughout the matrix. Carbon black is mainly employed in transport industries as a filler in rubbers and plastics. Carbon black is used for its economy, thermal and UV protection, electrical conductivity, and reinforcing properties. Commercial carbon blacks have average arithmetic particle sizes ranging from 10 - l00 µm and are typically generated utilizing channel, furnace, and thermal approaches. Another filler method popular among composite researchers is spherical fillers, which can be hollow or solid. The spheroidal shape, frequently regarded as the most suitable shape to perform tasks with, is one of this category's distinguishing features. Additional benefits include minimal impact on matrix viscosity and flow and the lack of unfavorable stress concentrations due to irregularly shaped and sharp-edged particle fillers, which result in significantly lower mechanical characteristics for composited products. Organic polymeric spheres can also be used as fillers, although they do not have the excellent performance attributes of glass or carbon fillers. The suspension polymerization procedure is typically used to produce them. Due to their reduced properties, they are only used in non-engineering applications. An additional filler method uses a dispersed phase, such as an elastomer, in a thermoset matrix system. During preparation, the dispersed phase is introduced to the epoxy, which cures to generate core-shell particles spread throughout the matrix.

Sand has been frequently employed as a protective shield in many military applications, but limited information is available about its energy absorption capability. A group of researchers from Singapore University (NUS) determined that sand can absorb more than 85% of the energy. Its ability to withstand the impact improves with the impactor's speed and ballistic velocity. On the other hand, steel plates have a lower energy absorption capability for high-speed projectiles. This indicates that sand might be a protective shield in defense applications at a lower cost, with less weight and more negligible environmental effects. The employment of sandbags for military shielding can be seen today. Still, precise information is not available about the impact resistance

behavior and how it varies depending on the velocity and shape of the impactor. The collision between sand and impactors creates considerable friction, which may cause the impactor damage. It may be because of the resistance offered by sand particles, which stretches and opposes the impactor's penetration. In the case of steel, penetration through the target with high velocity without any resistance may be because of the hydrodynamic effect in which steel acts as fluid without strength in material with higher velocity. Sand's unique properties could lead to exciting applications in fields that influence daily lives and defense. Because of higher energy absorption, steel is replaced by sand because of its lower cost, eco-friendliness, and weight (Chen 2016).

Due to the apparent scarcity of river sand, increasing emphasis has been given to using sea sand in recent years for many applications (Jin et al. 2017). To protect the ecosystem, several countries have considered banning the mining of river sands. The latest scientific innovations are attempting to use sea sand as a partial or total alternative, and attempts are being made to put the concept into practice (Zhou and Qiao 2018). Recent studies focus on how the sea sand can be used as filler material for different applications. Sea sand can improve composites' impact performance compared to standard fillers and investigate the feasibility of a more sustainable and cost-effective alternative.

1.2.5 Adhesive for sandwich materials

Among other conventional techniques, the adhesive bonding method proved an attractive and best method for joining the materials (Teixeira de Freitas et al. 2018). Adhesive, mechanical properties, and the bonded composite's stress concentration determine the bonded composite's failure behavior and strength (Afendi et al. 2011). There are various types of adhesives present, each with different mechanical properties. Therefore, adhesive selection plays a critical role based on the type of application and workplace environment (Ameen et al. 2015). The adhesive's main job is maintaining the bond between the skin and core in the sandwich composite. Synthetic and natural adhesives are the two types available for different applications. Some synthetic

adhesives are epoxy, vinyl-ester, iso-polyester, etc. Some natural adhesives are NR, polysaccharides, proteins, PLA- Poly (acid lactic), etc. NR-based gives the composite flexibility, and this flexible composite provides a uniform distribution of stresses with good bonding. Because NR blends have excellent natural adhesive. They can be applied to less sticky substances like synthetic rubbers to improve their cue; however, less research involves fabric composed of natural plant fiber and natural rubber. Researchers are working on a sandwich structure with different core and face sheet material combinations for multiple applications. These potential new sandwich materials must be carefully investigated for mechanical properties to predict their performance.

1.2.6 Functionally graded materials in sandwich materials

Functionally graded materials (FGMs) can be used as core materials in sandwich structures. FGMs are materials with varying properties such as composition, microstructure, and porosity in a controlled manner along the thickness of the material (Doddamani and Kulkarni 2012a). Using FGMs as core material in sandwich structures can offer several advantages over traditional core materials. FGMs can be designed to have a smooth variation in properties that can improve stress distribution and reduce stress concentrations. This can lead to better resistance to damage and fracture under external loads such as impact or bending. In addition, FGM cores can offer enhanced thermal insulation properties due to the variation in thermal conductivity along the thickness of the material (Doddamani and Kulkarni 2012b). They can also provide better acoustic insulation properties due to their graded porosity and stiffness. FGMs can be fabricated using various techniques, such as powder metallurgy, spray deposition, or additive manufacturing. The choice of fabrication technique depends on the desired properties of the FGM and the application requirements. However, the design and fabrication of FGM cores can be challenging due to the complexity of controlling the material properties along the thickness of the core. The material gradient must be carefully designed to ensure that the core material meets the desired mechanical, thermal, and acoustic properties. Overall, the use of FGM cores in

sandwich structures has the potential to improve the performance of the structure in terms of strength, stiffness, thermal insulation, and acoustic insulation. However, their use requires careful design and fabrication considerations to achieve the desired properties (M.R. Doddamani, S.M. Kulkarni 2011).

1.3 Sandwich Composite and Processing Methods

The facings materials are rigid, robust, and much thinner than the core, which is light and somewhat flexible. In conventional structural applications, the thickness of the facings rarely exceeds a few millimeters (mm), whereas the core can be over 50mm thick, but it is usually much thinner. There are exceptions to the dimensions mentioned here, but they rarely warrant the construction of a new theory for the study. A sandwich structure's facings and core do not have to be homogeneous. In place of a single metal layer, laminated composites are commonly used (Birman and Kardomateas 2018).

Composite sandwich panels are widely employed in the automobile, aerospace, marine, and defense industries to create lightweight components. They are subjected to various loading situations during serviceability, including targeted bullet impact. Even though these structures would not be suitable for usage as defensive or shielding structures against external object ballistic impact, their mechanical properties and failure modes should be studied appropriately (Ahmadi and Liaghat 2019). An experimental and numerical study can be conducted for several cases involving the impact response of composite sandwich panels. A review has been conducted on the impact effect of sandwich configurations (Abrate n.d.). Experiments have been conducted on the damage mechanisms, piercing energy, and ballistic range of composite sandwich panels subjected to HVI (Nasirzadeh and Sabet 2014). The failure initiation in affected sandwich panels was explored in a study, and it was claimed that the failure mechanism is determined by various parameters, including BC (boundary conditions), the nose of a projectile, and skin and core component properties. Deflection and global deformation of the sandwich laminate absorb a lot of energy. Deformation

is reduced with increased foam core thickness; the overall energy required for piercing the panels is reduced (Roach et al. 1998). An experimental investigation was carried out on the rupture of skin and core of different types and the sandwich panel combinations with varying impact velocities. Results show that the energy needed to perforate through the composite sandwich panels was substantially greater than pierce through individual parts, indicating that the layers interact during perforation (Goldsmith et al. 1997). Flat, conical, and hemispherical-nosed projectiles with impact velocities up to 305 meters per sec (m/sec) simulate LVI, HVI, and quasi-static impact on sandwich panels. Their experiments revealed that perforating a sandwich panel dynamically requires more energy than a sandwich panel quasi-statically (Wen et al. 1998). In a study, the effects of HVI on objects of different thicknesses were studied, and the results displayed delamination energy absorption presides over other mechanisms as the thickness increases (Mines et al. 1999). The composite's response to an HVI will significantly differ from an LVI's (Rajesh Mathivanan and Jerald 2010). It is not appropriate to generalize a composite sandwich behavior to an LVI to examine the consequences of an HVI.

Synthetic core composites (Synthetic foams) are closed-cell structures containing fillers spread in the resin matrix. When compared to open-cell, the closed-cell structure offers better mechanical properties and less moisture absorption (Gupta and Woldesenbet 2004). Synthetic core composites give the sandwich panel higher strength and stiffness than polymeric core foam (Choqueuse and Davies 2008; K. Ambika Devi, Bibin John, C. P. Reghunadhan Nair 2007). It also has civil engineering applications and is well-known in marine applications like boat bodies, submarines, underwater pipes, etc. (Gupta et al. 2014).

Some of the filler materials are used with the synthetic core structures like Fly ash particles (cenospheres), Soda lime-borosilicate (Engineering glass) micro-ballons as the filler material (Jayavardhan et al. 2017; Yung et al. 2009; Zhu et al. 2012). Researchers conducted several studies on the mechanical properties of syntactic core sandwich structures to determine their feasibility for various applications (Gupta et al.

2010; Shunmugasamy et al. 2013; Zhu et al. 2012). Several tests are conducted on a sandwich with a synthetic core, like modulus, compressive strength (Gupta et al. 2004), flexural strength (Tagliavia et al. 2012), and shear test (Kishore et al. 2005). A study shows that as the volume fraction of the Cenosphere increases, there is a decrease in failure strain and flexural strength, but some enhancement is observed in the flexural modulus (Garcia et al. 2018). The flexural characteristic of a sandwich with a syntactic core was examined, and the results show the micro-balloon shape influenced the flexural strength and showed the damage was like tensile tearing for skin and shear crack in the case of the synthetic core (Gupta and Woldesenbet 2004).

Sandwiches with synthetic cores with different fillers still haven't been investigated for ballistic impact applications, and some researchers have used this under quasi-static loading and LVI.

1.3.1 Processing of composites

The fabrication of FRP composite requires reinforcement fiber and matrix materials using various techniques. Several methods are used in the fabrication of FRP; some of the essential techniques are:

- **Open Molding:** In this type, resins and fiber reinforcements are exposed to air as they cure. It uses different processes, including hand lay-up, spray-up, casting, and filament winding.
- **Closed-Molding:** In this type, raw materials (fibers and resin) are cured within a two-sided mold or inside a vacuum bag. Special equipment is needed because closed molding is an automated process. These processes include Vacuum Bag Molding, Resin Transfer Molding, Compression Molding, Injection Molding, and Pultrusion.

Hand lay-up (HLU)

It is the basic and simple method in FRP fabrication. In the Hand lay-up process, wax or anti-adhesive is used to remove the mold easily; fibers, ply, and resin are added to dry plies using the brush; the procedure is continued to get the required size. Rollers ensure the bonding between resin and fiber, as shown in Figure 1.7 (Elkington et al. 2015; Gunge et al. 2019; Jamir et al. 2018). There are many curing techniques; a common strategy is to enable cure at room temperature for 24 hours. Another method is to speed up curing by heating the oven and applying pressure through a vacuum.

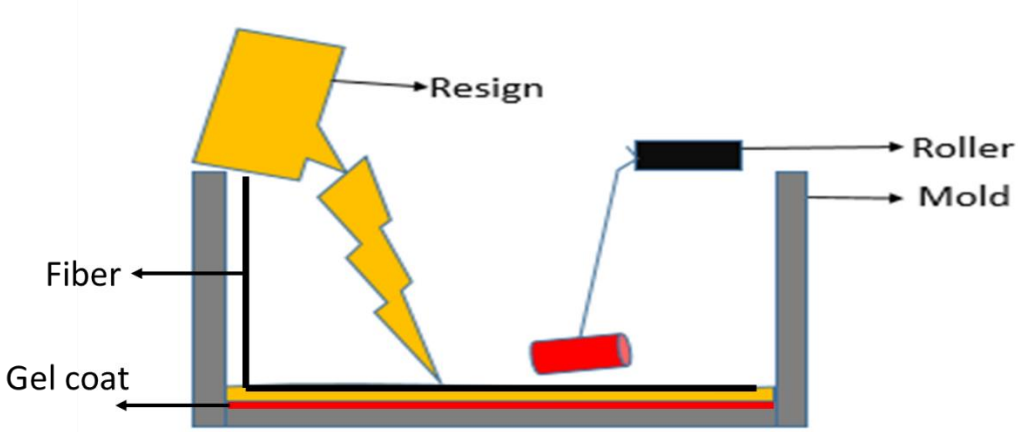

Figure 1.7 Hand lay-up process

Compression Molding (CM)

In this method, fiber reinforcement is kept between preheated molds and then pressed to get the required shape using a mechanical or hydraulic press, as shown in Figure 1.8 a) and Figure 1.8 b) shows the factors controlling compression molding. Compression molding provides less cycle time, more productivity, and a high level of automation, so this method is used in many applications in the automobile sector (Mitschang and Hildebrandt 2012)(Matveenko et al. 2018).

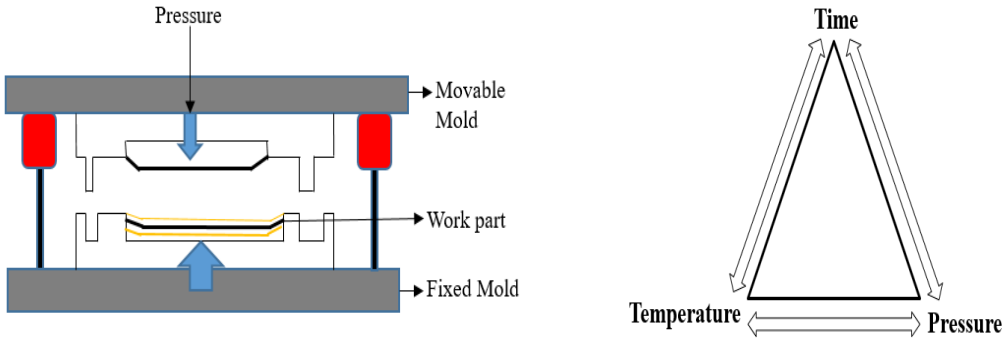

a) b)

Figure 1.8 a) Compression molding process, b) Controlling factors

This chapter discusses the foundations of composites, sandwich composites, functionally graded materials (FGMs), the processing of composites, and their methods. It begins by laying the groundwork for understanding composite materials, highlighting their significance in modern engineering applications due to their tailored properties and enhanced performance characteristics. The next chapter covers a comprehensive literature review emphasizing critical factors in selecting composite materials, identifying existing research gaps and potential areas for further investigation, and identifying the objectives.

CHAPTER 2

2 LITERATURE REVIEW

Many studies have been done on the importance of PMCs (Polymer matrix composite) on impact behavior in the last few years. The current research focuses on the performance evaluation of a jute/natural rubber/jute as skin material and Epoxy with sea sand as core material-based sandwich composite, the physical and mechanical characterization of the sandwich composite, and the study of the proposed composites for low and ballistic velocity impact behavior.

2.1 Impact properties of composites

The facing materials are rigid, robust, and much thinner than the core, which is light. The collision between two or more bodies is termed an impact, where a crash may be in the form of an individual or combination of elastic, plastic, or fluid. An area of great significance to the development, impact damage caused by laminated composites persists. This extreme level of responsibility arises from the fact that impact damage results in different ways, like cracks in the matrix, debonding in fiber/matrix, micro-buckling in the surface, delamination, and breakage in fiber; various forms of impact damage influence different degrees of the other properties of laminate (Razali et al. 2014). Because of their superior mechanical properties, lower production costs, and electromagnetic wave permeability, glass/polyester laminate structures are commonly used in applications like the airforce, marine, and automotive industries. These structures can be subjected to High-Velocity Impact (HVI) of low-mass components, but a better understanding of their response to impacts of this kind is needed. The minimal use of laminate-type composite materials is impact damage because, after impact, the strength will be decreased significantly and is not noticeable (S.I. Ibekwe, P.F. Mensah, G. Li 2007). Two distinct scenarios are there for impact problems, namely (Cantwell and Morton 1991):

1. Large mass (dropped weight) with a low-velocity impact.
2. Small mass (Gunfire) with a high-velocity impact.

The response of composite materials and metals differs in impact loading and dissipation of the projectile's incidence KE (kinetic energy). Metals absorb energy via elastic and plastic deformation for low and intermediate velocities. This may result in deformation, and the effects on the component's load-carrying capacity are generally less than on composites. Nevertheless, the potential of composites to endure plastic deformation is relatively low; as a result, the development of the area of fracture increases by decreases in strength and rigidity (Razali et al. 2014). Generally, the damaged area of a composite is dynamic and very hard to define. The absence of appropriate specifications or developed testing techniques for composite impact damage further complicates the problem. Based on the requirement, machines are built using suitable sample geometries, and most of the research reported in the literature has been carried out.

Consequently, direct comparisons between different material systems are sometimes difficult, and concluding is also challenging. Target perforation can occur at high-velocity impact, and the motion of the impactor can cause spalling, petalling, and cracking; where this damage will weaken the structure's load-bearing capability, the effects can be forecast by the principles of fracture mechanics (Avery 1981). For any object capable of being fired, the term projectile is used. The projectile identifies the target as any moving or stationary item hit. Based on the type of material and amount of deformation experienced during impact, projectiles may be classified as

- Soft projectiles (undergo substantial deformation)
- Semi-hard projectiles (undergo certain deformation)
- Hard projectiles (undergo minor or negligible deformations)(Zukas 1980).

For different applications like aircraft, structural applications, etc., the most critical characteristics of FRCs are damage resistance and tolerance under impact

loading since they are subjected to various forms of unanticipated impact during maintenance and production (Hirai et al. 1998).Some of the types of impact loadings:

1. Low-velocity impacts: It ranges from 0.001 to 0.01 km/s, which happens through bird and hail strikes, etc.
2. High-velocity impacts: It ranges between 0.01 to 0.2 km/s.
3. Ballistic velocity impacts: It ranges between 0.2 to 1.5 km/s, a significant concern in military applications.
4. Hypervelocity impacts: It is greater than two km/s, a significant concern in spacecraft applications.

2.1.1 Methods used for Impact Performance Assessment

There are three types of approaches to impact problems. An experimental investigation is the first approach involving instrumented or free-flying projectiles that contact the structures. During and after bullet penetration, the loss of kinetic energy of a projectile and impact damage to the targets are measured. Simple empirical curves or equations are developed for the tested targets and projectiles. These empirical findings are only reliable when applied to impact situations and structures identical to those used in the original testing. If the type of structure, material, target geometry, and shape and size of the projectile differ from the actual test conditions, their predictive potential is challenged. As a result, their applications are limited. Analytical modeling is the second approach in which the associated damage modes and penetration processes are discovered from these impact tests based on comprehensive analyses of the commencement, development, and progression of impact damage in the structures during projectile penetration.

Furthermore, employing these mechanisms to apply mechanistic theories for penetration problems is built. Since the damage processes in the models enable numerous impact and structural aspects to be addressed, this approach is the most versatile and practical approach to analyzing the ballistic performance of a wide range

of projectiles and targets. On the other hand, the validity of the analysis greatly depends on the accuracy of the initial assumptions or the suitability of the penetration mechanisms. Numerical modeling is the last approach to solve penetration difficulties; finite element analysis is used. Computer codes estimate composites' impact response, damage initiation, and growth. This type of modeling provides more information than experimental study and analytical modeling by revealing specific stress and strain distributions in structures. Formulating and predicting these are difficult because they rely on dependable constitutive models (XIANGYANG QUAN 1998). Impact analysis in composite materials might be as simple as an analytical technique or as complicated as a FE approach. As the methodology improves, damage estimation is also enhanced in impact analysis. The FE-based numerical method is used to predict the shape and type of damage based on the methodology used, but analytical and experimental approaches give quantitative dimensions of damage occurrence.

Theoretical Method

To decide on the appropriate design solution for a composite for a specific application, the designer should have a clear idea of the micro and macro-mechanical properties of the composite. Composite materials are isotropic, so mechanical characterization becomes more difficult. The composite's mechanical properties can be evaluated as follows:

- By taking the properties of each material and then determining the properties of composite using the rule of mixture, assuming that composite piles are to be homogeneous. It is essential to improve the properties at this phase, known as laminate micro-mechanics.
- A relationship between stress-strain is built, and from this, many properties relationships are obtained, known as laminate macro-mechanics.

The designer builds a laminate's macro-mechanics by understanding a single lamina's macro-mechanics. Stresses and failure theories are applied to each ply to determine laminate failure. Many scholars have proposed formulae to calculate

modulus based on various theories (Ishai and Cohen 1967; Harry S. Katz 1978; Wong and Truss 1994). Extensive research is on simulating responsive, flexible materials such as rubber (Bloch 1976; Christensen 1982; SCHAPERY 1987). Many scholars have also built several constitutive models for cyclic loading and dynamic behavior (Liu 2010; Liu and Hoo Fatt 2011). Rubber is widely utilized in many applications, but the study of mechanical responses and the absence of a constitutive model to accurately model rubber behavior are still insufficient. The main disadvantage of this method is the difficulty of managing materials with imperfections such as cracks, voids, and inhomogeneity. Compared to the analytical method, the FE method has become superior using modeling software (Nikhil Gupta 2002).

Numerical Method (FEM)

A composite design for a required application necessitates a detailed understanding of its performance under the desired stress. Finite Element M (FEM) proved superior to the theoretical method because material composition geometrical non-linearity can be built utilizing FE software. FEM has demonstrated its effectiveness in many engineering applications for a few decades. FEM begins with an analysis of structures and has already progressed to practically every engineering area, including the design of composite and mechanical components. FEM can effectively model and simulate the composite's behavior at the micro and macro scale levels. The following are the three analysis steps:

- Pre-processing: The main goal is to assign appropriate properties, materials, boundary conditions (BC), and meshing. Meshing is a process that divides the entire geometry into smaller elements, resulting in nodes BC can be applied. 2D (two-dimensional)/ 3D (three-dimensional) are elements used in meshing. The shell represents 2D, and 3D elements are represented by solid (thickness in all directions). The nodes determine the DOF (degrees of freedom) that define the movement. The challenging part of FEM is meshing; properties of materials must be specified based on the type of analysis. The density, tensile modulus,

poison's ratio, and thermal coefficient are essential for linear static analysis. The velocity and constraints are applied using BC (Vishwas M. 2020).

- Solution: After finishing the preprocessing model, the solution is identified. The numerical approach executes tasks like approximating unknown variables, discretizing models, and setting algebraic equations.
- Post-processing: It gives model results as outliners and can be saved as text documents for additional analysis. Animations are available for dynamic analysis. Many designers have used user-friendly software to use composite modeling (S.M. Kulkarni 2002). FEM is used to optimize the factors before manufacturing to reduce the cost and time of producing defective products. Some disadvantages are present with better advantages, like complexity in simulating the sandwich model and some assumptions that vary the results. Taking all the properties into the experimental method proved better than the theoretical and FE methods (Vishwas M. 2020).

Experimental Method

This experimental method is the best compared to other methods because it examines the composite mechanical behavior using standards without making assumptions and is executed in a practical situation.

The composite density is tested before it is finalized for the specific application. The void content is calculated using the density. Accordingly, tensile and tear tests are examined using the ASTM standard (D 412 and D 624). One of the essential features of composite is interlaminar shear strength (ILSS) (Garg et al. 2015; Wang et al. 2016). Using ILSS, the fiber and matrix interface bonding can be examined in order to improve individual fiber and matrix characteristics (Zahid et al. 2019).

Rather than static loading, the composites are subjected to dynamic loading while in use. Impact loading is one of the most significant dynamic loads composites bear. Before developing and completing the composite for a specific application, it is

imperative to thoroughly examine absorbed energy and the damage type that the flexible/stiff composite experiences from impact loads.

Different impact loadings, such as LVI (less than 10 m/s), intermediate impacts (High Strain rate) (10 to 50 m/s), HVI (50 to 1000 m/s), and hypervelocity impacts (2000 to 5000 m/s), can affect composites utilized in a variety of applications (Abrate 2011). There are two possible mechanisms for energy absorption in the composite: a) deformation of material and b) surface generation. Deformation of material happens when the initially created part of the task is retained as elastic deformation. In addition, crack initiation and propagation may occur with increased energy input. Increasing material deformation or creating a curved crack propagation route is crucial for improving energy absorption.

In composites, energy absorption can be evaluated using a gas gun HVI test, Split-Hopkinson Pressure Bar (SHPB) for intermediate impact test, and a drop weight impact test for LVI. The impact and residual velocities can be used in both scenarios (LVI and HVI) to calculate the energy absorption.

Impact testing machines with drop weights are used to conduct LVI tests. The impactor's shape might change based on the requirements. The sample is placed inside the sample holder, and the projectile is elevated to its required height with and without spring loads, causing it to fall upon the sample. It is possible to choose different heights to achieve varied impact velocities. Different impact energies could be achieved by altering the impactor's dropping height. The potential energy of the impactor increases with height. This test is used to study the composite’s energy absorption and mechanism of damage subjected to LVI.

One of the worst loading scenarios to which a composite structure may be exposed is ballistic impact; choosing a suitable material is crucial in these structures. Examine their resilience and damage tolerance abilities before using PMCs in ballistic impact applications (Lee et al., 2000). Designers and engineers frequently use flexible materials to enable protective structures designed to protect the primary structures from impact loads to absorb maximum energy (Khodadadi et al. 2019). The energy-

absorbing properties of flexible materials are thoroughly investigated by various researchers utilizing analytical and experimental methods (Yang and Chen 2016). The essential factor in evaluating the HVI response of the composites is to determine the ballistic limit- the mean of the higher partial piercing velocity and lowest piercing velocity of a projectile and target. Table 2.1 shows the different methods used to determine the impact behavior.

Table 2.1 Research work on composites to assess impact behavior.

Method Used	**Impact Test**	**Composite materials**	**Software/ Equipment**
FE (Ansari and Chakrabarti 2016)	Low to hyper	Glass /epoxy	ANSYS/ AUTODYN
FE (Nalla Mohamed et al. 2016)	Ballistic	Carbon, glass, and Kevlar FRPs are used as the skin, and Aluminium foam is used as the core in sandwich composites.	ABAQUS/ Explicit
FE (Žmindák et al. 2016)	Ballistic	Carbon/PEEK	ABAQUS/ Explicit
FE (Park et al. 2015)	Ballistic	Kevlar/STF (Shear thickening fluid)	LS-DYNA
Experimental and FE (Bandaru et al. 2016)	Ballistic	Kevlar-polypropylene composite	ANSYS AUTODYN Gas gun
FE(Fawaz et al. 2004)	Ballistic	Ceramic-composite	LSDYNA3D
FE (Nasir Hussain et al. 2017)	Crash	GRRP	LSDYNA

Experimental (VanderKlok et al. 2018)	Ballistic	Glass/epoxy	Gas gun
Experimental	Ballistic	Glass epoxy/ Dyneema	Sub-machine carbine gun
FE, Analytical model (Palta et al. 2018b)	Ballistic	Kevlar composites	LS-DYNA Recht–Ipson model
FE (Sudhir Sastry et al. 2014)	Ballistic	Kevlar, Glass, and Carbon fiber-reinforced composites	ABAQUS
Experimentation (Reddy et al. 2015)	Ballistic	Glass/phenolic composites	Gas gun
FE (Sangamesh et al. 2018)	Ballistic	Jute/Epoxy,	ABAQUS/ Explicit

2.1.2 Impact Events in Applications of Composite Materials

High-kinetic-energy projectiles will perforate the structure, eventually causing it to fail. Low-kinetic-energy projectiles may not pierce the structure but may cause undesired damage. As a result, it is critical to examine the onset and progression of damage in composites after foreign object impact and how they absorb impact energy to anticipate the structural behavior of damaged composites under subsequent loads (XIANGYANG QUAN 1998).

Figure 2.1 represents the development from simple analytical models to complex micro models using finite element systems at a high level. As predicting capabilities improve, so does the amount of analysis time required. Impact analysis's primary purpose is to estimate damage, and analytical expressions are employed to offer

data on damage initiation. Numerical models can assess the type and pattern of damage to varying degrees of accuracy depending on the modeling technique.

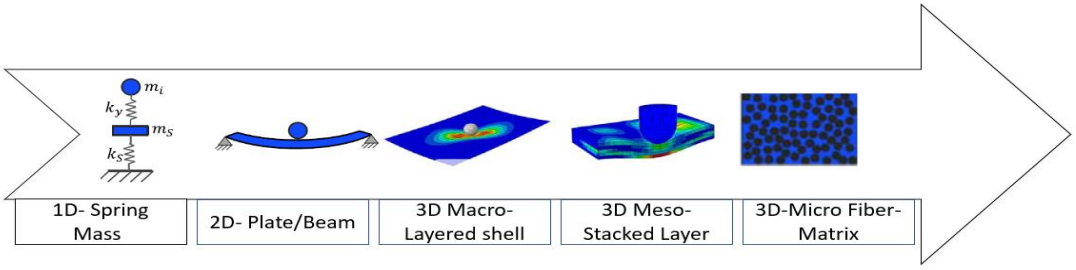

Figure 2.1 Developmental steps for impact analysis methods (Bogenfeld et al. 2018).

Impact analysis in composite materials might be as simple as an analytical technique or as complicated as a FE approach. As the methodology improves, damage estimation is also enhanced in impact analysis. The FE-based numerical method is used to predict the shape and type of damage based on the methodology used, but analytical and experimental approaches give quantitative dimensions of damage occurrence. Analytical techniques used on a spring-mass structure were introduced to evaluate the impact response. (Abrate 1991; Christoforou and Yigit 1998). Furthermore, researchers used the beam plate model and were able to define the initiation of damage in composites. Damage type, shape, and extent were identified using a layered shell model 2009 (Kärger et al. 2009). In 2015, a layered stack model was used to predict microdamage. Finally, in 2016, fiber/matrix models were created.

All the models are used in the developmental steps for impact analysis methods, summarising the essential aspects of the techniques. For these modeling approaches, the scale of approaches, analysis environment, inter-fiber, fiber failure, Delamination, and damage evolution are shown in Table 2.2.

Table 2.2 Basic approaches in modeling.

Model	Scale of Abstraction	Analysis	Fiber failure	Delamination	Inter-fiber Failure	Damage Evolution
Spring mass (Abrate 1991)	Global impact system	Scilab	---	Threshold force	---	---
Plate / Beam (Dobyns 1981; Olsson 1992)	Macro	Scilab	---	Threshold force	---	Secant stiffness limit
Layered shell (Kärger et al. 2008; Yap et al. 2003)	Macro	Abaqus standard	Max strain	Quad strain	Hashin	Bilinear
Stacked shell (Chen et al. 2017)	Macro-meso	Abaqus explicit	Max strain	Quad strain	Hashin	Bilinear
Stacked-solid (Liu et al. 2016)	Meso	Abaqus explicit	Max strain	Quad strain	Quad strain	Bilinear
Fiber Matrix (Hongkarnjanakul et al. 2013)	Meso	Abaqus explicit	Max strain	Quad strain	Quad strain	Bilinear

2.1.3 Ballistic Impact Test (High-Velocity impact -HVI)

HVI testing causes more severe damage, resulting in sudden material failure (Rajesh Mathivanan and Jerald 2010). Application areas include high-speed projectiles to provide structural survivability against impact. Composites are used and engineered to withstand HVI of damaging parts of the engine, blades of a turbine, and other obstacles in aircraft and automobiles (Sunt and Potti 1996). HVI testing means the impact between two or more components. Two types of single-stage guns are used in HVI they are:

- Powder gun: Gunpowder is used, and the velocity range is between 2000 to 2200 m/s.
- Gas gun: The propellant is compressed helium or hydrogen gas (Bernier 2005).

HVI/Ballistic impacts penetrate the target entirely, whereas non-penetrating impacts are referred to as LVI (Abrate 1998). The ballistic impact is an HVI event in which a component drives a low-mass, high-velocity projectile toward a target. Penetration or perforation may be achievable depending on the target's geometry, materials properties, and projectile parameters. If the initial kinetic energy of the projectile is less than the energy the object can absorb, the bullet will either stick or rebound. If the projectile's initial KE is more than the energy that the object can absorb, perforation occurs with a given residual velocity. The ballistic limit (VBL) refers to the starting velocity of a projectile of a given mass when it completely perforates the target with zero residual velocity (Naik and Doshi 2008). Because the penetration process involves multiple complex phases and always some unpredictability, the ballistic limit is sometimes defined as complete penetration with minimal impact velocity (Abrate 1998). Energy is transferred from the bullet to the target during the ballistic impact. By absorbing the projectile's KE, polymer composites slow it down. During an impact, various mechanisms occur, including cone formation on the target's back face, the tension in primary fibers, secondary yarn deformation, matrix cracking, shear plugging, delamination, and friction between the target and projectile.

Projectile energy will be transferred to the target material whenever the projectile hits a target material. A fabric system or composite target absorbs the energy in one of three ways:

- No penetration: When the projectile collides with the target material, it bounces/rebounds.
- Partial penetration: Penetrates the target material partially before resting within it.
- Complete penetration: Penetrates completely by damaging the target material (SANGAMESH 2019b).

In the situation where there is no penetration or partial penetration, there is no exit (residual) velocity, and so the equation for the energy absorbed (EA) is given by

$$E_A = {}^1\!/_2\, m(V_i^2) \tag{1}$$

The energy absorption phenomena are controlled by the fiber's tensile characteristics, the matrix's properties, the fiber arrangement in the composite, and the interfacial strength. A projectile's residual KE is proportional to its initial KE. As a result, the energy required to perforate the target is constant, and energy conservation can be expressed as (Abrate 1998):

$$E_A = {}^1\!/_2\, m(V_i^2) = E_{PF} + {}^1\!/_2\ m(V_r^2) \tag{2}$$

Where m_p = mass, V_P= incident impact velocity, V_r = residual velocity of the projectile, and E_{PF} = perforation energy, according to the preceding equation, projectile velocity is unaffected by the amount of energy required to perforate the target (Kumar et al. 2010). Table 2.1 details the processing and modeling methods used under ballistic impact. Some studies show the absorption and perforation of FRPs utilizing conical tips, hemispherical corners, and flat-faced (Wen 2000). Early research indicates most of the research work was carried out on thinner laminates, generally not above 0.002-0.033 m. Some researchers suggest thick laminates are used in the study of the HVI test. This review from Table 2.3 comprises the FE analysis and processing method of composites for ballistic impact analysis.

Table 2.3 Fabrication and FE modeling of composites for ballistic impact and composites for ballistic impact.

Fiber Used	Matrix	Processing Method	Modeling methods and FEM software	Summary	References
Kevlar	Epoxy	HLU (Hand Lay-Up)	Variables used: Thickness, Number of Layers, Input Velocities	Ballistic impact: GAS gun firing setup • The ballistic limit and the composite laminate thickness have a linear relationship. • The composite target's energy absorption and ballistic limit increase as thickness increases for specific impact velocity.	(Patel et al. 2004)
Twaron	Natural rubber	Coating technique	Experimentally Variation in coating thickness	Ballistic Impact: Test Gun at 0^o obliquity. • Ballistic impact resistance. It is improved with fabric treated with natural rubber.	(Ahmad et al. 2007)
Polyethylene	Polymeric-matrix	HLU	ANSYS/Autodyn version 11.0	Ballistic Impact: • Starting phase- shearing or cutting • Intermediate phase- debonding	(Grujicic et al. 2009)

Fiber Used	Matrix	Processing Method	Modeling methods and FEM software	Summary	References
				• Back phase- stretching of armor, which leads to buckling	
Kevlar yarn	Soft and Stiff matrix	HLU	LS-DYNA	Ballistic impact: Body armor application • Stiffer polymer materials absorb maximum KE.	(Gopinath et al. 2012)
Kevlar	Polyester-Al2O3	HLU	ANSYS/AUTODYN 3D- v.12	Ballistic Impact: GAS gun Firing Setup (160-400 m/s). • The target's thickness influences the composite's ballistic response.	(Ramadhan et al. 2012)
E-Glass	Epoxy	HLU	ABAQUS/Explicit	Ballistic Impact: GAS gun Firing Setup. • The FE simulation and experimental findings matched the varied thicknesses of the composites simulated.	(Phadnis et al. 2013)

Fiber Used	Matrix	Processing Method	Modeling methods and FEM software	Summary	References
Kevlar	Polypropylene matrix	HLU, CM (compression Molding)	ANSYS/AUTODYN	Ballistic Impact: • Other fabric armor composites failed to intercept the 9mm FMJ bullets, while 3D orthogonal and interlock fabric armor composites arrested the bullet.	(Bandaru et al. 2016)
Polyethylene	polymeric-matrix	HLU	LS-DYNA	Ballistic Impact: • Enhanced combat helmets find that the helmets created can stop a 9 mm bullet; however, they fail to stop bullets with a Caliber of 223mm.	(Palta et al. 2018a)
Carbon fiber	Vinyl ester Core: Epoxy/ cenosphere	VARTM (Vacuum-assisted resin	Finite element model	Dynamic impact loading: An increased volume fraction of the Cenosphere (60%) shows better mechanical properties.	(P. Breunig et al. 2018)

Fiber Used	Matrix	Processing Method	Modeling methods and FEM software	Summary	References
		transfer molding)			
Jute	Epoxy/Rubber	CM	ABAQUS/Explicit	Ballistic Impact: GAS gun Firing Setup (150-350 m/s). Bullet-proofing application	(Sangamesh et al. 2018)

2.2 Material selection approaches

The designer's most important responsibility is decision-making. Figure 2.2 illustrates the eight steps that are included in the process of decision making.

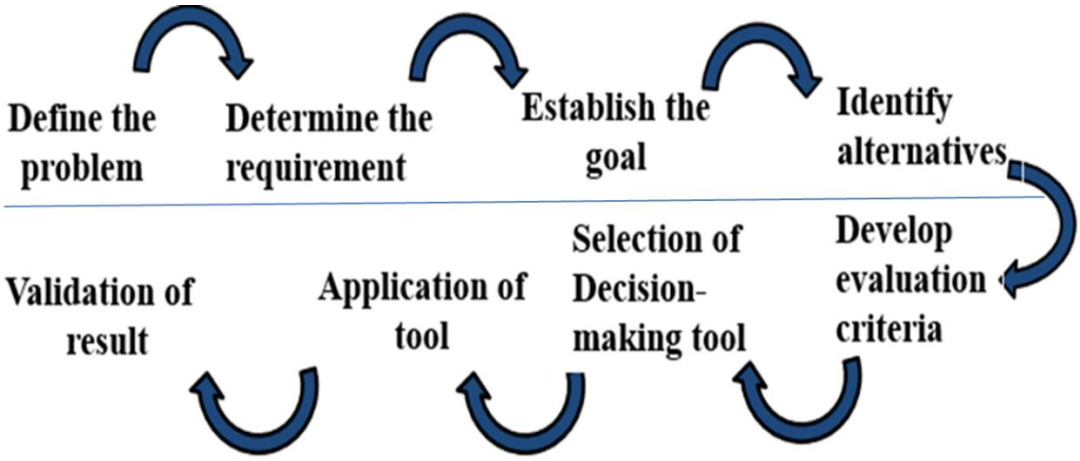

Figure 2.2 The Decision-Making Process (Jackson and Pascual 2008; Navneet Bhushan 2004).

The initial decision-making phase is selecting suitable tools for achieving desired strategic goals (Belton 1986). In addition, scientific groundwork or expert opinions should be developed to validate the outcome. After the problem has been identified, the criteria for achieving the desired outcome should be determined. Additionally, it is critical to developing essential goals. After the objective has been decided, the designer should prepare a set of several alternatives from which to choose (Krupa et al. 2015). Generally, it isn't easy to find the optimum alternative for the solution in the initial phase. Therefore, the designer chooses many evaluation criteria to use as a framework to analyze the alternatives (Mateo 2011).

In the subsequent step, care should be taken to select the best tool for decision-making and implement it to obtain the desired outcome. In terms of material selection, for any engineer, the most challenging job is to choose the suitable materials, volume

fraction, and stacking sequence of the selected composites (Yogesha 2019), all of which impact the product's performance.

It is essential to remember that there is no set of rules that engineers must adhere to as a guideline. This also makes the job of engineers much more difficult. In composites, multiple factors are considered when choosing a material for a specific purpose, and these specifications could be inconsistent. As a result, engineers play a crucial role in selecting materials. Figure 2.3 shows the variety of ranking techniques for material selection.

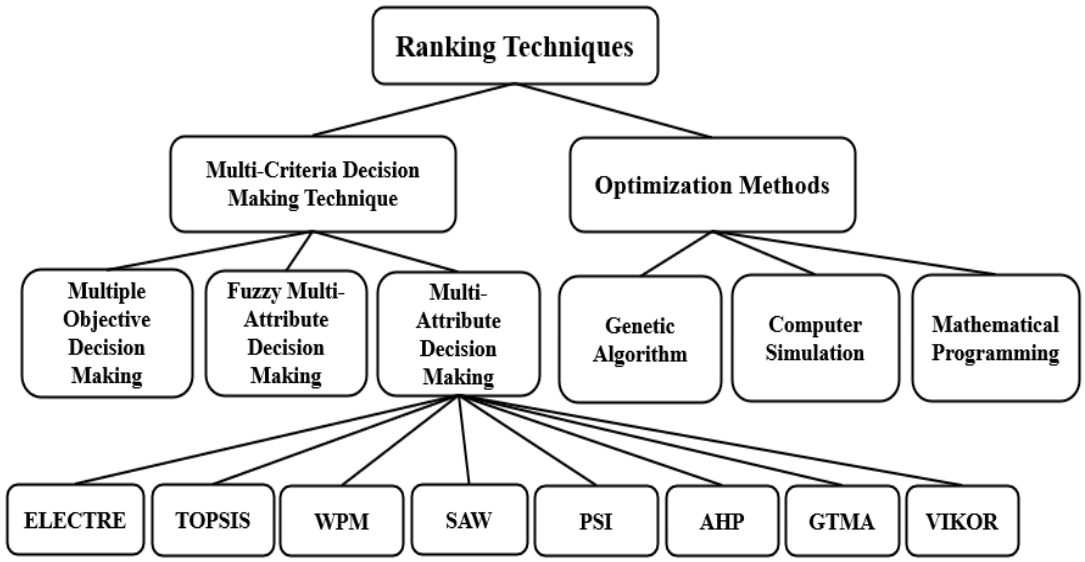

Figure 2.3 Ranking techniques used to select materials (Jahan et al. 2010).

MADM reduces the engineer's effort and time and produces realistic results. This is why material selection has proved to be an effective tool in ranking techniques. TOPSIS proved better than all other ranking techniques because it considers both the positive and negative optimized solutions when selecting the material(Kumar et al. 2018; Patel and Rawat 2017; Vinay Kumar Patel 2016). If there is a disagreement between the criteria selected, TOPSIS and VIKOR techniques are the best methods to resolve the problem. In VIKOR, the materials are ranked according to the alternative's closeness to the correct response (Gangil and Pradhan 2018).

PSI is another simple technique used for material selection (Maniya and Bhatt, 2010). It is considered the simplest method because it does not require weight allocation to each factor. Many studies have employed the MCDM methodology for suitable material selection, and Table 2.4 summarizes.

The literature reports that the MADM approach has shown considerable potential to effectively select material, especially in complex engineering applications where numerous variables must be evaluated simultaneously. While evaluating multiple material alternatives based on various criteria like mechanical properties, cost, environmental effect, and manufacturing flexibility, MADM approaches offer an organized and methodical framework. These methods quantify trade-offs and prioritize material properties that meet specific design requirements, enabling design engineers to make accurate selections. However, an assessment of the research on the selection of material available is less, indicating the need for additional exposure for designers to MADM techniques (Mardani et al. 2015). This indicates that engineers and designers could not take full advantage of MADM in their material selection procedures because they are unfamiliar with the methods or have not had enough exposure to their real-world uses. A critical need exists for further research incorporating MADM approaches into the material selection process, as evidenced by the insufficient study and implementation. By implementing this, designers will be more capable of managing the intricacies of choosing contemporary materials, ultimately resulting in more sustainable and efficient solutions to design. Table 2.4 shows an extensive overview of these investigations, highlighting the various MCDM approaches utilized, the standards for assessment, and the particular situations or uses for which the materials had been selected.

Table 2.4 Methods of multicriteria decision-making used for selection of materials.

Approach	Techniques used	Summary	References
MADM	TOPSIS	Material Selection for roofing	(Rahman et al. 2012)
	TOPSIS	Composite optimization for Impact application	(Alemi-Ardakani et al. 2016)
	VIKOR	Used for selection of material	(Chatterjee 1997; Mahesh et al. 2021a)
	PSI	Used for selection of material	(Mahesh et al. 2021a)
	AHP	Selection of material for designing a component	(Desai et al. 2012)
Hybrid MADM	TOPSIS and AHP	Selection of material for hydropower plants and the sugar industry	(Kumar and Singal 2015), (Rao and Davim 2008), (Anojkumar et al. 2015)
	TOPSIS and ANP	Material-handling equipment selection	(Onut et al. 2009)
	DOE and TOPSIS	Robots related	(Iç 2012)
	VIKOR and TOPSIS	Covering material selection	(Huang et al. 2009)
	ELECTRE and FEA	for the selection of gas turbine components	(Milani 2012)
	Six Sigma DMAIC approach	Used for the selection of Natural fiber	(Yusof et al. 2020a)

2.3 Research gap

Though much research is being carried out on the ballistic impact behavior of composites, a majority of it has been focused on traditional PMCs, specifically synthetic fiber-based sandwich composites. Not many studies have been carried out on natural fiber-based sandwich composites. The following are some of the research gaps that have been identified:

- For material selection, the Six Sigma DMAIC methodology has been used less than other material selection methods in ballistic impact applications.
- Though flexible Composites can absorb and distribute impact energy by reducing the impact force transmitted to the core when subjected to a ballistic impact, very little work has been carried out on flexible materials.
- Sandwiches with synthetic cores with different fillers still haven't been investigated for ballistic impact applications, and some researchers have used this under quasi-static loading and LVI.
- Even though sea sand is a good absorber of energy, no literature has been found that uses it as a composite for ballistic impact applications.
- The literature review found that NFs are often employed to fabricate stiff PMCs, and few studies are used to fabricate flexible PMCs. In contrast, very little or no research has been carried out on natural fibers fabricating both flexible skin material and stiff core material for ballistic impact applications.
- Hybridizing composite materials is an essential and economical method to reinforce and improve performance. Selecting the best material and combination of these materials should be done carefully to get the required output.
- There are limited experimental studies specifically focusing on functionally graded sandwich composites for different material combinations for ballistic

impact behavior. Conducting comprehensive experimental investigations can help bridge this gap.

2.4 Objectives of proposed work

Based on the literature review, there are very few or no reports on the ballistic impact behavior of the functional grade core sandwich composites planned to be used as a novel structure. The following are the objectives for the present study.

1. To propose a hybrid sandwich composite material for ballistic impact applications.
2. To identify the different configurations of the proposed composite and study their impact properties using FE modeling and analysis.
3. To optimize the configuration of the proposed hybrid sandwich composite for better impact performance and identify a capable sequence.
4. To experimentally evaluate the mechanical properties of hybrid composite coupons with optimized stacking sequence as per ASTM standards.
5. To optimize the configuration using FE modeling and analysis for optimized composite coupons.
6. Fabricate composite sandwich plates, evaluate the ballistic impact behavior of the proposed composite experimentally, and study the nature of the damage.

2.5 Scope of the proposed work

- The proposed material for the sandwich was selected using a scientific statistical optimization approach using the Six Sigma DMAIC methodology. The proposed sandwiches are made of jute/rubber/jute skin material, Epoxy as core, and sea sand as filler material to investigate the ballistic impact behavior.
- Study the sandwich composite for ballistic impact properties using commercially available FE software (ABAQUS). Modeling and simulation of

sandwiches under the ballistic impact for different configurations by increasing the thickness of core from 10 to 30 mm (Increment of 10mm) and sea sand composition for core 10 to 30% (Increment of 10%) of the bullet impacting at velocities from 200 to 350 m/sec (Increment of 75 m/sec).

- To determine the optimum configuration of the composite through FE modeling.
- Prepare samples of best configurations and evaluate mechanical properties (Tensile, Compression, and Flexural) according to ASTM standards.
- To determine the optimum configuration of the composite through FE modeling for the optimized composite coupons.
- Fabrication and testing for optimized configurations for ballistic impact and study of the nature of damage.

This chapter comprises a comprehensive study of the literature focusing on the applicability of naturally occurring materials as components for polymer matrix composites used in impact applications. According to the literature review findings, NFs/matrices have often been employed to fabricate stiff PMCs, and few studies have used flexible PMCs. In contrast, little research has been conducted on natural fibers fabricating flexible and stiff hybrid PMCs for ballistic impact applications. Although researchers have made a considerable effort to evaluate the composite's experimental impact responses, it has been discovered that FE analysis is increasingly important during the initial feasibility study to reduce the time and cost associated with experimentation. Additionally, it was found that FE simulation effectively optimizes the composites. The next chapter discusses the materials used, processing methods, and methodologies used for the current work.

CHAPTER 3

3 METHODOLOGY

This chapter deals with the materials, processing, and methodologies used for the current work. The methodology of the proposed work is shown in Figure 3.1 to achieve the desired objectives.

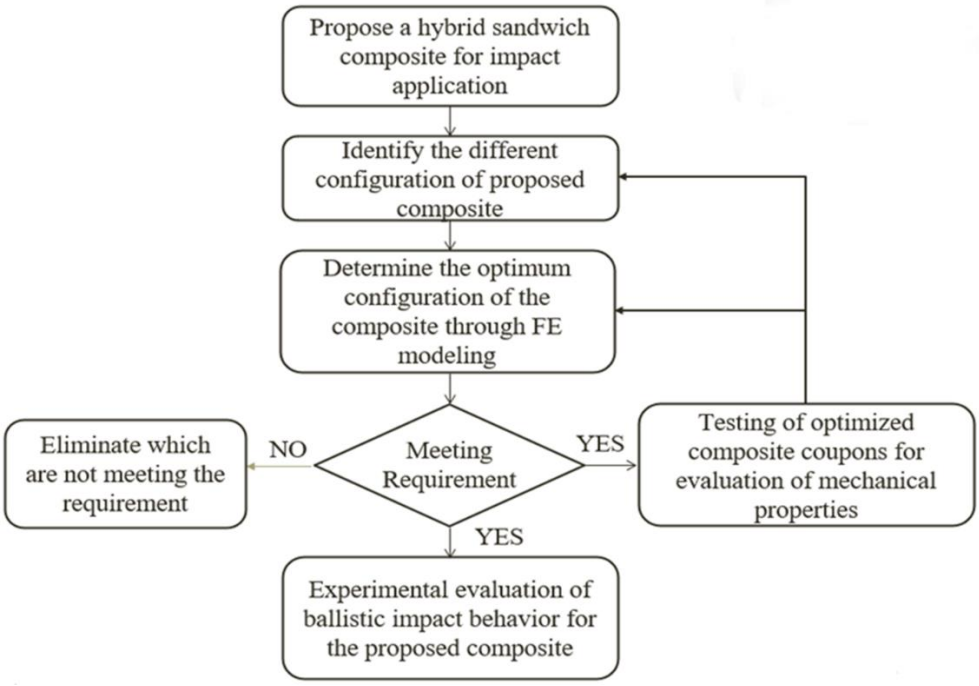

Figure 3.1 Methodology of proposed work.

The methodology involves selecting materials using Six Sigma DMAIC methodology, incorporating qualitative and quantitative analysis. Initial finite element (FE) analysis estimates composite properties using the rule of mixtures. Composite coupons are fabricated and tested for physical and mechanical properties, including gradation, hardness, flexural strength, and impact strength. The results from coupon testing are used to refine the FE models for low and ballistic velocity impact simulations. Finally, experimental ballistic testing validates the FE analysis and assesses the damage resistance of the composites.

3.1 Materials selection using Six Sigma DMAIC methodology

For the past two decades, the researcher's ultimate focus has been to outline the design process precisely, which is the most crucial task in selecting materials. If the suitable material is not selected, it may lead to failure or a reduction in performance. Low cost is not the only criterion for selecting materials, so several MCDM (multi-criteria decision-making) methods have gained popularity in the material selection domain (Yusof et al. 2020b).

This review uses the six sigma (6σ) DMAIC (D-Define, M-Measure, A-Analyze, I-Improve, and C-Control) methodology to select materials for ballistic impact applications. Six Sigma has already been employed in product development to improve quality using quality tools and techniques (Montgomery and Woodall, 2008). Six Sigma is the statistical method with 3.4 DPMO (Defects per million opportunities) or 99.9997% success rate (Kumar 2019). Six Sigma uses 5 phases of DMAIC to improve the quality of the product by reducing waste (Aized 2012). Few researchers have used the Six Sigma DMAIC methodology to select natural fiber, matrix, and fillers for hybrid sandwich polymer composite for ballistic impact applications. DMAIC methodology is beneficial for selecting materials because it considers all process stages, from raw materials to finished products. It also analyses material selection before the production process (McKergow 2014). Figure 3.2 shows the 5 phases of the Six Sigma DMAIC methodology and the essential tools used in each phase to select material.

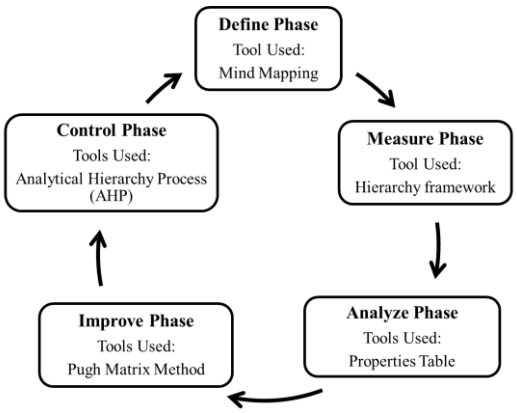

Figure 3.2 DMAIC methodology process flow for selection of materials

Step 1: Define Phase

Define Phase is the first phase in the Six Sigma DMAIC methodology, wherein this phase goal will be set, and the problem will be identified for this mind mapping tool used to develop the chart by collecting the information. The materials selection criteria and alternatives were then developed based on the critical aspects in the constructed chart. Before initiating the materials selection process, it's critical to comprehend the factors that affect the material selection. Cost is a primary and significant aspect when selecting materials for particular products. Variation in the cost of a product changes over time due to increased demand and the availability of the material in the business. Other selection criteria that were examined to ensure the product's extended life span included biodegradability, reusability, recycling, and corrosion-free materials. The Department of Crashworthiness in automotive industries is trying to acquire high performance by reducing weight by selecting lightweight materials. Toughness is defined as the deformation energy to the unit volume preceding fracture, and it can also be described as the ability to absorb kinetic energy till failure. Toughness is the most crucial criterion for impact applications, as higher toughness means better energy absorption (Monteiro et al. 2009). Toughness qualities need strength and ductility stability.

Step 2: Measure Phase

In the second (measure) phase, hierarchical frameworks produce good results by specifying the hierarchy levels. Priority criteria for material selection were established at every hierarchy stage depending on the data collected during the define phase. This hierarchical structure was categorized into five levels in the measure phase, with the first hierarchy level specifying the ultimate objectives (selection of materials). Basic requirements or parameters affecting the defined purpose, such as material performance, sustainability, and lightweight to maintain wellness while being eco-friendly, with comprehensive definitions, are highlighted in the second level. Parameters 1 was the third level in the hierarchy, broken down into precise parameters

to achieve the objective. Parameter 2 was the fourth level in the hierarchy, which outlined all NF by prioritizing the parameter 1 factor. The fifth and last levels set the choices that identify potential methods for selecting the best-suited natural fiber to fulfill the objectives. A study highlighted the VOC (voice of the customer) and the VOE (voice of the environment), and parameters are given consideration. During the bilateral decision analysis, the properties specification aids in understanding the precedence of natural fiber features (Joshi et al. 2004; Mastura et al. 2017)

Step 3: Analysis Phase

In the third (analyze) phase, the properties of natural fibers/ Matrix that might be employed to reinforce hybrid sandwich composites are highlighted with material qualities that need to be fabricated. Before beginning the material selection process, the "analyze" phase determines the ability of natural fibers/ matrix material properties selection. This stage assists in identifying the benefits and drawbacks of specific material properties and any issues that may arise during manufacturing.

Step 4: Improve Phase

Evaluation and actual outcome are completed using the Pugh matrix method qualitative tool in the fourth (improve) phase (Frey et al. 2008). In the improve phase, the Pugh selection method tool is used in this review, aluminum is set as the datum, and all other parameters of natural fibers are examined.

Step 5: Control Phase

The fifth (control) and last stage are used to verify and monitor whether the obtained results from the improved phase are accurate. The analytical hierarchical process (AHP) tool is used in the control phase to propose selecting the material framework and finding the best appropriate material. Based on the improved phase results, the Pugh selection method decision-making methodology has an advantage over other methods by managing various decision parameters. On the other hand, the

quality of the selection criteria is primarily connected with the quality of the Pugh method decision. There are three elements to this quality, and they are:

- The use of inappropriate selection criteria could result in poor decisions. Using opinions to identify criteria can, of course, result in incorrect criteria.
- On the other hand, inadequate selection criteria refer to a set of selection criteria that isn't complete.
- Insufficient selection criteria are inadequately defined and can have various perceptions.

As a result, the AHP (analytical hierarchy process) tool is used to assess and validate the reliability of the results. Data from the improve phase was accessed and validated in the control phase to select the best NF for ballistic impact application. The decision in the study is correct only when the consistency ratio is less than 10%. After the pairwise comparison, the AHP software calculator is used to get the decision matrix and priority weightage values for natural fiber attributes.

The selection of materials process typically begins by defining a set of requirements, which can be divided into rigid requirements (constraints) and soft constraints (objectives). Rigid requirements are those that must be met without fail. These could include minimum strength or durability requirements, maximum weight or size limitations, or regulatory requirements such as restrictions on using specific materials. Soft constraints are more flexible and guide the selection process towards materials that meet specific desirable criteria. These could include cost, environmental impact, ease of manufacturing or processing, or aesthetic considerations. By defining rigid and soft constraints, engineers can evaluate different materials and identify those that meet the requirements while satisfying the desired objectives.

This review confirmed the research objectives, indicating that the natural fibers and matrix chosen must bridge the gap between ecological and economic concerns. The preferred fibers must have high energy absorption, low cost, high availability, low density, high toughness, acceptable tensile strength, and biodegradability.

3.2 Raw Materials

The proposed hybrid sandwich composites are fabricated using naturally available woven jute fiber, rubber sheet, and B-stage cured pre-peg (NR-based).

Jute

Jute fiber is called "Golden fiber" in the industry due to its importance and color. Regarding productivity, it is ranked 2nd after cotton and is among the most efficient NF. Jute is inexpensive to cultivate, produces a high yield/acre, and requires minimal fertilizer, making it environmentally sustainable. Jute is biodegradable since it is made up of cellulose and lignin. India and Bangladesh are the leading producers of jute (Jayaraman n.d.).

Furthermore, jute fiber was selected instead of synthetic fibers such as glass, carbon, or aramid because of its eco-friendly nature, lower cost, and good mechanical properties. Figure 3.2 shows a woven jute fabric with a density of 1.450 g/c^{-3} and 350 GSM. Table 3.1 lists the physical and mechanical properties of jute fibers.

Figure 3.3 Woven Jute Fabric

Table 3.1 Physical and Mechanical Properties of Jute.

Properties	Jute fiber	Properties	Jute fiber
Cellulose	50-57 %	Density	1400-1500 kg/m^3
Hemi-Cellulose	13.6-20.4 %	Tensile strength	400–780 MPa
Lignin	12 to 14 %	Young’s modulus	13–30 GPa
Ash	0.5-2 %	Percentage of Elongation	1.1-1.9 %
Pectin	0.2 %	Specific Gravity	1.3
Moisture	12.6 %	Diameter	160-185 μm
Wax	0.5 %	Lumen size	12 μm

Natural Rubber

Natural Rubber (NR) exhibits sufficient tensile strength, high resilience, and tear and wear resistance. It also provides moderate persistent properties with better flexibility capabilities at low temperatures. NR is one of the most flexible rubbers compared to all other rubbers available, and it is water and chemical-resistant. NR used as the matrix has an advantage in ballistic impact applications because of its flexibility, which results in tearing instead of matrix cracking, thus freeing the composite from catastrophic failure. Flexibility doesn't restrict the yarns through which the fabric resists projectile energy. Figure 3.3 shows NR sheets purchased from Manjunath Rubber, Baikampady, Mangaluru, India. Table 3.2 lists the characteristics of natural rubber.

Figure 3.4 Natural rubber sheet

Table 3.2 Characteristics of natural rubber.

Properties	Tensile Strength (MPa)	Ultimate Strain (%)	Modulus (MPa)	Density (kg/m^3)	Tear Strength (N/mm)	Hardness value
Natural Rubber	0.05	210	0.45	987.18	7.64	24

Pre-peg (B-stage cured)

Figure 3.4 shows that pre-peg (NR-based B-stage cured) is used as a bonding agent for fiber jute and natural rubber, which work together as a matrix. It acts as a matrix and protects natural rubber and jute from the effects of the outside environment. Table 3.3 lists the pre-peg (NR-based B-stage cured) properties.

Figure 3.5 Pre-peg (NR-based B-stage cured)

Table 3.3 Pre-peg (NR-based B-stage cured) properties.

Tensile Strength (MPa)	Modulus (MPa)	Elongation (%)	Hardness Value
15.69-16.67	7.35-8.33	475-575	56-60

Epoxy

Epoxy: Epoxy resin is grouped in the thermosetting polymer group. It is formed by a reaction between epichlorohydrin and acids or amines, hydroxyl (Bhd 1996). Schade prepared the first epoxy resin from Epichlorohydrin in 1927, while Custon and Lee synthesized Epichlorohydrin and Bisphenol. Epoxy resins are related to the chemical group formed by a three-numbered ring containing an atom of oxygen surrounded by two carbon atoms. Epoxies are generally found in maritime, aerospace, and electrical applications. Epoxy matrix has better mechanical properties than synthetic and natural matrices (T. S. Mohan Kumar et al. 2020). Figure 3.4 shows the epoxy and the hardener used. Table 3.2 lists the properties of Epoxy.

Figure 3.6 Epoxy and Hardner

Table 3.4 Properties of Epoxy.

Properties	Tensile strength (MPa)	Compressive strength (MPa)	Elastic modulus (GPa)	Percentage elongation (%)	Density (g/cm^3)
Epoxy	40–90	90–250	2–4.5	2	1.2–1.5

Sea sand

Fine aggregates are described by IS: 383-1970 as particles that pass through a 4.75mm (IS sieve) and are considered sand. Sea sand is commonly referred to as marine/ offshore sand and is abundantly available in coastal regions. However, these sands must be treated before use because of the excessive chlorides deposited in saline water. Sea sand has a round/cubical shape like river sand. These are naturally available and can be mined at a significantly lower cost.

Sea sand is more stable than river sand (high SBC - Safe Bearing Capacity). The sea sand is carried in by moving water, driven by the shoreline, or forced by the river during continual moving between water layers in rivers and sea shore sand. Continuous exposure to larger particles degrades gradually as they move towards the sea and finally degrade into very fine particles. The fine particles that reach the seashore would be significantly more powerful than any other sand on the planet (Chotaliya et al., 2020).

Figure 3.7 Sea Sand before and after wash/drying

The grain size of sea sand is estimated using sieve analysis. This method involves passing the sample through a series of sieves with progressively smaller mesh sizes, separating the larger particles from the smaller ones. The mechanical vibrator was used to sieve the sea sand. Figure 3.7 (a) shows the weight retained graph, which provides information about the amount of material retained on each sieve and can be used to identify the particle size fractions in the sample. Figure 3.7 (b) shows the cumulative graph, which provides information about the percentage of material that has passed through each sieve and can be used to identify the particle size fractions in the sample. By analyzing both graphs, you can determine the dominant particle size fractions, the range of particle sizes present in the sample, and the uniformity or variability of the particle size distribution for 50% cumulative, the % retained sand is taken, and the average size of the sea sand is found to be 182.5 microns.

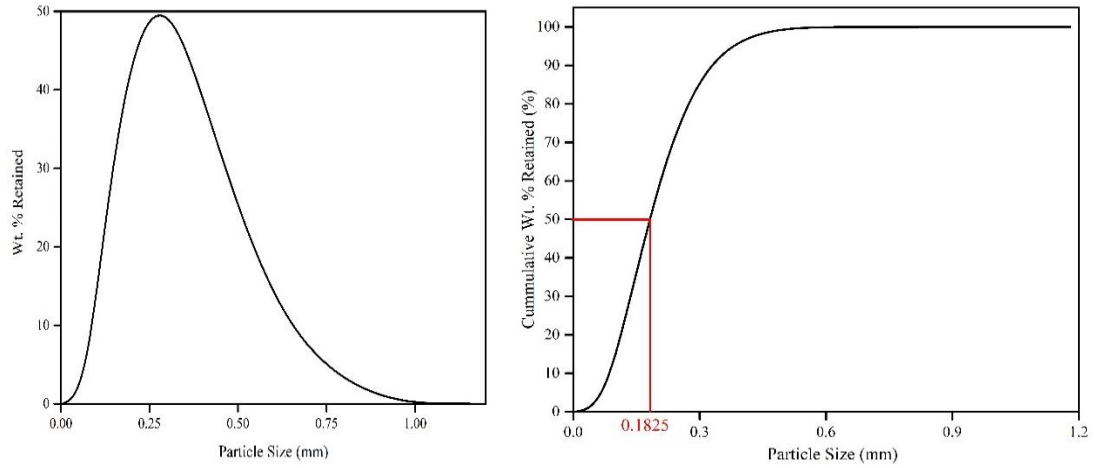

a) b)

Figure 3.8 Sieve analysis a) Distribution of participle size b) Cumulative % of retained sea sand

Table 3.5 Properties of sea sand (B. H. Shinde 2016; Chotaliya et al. 2020).

Properties	Sea sand	Properties	Sea sand

Specific gravity	2.76	Particle shape, Size	Round, 4.75mm
Fineness modulus	2.576	Silt/Dust content	2.1%
Bulk density	1291.70	Water Absorption	1.7%
Chloride Content (mg\lit)	Without Wash - 420 With wash - 270	Hardness values	Without Wash – 515 With wash – 573
pH values	Without Wash – 8.68 With wash – 8.97	Permissible Limits	Without Wash – 2141 With wash – 301

3.3 Modeling of Sandwich Composite

The foundation and comprehension of FE analysis will be discussed in this section. In particular, the type of elements included in the model—which could consist of solid 2D and 3D elements—and their importance in accurately capturing the geometry and material behavior of the composite structure. A comprehensive meshing approach that emphasizes mesh density, element size, and quality is essential for achieving result accuracy. Inaccurate results or problems with convergence may result from poor meshing, especially in dynamic simulations like ballistic impact. Since the FE model discretizes the entire geometry into a network of nodes and elements that cooperate to produce a continuum-based solution, explaining the concept of continuum via nodes is also necessary.

Abaqus is frequently used to solve complicated engineering problems, particularly those including dynamic loads like ballistic impact. In the current research, solid 3D elements, like C3D8R in Abaqus, were employed to accurately characterize the mechanical behavior of the sandwich composite structure during ballistic impact.

The nodal continuum technique assures that deformations, stress distributions, and strain computations are integrated throughout the structure, resulting in a thorough understanding of energy absorption and damage mechanisms. Furthermore, decreased integration approaches (used in elements such as C3D8R) maximize computational efficiency while avoiding numerical difficulties such as locking, especially in large deformation scenarios. Abaqus advanced contact algorithms accurately describe projectile-target interactions during dynamic impact simulations, essential in understanding stress wave propagation and material failure. The benefits of using Abaqus for this type of simulation include the ability to accurately model complex geometries, nonlinear material behavior, and dynamic loads and the ability to simulate complex damage mechanisms such as delamination, matrix cracking, and fiber breakage in composite structures. The disadvantages of FE, such as its reliance on accurate material models, high cost of computation, and potential numerical issues, are recognized; however, these can be minimized by careful model setup, experimental data validation, and mesh refinement. Abaqus/Explicit is particularly well-suited for high-velocity impact simulations that need extensive modeling of dynamic contact, material failure, and energy absorption. It would be difficult and expensive to replicate such instances experimentally, particularly when studying a wide range of core thicknesses, filler percentages, and projectile velocities.

The FE approach enables Comprehensive parametric investigations and parametric simulations, which eliminates the need for significant physical testing and permits the investigation of several design configurations.

FE analysis for functionally graded sandwich structure for ballistic properties.

Commercially available FE (finite element) software ABAQUS explicit is used for simulations. ABAQUS software package is structured into three distinct stages: preprocessing (sample geometry is created and material properties are entered), processing (Meshing and boundary conditions are given), and post-processing (Result of simulation).

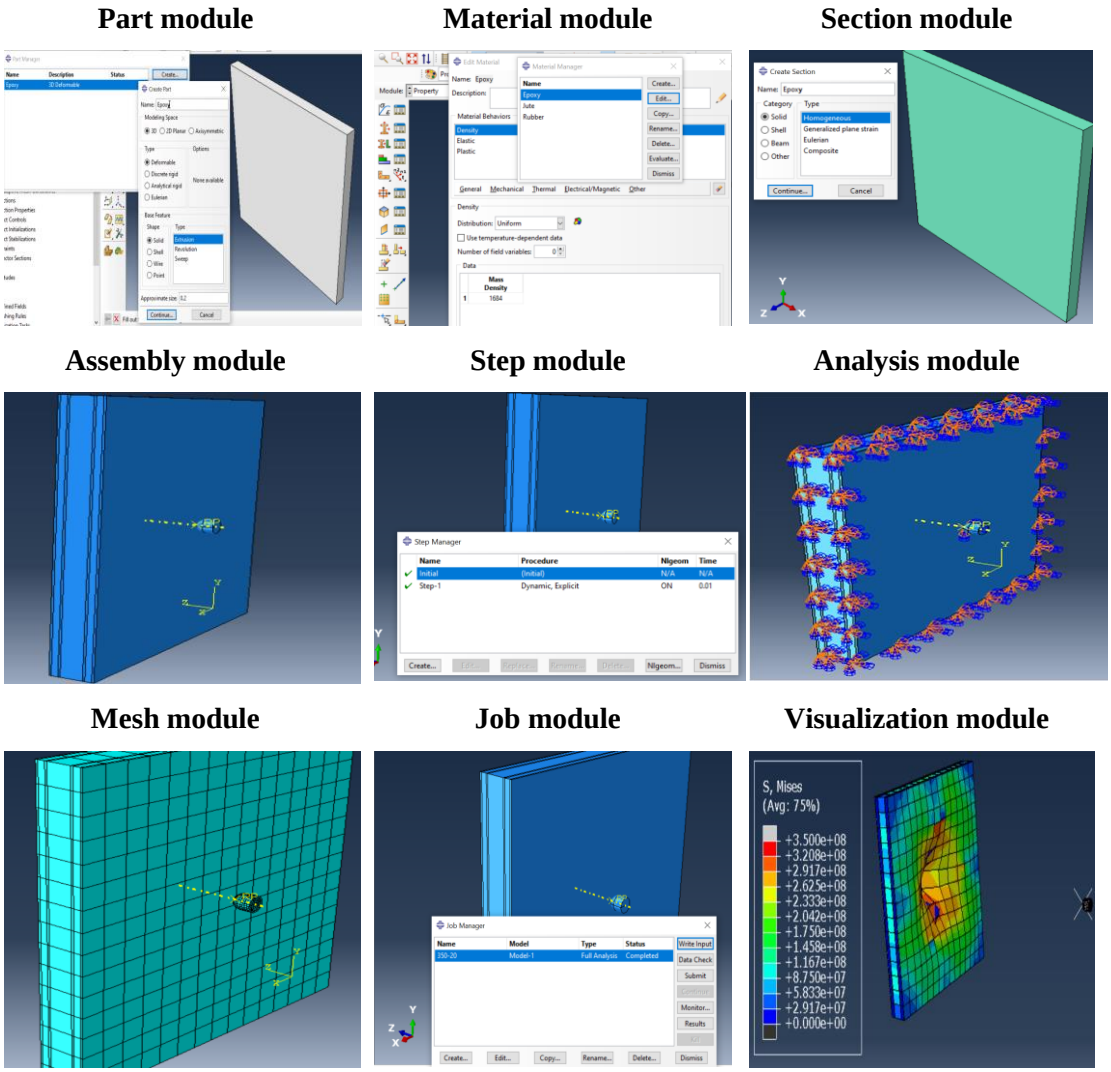

Figure 3.9 Modules used in ABAQUS software

- Part module: Sample geometry is created, and material properties are entered in this module.
- Material module: In this module, parameters such as Young's modulus, yield stress, Poisson's ratio, and yield strain are entered.
- Section module: Assign sections for all the materials in this module.

- Assembly module: In this module, individual parts are assembled to make a single component. Created geometries are initially independent of other sections when they are created. However, a model is utilized to place the portions and apply constraints. Instances can be defined in two ways: dependent and independent. Independent instances are employed in this case.
- Step module: In this module, an analysis step is built, and output requests are specified. If the loading circumstances or the boundary conditions change, several analysis steps may be required; normally, a static, general step type is utilized for analysis.
- Analysis module: To analyze the data.
- Mesh module: The fineness of the mesh is determined by the required situation, with a finer mesh demanding more significant amounts of memory storage. For 2D systems, the mesh type can be either triangular or quadrilateral, while for 3D systems, the mesh type is typically tetrahedral. These mesh types allow for an accurate representation of the geometry and facilitate system analysis.
- Job module: The job to be analyzed is selected and submitted for processing. Additionally, it is possible to schedule the job to start at a specific desired time, allowing for the flexibility of delaying the start as needed. This feature enables better control and coordination of the analysis workflow, especially when timing considerations are involved.
- Visualization module: This post-processing stage is where the simulation results are obtained. The processed output requests, such as stress boundaries, are used in this module to get and produce the required results.

3.3.1 Influence of velocity, filler composition, and core thickness

Figure 3.10 illustrates the sandwich structure used in the study. The face sheet on both sides of the core is modeled with dimensions (all dimensions are in (millimeter) mm) 300x300x10mm face sheet thickness. 20 mm thick core is used, which is two times

the thickness of the skin for hybrid bio-composites (J-Jute, R-Rubber, J-Jute, E-Epoxy (with different percentages of sand) J-Jute, R-Rubber, J-Jute) JRJE(%S)JRJ, similarly for (J-Jute, R-Rubber, J-Jute, R-Rubber (with different percentage of sand) J-Jute, R-Rubber, J-Jute) JRJR(%S)JRJ also skin thickness is maintained at 10mm, Core thickness is of 20mm the configuration is as shown in Table 3.6. For the optimized sandwich structure, the bullet's velocity of 350 m/sec and composition of 30% sand is kept constant, and the thickness of the core is varied for 10, 20, and 30 mm; the configuration is shown in Table 3.7.

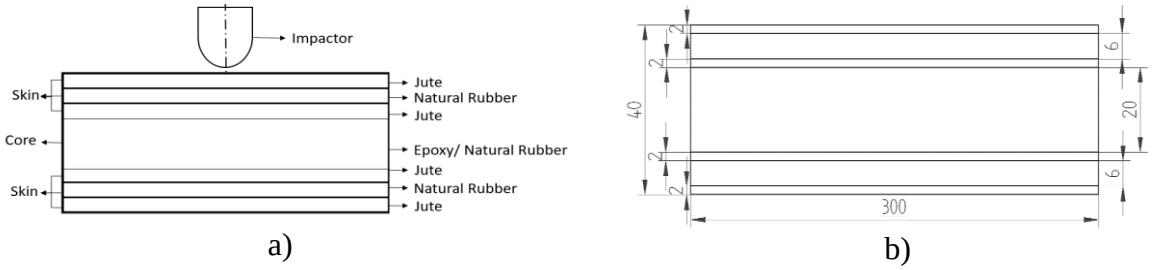

a) b)

Figure 3.10 Sandwich composite subjected to impact a) Sequencing of materials for sandwich structure, b) Dimensioning of sandwich structure (core and skin)

Table 3.6 Configuration of sandwich composites for the present study

Sl. No.	Sandwich Structure		The composition of filler in the core (%)	Velocity (m/sec)
1	FESF	F-JRJ (J-Jute, R- Natural Rubber, J-Jute)	FE0F-0% Sand filler FE10F-10% Sand FE20F-20% Sand FE30F-30% Sand	• Low Velocity 10 m/sec • Intermediate
		ES (core) - Epoxy and sand		
		F- JRJ (J-Jute, R- Natural Rubber, J-Jute)		
		30- 30% sand with Epoxy as a core material.		

2	FRSF	F-JRJ (J-Jute, R- Natural Rubber, J-Jute) R (core) – Natural Rubber and sand S-Sand (filler) percentage F- JRJ (J-Jute, R- Natural Rubber, J-Jute)	FR0F-0% Sand filler FR10F-10% Sand FR20F-20% Sand FR30F-30% Sand	velocity 50m/sec. • High Velocity: 100 and 350 m/sec

Table 3.7 Optimized Sandwich Composites

Sl No.	Sandwich Structure	The thickness of the core (mm)	Velocity (m/sec)
1	FE30F	10,20, and 30	350

The composite structures are modeled as a 3D deformable body using widely viable explicit (ABAQUS/CAE) software, while the projectile (hemispherical shaped) as a rigid body was modeled with inertia 2kgs. The right combination of the skin and core is modeled and assembled. The sandwich structure's four sides are constrained by the BC (boundary condition), and the projectile motion is limited to the Z-axis with different velocities. The boundary condition is set for the sandwich structure, which is replicated for all other combinations. The properties of the materials are taken from Table 3.8.

3.3.2 Optimization of process parameters

The composite's hybrid sandwich composite and sequence, where a jute thickness of 2mm and a natural rubber thickness of 6mm, are modeled using different core thicknesses, such as 10, 20, and 30mm. The face sheet and core materials are modeled and assembled in the correct sequence as 3D deformable-body and different shape projectiles, as shown in Figure 3.11, are modeled. The proposed JRJE(%S)JRJ

hybrid sandwich composite parameters are necessary for FE analysis. Ballistic impact behavior of the composite for different core thicknesses (10, 20, 30mm) and different filler compositions (0, 15, 30%) subjected to impact at 350 mps using different shaped projectiles like flat (F), conical (C), and hemispherical (H) using ABAQUS/CAE FE software approach.

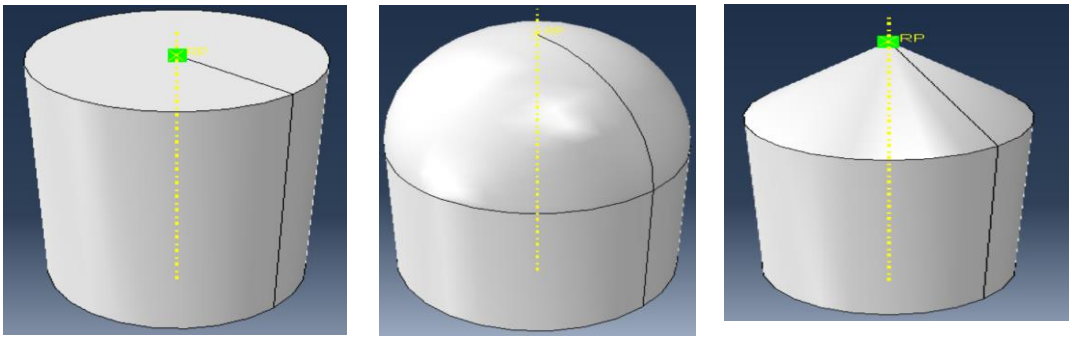

a) b) c)

Figure 3.11 Modelling of different shaped projectile: (a) Flat, (b) Hemispherical, and (c) Conical

Table 3.8 Parameters used for FE analysis (Mohan Kumar et al. 2022)

Sl No.	Materials	Density (kg/m^3)	Ultimate stress (GPa)	Young's Modulus (GPa)	Poison's ratio
1	Skin-Natural fiber (Jute)	1.45×10^{3}	3.50×10^{-1}	20	0.38
2	Skin-Matrix (Natural Rubber)	9.87×10^{2}	5.00×10^{-5}	4.50×10^{-4}	0.49
3	Core (Epoxy)	1.20×10^{3}	0.72×10^{-1}	3.4	0.30
4	Sand (Filler with core)	2.410×10^{3}	1.00×10^{-1}	70.6	0.17

3.4 The processing method of functionally graded sandwich structure

Characteristics of materials utilized for key constituents of sandwiches (core and skin) are described below.

Processing of Skin

The proposed hybrid sandwich composites are fabricated using a compression molding technique for skin material. The materials are cut into the required dimensions and sequenced into the necessary configuration. Pre-peg (NR-based B-stage cured) is added between layers to bond the layers effectively. The complete set-up is retained within a compression molding machine under a pressure of 25kg/cm^2 and at a temperature of 138°C for 7 minutes (Vishwas M. 2020). this pressure and temperature were applied, and sandwiched samples were placed between two aluminum sheets. Figure 3.12 illustrates the stages required in the fabrication of skin material. The samples are cut after curing in accordance with the applicable ASTM standards.

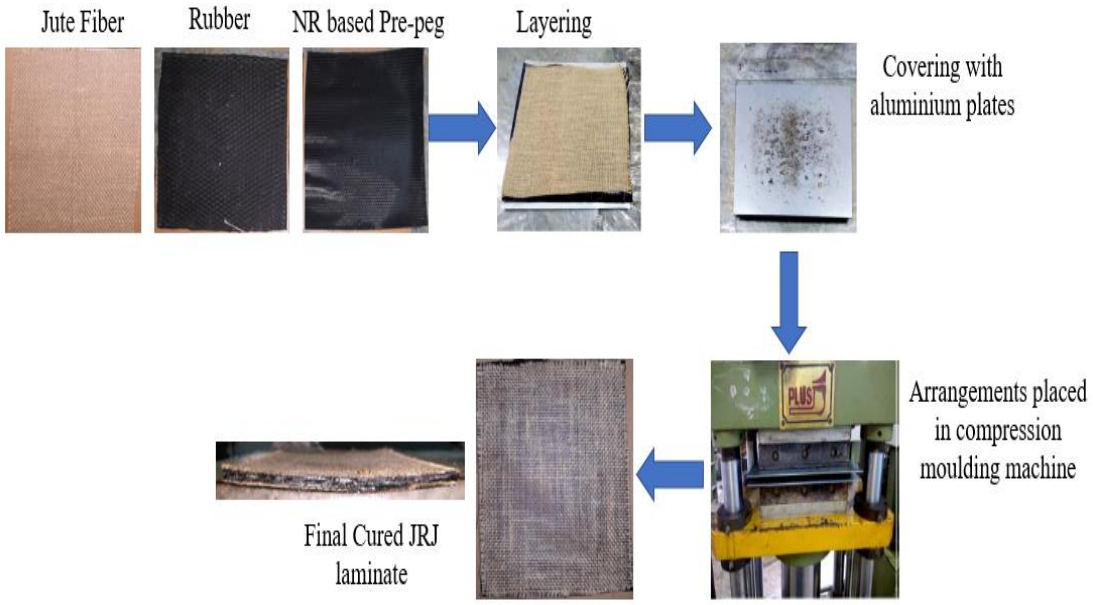

Figure 3.12 Stages in the fabrication of skin materials

The stages in fabricating the proposed flexible skin material are provided below: A mold of 150 mm x 150 mm is used. The skin material can be readily removed by using a releasing agent (high vacuum silicone). The following lists the stages involved in composite fabrication: Stage 1: Jute fiber, Natural rubber, and Pre-peg (NR-based B-stage) have been cut to the required shape and size and stacked in the proper sequence. After positioning, the entire setup is placed between the molds and the mold is placed inside the compression molding machine. Stage 2: The compression molding machine sets the temperature and pressure to 25 kg/cm2 and 138^0c. Stage 3: After they reach the desired temperature, they are heated for 7min. Stage 4: The temperature turned off after seven minutes, and the pressure was kept at that same level for an additional two hours. Stage 5: The mold was removed from the compression molding machine, and the composite was removed from the molds.

Processing of functionally graded core

Functionally Graded Materials (FGMs) are often considered as expensive as they are developed using polymeric methods. Therefore, it has been proposed that the effect of varying the composition of filler and thickness of the core on the mechanical properties of FGMs be investigated by using sea sand, which is widely available and used as filler material for the core (epoxy). The current work employs polyamine hardener (K-6) that can be cured at room temperature and medium viscous epoxy resin (LAPOX L-12) for the core material, supplied by ATUL India Ltd. Filler Sea sand, which was collected from NITK beach in Karnataka, is used. Whenever employed with validated matrix systems, these relatively inexpensive filler materials with good mechanical characteristics significantly minimize the overall cost while maintaining desirable mechanical properties.

The appropriate proportion of sea sand was added to a measured amount of epoxy, and the hardener was added and mixed well while gently stirring to minimize the occurrence of air bubbles. The stirred epoxy was gradually poured into a mold coated with a silicone-releasing agent; then, at room temperature, it was left to cure for

about 24 hours. After being removed from the mold, the samples had their corners trimmed. A series of composites with different compositions of sea sand FGPC samples are fabricated using the same method.

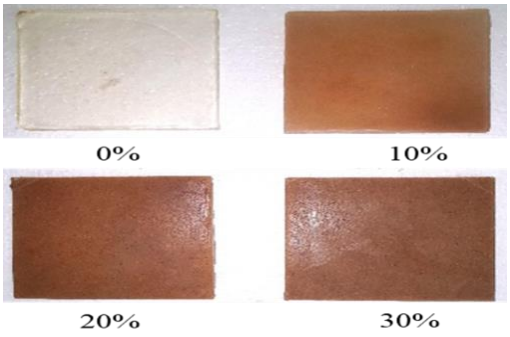

Figure 3.13 Core (Epoxy/Different composition of sea sand)

Processing of sandwich

In the sandwich structure, the sandwich skins, which comprise Jute/Natural rubber/jute and pre-peg (NR-based B-stage cured), are added between layers for bonding. The thickness of jute fabric (2mm) and NR thickness (6mm) are taken, and the required dimension of 300X300 mm is cut, sequenced, and bonded using NR-based B-stage cured pre peg. After positioning the entire setup between the molds, the mold is put inside the compression molding machine. The core measured amount of epoxy and hardener (1:10 ratio) is taken, and filler sea sand is mixed with different compositions of 10%, 20%, and 30%. The mixture is poured into the mold and cured at room temperature for 24 hours. The core with different 10, 20, and 30mm thicknesses are taken. Using data, the necessary top and bottom skin material base fabric (last jute fabric) are rinsed with epoxy/hardener mixture and stacked on the core (top and bottom) to make the sandwich structure. The weights are added to the structure to achieve a higher degree of resin spread over the skin and core to remove the excess resin. The structure is cured at room temperature for 24 hours, then removed and cut into the required dimensions. Similarly, all the specimens

were prepared by varying the composition of sea sand and the thickness of the core, as shown in Figure 3.14. The different layers used are detailed in Table 3.9.

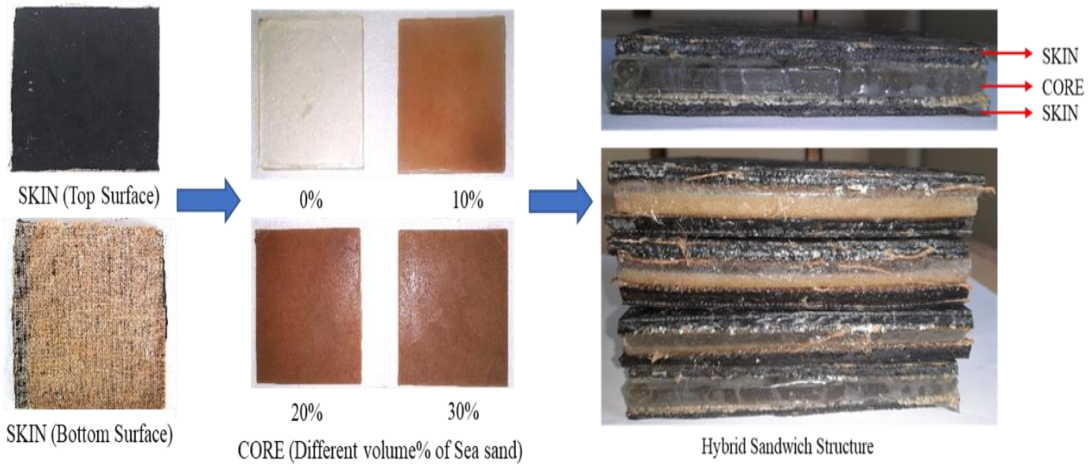

Figure 3.14 Functionally graded sandwich

Table 3.9 Layer Distribution and Dimensional Specifications of Sandwich Composites

No. of layers above the core	No. of layers below core	Core Thickness (C) (mm)	Sandwich Thickness (H) (mm)	C/H Ratio
Jute - 2	Jute - 2	10	30	0.3
NR- 1	NR- 1	20	40	0.5
Pre-peg- 3	Pre-peg- 3	30	50	0.6

3.5 Experimental Analysis of FG Cores and Sandwiches

As FG composites are a relatively recent addition to the engineering field, getting an accurate database of these new materials is challenging. Thus, creating material databases is a crucial component of using FG composites. The conventional test methods used for metals are not always applicable, requiring the development of specialized testing standards for composites by organizations like ASTM. The present

thesis adheres to ASTM standards for testing FG composites and their sandwich structures.

3.5.1 Functionally graded sandwich Testing

The basic physical properties of FG sandwich composites are evaluated through experimentation. Physical properties refer to any measurable attribute that can describe the physical state of a system. These properties can describe the transformations or changes between the system's momentary states. Without affecting its identity, an object or substance can be measured. Physical properties can be classified as either intensive or extensive, with intensive properties remaining constant regardless of the amount or size of matter present, while extensive properties vary in proportion to the quantity or magnitude of the object. Physical properties can be further categorized as isotropic or anisotropic, depending on whether their values are directionally dependent. These properties are also referred to as observables. In composite materials, the physical properties are typically orthotropic, meaning that they vary depending on the direction of the applied force or load rather than being independent.

It is essential to comprehensively comprehend the physical properties of FG particulate-reinforced polymer matrix composites to assess their suitability for a given application. The fundamental properties such as density, void content, and gradation characterization may undergo alterations due to the influence of the processing methods, leading to changes in physical properties. The physical properties highlighted in the overview of this study are explained below.

3.5.1.1 Physical properties of functionally graded sandwich structure

Gradation Test for FG core

Functionally graded polymer composites (FGPCs) exhibit graded composition, microstructure, and properties variations. FGPCs are designed to provide specific combinations of mechanical, thermal, electrical, or other functional properties as

required by their intended applications. Overall, the testing of FGMs requires a multidisciplinary approach involving additional testing and analysis. It is essential to choose the appropriate testing techniques that are most relevant to the properties of the material being tested.

Functionally graded polymer composites (FGPCs) are designed to exhibit gradual variations in their composition and properties across different material regions. The gradation test measures the degree and direction of gradation in FGPCs. The gradation test involves preparing cross-sectional samples of the FGPCs and analyzing them using various techniques. For the gradation test (Figure 3.15), a separate test piece is cut from the specimen for physical quantification using the burn-out test and weight method (Doddamani and Kulkarni 2012a; b; M.R. Doddamani, S.M. Kulkarni 2011; Mohan Kumar T. S., Sharnappa Joladarashi and Doddamani 2023).

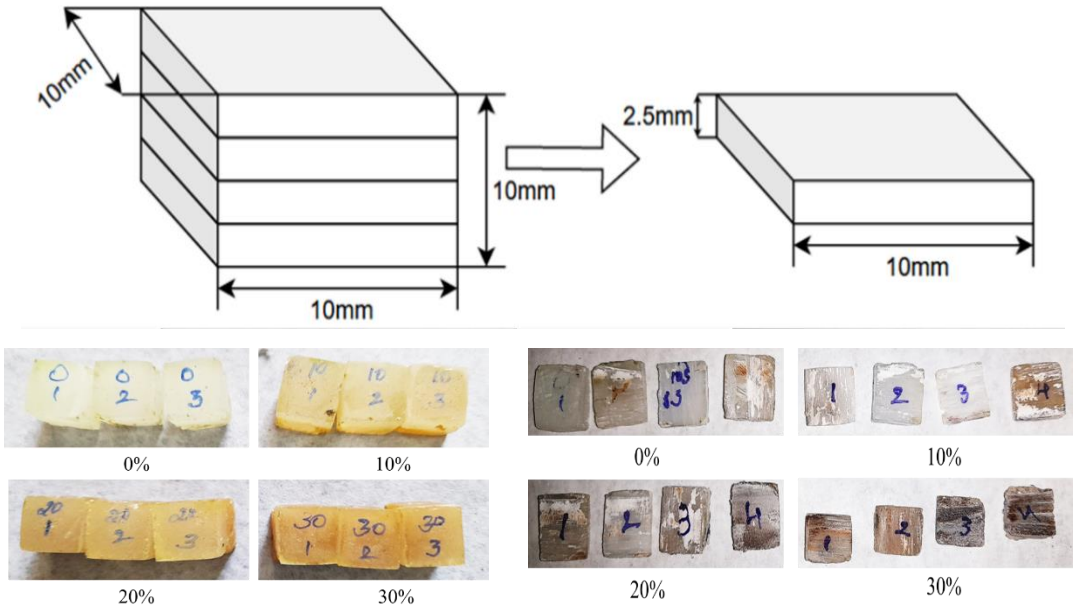

a) b)

Figure 3.15 Functionally gradability test (a) Sample used (b) Sample cut into slices for test

The specimen was cut into the required dimension, as Figure 3.15(a) shows. Figure 3.15 (b) shows the further divided into four smaller slices. Weights are noted for

the cut slices to determine the filler content, and the two methods used for the gradation burn-out test and the weight method are also indicated.

Burn-out test

Each 10%, 20%, and 30% weight fraction slice is weighed and burned until the epoxy is burnt completely. Once the epoxy is burnt, sea sand is separated, then the weight of sea sand (residual) is recorded. The weight percentage of sea sand in all the slices is estimated using an equation (3).

$$Wt.\%\ of\ fly\ ash = \frac{Wt.of\ residue}{Wt.of\ slice} \times 100 \quad (3)$$

Three replicates are tested for all the samples, and the average is taken. The same steps are followed for other samples with 10% - 30% weight fractions of filler.

Weight Method

The slices were cut from the neat epoxy specimen, similar to the dimensions of the FGPC sample, and weighed. Equation (4) determines the weight percent of sea sand in each layer.

$$Wt.\%\ of\ sea\ sand = \frac{Slice\ Wt.with\ sea\ sand - Slice\ Wt.of\ neat\ epoxy}{Slice\ Wt.with\ sea\ sand} \times 10 \quad (4)$$

Density and Void

Density refers to the amount of mass or substance present in a given volume of space. It is usually expressed in terms of mass per unit volume, such as kilograms per cubic meter (kg/m^3) or grams per cubic centimeter (g/cm^3). Void, conversely, refers to the space or absence of substance in a given volume of space. Void can refer to both the absence of matter and energy. While material selection for a particular application, density is among the most crucial factors. The composite's experimental density ($\rho_{Experimental}$) is estimated by the traditional water displacement technique to calculate

the density of sea sand, as shown in Figure 3.16 (a). A density Kit is used to calculate the density of the composite, as shown in Figure 3.16 (b).

In contrast, the composite's theoretical density (ρ Theoretical) is derived using the rule of mixtures. Whenever filler is added to the matrix or during the mixing process, air/other volatiles may be trapped inside the material, causing voids and affecting physio-mechanical properties. Equation (5) is used to determine the composite's void percentage.

$$Void\ \% = \frac{\rho_{Theoretical} - \rho_{Experimental}}{\rho_{Theoretical}} \times 100 \quad (5)$$

a) b)

Figure 3.16 Density Calculation a) Conventional method, b) Density kit

3.5.1.2 Mechanical properties of functionally graded sandwich structure

Hardness test

Hardness is measured by the resistance offered by the material to the penetration depth of an indenter. A material's resistance to penetration by a spring-loaded needle-like indenter is measured by its shore hardness. Two shore hardness scales are employed to determine the shore hardness of elastomers (shore A) and other polymers (shore D). The hardness testing is carried out at room temperature using Shore D

hardness and following ASTM D-2240 standard, as shown in Figure 3.17. Five readings from each sample are taken, and the average is calculated.

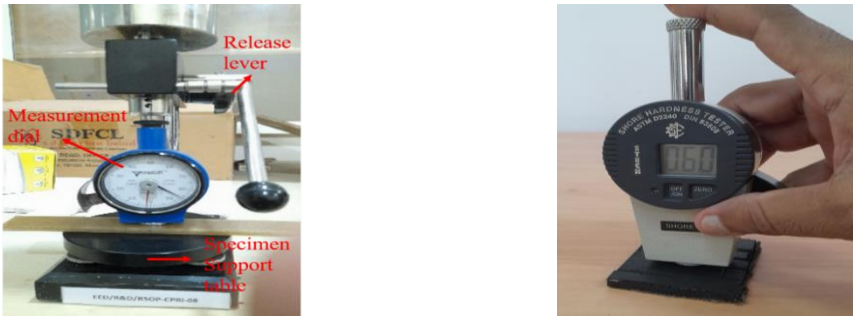

a) b)

Figure 3.17 Hardness a) Shore D hardness, b) Share A hardness

Tensile testing

UTM (universal testing machine), Tinius Olsen H75KS, manufactured with a cross-head speed of 1mm/min, determines the tensile properties. According to the ASTM 3039 M standard, samples were cut; it consists of the gauge length, a critical area where failure is anticipated, and the two end portions used to grip the sample and are connected to UTM, as shown in Figure 3.18. Specific strength, the ratio of tensile strength to the specimen's density, was calculated using this relation.

Figure 3.18 Universal Testing Machine for Tensile Specimens

Flexural Test

UTM (universal testing machine), Tinius Olsen H75KS, manufactured with a cross-head speed of 1mm/min, is employed to determine the flexural properties. The

three-point bending method is used; it consists of the length of the beam span with three essential points: two end supports and one main charge point. According to the ASTM 7264 standard, samples were cut UTM, as shown in Figure 3.19.

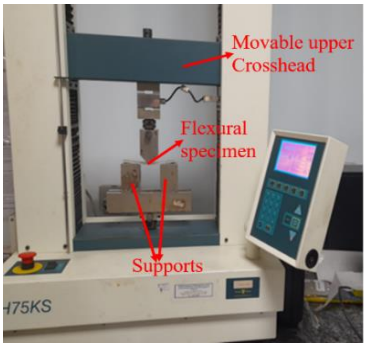

Figure 3.19 Universal Testing Machine for Flexural Specimens

Impact test

Impact tests are used to examine a material's resistance under sudden load. The energy needed to cause material fracture is determined to investigate the brittleness. Izod and Charpy tests are typically used to investigate impact characteristics. The Izod test is used in this study in accordance with ASTM D256 standards (length=64mm, width=13mm, and thickness=5 mm). Five specimens for each composition were taken. The average is determined for unnotched specimens used for polymer composites (ASTM D256-10e1 2010).

High Strain Rate Compression Test

Split-Hopkinson Pressure Bar (SHPB) is extensively employed for HSR testing (10^2-10^4 s^{-1}); since the traditional machines (servo-hydraulic) can only test at lower strain rates (less than10 s^{-1}), it is widely applied (Elmahdy et al. 2021). It is composed of a gas gun, transmission bar (TB), incident bar (IB), and a striker bar (SB); it works on one-dimensional wave propagation, as shown in Figure 3.20.

The specimen is placed in between IB and TB. The materials used and the c/s area are the same for all the bars. The TB, IB, and SB must stay elastic during the

operation. A compressive stress wave propagates towards the IB when gas pressure accelerates the SB. A proportion of the wave is reflected into the IB as it contacts the IB and the sample.

In contrast, the remaining wave transmits through the sample into the TB. A thin lubricant coating was added to the contact surface of the bars and specimen to reduce interfacial friction. Strain rate can be obtained by altering the specimen size and impact velocity. Each bar has a strain gauge installed as a half Wheatstone bridge. These gauges measure axial strain and eliminate bending impacts. Fiber optic amplifier-based measurement technology and a response speed range of 10 to 2000 μs, with this system's velocity capture, is exceptionally accurate. Utilizing LAB VIEW architecture, data collecting, analysis, and reporting are automated. Equation (6) can be stated, assuming that the dynamic force in the incident and transmitter bars is equal.

$$\varepsilon_r = \varepsilon_t - \varepsilon_i \tag{6}$$

Calculating the stress-strain in the specimen involves using the elastic strain produced in the IB and TB. The length of the sample has an inverse relationship with the nominal strain rate in the specimen, computed employing Equation (7) (Li et al. 2021).

$$\dot{\varepsilon}(t) = \frac{2C_0}{L}\, \varepsilon_r(t) \tag{7}$$

C_0 = wave velocity of the bar, L = length (sample), and time-resolved strain connected to the reflected pulse in the IB are denoted by $\varepsilon_r(t)$. In the perspective of E (Young's modulus) and ρ (density) of the bars, bar wave velocity can be calculated using Equation (8).

$$C_0 = \sqrt{E}/\rho \tag{8}$$

Wave analysis determines the nominal stress and normal strain using Equation (9).

$$\sigma(t) = \frac{A_t}{A_s}\, E\, \varepsilon_t(t)$$

$$\epsilon_n(t) = -\frac{2C_0}{L} \int_0^t \varepsilon_r dt \tag{9}$$

Where A_s and A_t are c/s area of sample and TB, $\varepsilon_t(t)$ time-resolved strain connected to the axial strain in the TB True stress and strain are determined using Equation (10).

$$\varepsilon_t(t) = -\ln(1 - \varepsilon_n(t))$$
$$\sigma_t(t) = \sigma_n(t)[1 - \varepsilon_n(t)] \quad (10)$$

As compared to quasi-static tests, the compressive strength increases at HSR. Most of the applied energy is used to develop damage at LSR gradually. In HSR, there isn't sufficient time for damage to develop and spread. Additional effort is needed in these circumstances to prevent damage from developing and spreading, showing results of improvement in compressive strength at HSR loading. Also, compressive strength increases under HSR loading due to the visco-elastic nature of the polymeric material (Colak et al. 2020).

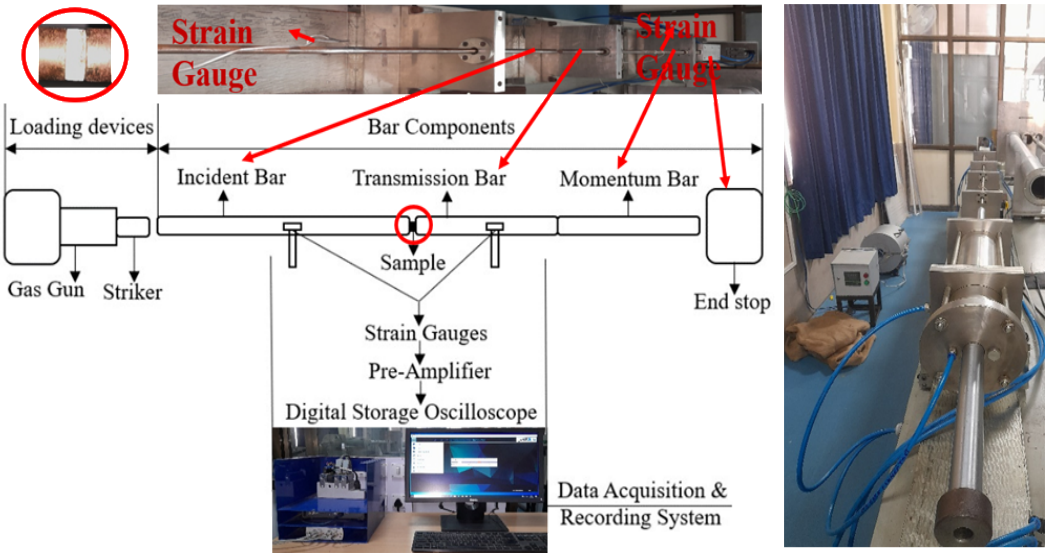

Figure 3.20 SHPB Experimental Set-up.

Scanning Electron Microscopy

Scanning Electron Microscopy (SEM) produces magnified images for study by scanning specimens with an electron beam. The technique, also referred to as SEM analysis and SEM microscopy, is highly successful when it comes to microanalysis and

failure analysis of the specimen. High magnifications, high-resolution images, and accurate measurements of microscopic features and objects are produced by electron microscopy. SEM testing involves several significant processes. The sample must first be carefully prepared by cutting it to the required size, generally by mounting it on a conductive substrate. Then, the sample is put into the SEM's vacuum chamber. After that, the chamber is pumped down to produce a high vacuum, essential to keeping air molecules out of the way of the electron beam. After that, a concentrated electron beam produced by the SEM's electron source is directed onto the specimen's surface. Several signals are released or scattered when this electron beam is scanned over the material. These signals include cathodoluminescence, X-rays (EDS), backscattered, and secondary electrons. The generation of precise spectra and images is made possible by collecting and detecting these signals using specialized detectors. By carefully adjusting the beam parameters and scanning techniques, investigators can get essential data regarding the specimen's morphology, composition, and crystallography. The collected data is next examined and interpreted to derive relevant inferences regarding the characteristics of the specimen.

Figure 3.20 shows the SEM set-up where the fracture sample surfaces were evaluated using a Scanning Electron Microscope (SEM) EVO MA18 equipped with Oxford EDS(X-act). The magnification range used for the analysis was between 1x and 100,000x. To analyze the influence of sea sand morphological characteristics and weight percentage on the failure patterns of the FGPC composites. To avoid damage to the SEM equipment, the specimens were dusted at a sputtering deposition rate with gold using sputtering equipment.

Figure 3.21 SEM set-up

3.6 FE study for optimized composite coupons

The rule of mixtures (ROM) can be used to theoretically calculate the properties of composite materials by utilizing the characteristics of their constituent materials and their volume fractions. It works with composite materials whose constituents' properties are known. It is predicated on mathematical models and assumptions from theory by considering the elastic modulus, volume fractions, and other mechanical characteristics of the component materials. It may not always represent the complex relationships and variances of the real world since it makes assumptions of uniform distribution and ideal conditions.

The physical characteristics that are measured through testing are referred to as experimentally obtained mechanical properties. They are based on direct measurement, done under controlled conditions through physical experiments and standard tests. They consider variances seen in the real world, such as defects, deviations, and other elements that influence the behavior of materials. They consider fatigue characteristics, failure modes, and actual stress-strain behavior.

For the initial FE study rule of mixture, calculated values and the energy absorption on the sandwich structure at ballistic impact velocity are taken. The next step is to take the optimized sequence of the sandwich coupons and test for the mechanical properties. The optimized coupons' mechanical properties were tested for the FE study, and energy absorption and residual velocity were determined. Table 3.10 shows the proposed sandwich properties required for FE simulation.

Table 3. 10 Properties of sandwich (Experimental values)

FGSCs	**Density (kg/m^3)**	**Ultimate stress (GPa)**	**Young's Modulus (GPa)**	**Poison's ratio**
SKIN (JRJ)	1044.98	0.003	0.027	0.45
SC0S	1175.40	0.037	0.991	0.3
SC10S	1314.27	0.021	0.804	0.32
SC20S	1453.14	0.015	0.786	0.34
SC30S	1592.01	0.015	0.749	0.36

3.7 Low-velocity Impact test on functionally graded sandwich composite structure

LVI tests were performed employing drop-weight impact testing equipment. by positioning the sample in the holder and elevating the impactor to the required height. The test is performed at different impact velocities by varying the drop height of the impactor. The impact velocity can be calculated using the formula v = (2gh)^0.5, where v is the impact velocity, g is the acceleration due to gravity, and h is the drop height of the impactor. During the test, the energy absorbed by the specimen upon impact is recorded, and the sample is visually inspected for damage. The test can be repeated at different impact energies or velocities to determine the specimen's impact resistance and damage threshold. Overall, the low-velocity impact test set-up and testing involve carefully controlled conditions to ensure accurate and repeatable results that can provide valuable information for designing and optimizing materials for impact

protection applications. Four configurations with varying filler compositions, including neat epoxy (0%), 10%, 20%, and 30% sea sand, are shown in Figure 3.22.

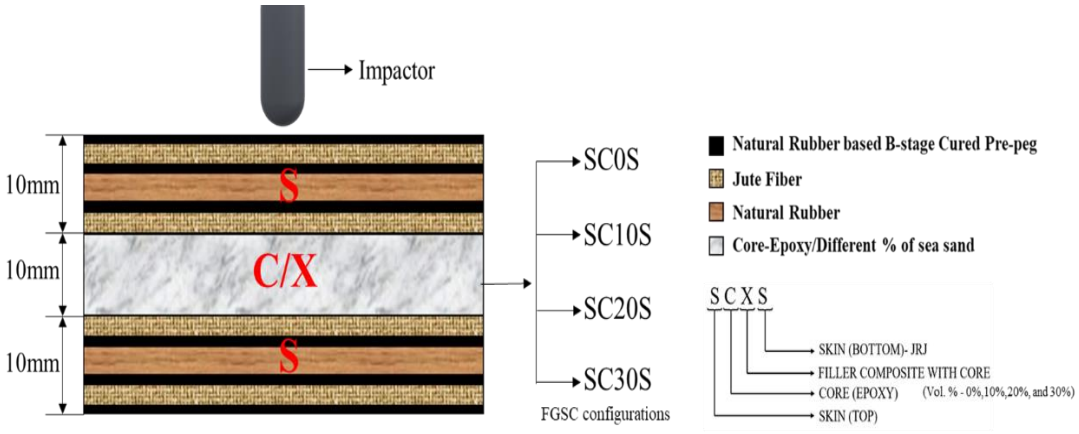

Figure 3. 22 Schematic representing the sample cross-section with different configurations

The hemispherical-shaped projectile is used with a net set-up weight of 8.09 kg. The impactor was dropped from heights of 0.5m, 1m, and 1.5m with spring compression loads of 10, 20, and 40 N, respectively, to produce impact velocities of 5.89 m/s, 10.92 m/s, and 15.18 m/s, and impact energy of 140.44 J, 482.47 J, and 931.91 J respectively. The tests were conducted at room temperature, and the impact energy was varied by changing the impactor's drop height. The impactor's potential energy increased with increasing drop height, which was then converted into kinetic energy upon release. The LVI equipment used for testing has a rebounding arresting mechanism. D7136 ASTM standard is used for testing for Figure 3.23.

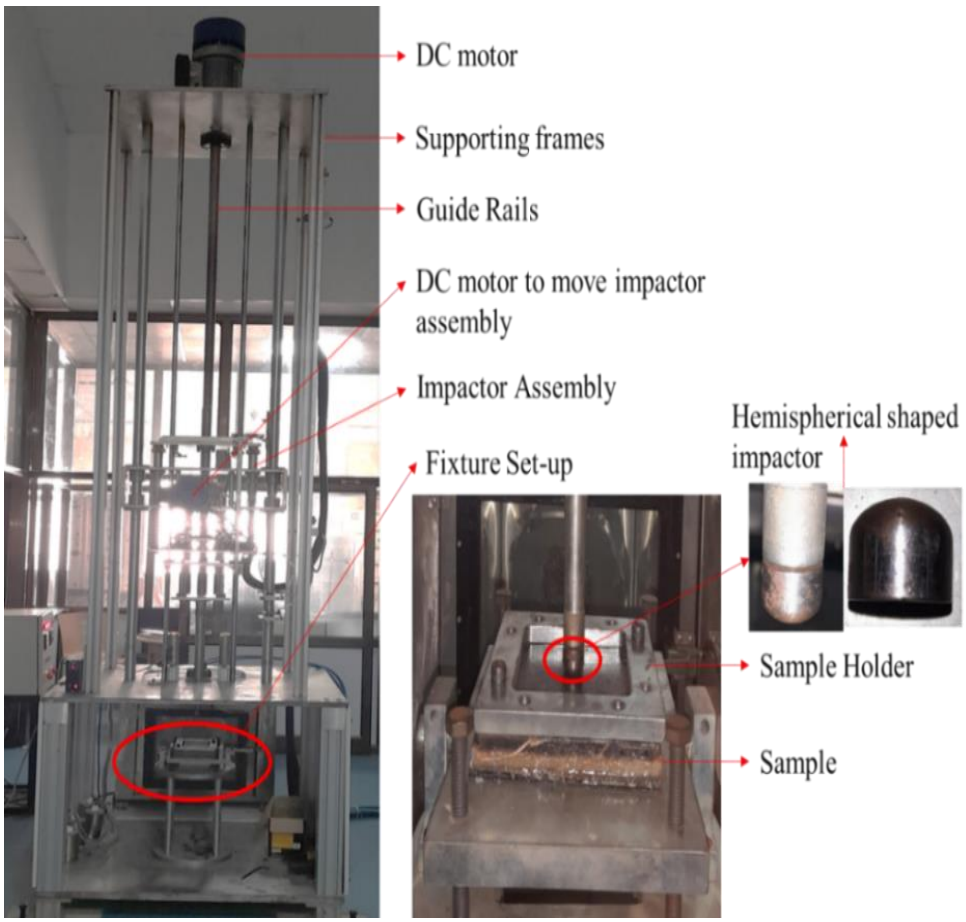

Figure 3.23 Low-velocity impact test Set-up

3.7.1 Finite Element Modelling for LVI

A finite element (FE) model was created using the ABAQUS explicit software to provide more accurate data about the impact response of the sandwich structure, such as the energy absorbed by each component and the development of the stress within the front skin. Due to the symmetry of the configuration, the simulation was developed in accordance with the experimental set-up, and the sandwich panel (Element type C3D8R) and impactor (Element type R3D4) assembly were created to increase computational efficiency. The impact velocities (5.89 m/s, 10.92 m/s, and 15.18 5 m/s) were taken using a hemispherical-shaped impactor. A hemispherical shape impactor was selected because it is a common impactor used in low-velocity impact testing of

sandwich composites. The studies show that conical-shaped impactors absorb maximum energy with lesser damage, and flat-type impactors absorb lesser energy with localized failure and maximum damage (Mohan Kumar et al., 2023). The skin and core materials are modeled into a 3D deformable body in the proper sequence.

Impactor deformation is neglected because of its minimal deformation after examination in the experiment. As a result, the impactor was considered to be rigid and simulated. Auto-mesh selection is chosen for the sandwich structure and projectile. A quad mesh includes 1944 elements, and 3939 nodes have been used. To reproduce the fixed boundary condition (BC), the DOF (degrees of freedom) of the nodes within the clamped region of FGSC were constrained, and a symmetric BC was imposed on the planes of symmetry of the sandwich structure and impactor. The impactor, with a net set-up mass of 8.09 kg, was constrained to translate only along the z-axis, and the impactor was given beginning velocities consistent with those in the impact tests. To ensure the integrity of the layers, interaction attributes have been established for all the layers in the software's module (interaction). Based on the reported studies, the algorithm of penalty contact was employed to determine the interaction between the impactor and the skin (top surface). The automated surface-to-surface contact method was utilized to establish the possible interaction among any two sandwich components. A friction coefficient of 0.3 was taken, which may happen because of hard contact and pressure, and the general contact method was used to measure the interaction between the laminates. (Mohan Kumar et al., 2022).

FGSC configurations, SC0S, SC10S, SC20S, and SC30S, subjected to LVI (5.89, 10.92, and 15.18 m/s). FE analysis can be used to examine the low-velocity impact behavior. The impact energy (E_I) of the bullet striking the target is given by Eq. (11).

$$E_I = 0.5\, m\, V_I^2 \tag{11}$$

Where V_I= velocity of impact (m/sec), and m = impactor mass (kg). The impactor's Kinetic energy (KE) and velocity decrease as it transfers energy to the target, resulting in damage dispersion within the composite. The velocity reduced is known as

residual velocity (V_R). Depending on the impact conditions and the properties of the target composite, the impactor may pierce or rebound the composite at a velocity lower than the V_I. In addition, if the bullet stops inside the composite, it results in a residual velocity of zero. The impactor's V_R is critical as it determines the amount of energy the composite absorbs during the impact event. Energy absorption is measured by determining the difference between the impactor's impact energy (E_I) and the residual energy (E_R) after impact. The energy absorption (E_A) and residual velocity are calculated using Equations (12)-(13).

$$E_A = E_I - E_R \tag{12}$$

$$E_R = 0.5\, m\, V_R^2 \tag{13}$$

Coefficient of restitution (CoR) and Energy loss percentage (ELP)

The proportion of residual velocity to the initial velocity is known as the CoR. After solving the linear momentum calculation, the plastic deformation related to both objects makes estimating the object's velocity challenging after an impact with two separate bodies; in this situation, CoR is applied. The CoR ranges from 0 to 1, with 0 indicating a plastic nature of impact and 1 indicating an elastic nature (Aryaei et al. 2010). If one of the two impacting objects occurs to be resting, the CoR may be expressed as given in Equation (14).

$$CoR = {}^{V_R}/_{V_I} \tag{14}$$

where V_R is the residual velocity, and V_I is the initial velocity. Composite drop weight impact testing for LVI behavior is considered. When the impactor is forced to fall from height 'h' into the composite laminate, the air resistance is ignored, as stated in different studies (Minamoto and Kawamura 2009; Weir and Tallon 2005; Wong et al. 2009).

During an impact occurrence, energy loss typically occurs, and the ELP is determined using Equation (15).

$$ELP = (1 - CoR^2) \times 100 \tag{15}$$

The two bodies colliding do not experience tangential forces as they make contact. As a result, friction has no effect during normal impact (Vu-Quoc et al. 2001). Because the current study is concerned with the usual impact loading situation, frictional forces are ignored. Many parameters affect the CoR, such as the shape of the materials in contact, the approach velocity, the material qualities, contact duration, and friction (Arya et al. 2016).

3.8 Ballistic Impact test on functionally graded sandwich structure

Functionally graded sandwich structures are composite materials that have different material properties across their thickness. They consist of two outer layers (skins) made of a jute/rubber flexible composite and a core made of epoxy with different filler (sea sand) compositions. The core material can be graded to have different properties, such as density, strength, and stiffness, in different structure regions.

The samples are prepared for a required dimension of 300 X 30 mm and are subjected to a ballistic impact test. Figure 3.23 shows the schematic test setup.

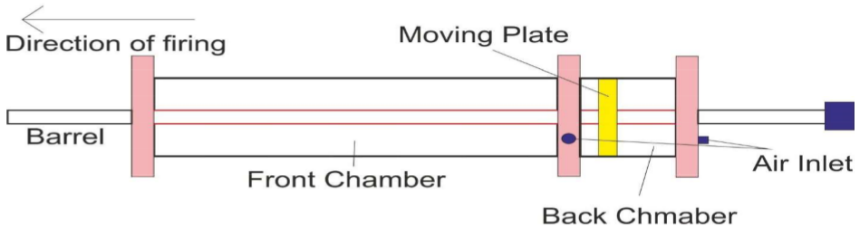

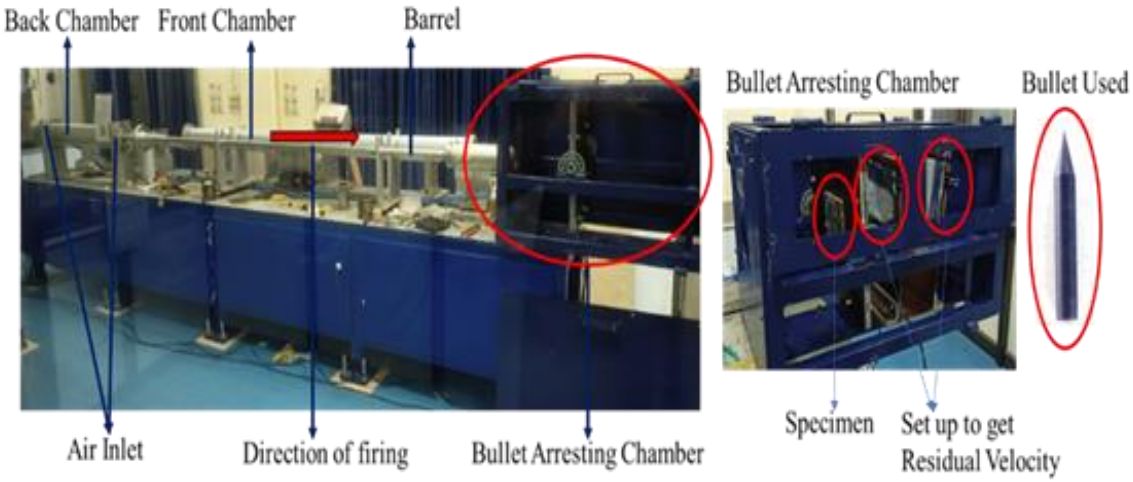

Figure 3.24 Ballistic impact setup

The ratios describe the damage caused by a ballistic impact As/A_B and A_B/A_E, where (As) is the skin pull-out area, (A_B) is the damaged area of the back/exit side of the sandwich composite, (A_E) is the area of the hole at the entry of sandwich composite, A_B/A_E ratio is dependent on the thickness of the core material and indicates the amount of energy dissipated or absorbed by the material as the bullet travels from the entry to the exit. On the other hand, the As/A_B ratio indicates the amount of energy available in the bullet for skin pull-out. Figure 3.24 provides a schematic representation of the hole created and its relevant terminology.

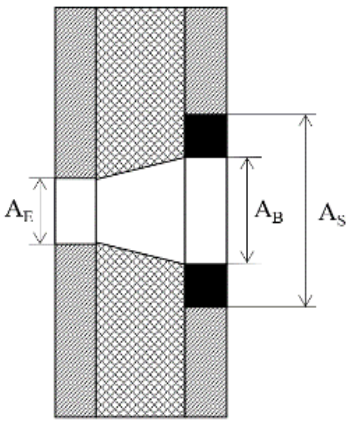

Figure 3.25 Terminology associated with the ballistic test

The mathematical model developed to determine the residual velocity (V_R) of a rigid bullet that normally impacts the target plate is represented by Equation (16). The above Equation assumes a target plate is thin enough to produce an ejected plug of fractured material (Anish et al. 2018; Iqbal et al. 2012; Rajole et al. 2020; Recht and Ipson 1960).

$$V_R = \frac{\left[\sqrt{\left(V_I{}^2 - V_{xn}{}^2\right)}\right]}{1+\Omega\left({}^{D}/_{d}\right)^2\left({}^{T}/_{L}\right)} \quad \text{at } \left(\frac{T}{L} < 0.5, \frac{T}{d} < 0.5\right) \tag{16}$$

Where V_I (m/sec) is Initial/Impact velocity, V_{xn} (m/sec) is Perforation velocity minimum, D is the diameter of a plug (7.62mm), d is the diameter of a bullet (7.62mm), Ω is the proportion of plate and bullet material densities, T is the thickness of plate, and L is the length of the bullet.

Similarly, considering the bullets, V_R is essential for the thick plate to calculate the composite's energy absorption capability. The mathematical Equation to determine V_R for a thick plate is given by Equation (17) (Doddamani et al. 2023b; Recht and Ipson 1960).

$$V_R = \left\{\frac{V_I - V_{xn}{}^2)}{\left[1+\frac{M_{snr}}{M_P}\right]\left[1+\Omega\left({}^{D}/_{d}\right)^2\left({}^{T}/_{L}\right)\right]}\right\}^{0.5} \tag{17}$$

Where M_P (g) is bullet mass, M_{snr} (g) is plug mass discharged from the back of the plate. Assuming that the observed mean dynamic shear strength stays constant, an equation for the minimal perforation velocity is given by Equation (18).

$$V_{xn} = \frac{4\Omega T^2 \varphi \eta}{Ld}\left\{1 + \left[\frac{(L+\Omega T)}{\Omega T}\left(1 + \frac{d}{4\rho_s T \eta \varphi^2}\right)\right]^{0.5}\right\} \tag{18}$$

Where, $\varphi = \left[\frac{\rho_P C_P + \rho_S C_S}{\rho_P C_P \rho_S C_S}\right]$, ρ_P *and* ρ_S (kg/m^3)is the Density of the bullet and target, η is the constant function with dimensions of stress according to the dynamic shear strength of plate material (η =0.5 σ_u) (82 X 10^6 (Pa)) (Doddamani et al. 2023a).

Equation (19) can be used to determine the longitudinal acoustic-wave velocities of bullet and target materials, CP and Cs, respectively.

$$C = \sqrt{K/\rho} \tag{19}$$

Where K (N/m^2) is the material Bulk modulus $K = E/3(1-2V)$, and σ_u (N/m^2) is the material Tensile strength. Equation (20) can be used to determine the energy absorbed (E_A) by the material from the residual velocity (Ahmad et al. 2007):

$$E_A = \frac{1}{2} M_P \left({V_I}^2 - {V_R}^2 \right) \tag{20}$$

The ballistic limit is determined using Equation (21),

$$V_B = \sqrt{V_I^2 - V_R^2} \text{ m/sec} \tag{21}$$

This chapter comprises a comprehensive methodology employed in this study that has effectively guided the material selection, fabrication, and analysis of functionally graded sandwich composites for ballistic impact applications. The Six Sigma DMAIC approach ensured a systematic and precise selection process, resulting in a composite structure demonstrating significant improvements in energy absorption, structural integrity, and cost efficiency. The integration of jute, rubber, epoxy, and sea sand, along with the validation through both FE analysis and experimental testing, has laid a robust foundation for the subsequent analysis. The next chapter discusses the detailed outcomes of the experimental and FE analyses, highlighting the influence of varying filler compositions and core thicknesses on the mechanical and physical properties of the composite. It will also explore the effectiveness of the sandwich composite in resisting low-velocity and ballistic impacts, supported by statistical analyses and fractography insights, to provide a comprehensive understanding of its performance in real-world applications.

CHAPTER 4

4 RESULTS AND DISCUSSION

This chapter discusses the results of the properties studied in three phases. The first phase focuses on material selection, the second phase focuses on characterizing the properties of Functionally Graded (FG) cores, and the third phase examines the sandwiches with FG cores for ballistic impact. Five replicates undergo various loading conditions in all the phases, and the average values obtained from these are used for analysis.

4.1 Material selection using Six Sigma DMAIC Methodology

Step 1: Define Phase

Before initiating the materials selection process, it's critical to comprehend the factors that affect the material selection, as illustrated in Figures 4.1 and 4.2.

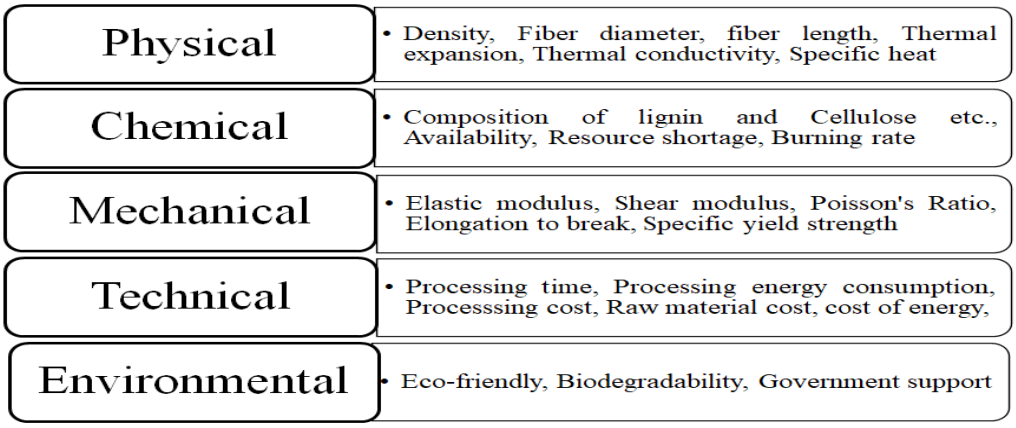

Figure 4.1 Parameters for selecting the materials

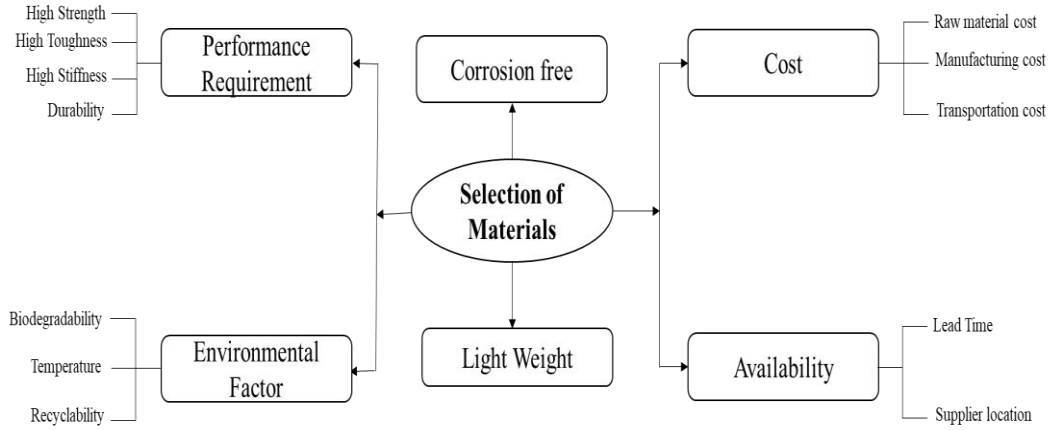

Figure 4.2 Material parameters mind mapping

Figure 4.2 shows the graphical tool representing mind-mapping material parameters for material selection. It can be a useful tool in selecting materials for a specific application, as it can help to organize and categorize the different factors that need to be considered. It starts with a central idea and branches out with the main factors to consider. Then, it is organized and compares different materials based on their performance, environmental suitability, cost, and availability. Finally, the mind map decides the best material(s) for the ballistic application. Properties of toughness necessitate ductility and strength stability (HARTNESS 1988); as highlighted in Table 4.1, additional criteria are needed when choosing the best natural fibers and matrix. The PDS (product design specifications) was developed at the initial stage of the research and was used to examine crucial design variables during the material selection process. However, for the sake of brevity, it has not been included here. To obtain the lightweight component, the material must show a significant increase in density (Liu et al. 2013). The material must also have a high elongation at break value to provide better toughness. Furthermore, the selected material must always be readily available, have good durability with high tensile strength, prevent fiber cracking with lower moisture content, and be eco-friendly with high biodegradability.

Table 4.1 PDS for selecting NF (natural fibers) and matrix.

NF	Matrix (Face and bottom Sheet)	Matrix (Core)
Density(g/cm^3)- LTB	Density(g/cm^3)- LTB	Density(g/cm^3)- LTB
Elongation at break (toughness) - HTB	Tensile Strength- HTB	Tensile Strength- HTB
Tensile Strength- HTB	Tensile Modulus- HTB	Tensile Modulus- HTB
Tensile Modulus - HTB	Flexibility- HTB	Adhesion- HTB
% Hemicellulose- HTB	Toxicity- LTB	Toxicity- LTB
Availability- HTB	Availability- HTB	Availability- HTB
Cost/(Rs/kg)- LTB	Cost/(Rs/kg)- LTB	Cost/(Rs/kg)- LTB

LTB = Lower the better; HTB= Higher the better

The hybrid and non-hybrid forms and their usage data as PMC are shown in Figure 1.3. The percentage of NF and their usage data from the past 20 years as PMC for impact application are shown in Figure 1.4. Non-hybrid PMCs employ NF more than hybrid PMCs. Even though jute fiber has acceptable mechanical properties, the researchers have not completely exposed it for impact application, as shown in Figure 2.2 (Célino et al. 2014). Very few or limited numbers of literature use jute fiber in PMC. These studies also focus more on bio-composites for use in impact applications. However, all existing studies focus on producing composites for impact applications. The gap has been identified in producing hybrid sandwich composites for ballistic impact applications.

To obtain PMC, several matrices are used to reinforce the natural fibers. As shown in Figure 1.5, epoxy is the maximum and widely used matrix in PMC when natural fibers are employed as reinforcement. Synthetic fibers are employed in the majority of PMCs for impact applications. Figure 1.6 shows the matrix percentage used in impact applications with natural and synthetic fibers, which indicates epoxy is the

most used matrix in combination with natural and synthetic fiber for impact applications. Natural rubber and STF (shear-thickening fluids) are used as matrix material, and synthetic fibers are used for flexible composites. In the case of natural fibers, very few matrix materials like epoxy, PE, PP, and PU are used. Some investigators have studied the impact behavior of the PMC utilizing a variety of polymer-based matrices. Most studies focused on determining the LVI of composites used in structural applications. Natural rubber capable of being employed in PMC exposed to ballistic impact loading (Vishwas et al. 2017, 2019) is not fully exposed in research. The matrix defines the deformation amount in PMCs, which impacts the local strain and impact resistance.

According to the review, rubber is a better matrix material for flexible composites than others, preceded by polypropylene (PP), Phenolics, and polyurethane (PU). Since rubber is a naturally occurring biodegradable material, it contributes to producing flexible composites. Less cost made this the best choice as a matrix with the jute fiber. The synthetic matrix used is effectively used in PMC and is subjected to impact application. The most popular and best synthetic matrix is epoxy, followed by vinyl ester and polyester. Epoxy has a better mechanical property than other matrices, so it best fits core material in hybrid sandwich material (Mahesh et al. 2020). After the literature review, some rigid requirements can be set as toughness, strength, and density, and soft constraints can be set as cost and eco-friendly.

Step 2: Measure Phase

The hierarchical structure was categorized into five levels in the measure phase, with the first hierarchy level specifying the ultimate objectives (selection of materials). The rank standards in this hierarchy structure were obtained from Table 4.1. As shown in Figure 4.3. the 4 levels of the hierarchy framework for matrix selection are described in Figure 4.4. Similarly, the 4 levels of the hierarchy framework for the selection of core material and filler material with core are described in Figure 4.5 and Figure 4.6, respectively.

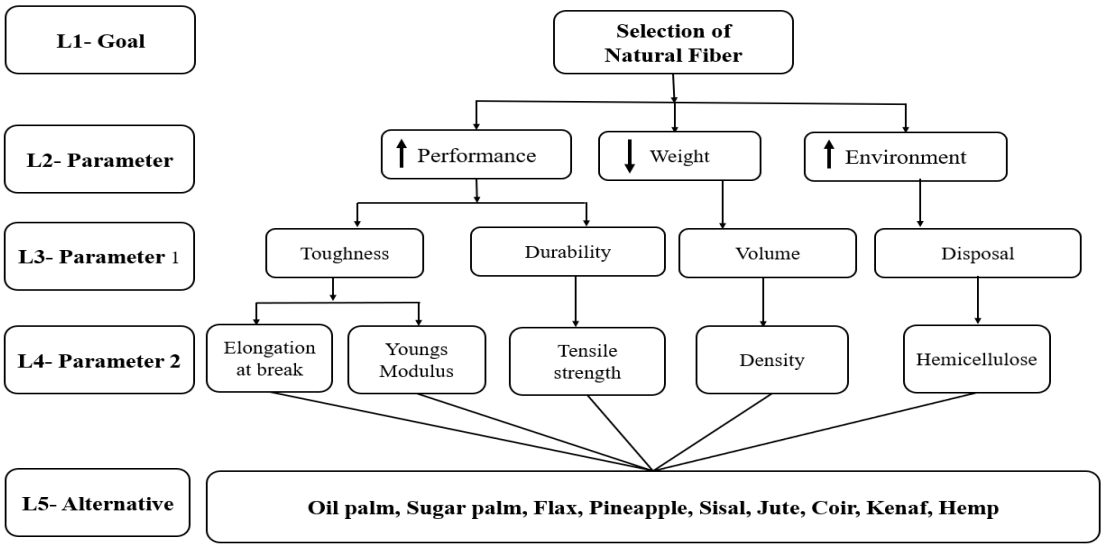

Figure 4.3 Five-level hierarchy frameworks for material selection (natural fibers) skin material

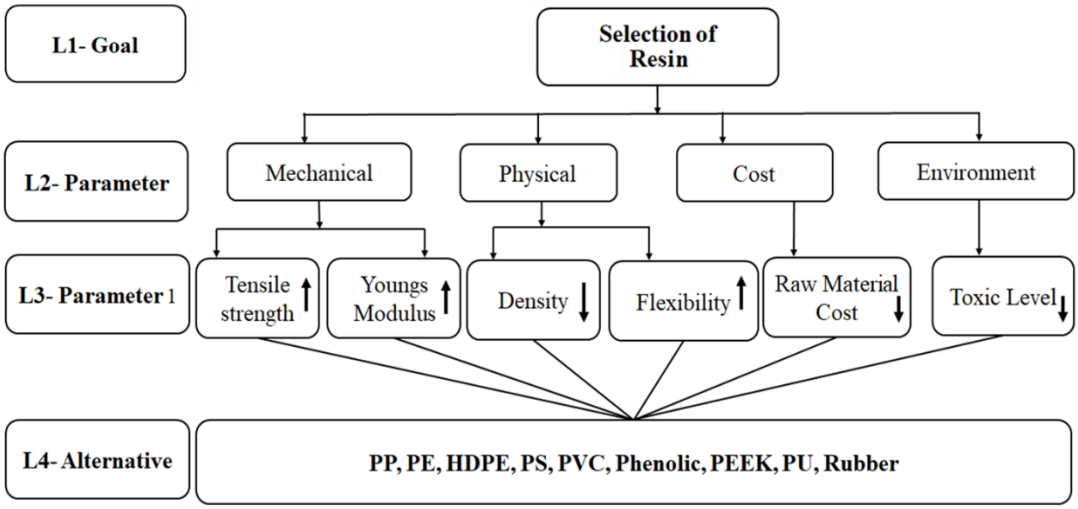

Figure 4.4 Four-level hierarchy frameworks for the material selection (Resign) for skin reinforcement

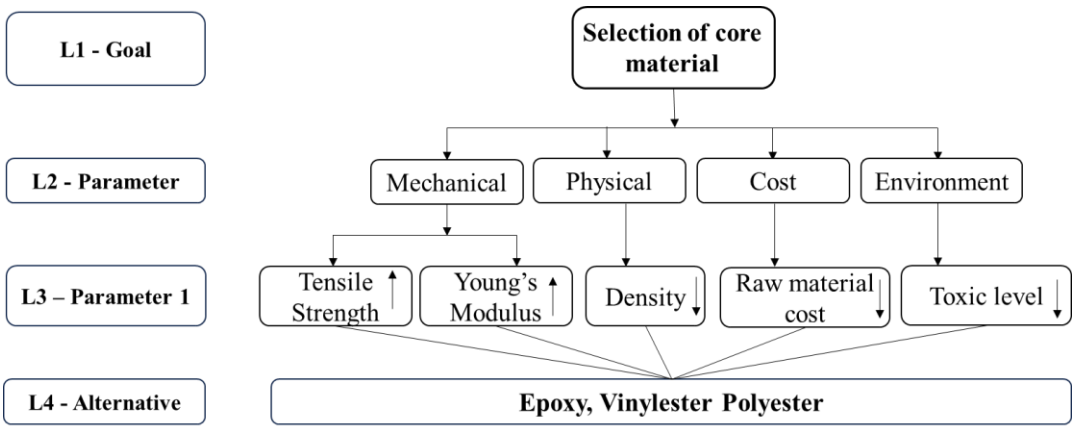

Figure 4.5 Four-level hierarchy frameworks for the material selection for core material

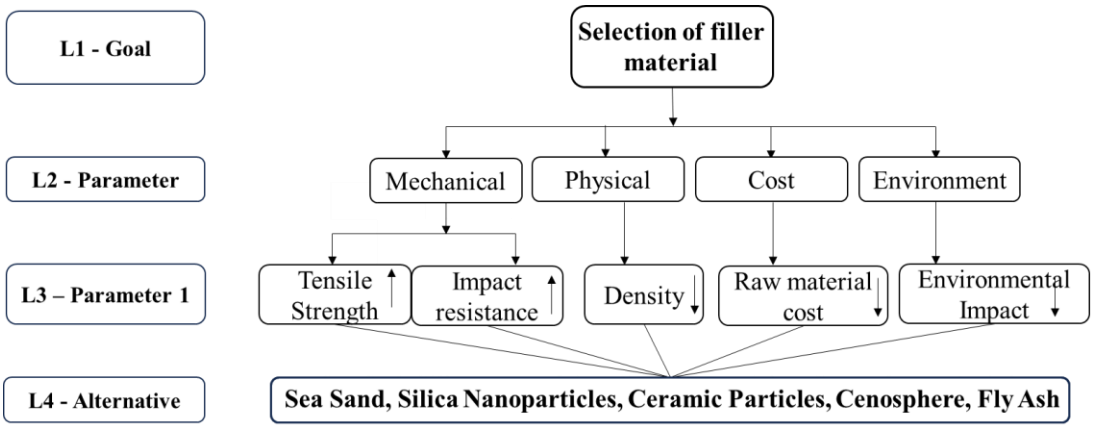

Figure 4.6 Four-level hierarchy frameworks for the material selection for filler material with core

Step 3: Analysis Phase

Before beginning the material selection process, the "analyze" phase determines the ability of natural fibers/ matrix material properties selection, as indicated in Table 4.2. This stage assists in identifying the benefits and drawbacks of specific material properties and any issues that may arise at the time of the manufacturing process. 9 NFs are chosen with aluminum to analyze material properties like Young's modulus, TS, SEA (specific energy absorption), density, and cost.

Table 4.2 Material Properties of Natural Fibers for Skin Material (Mahesh et al. 2021b; Nurazzi et al. 2020; Yusof et al. 2020b)

Natural fibers	YM (GPa)	TS (MPa)	Density (g/cm^3)	Elongation at break (%)	Hemicellulose %	Cost (Rs/kg)	SEA (kJ/kg)
Oil palm	3.2	248	1.55	25	14.95	50.00	---
Sugar palm	5	277	1.26	22.3	13.3	37.73	---
Hemp	69.5	687.5	1.47	1.6	15	90.57	---
Flax	27.5	1000	1.49	3.2	20	113.21	---
Jute	30	710	1.3	1.8	20	26.42	---
Sisal	19	700	1.45	2.25	12	27.17	---
Kenaf	38	612	1.4	1.6	20.3	98.11	---
Pineapple	1.44	700	1.55	14.5	18.8	3.77	---
coir	5	175	1.195	30	0.25	94.34	---
Aluminium	5	700	2.7	---	---	279	23.0

Eight thermoplastic and naturally available matrix matrices were selected to analyze the material properties like YS, TS, density, cost, and flexibility, as shown in Table 4.3. Flexibility is scaled from 1 to 9, where 9 is very flexible and 1 is less flexible.

Table 4.3 Material Properties of Matrix for Skin Material (Mahesh et al. 2021b; Yusof et al. 2020b)

Matrix	YM (GPa)	TS (MPa)	Density (g/cm^3)	Cost (Rs/kg)	Flexibility using a scale (1-9)
PP	1.6	40	0.91	75	5

PE	0.5	45	0.95	71.25	8
HDPE	1.1	40	0.97	94.56	7
PS	3.5	60	1.05	143.33	3
PVC	3	53	1.38	86.30	4
Phenolic	4.8	62	1.29	191.11	1
PEEK	3.6	95	1.32	102.52	2
PU	1.31	40	1.12	760.23	6
Rubber	0.0025	32	0.92	67.5	9

The thermoset matrix for core material is used to analyze properties like YS, TS, density, cost, and environmental impact, as shown in Table 4.4. Table 4.5 shows the material properties of filler materials.

Table 4.4 Material Properties of Matrix for Core Material

Matrix	**YM (GPa)**	**TS (MPa)**	**Density (g/cm^3)**	**Cost (Rs/kg)**	**Izod Impact Notch (J/cm)**
Epoxy	3–6	35–100	1.1–1.4	312-1500	0.3
Polyester	2–2.45	69–83	1.2–1.5	104-208	0.15–3.2
Vinylester	3.1–3.8	40–90	1.2–1.4	208-416	2.5
Polyurethane	0.00114 - 3.54	0.138 - 79.3	0.0400 - 1.74	850- 1000	0.160 - 7.47

Table 4.5 Material Properties of filler Material

Property	**Synthetic Foams**	**Silica Nanoparticles**	**Ceramic Particles**	**Fly Ash**	**Cenosphere**	**Sea Sand**
Density (kg/m^3)	20 - 150	1800 - 2200	3000 - 4500	2100 - 2500	150 - 800	1500 - 1900

Hardness (Mohs scale)	0.5 - 2	7	6 - 8.5	4 - 6	3 - 5	7
Young's Modulus (GPa)	0.01 - 0.5	170 - 180	150 - 400	10 - 40	0.1 - 10	20 - 30
Thermal Stability (°C)	80 - 200	1600	> 1700	Varies depending on the composition	600 - 800	Up to 1500
Cost (Rs/kg)	0.5 - 5	10 - 50	1 - 10	0.1 - 0.5	0.1 - 0.3	0.01 - 0.1

Step 4: Improve Phase

As shown in Table 4.6, aluminum (Al) is chosen as the datum because it has a higher specific energy absorption capacity than steel (15.77kJ/kg) (Abbas et al. 2016), balanced properties, cost-effectiveness, and wide applicability across many industries.

Table 4.6 shows the selection of fiber 6 material properties and 2 (low cost and ease of availability); additional properties are compared with the datum aluminum. The results of the Pugh selection method reveal that flax and jute are the best natural fibers for fabricating. Flax and jute fibers came in first with a total score of 6, followed by sisal, hemp, and kenaf, which came in second with a total score of 5. However, the authors believe that jute can be employed as a reinforcement in hybrid sandwich composites due to these fiber's availability and low cost.

Similarly, PP is set as a datum for selection, and all other matrix parameters are examined. As shown in Table 4.7, PP is taken as a datum because, from Figures 1.5 and 1.6, after a synthetic matrix epoxy, it is the most used matrix with NF and for impact applications. The Pugh selection method results in Table 4.7 reveal that rubber is the

best matrix for fabricating. Rubber came in first with a total score of 4, followed by PE, Phenolic, and PEEK, which came in second with a total score of 3. Four materials with three additional properties (low cost, ease of availability, and biodegradability) are taken and compared with datum PP. As per the results, rubber is the most suitable matrix for impact applications, followed by PE, Phenolic, and PEEK.

Polyurethane (PU) is set as a datum for core material selection because it is widely used in various industries, including construction, automotive, aerospace, and consumer goods. Its prevalence makes it a suitable reference point for comparison against other materials. Polyurethane is the datum (reference) material used in the Pugh matrix method for comparing materials such as epoxy, polyester, and vinyl ester.

The Pugh selection method results in Table 4.8 reveal that epoxy is the best matrix for fabricating, which gives structural stability and stiffness to the sandwich structure. Epoxy came in first with a total score of 5, followed by Polyester, which came in second with a total score of 3, and Vinylester with a score of 2. Three materials with five additional properties (low cost, ease of availability, and biodegradability) are taken and compared with datum PU. As per the results, epoxy is the most suitable matrix for the core for impact applications, followed by Polyester and Vinylester.

The Pugh selection method selects the best filler material with the core in the improve phase. As shown in Table 4.9, synthetic foam is set as a datum in the Pugh Matrix, Synthetic foam is a commonly used or widely known filler material in the industry. The properties and performance of synthetic foam may be well understood or documented, making it a reliable reference point for comparison. The Pugh selection method results in Table 4.9 reveal that sea sand is the best filler material, conducted using DMAIC methodology, including criteria such as cost, availability, density, and mechanical properties, sea sand emerges as a compelling choice for ballistic material applications. Sea sand came in first with a total score of 4, followed by flyash, which came in second with a total score of 3, Cenosphere and silica nanoparticles with a total score of 2, and ceramic particles with a score of 1.

Table 4.6 Pugh selection method for skin material

Properties	Datum (Al)	Sugar Palm	Kenaf	Oil Palm	Sisal	Jute	Hemp	Flax	Pineapple	Coir
YM	Aluminum	=	+	-	+	+	+	+	-	=
TS		-	-	-	=	+	-	+	-	-
Density		+	+	+	+	+	+	+	+	+
Hemicellulose		-	-	-	-	-	-	-	-	-
Microfibril angle		-	-	-	-	-	-	-	-	-
High biodegradability		+	+	+	+	+	+	+	+	+
Ease of availability		+	+	+	+	+	+	+	+	+
Cost		+	+	+	+	+	+	+	+	+
Total		**4**	**5**	**4**	**5**	**6**	**5**	**6**	**4**	**4**

(+) = better; (=) similar, (–) worse, compared to datum.

Table 4.7 Pugh selection method for matrix skin material

Properties	Datum	PE	HDPE	PS	PVC	Phenolic	PEEK	PU	Rubber
YM	PP	-	-	+	+	+	+	-	-
TS		+	=	+	+	+	+	=	-
Density		-	-	-	-	-	-	-	-
Flexibility		=	=	=	=	=	=	=	+
High biodegradability		+	=	=	=	+	+	+	+
Ease of availability		-	-	-	-	-	-	-	+
Cost		+	-	-	-	-	-	-	+
Total		**3**	**---**	**2**	**2**	**3**	**3**	**1**	**4**

(+) = better; (=) similar, (–) = worse, compared to datum.

Table 4.8 Pugh selection method for core material selection

Properties	**Datum (PU)**	Epoxy	Polyester	Vinyl ester
YM	Polyurethane	+	-	=
TS		+	-	=
Density		+	+	+
Chemical Resistance		+	-	=
Ease of availability		-	-	-
Cost		-	+	+
Processing Ease		+	+	-
Environmental Impact		=	=	=
Total		**5**	**3**	**2**

(+) = better; (=) similar, (–) = worse, compared to datum.

Table 4.9 Pugh selection method for filler material selection

Properties	Datum	Silica Nanoparticles	Ceramic Particles	Fly Ash	Cenosphere	Sea Sand
Tensile Strength	Synthetic Foams	+	+	-	=	-
Density		-	-	+	=	=
Impact Resistance		+	=	-	=	-
Cost		-	=	+	=	+
Availability		=	=	+	+	+
Processing Ease		=	=	=	+	+
Environmental Impact		=	=	=	=	+
Total		2	1	3	2	4

Step 5: Control Phase

Based on the improved phase results, flax and jute fibers were indicated as the best acceptable potential material for impact application. The intensity scale is highly desirable, followed by quality and weight, as shown in Table 4.10.

Table 4.10 Intensity scale pairwise comparison as a selection basis

AHP scale	Summary
1	Equal
3	Moderately important
5	Strongly important
7	Very strongly important
9	Extremely important
2-4-6-8	Middle

Case-1

The decision matrix was prepared by giving the scale of rating for each parameter based on the AHP scale and priority weightage. The decision matrix resulting weights are based on the principal eigenvector of the decision matrix. The value of the eigenvector is 6.483 for six iterations. The resulting weights for the criteria based on your pairwise comparisons top priority percentage was given to cost and biodegradability (23.6%) each followed by density (19.2%), Tensile strength (14.5%), Young's modulus (11.5%) and Elongation at break (7.6%)). Based on the software results for the number of comparisons (15) and the CR (7.7%), it can be concluded that the decision-making is agreed upon. Then, the parameters were normalized by taking the weightage value based on Table 3.1. Then, the values are normalized and calculated to get a Performance value based on the performance value raking assigned to each natural fiber using software, as shown in Table 4.11. Flax fiber ranked first, followed by oil palm and jute. Based on the ranking first, three ranked natural fibers were taken for further consideration.

Table 4.11 Ranking table for natural fiber

NF	Statistical results			
	Ideals	**Normal**	**Raw**	**Rank**
Coir	0.5143	0.1235	0.0926	5
Flax	1.0000	0.2402	0.1801	1
Hemp	0.2969	0.0713	0.0535	8
Jute	0.5788	0.1390	0.1043	3
Kenaf	0.2973	0.0714	0.0536	7
Oil Palm	0.5999	0.1441	0.1081	2
Pineapple	0.5267	0.1265	0.0949	4
Sisal	0.3496	0.0840	0.0630	6
Sugar Palm	0.2929	0.0703	0.0525	9

The main criterion for selecting a material is the availability of fiber. Table 4.12 shows the anticipated production quantities of various natural fibers in composite fabrication. Jute fiber has a relatively high yearly output in the native region and has good, acceptable mechanical properties.

Table 4.12 Yearly production of selected fibers in different countries (Asim et al. 2018)

NF	Origin countries	Estimated production (tons)
Flax fiber	Canada, France, Belgium	$810X10^3$
Oil palm fiber	Indonesia, Malaysia, Thailand	Abundant
Jute fiber	India, Bangladesh	$2500X10^3$

Flax is mainly harvested in Canada, France, and Belgium. The main drawback of flax fiber is the variation in its properties. The tensile characteristics of flax fibers will deteriorate due to environmental factors. Also, flax fibers in composites have several drawbacks, like poor bonding between fiber/matrix, resulting in lower tensile properties (Yan et al. 2014). Oil palm is harvested for the oil refining process, and a by-

product of this is oil palm fiber, which is abundant in Malaysia and Indonesia. In the case of oil palm fibers, the properties are influenced by the structure of fibers, cell defects and dimensions, chemical compositions, and micro-fibril angle, which varies from part to part and area to area of a plant. Due to their drawbacks like less strength, a sensitive environment, and weak resistance to moisture, which causes natural fiber-reinforced materials to degrade in strength and stiffness, the oil palm biomass fibers are not suitable for high-performance applications (Norsuzila Ya'acob et al. 1989).

Because of the importance and color of jute fiber, it is sometimes known as "Golden fiber" in fiber production industries. Jute ranked 2nd only to cotton in the world's total production and is among the strongest NF. Jute is inexpensive to cultivate, produces a high yield/acre, and requires minimal fertilizer, making it environmentally sustainable. Jute is biodegradable since it is made up of cellulose and lignin. India and Bangladesh are the leading producers of jute (Jayaraman n.d.). Thus, jute is the most promising option for composites among the selected natural fibers when cost, mechanical properties, availability, and biodegradability are considered.

Similarly, a decision matrix was prepared to select the matrix by giving the rating scale for each parameter based on the AHP scale and priority weightage. The decision matrix resulting weights are based on the principal eigenvector of the decision matrix. The value of the eigenvector is 5.401 for 6 iterations. The resulting weights for the criteria based on your pairwise comparisons (top priority percentage were given to flexibility (41.1%) followed by density (19.6%), cost (18.8%), Tensile strength (16.7%), and Young's modulus (3.8%)). Based on the software results for the number of comparisons (10) and the CR (8.9%), it can be concluded that the decision-making is agreed upon. Then, the parameters were normalized by taking the weightage value based on Table 3.6. Then, the values are normalized and calculated to get a Performance value based on the performance value raking assigned to each matrices-using software as shown in Table 3.11. Polyurethane ranked first, followed by phenolic and rubber.

Based on the ranking, the first three ranked matrices were taken for further consideration.

Table 4.13 Ranking table for Matrix

Matrix	Statistical results			
	Ideals	**Normal**	**Raw**	**Rank**
HDPE	0.3583	0.0870	0.0652	6
PE	0.3282	0.0797	0.0597	7
PEEK	0.2282	0.0737	0.0537	8
Phenolic	0.7162	0.1738	0.1304	2
PS	0.6208	0.1507	0.1130	4
PU	1.0000	0.2427	0.1820	1
PVC	0.4598	0.1116	0.0837	5
Rubber	0.6369	0.1546	0.1159	3

Phenolic resin is quite harmful when exposed; long-term exposure to humans may cause a gradual loss in weight, dark urine release, and sometimes damage to the liver and blood. Their main drawbacks are low strength and a curing reaction that produces water. This water might be trapped within the composite, harming the material's structure. Mechanical properties are reduced due to the brittle nature because of the condensed nature of the curing process, voids, and defects in the surface (Gardziella and Mueller 1990). One of the significant disadvantages of polyurethane materials is their short lifespan. It absorbs moisture and gradually deteriorates, losing its structural integrity. Polyurethane products are quite harmful, which will not lead to death but annoy persons with breathing disorders—toxic material isocyanates, which are sometimes used for curing purposes. PUs hybridize with other resins because of the significantly lower mechanical properties of laminate under compression (Radzi Ali et al. 2017). Natural Rubber (NR) exhibits sufficient tensile strength, high resilience, and tear/wear resistance. It also provides moderate persistent properties with better

flexibility capabilities at low temperatures. NR is one of the most flexible rubbers compared to all other rubbers available, and it is water and chemical-resistant. NR used as the matrix has an advantage in ballistic impact applications because of its flexibility, which results in tearing instead of matrix cracking, thus freeing the composite from catastrophic failure. Flexibility doesn't restrict the yarns through which the fabric resists projectile energy. Therefore, among different selected matrices, natural rubber is the most promising option over other matrices in composites when flexibility, cost, availability, and biodegradability are considered.

Pugh's selection method uses qualitative data to select materials by evaluating paired priorities (Pugh 1996). Pugh technique has limitations in adding significant assessments to confirm correct results. As a result, the AHP approach was used to analyze and validate the best material selection outcome. Nevertheless, the priority vectors of the AHP approach connected to the key parameters significantly impacted the fibers and matrix priority (Chang et al. 2007), demonstrating that a slight adjustment in the factor weights can vary the material hierarchy decision's overall ranking. Because of the highly qualitative decisions of the priority vector, the durability of the results obtained in the control process by modifying the criteria weights must be checked (Mansor et al., 2013). By increasing or decreasing the weight of the criteria, the testing process might apply to a specific situation. Because of changing the weights for individual factors, changes in priority and varied rankings of the alternatives may be tracked. As a result, ANP (Analytic Network Process) sensitivity analysis may be used to present the ranking's stability data for selecting the most appropriate material (Mastura et al. 2017). ANP is a strategy to boost the AHP for complex challenges with non-hierarchical structures based on the analysis performed by the human brain. ANP employs a complete framework for all interactions and relationships between decision-making levels, resulting in a network structure (Zare et al., 2018).

Using the available decision-making software, four parameters were chosen to change the priority vector of the sensitivity analysis. For natural rubber, the priority percentage for density is 19.2%, increasing by 20% to 39.2%. Similarly, all the parameter percentages are increased, as shown in Figure 4.7. The case of the matrix also followed the same procedure as shown in Figure 4.8. Flax is a better material, followed by oil palm and jute, with maximum priority percentage values. PU is a better matrix, followed by Phenolic and rubber with maximum priority percentage values. These results show consistency with the decision that we made earlier. Flax, oil palm, and jute are three recommended materials when the priority percentage value increased by 20% for all the parameters like density, tensile strength, hemicellulose, and cost. Similarly, in matrix selection, PU, followed by phenolics and rubber, are the top three recommended materials when the priority percentage value increased by 20% for all the parameters like density, tensile strength, flexibility, and cost.

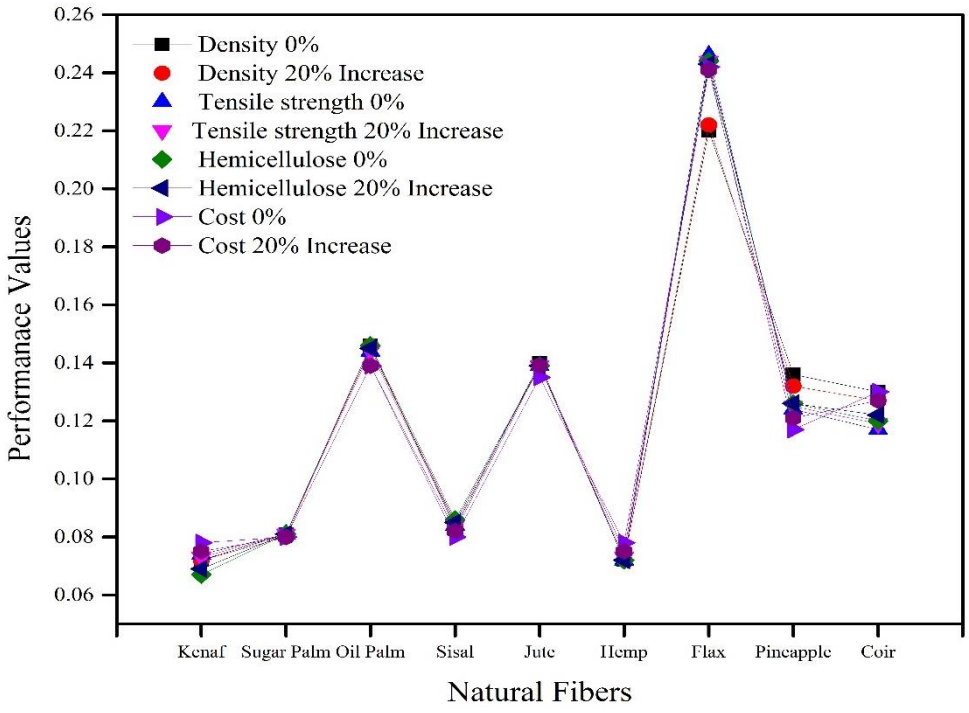

Figure 4.7 Priority percentage values of different parameters when increased by 20 % for NF

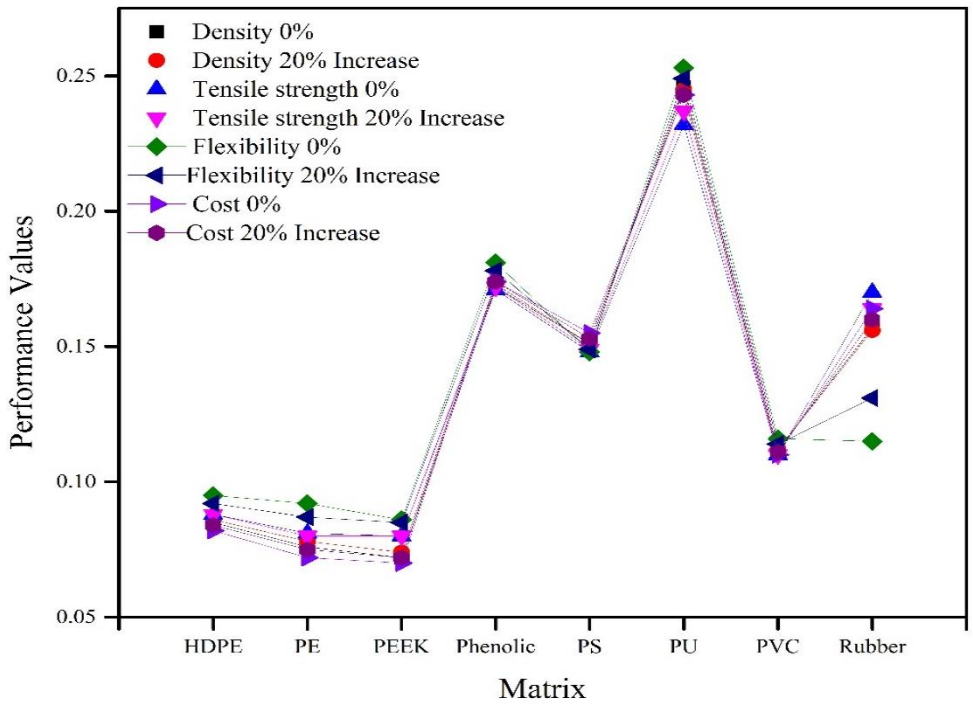

Figure 4.8 Priority percentage values for different parameters when increased by 20 % for matrices

An ANP sensitivity analysis was performed to investigate the effects of several parameters on finding the optimal alternative. The priority vectors associated with the key criteria heavily influenced the selection priorities. It would be difficult if the "improve" and "control" phases produced conflicting results. However, in this case, the results consistently showed the same results with significantly less deviation. This indicates that flax, oil palm, and jute are the best members of natural fibers. PU, phenolics, and natural rubber are the better matrix members for the skin part of the hybrid sandwich composite for ballistic impact application.

For hybrid sandwich composites for impact applications, skin material (front and bottom sheets) is chosen as natural fiber. Jute is a promising fiber over other natural fibers by considering cost availability and acceptable mechanical properties. Natural rubber is selected for the matrix because of its high flexibility, which suits impact applications. The core provides flexural stiffness and improved energy absorption

without compromising its performance in the composites during an impact. The core absorbs most shear stress, whereas the face sheets absorb most bending stresses. Using such composite structures, high bending strength can be achieved without increasing the weight of the composite (Chatterjee et al. 2021). We require good stiff material with better stiffness and mechanical properties for a core material. According to the review and Table 1.3, epoxy is the most used synthetic material for impact application. Figure 1.5 shows the percentage of polymers used with natural fibers as a matrix, and Figure 1.6 shows the matrix % used with natural and synthetic fibers for the applications of impact; in both cases, epoxy stands top on the list and, without any doubt, it is the better stiff core material used for impact application. One more important reason for selecting jute as skin and epoxy as the core is these jute fibers are less hydrophilic; they have a better jute/epoxy bonding. Because of this bonding and the high tensile strength of the jute, both flexural and tensile properties can be improved. So, the combination of the sandwich structure may be jute/rubber /jute, as the skin surrounding the core material is epoxy.

This review confirmed the research objectives, indicating that the natural fibers and matrix chosen must bridge the gap between ecological and economic concerns. The preferred fibers must have high energy absorption, low cost, high availability, low density, high toughness, acceptable tensile strength, and biodegradability.

Case-2

In the second case, the same procedure is adopted as in case 1. The weightage for cost, availability, biodegradability, and density is increased. The decision matrix was prepared by giving the scale of rating for each parameter based on the AHP scale and priority weightage. The decision matrix resulting weights are based on the principal eigenvector of the decision matrix. The value of the eigenvector is 5.483 for six iterations. The resulting weights for the criteria based on your pairwise comparisons (top priority percentage were given to cost (30%) and biodegradability (15%) each followed by density (10%), Tensile strength (10%), Young's modulus (10%) and

Availability (25%). Based on the software results for the number of comparisons (10) and the CR (8.7%), it can be concluded that the decision-making is agreed upon. Then, the parameters were normalized by taking the weightage value based on Table 4.1. Then, the values are normalized and calculated to get a Performance value based on the performance value raking assigned to each natural fiber using software, as shown in Table 4.12. Jute and Flax fiber ranked first with the same score, followed by sugar palm and sisal. Based on weightage given more on cost, Availability, and biodegradability, jute and flax have the same score with first rank, and from Table 4.10, based on availability and cost, jute is the better member compared to the other natural fibers.

Table 4.14 Ranking table for natural fiber

NF	Statistical results			
	Ideals	**Normal**	**Raw**	**Rank**
Jute	1.00	0.12	0.84	1
Oil Palm	0.72	0.24	0.61	5
Sugar Palm	0.83	0.07	0.70	3
Hemp	0.90	0.13	0.76	2
Flax	1.00	0.07	0.84	1
Sisal	0.75	0.14	0.63	4
Kenaf	0.67	0.12	0.57	6
Pineapple	0.57	0.08	0.48	7
Coir	0.44	0.07	0.37	8

Similarly, for matrix material for skin, the decision matrix's resulting weights are based on the principal eigenvector of the decision matrix. The value of the eigenvector is 5.383 for six iterations. The resulting weights for the criteria based on your pairwise comparison's top priority percentage were given to Flexibility (39.7%), cost (29.4%) each followed by density (5.8%), Tensile strength (13.2%), and Availability (11.9%). Based on the software results for the number of comparisons (10)

and the CR (8.5%), it can be concluded that the decision-making is agreed upon. Then, the parameters were normalized by taking the weightage value based on Table 4.1. Then, the values are normalized and calculated to get a Performance value based on the performance value raking assigned to each matrix using software, as shown in Table 4.13. Rubber ranked first, followed by phenolic and PU. Based on weightage gives more flexibility, cost, availability, and biodegradability. With the first rank based on flexibility, availability, and cost, the Rubber is a better member than the other matrix.

Table 4.15 Ranking table for matrix for skin

Matrix	**Statistical results**			
	Ideals	**Normal**	**Raw**	**Rank**
Rubber	0.3583	0.0870	1.00	1
Phenolic	0.3282	0.0797	0.9375	2
PU	0.2282	0.0737	0.875	3
PS	0.7162	0.1738	0.8125	4
PVC	0.6208	0.1507	0.75	5
HDPE	1.0000	0.2427	0.6875	6
PE	0.4598	0.1116	0.625	7
PEEK	0.6369	0.1546	0.5625	8

The decision matrix was prepared by giving the scale of rating for each parameter based on the AHP scale and priority weightage. The decision matrix resulting weights are based on the principal eigenvector of the decision matrix. The value of the eigenvector is 5.388 for six iterations. The resulting weights for the criteria based on your pairwise comparison's top priority percentage were given to Tensile strength (40.2%), Young's modulus (21.5%), each followed by density (18.4%), cost (8.7%), and environmental impact (11.3%). Based on the software results for the number of comparisons (10) and the CR (8.6%), it can be concluded that the decision-making is agreed upon. Then, the parameters were normalized by taking the weightage value

based on Table 4.1. Then, the values are normalized and calculated to get a Performance value based on the performance value raking assigned to each natural fiber using software, as shown in Table 4.14. Epoxy ranked first because of its better mechanical properties than its counterparts, followed by vinyl ester and polyester.

Table 4.16 Ranking table for matrix for core

Matrix	**Statistical results**	
	Performance value	**Rank**
Epoxy	0.3354	1
Vinyl Ester	0.3239	2
Polyester	0.2916	3

The decision matrix was prepared by giving the scale of rating for each parameter based on the AHP scale and priority weightage. The decision matrix resulting weights are based on the principal eigenvector of the decision matrix. The value of the eigenvector is 5.388 for six iterations. The resulting weights for the criteria based on your pairwise comparison's top priority percentage were given to Tensile strength (11.3%), Impact resistance (18.4%), followed by density (8.7%), cost (40.2 %), and environmental impact (21.5%). Based on the software results for the number of comparisons (10) and the CR (8.7%), it can be concluded that the decision-making is agreed upon. The parameters were normalized by taking the weightage value. Then, the values are normalized and calculated to get a Performance value based on the performance value raking assigned to each filler material using software, as shown in Table 4.17. Sea sand ranked first because of its availability and cost compared to its counterparts, followed by silica nanoparticles and ceramic particles.

Table 4.17 Ranking table for filler with core

Filler	Performance value	Rank
Sea Sand	4.4	1

Silica Nanoparticles	4.0	2
Ceramic Particles	3.8	3
Cenosphere	3.4	4
Fly Ash	2.4	5

4.2 Results of FE modeling on Sandwich composites

Mesh convergence Analysis

In Finite Element Analysis (FEA), mesh convergence analysis is crucial in ensuring that the numerical results are independent of the discretization factors, including element size. To determine the ideal mesh size where the results stabilize and show convergence, analyze how the values of residual energy change with varying element sizes. Quad-mesh is chosen for meshing, and the element S4R, a 4-node double curved with thin or thick solids, hourglass control, finite membrane strains, and decreased integration, is used for meshing the plate, and R3D4, a 4-node 3-D bilinear rigid quadrilateral, is used for meshing the impactor. The total number of elements and nodes employed in this study is 3939 and 1944, respectively. A mesh convergence analysis was conducted using a range of mesh sizes from 3 mm to 10 mm with an increment rate of 1 mm to choose an optimal mesh size in terms of convergence and computing efficiency.

The FE model simulates the sandwich composite structure's impact response under specified loading conditions. Boundary conditions and material properties are constant throughout all simulations. Once the simulation is complete, residual energy data are noted for every mesh configuration. The objective is to determine the element size at which the findings converge, meaning that increasing the mesh's fineness does not appreciably change the outcomes. In this analysis, we will assume that the findings have converged if the residual energy differs between consecutive element sizes of less than 1%. Initially, the percentage difference between successive element sizes for residual energy will be determined to perform mesh convergence analysis. The results

show that residual energy begins to stabilize at about the element size of 5 mm based on the calculated percentage differences. The percentage disparities decline beyond this point, suggesting convergence, as shown in Figure 4.9. The element size of 5 mm appears to be the optimal choice for this mesh convergence analysis, as it shows a consistent trend toward convergence for both residual energies. By completing this mesh convergence investigation, we have determined the ideal mesh size (5 mm) that yields converged results for the specified simulation. This analysis helps determine the proper mesh density for upcoming simulations and ensures the accuracy and dependability of the Finite Element Analysis (FEA) model.

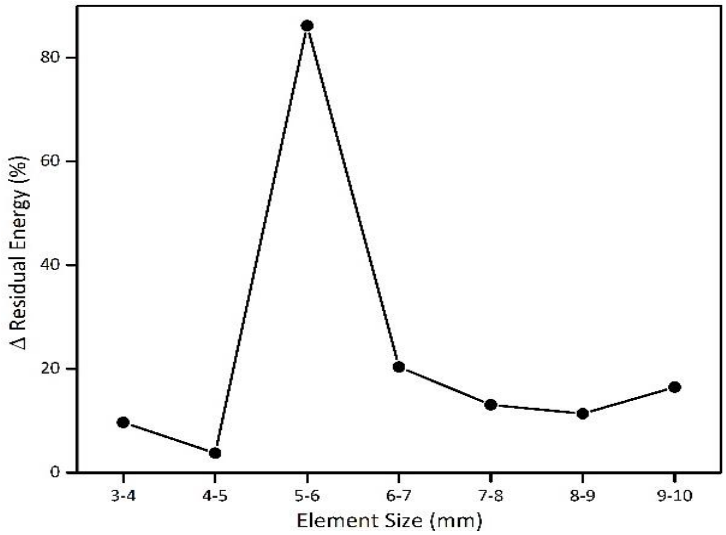

Figure 4. 9 Mesh convergence for the difference in residual energy % with Element size.

4.2.1 Influence of Composition of Filler on Sandwich Structure

Figure 4.10 gives the energy absorbed for different percentages of sand (0%,10%,20%,30%) with core materials Epoxy and Rubber for different velocities like 10m/sec, 50m/sec, 100m/sec, 350m/sec. The percentage increase of energy absorption from 0 to 30 percent is 5.26% for FESF and 5.21% for FRSF at a low velocity of 10 m/sec. Similarly, 1.35% for FESF and 8.44% for FRSF at an Intermediate velocity of

50 m/sec, 11.30% for FESF, and 5.07% for FRSF at a high velocity of 100m/sec and 9.34% for FESF and 1.37% for FRSF at high velocity 350 m/sec. The bullet loses energy when it strikes the composite by decreasing its KE, dispersed in damages like matrix cracking, fiber breaking, etc. The projectile velocity is lowered, referred to as residual velocity (Vr). After transferring the KE, the impactor may move inside and get stuck in the composite with less impact velocity or rebound at a lesser velocity. If the impactor struck inside the laminate, then Vr=0.

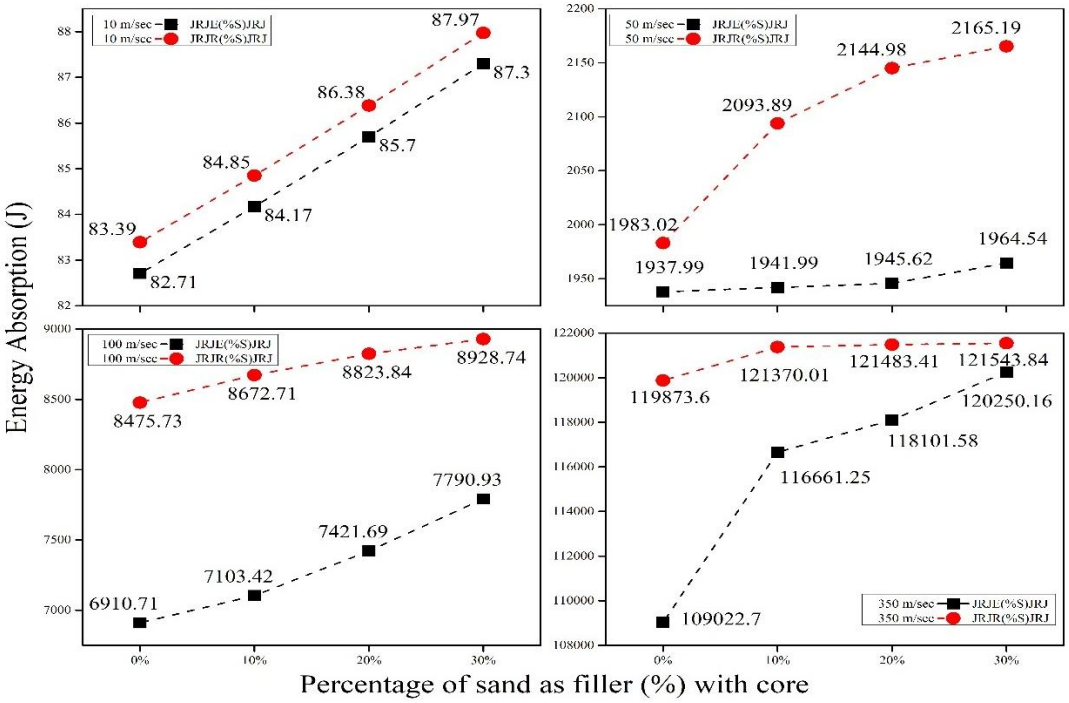

Figure 4.10 Energy absorption for FESF and FRSF for different Velocity a) Low (10 m/sec), b) Intermediate (50 m/sec), c) High (100 m/sec), and d) Ballistic (350 m/sec)

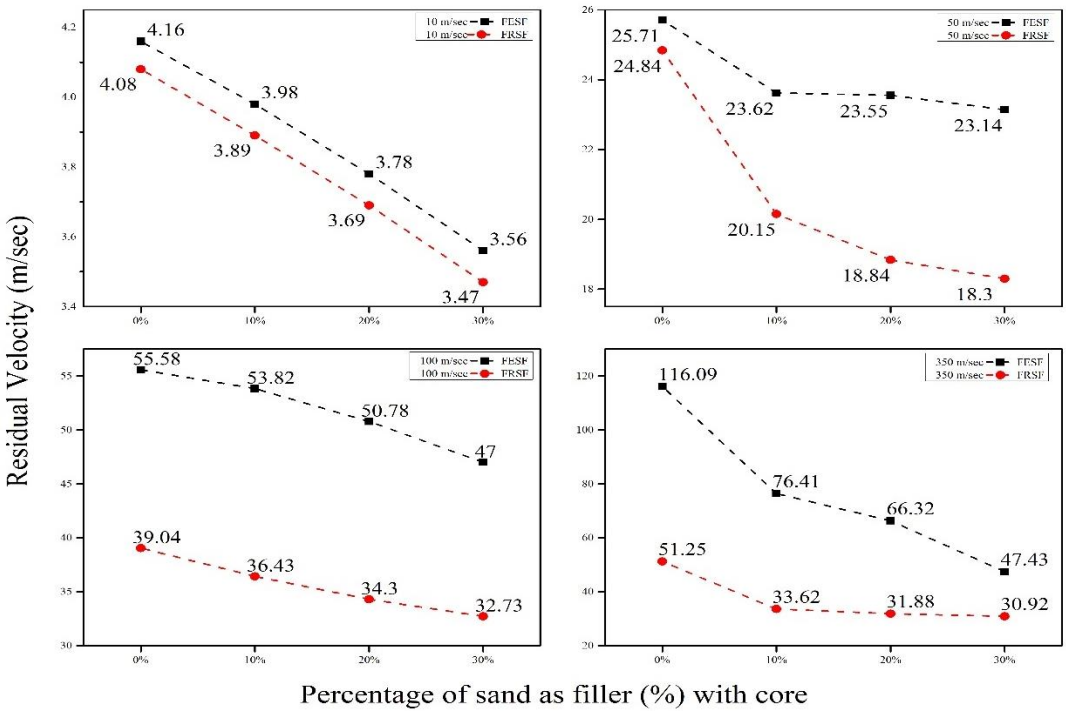

Figure 4.11 Residual Velocity for FESF and FRSF for different Velocity a) Low (10 m/sec), b) Intermediate (50 m/sec), c) High (100 m/sec), and d) Ballistic (350 m/sec)

Figure 4.11 shows the residual velocity for different percentages of sand (0%,10%,20%,30%) with core materials Epoxy and Rubber for different velocities like 10m/sec, 50m/sec, 100m/sec, 350m/sec. The percentage decrease of residual energy from 0 to 30 percent is 14.42% for FESF and 14.95% for FRSF at a low velocity of 10 m/sec. Similarly, 10% for FESF and 26.33% for FRSF at an Intermediate velocity of 50 m/sec, 15.44% for FESF, and 16.16% for FRSF at a high velocity of 100m/sec and 59.14% for FESF, and 39.67% for FRSF at a ballistic velocity of 350 m/sec residual velocity shows the more significant value.

4.2.2 Influence of core thickness on sandwich structure

Core thickness can significantly influence the impact behavior of a sandwich structure under ballistic impact. A thicker core provides excellent energy absorption

and improved resistance to penetration. However, a thinner core can reduce weight and improve flexibility, making it better suited for specific applications. The choice of core thickness depends on the application's particular requirements and trade-offs, such as weight, stiffness, and resistance to impact damage. It is essential to consider the properties of the core material and its bonding ability with skins to optimize the sandwich structure's overall performance under ballistic impact. 40% of sand with the core material for different compositions shows better energy absorption capabilities. The composition shows better energy absorption and the ballistic velocity of 350 m/s is limited and taken for further study; the high-velocity impact response of sandwich composites of different thicknesses at 350 m/sec impact velocity. Figure 4.12 (a) and (b) indicate the effect of KE and deformation for various configurations for FE30F and FR30F, respectively. The initial velocity (350m/sec) is the same for all configurations. Equation (1) gives the energy Ei (Joules) at which the target gets hit by the impactor.

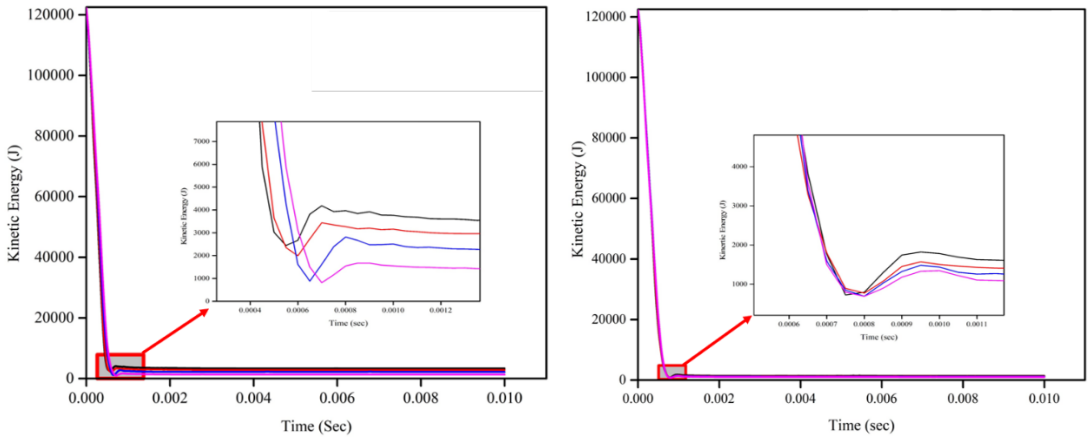

a) b)

Figure 4.12 Variation in Kinetic energy (J), (a) FE30F, (b) FR30F

The effect of core thickness on sandwich structure FE30F under ballistic-velocity impact loading (350 m/sec) can be analyzed using Figures 4.12 (a) and (b). The main conclusion drawn from the graph is that as the core thickness increases, it is observed to increase energy absorption and decrease residual velocity. This could

indicate that thicker cores are better able to absorb and dissipate energy, resulting in a lower residual velocity after impact. However, it's challenging to provide a definitive answer without seeing the graph and understanding the specifics of the experiment. It's important to carefully analyze and interpret data to draw accurate conclusions about the behavior of a material or structure under specific loading conditions. The figure shows that as the laminate thickness improved, the Vr decreased, increasing EA. The trend in variance in residual energy and velocity for different thicknesses of the sandwich structure remains the same for all the configurations. In addition, it has been discovered that a sandwich structure with a core thickness of 30 mm has less residual velocity and absorbs more energy.

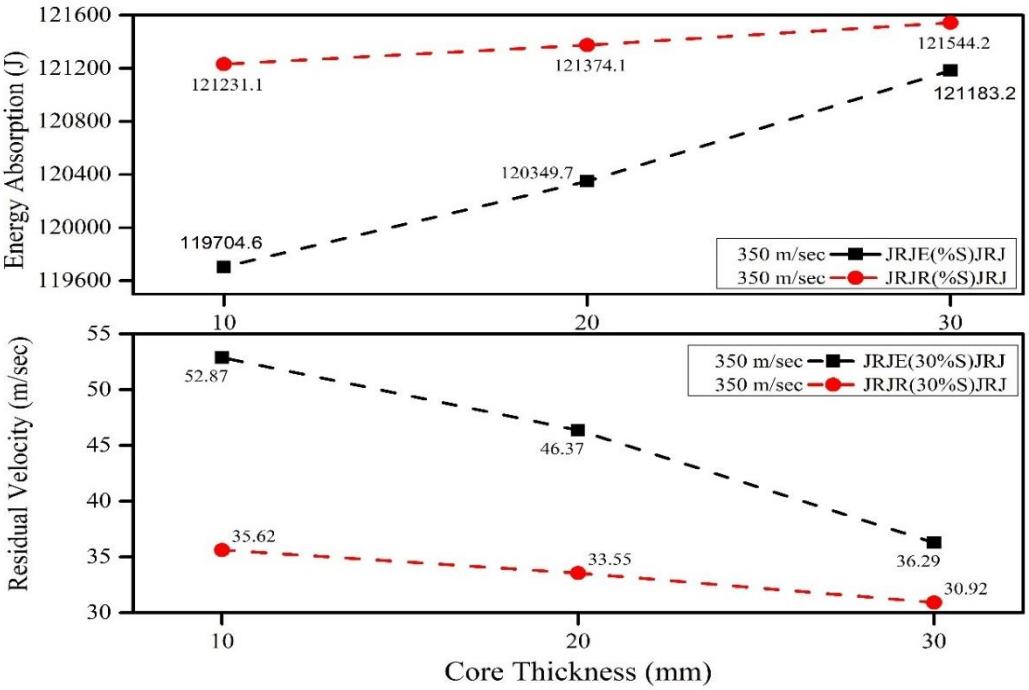

Figure 4.13 (a)Energy Absorption for different core thicknesses, (b) Residual velocity of different core thicknesses

Figure 4.13 shows the percentage increase of energy absorption for different core thicknesses (10, 20, 30mm) is 0.37% for FR30F and 1.70% for FE30F. Similarly, the percentage decrease in residual velocity is 21.15 % for FR30F and 59.33% for

FE40F. Figure 4.13 shows that an increase in core thickness Vr decreases with Ea improvement. However, for different thicknesses, the difference in Vr and Ea follows a similar pattern for all the configurations.

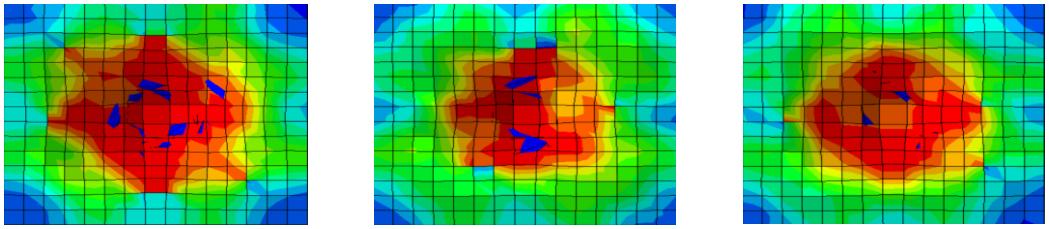

a) b) c)

Figure 4.14 Damage Behaviour for different core thicknesses in FESF30 a) 10mm, b) 20mm, c) 30mm.

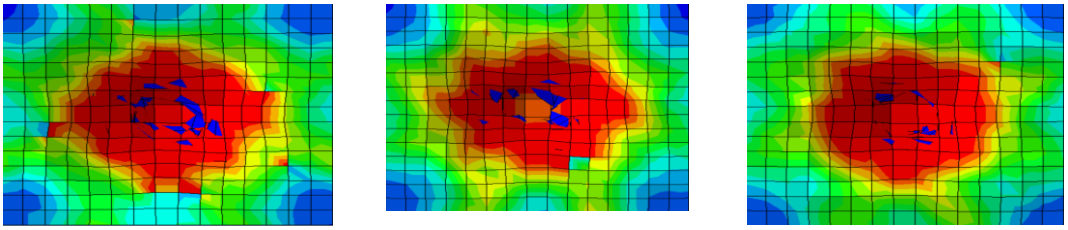

a) b) c)

Figure 4.15 Damage Behaviour for different core thicknesses in FRSF30: a) 10mm, b) 20mm, and c) 30mm.

Figures 4.14 and 4.15 illustrate the damage caused by projectile striking sandwich structures FE30F and FR30F for different core thicknesses. Damage analysis was performed for this study's ballistic velocity of impact (350m/s). Results reveal that the sandwich structure impacted by the projectile causes an increase in the level of damage with decreased localized damage because the damage spreads widely from the area of impact. Increasing the core thickness reduces the extent of damage in both cases, but the extent of damage is more significant in FE30F compared to FR30F. This may be because rubber as a core material can help prevent further progression of damage in a composite structure. Rubber's elastic nature allows it to absorb and distribute stress and strain, reducing the likelihood of cracks or fractures propagating through the

material. This is why rubber is often used as a shock-absorbing material in applications where impact or vibration is a concern. Finally, the comparative analysis on the impact responses of sandwich composites with stiff and compliant core materials suggested that the core material used substantially impacts the composite's behavior. Sandwich composites with stiff cores demonstrated increased stiffness and resistance to deformation, making them appropriate for structural integrity and load-bearing capacity applications. Sandwich composites with compliant cores, on the other hand, demonstrated greater energy absorption characteristics, making them appropriate for applications that prioritize impact mitigation and damage tolerance. When selecting between stiff and compliant core materials, the study stressed the need to consider weight, cost, and particular application requirements. Compliance core materials offer energy absorption, impact resistance, weight reduction, flexibility, and vibration-damping advantages. However, it is essential to consider the application's specific requirements, as compliant cores may have structural rigidity or load-bearing capacity limitations compared to stiff cores.

FE for ballistic Impact

The energy absorption values were determined by the use of mechanical and physical properties obtained from the rule of mixture (RoM) in the finite element (FE) analysis depicted in the figure. In accordance with NIJ standards, ballistic impacts with 7.62mm bullets (9.63 grams) impacted at 200, 275, and 350 m/sec were examined in this study. The different percentages of sea sand (0%, 10%, 20%, and 30%) and the core thicknesses (10 mm, 20 mm, and 30 mm) were included in the material configurations. Figure 4.15 shows the energy absorption for 10mm and 20mm thick core.

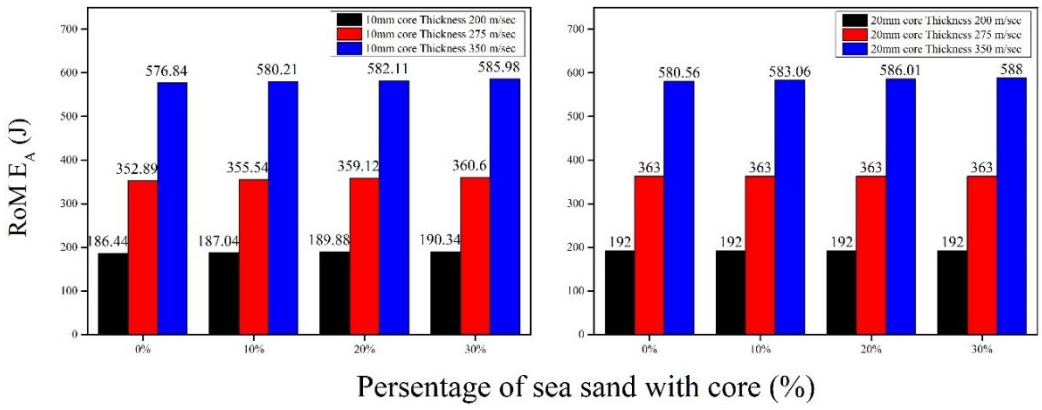

a) b)

Figure 4.16 Energy Absorption for different core thicknesses at 200, 275, 350 m/sec a) 10mm b) 20mm

From Figure 4.16, it was evident from the results that the composite's ability to absorb energy increased with the increase in the percentage of sea sand and core thickness. The energy absorption values for the sandwich composite with a 10mm core demonstrate that the energy absorption capacity increases as the percentage of sea sand filler increases. At 200 m/sec, the energy absorption increases from 186.44 J for 0% sea sand to 190.34 J for 30% sea sand, corresponding to approximately 2.09%. At 275 m/sec, the energy absorption rises from 352.89 J at 0% sea sand to 360.60 J at 30% sea sand, indicating an increase of 2.19%. Finally, at 350 m/sec, the absorption values increase from 576.84 J with 0% sea sand to 585.98 J with 30% sea sand, an increase of 1.58%. The results indicate a consistent trend increase in energy absorption with the addition of sea sand filler across all tested velocities. The increased energy absorption can be attributed to the improved structural integrity and energy-dissipating characteristics of sea sand within the composite matrix. As the filler content increases, the composite is better able to absorb and dissipate the energy from the impacting bullet, leading to higher energy absorption values. Despite the increase in energy absorption, the composite still fails to prevent bullet perforation at all tested velocities, indicating

that the current thickness and composition may not be sufficient for effective ballistic protection.

Similarly, the 20mm core demonstrates a notable relationship between the percentage of sea sand filler and the material's ability to absorb energy during ballistic impact. At 200 m/sec and 275 m/sec, the energy absorption remains consistent across all sea sand compositions, with values at 192 J and 363 J. This indicates that the composite successfully arrests the bullet at these velocities. However, at 350 m/sec, the energy absorption values show variation with the sea sand composition. For 10% and 20% sea sand, there are slight increases in energy absorption of 0.43% and 0.33%. The bullet still perforates the composite at this velocity. In contrast, when the composition reaches 30% sea sand, the energy absorption increases to 588 J, a 0.34% increase over the previous composition. Importantly, this adjustment leads to the successful arrest of the bullet at 350 m/sec, showcasing the enhanced performance provided by the higher filler content. The transition from perforation to arresting the bullet at 350 m/sec with 30% sea sand underscores the critical role that filler composition plays in improving ballistic resistance. This shows that even though the material was able to absorb the bullet's kinetic energy, the energy was not dissipated efficiently enough to prevent damage to the back skin.

For the thickest core of 30mm, the sandwich composite could arrest the bullet for all the velocities (200 m/sec, 275 m/sec, and 350 m/sec). Even though the bullet was arrested, there was noticeable back skin damage for sea sand compositions of 0%, 10%, and 20%, indicating that the energy was absorbed but not completely dissipated without damaging the structure. Remarkably, the 30mm core composed of 30% sea sand could arrest the bullet without damaging the back skin, highlighting the effectiveness of this configuration in dissipating energy within the sandwich composite structure.

The optimal configuration observed was a 30mm thick core with 30% sea sand, which provided maximum energy absorption while minimizing damage by arresting the bullet within the sandwich composite.

4.2.3 Optimization of process parameters

Figure 4.17 shows the ballistic impact behavior of (JRJ-ES-JRJ)0, (JRJ-ES-JRJ)15, and (JRJ-ES-JRJ)30 hybrid sandwich composite for different core thicknesses (10, 20, 30 mm) subjected to impact at 350 mps using different shaped projectiles like flat (F), conical (C), and hemispherical (H). The projectile's KE (kinetic energy) and velocity are reduced when they strike the target, which is dispersed as damage. Reduced velocity is termed the projectile's residual velocity (VR). After imparting all of its KE, the projectile may rebound or penetrate at a lesser velocity than the impact velocity. A projectile can also arrest the composite, losing all of its KE, and the residual velocity will become zero. The projectile residual velocity is significant because it determines how much energy is absorbed.

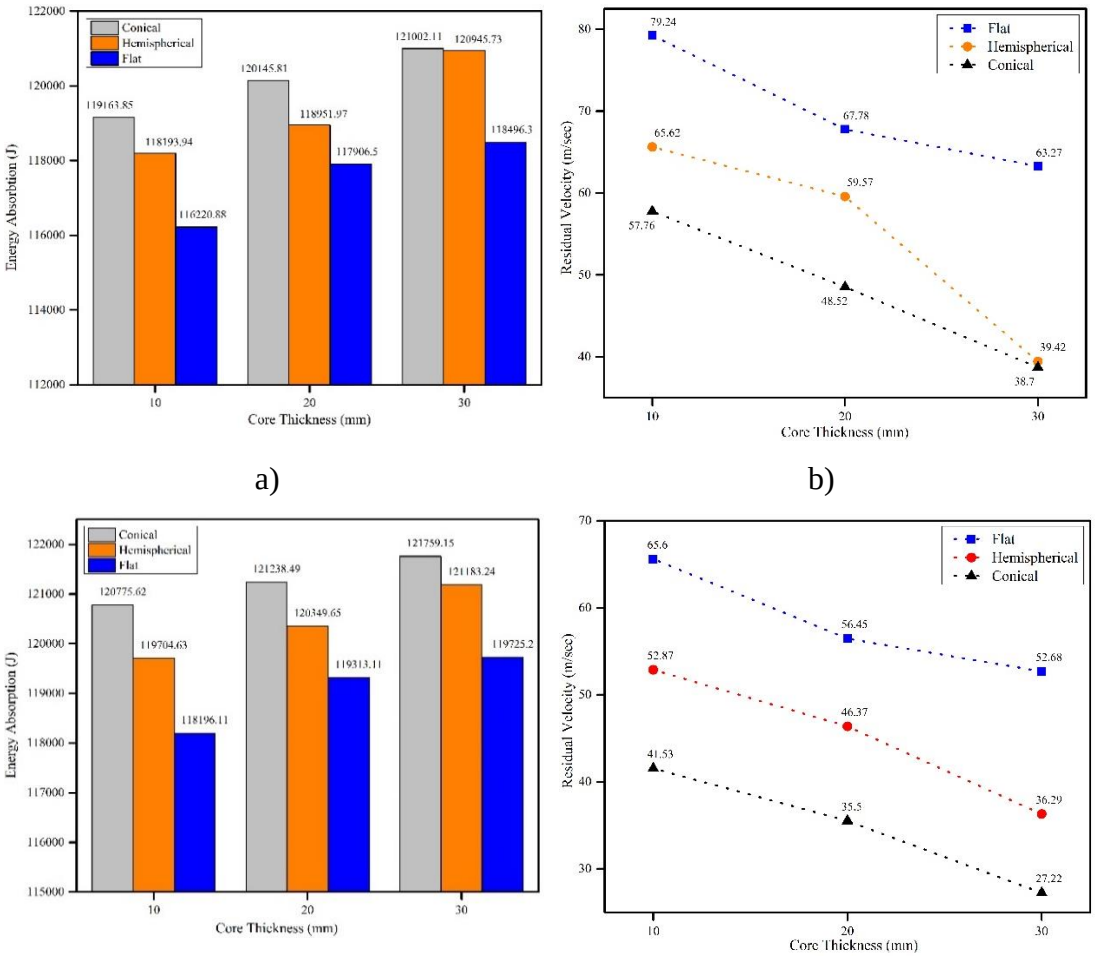

a) b)

c) d)

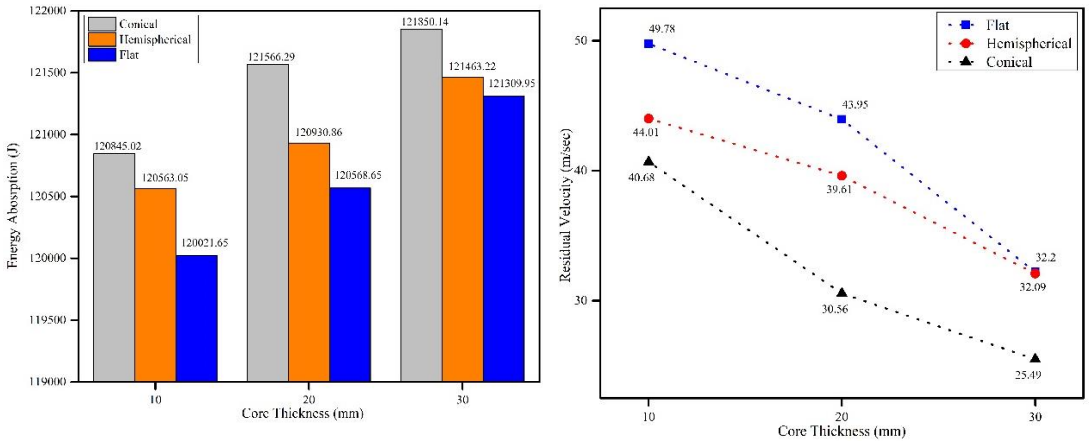

e) f)

Figure 4.17 Represents the Energy absorption, Residual velocity Vs. Core thickness for (a, b) conical, (b, c) hemispherical, (e, f) flat projectile

Figure 4.17 shows that when the composition of filler and the thickness of the core is increased, the energy absorption increases with a decrease in the residual velocity; no change in the pattern is observed for a different composition and core thickness of JRJE(%S)JRJ hybrid sandwich composite when different types of projectiles used. In addition, it has been determined that JRJE(%S)JRJ hybrid sandwich composite has a core thickness of 30mm and a filler composition of 30% that absorbs maximum energy with reduced residual velocity. Maximum energy is absorbed by a conical shape projectile, followed by hemispherical and flat projectiles.

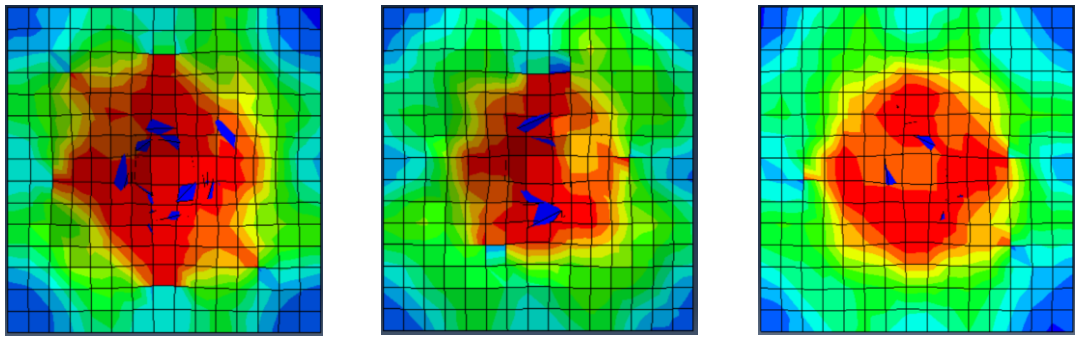

a) b) c)

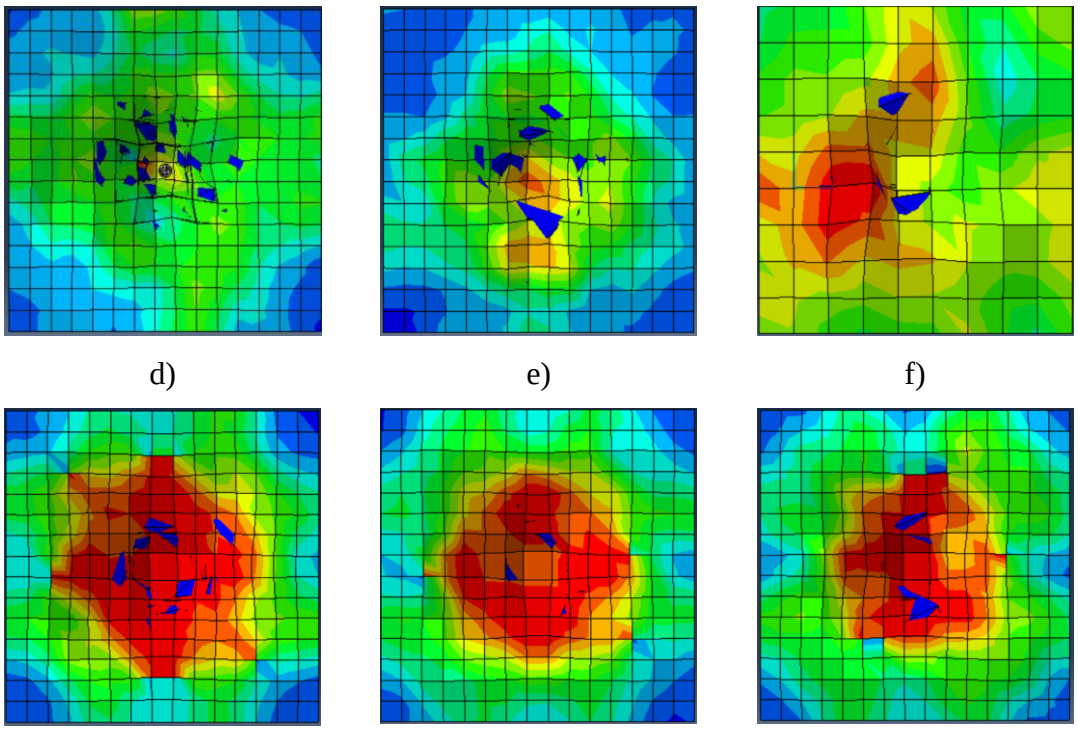

d) e) f)

g) h) i)

Figure 4.18 (JRJ-ES-JRJ)30 hybrid composite at 350 m/sec for 10,20,30mm core thickness, respectively. (a, b, c) hemispherical, (d, e, f) flat, and (g, h, i) conical shape projectile.

Figure 4.18 displays the damage that different projectiles impact the (JRJ-ES-JRJ)30 hybrid sandwich composite. A damage study was conducted for 30% of the filler composition of all the composite configurations for different core thicknesses at 350 mps. Figure 4.18 (a) shows the damage level induced by the hemispherical shape projectile for 10mm core thickness at 30% filler composition. Figure 4.18 (b) for 15mm and Figure 4.17 (c) for 20mm core thickness. Similarly, Figure 4.18 (d), (e), (f) for flat shape projectile and Figure 4.18 (g), (h), (i) for conical shape projectile. The analysis shows that whenever a conical projectile hits the composite, it undergoes localized damage to a lower extent than hemispherical and flat projectiles. When a hemispherical

projectile hits the composite, localized damage is not found, and the amount of damage spreads widely from the area of impact.

Moreover, more damage happens to the composite when it is affected by a flat projectile. The area of damage decreases with an increase in thickness; the area of damage is calculated for all the projectile shapes and the thicknesses of the core. The flat-shaped projectile shows the maximum area of damage, in contrast to the conical and hemispherical projectiles. The maximum area of damage is 15323mm^2 in $(JRJ\text{-}ES\text{-}JRJ)_{30}$ for 10mm thickness with a flat-shaped projectile, and the minimum area of damage is 9740mm^2 for 30mm thickness with the conical-shaped projectile. The damage study's results can state that the projectile's contact area with the composite is directly proportional to the level of damage.

4.2.3.1 Taguchi's Design of Experiment (DOE) Technique

Taguchi's method is an organized methodology widely utilized to optimize the design and ensure quality and performance. Taguchi's orthogonal array concept assists the variations of the experiments or condensed irregularities with an ideal design parameter setting that controls the process. Taguchi's concept gives an effective and modest methodology to determine the outstanding choice of designs for performance, quality, and cost. Taguchi's design of experiments (DOE) requires minimal experimental sets. In this case, the three factors with three levels were chosen, listed in Table 4.18. The effect of the process parameters is evaluated by analyzing variance and means of outcomes of experiments.

Table 4.18 Levels for various control factors

Factors	Level 1	Level 2	Level 3
Composition (%) of filler	0	15	30
Projectile shape	Flat	Hemispherical	Conical
Thickness of Core	10	20	30

A numerical condition was laid out to conjecture the energy absorption capacity of the said composite by multiple linear regressions. Consequently, the fundamental point of the ongoing review is to break down the impact of boundaries like the filler composition, the projectile's shape, and the core's thickness on the energy absorption capacity of said composite utilizing the Taguchi method.

The ballistic impact simulations were conducted per the design of experiments (DOE) by Taguchi's L27 orthogonal array (Table 4.19). The selection of Taguchi's L27 orthogonal array is based on its degree of freedom, which must be more than or equal to the sum of process parameters. The energy absorption process parameters/factors selected for the experiment were the composite's composition, the projectile's shape, and the target's thickness. The process parameters and their levels utilized are listed in Table 4.19. In Taguchi's orthogonal array, individual experiments are represented by rows, and columns represent the different parameters. In this technique, the results obtained through simulation were converted into a signal-to-noise (S/N) ratio; further, the S/N ratio was utilized to determine the quality characteristics. In the current work, the quality characteristic instigated is 'the-higher-the-better' for the energy absorption of the said composites, as higher values of energy absorption are necessary. The results obtained by the simulation analysis were inputted into Taguchi's analysis, and the S/N ratio was determined.

Table 4.19 Design of Experiments using Taguchi's L27 orthogonal array.

Sl No.	Composition of Filler	Shape of Projectile	Thickness of Core	Energy Absorption (J)	SNRA1
1	0	F	10	116220.88	101.3057
2	0	F	20	117906.5	101.4308
3	0	F	30	118496.31	101.4741
4	0	H	10	118193.94	101.4519
5	0	H	20	118951.97	101.5074
6	0	H	30	120945.73	101.6518

7	0	C	10	119163.85	101.5229
8	0	C	20	120145.81	101.5942
9	0	C	30	121002.11	101.6559
10	15	F	10	118196.11	101.4521
11	15	F	20	119313.11	101.5338
12	15	F	30	119725.29	101.5637
13	15	H	10	118193.94	101.4519
14	15	H	20	118951.97	101.5074
15	15	H	30	120945.73	101.6518
16	15	C	10	120775.62	101.6396
17	15	C	20	121239.49	101.6729
18	15	C	30	121759.15	101.71
19	30	F	10	120021.65	101.5852
20	30	F	20	120568.65	101.6247
21	30	F	30	121309.95	101.6779
22	30	H	10	120563.05	101.6243
23	30	H	20	120930.86	101.6507
24	30	H	30	121463.22	101.6889
25	30	C	10	120845.02	101.6446
26	30	C	20	121566.29	101.6963
27	30	C	30	121850.14	101.7165

ANOVA (analysis of variance) analysis is carried out to find the statistically significant process parameters. ANOVA, along with S/N ratio analysis, is likely to attain the forecasting of the optimal mixture of energy absorption parameters to an acceptable level of accuracy. Table 4.19 also displays the response for S/N ratios and the average characteristics for each parameter level. Minitab software has been utilized

to plot the Mean-response graphs and determine each parameter's contribution percentage.

Taguchi's analysis cannot analyze the individual parameters; thus, ANOVA is employed to analyze each parameter. ANOVA examines the influence of parameters, such as the filler's composition, the projectile's shape, the core's thickness, and its optimal level. ANOVA is performed for the significance level of 0.05. i.e., for the confidence level of 95 % and above. Carrying out the ANOVA will decide the influence of parameters and their percentage on the energy absorption of said composite for each of its values. The analysis outcomes are given in Table 4.20 for the energy absorption, process parameters, and their levels. Also, the percentage of individual factors contributing to energy absorption is determined.

Table 4.20 Analysis of variance (ANOVA) for means for the energy absorption

Source	**DF**	**Adj SS**	**Adj MS**	**F-Value**	**P-Value**	**% Contribution**
Composition of filler	2	18253991	9126996	24.43	0.000	33.7
Shape of Projectile	2	15350348	7675174	20.54	0.000	28.4
The thickness of the core	2	13050153	6525077	17.46	0.000	24.1
Error	20	7472439	373622			13.8
Total	26	54126931				100.0

From the outcomes of the ANOVA, it is observed that the composition of filler is the most influencing parameter, i.e., by 33.7%. The energy absorption depends on the properties of the material. Followed by composition, the thickness of the core

(24.1%) and the shape of the projectile (28.4%) will also influence the energy absorption of the composite.

The outcomes from the FE simulations were the inputs for Taguchi's analysis. The results were transformed into the S/N ratio (signal to noise), which describes the quality of the process. The "Larger is better" quality characteristic is employed to analyze the energy absorption data.

The main effects plot for S/N ratios for energy absorption process parameters is shown in Figure 4.18. The filler compositions significantly impact energy absorption, followed by the core's thickness and the shape of the projectile. From Figure 4.19, it is also observed that as the composition and thickness of the core increase, the energy absorption capacity increases. However, the energy lost by the flat bullet is lower, whereas the conical shape of the bullet will lose more energy, so higher energy absorption is obtained.

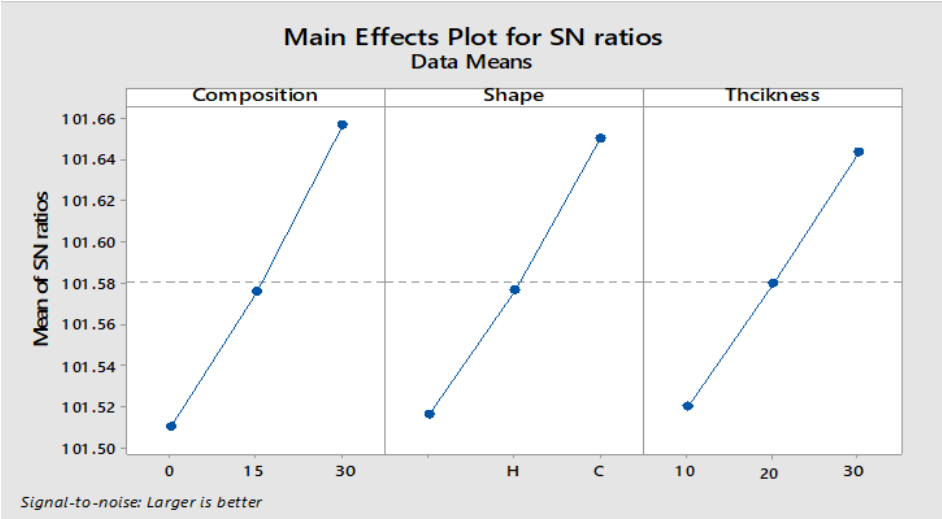

Figure 4.19 Main effect plots for SN ratios-energy absorption of composites.

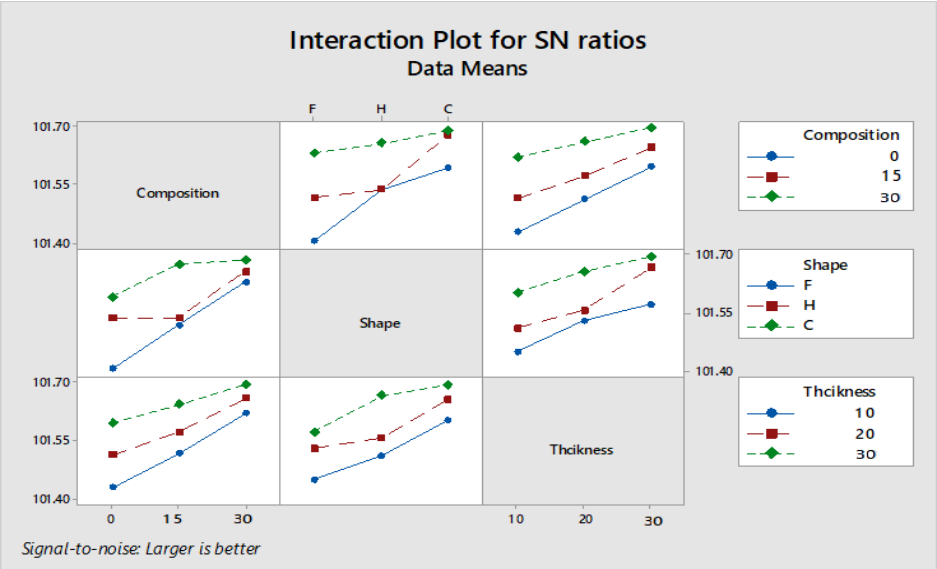

Figure 4.20 Interaction plots-energy absorption of composites.

Fig 4.20 shows the interaction of process parameters on the energy absorption of the said composites. It is observed that as the composition of the filler material increases, the energy absorption increases. The highest energy absorption can be obtained for 30% composition, 30mm thickness, and from the conical-shaped projectile. Also, the interaction of other process parameters shows the same results.

Using the Minitab statistical program, a multiple linear regression model was developed for the energy absorption of composites. The developed model gives the linear dependency of the unidentified variable on the identified variables. In the present work, the linear dependence of energy absorption of the composite can be noticed by the process parameters such as filler composition and core thickness. The developed linear regression equation for the energy absorption is given in Equation (22):

EA= 116413 + 50.3 X Composition of filler + 170.3 X Core thickness (22)

This expression is suitable for a specified energy regime as it covers the most influencing parameters. From the equation, the positive sign indicates that the energy absorption increases with an increment in the composite's composition and the target's thickness. Table 4.21 lists Taguchi's DOE's calculated energy absorption values using Equation (4). Table 4.21 also compares the results obtained through simulation analysis

and Taguchi's analysis. Both results were observed in close agreement with the comparison, with an error percentage of 1.4. Thus, there is a significant endorsement that the model is acceptable.

Table 4.21 Comparison of energy absorption.

Sl no	Composition	Shape	Thickness	Energy absorption (J)		% Error
				Simulation	Eq (4)	
1	0	F	10	116220.88	118116.0	1.6
2	0	F	20	117906.5	118967.5	0.9
3	0	F	30	118496.31	119819.0	1.1
4	0	H	10	118193.94	118116.0	-0.1
5	0	H	20	118951.97	118967.5	0.0
6	0	H	30	120945.73	119819.0	-0.9
7	0	C	10	119163.85	118116.0	-0.9
8	0	C	20	120145.81	118967.5	-1.0
9	0	C	30	121002.11	119819.0	-1.0
10	15	F	10	118196.11	119122.0	0.8
11	15	F	20	119313.11	119973.5	0.6
12	15	F	30	119725.29	120825.0	0.9
13	15	H	10	118193.94	119122.0	0.8
14	15	H	20	118951.97	119973.5	0.9
15	15	H	30	120945.73	120825.0	-0.1
16	15	C	10	120775.62	119122.0	-1.4
17	15	C	20	121239.49	119973.5	-1.1
18	15	C	30	121759.15	120825.0	-0.8
19	30	F	10	120021.65	120128.0	0.1
20	30	F	20	120568.65	120979.5	0.3
21	30	F	30	121309.95	121831.0	0.4

22	30	H	10	120563.05	120128.0	-0.4
23	30	H	20	120930.86	120979.5	0.0
24	30	H	30	121463.22	121831.0	0.3
25	30	C	10	120845.02	120128.0	-0.6
26	30	C	20	121566.29	120979.5	-0.5
27	30	C	30	121850.14	121831.0	0.0

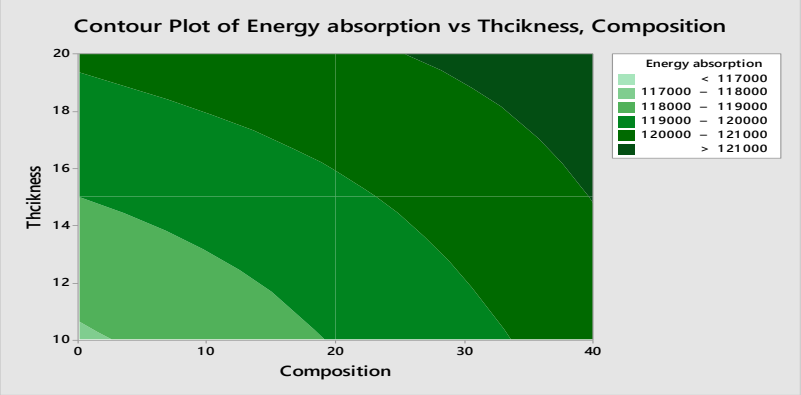

Figure 4.21 Contour plot for energy absorption of composites-Thickness (mm) Vs. Composition (%).

Figure 4.21 shows the contour plots indicating the relationship between the process and its parameters, which influence the energy absorption capacity of the composites. From Figure 4.21, it was noticed that high energy absorption was obtained at higher levels of thickness of the core and composition of fillers in the mentioned composites.

4.3 Experimental Investigation on Cores and Sandwiches

FG cores and their sandwich are prepared and tested under different loading conditions, as discussed in the following section.

4.3.1 Results of Gradation test FG cores

For FGPC reinforced with sea sand, gradation analysis is performed using two tests (burn-out and weight technique). For both methods, layer-1 refers to the top layer,

which is an epoxy layer, while layer-4 refers to the bottom layer, which is rich in sea sand for both the methods. Table 4.22 illustrates the burn-out test results, and Table 4.23 displays the weight method results. At the same time, a comparison of the sea sand present in FGPC samples for both experiments is presented in Figure 4.22. Figure 4.23 shows the Wt.% of sea sand in each layer. Sea sand distribution in layers, as determined by the weight method for larger weight fractions of sea sand, is illustrated in Figure 4.24.

Table 4.22 Burn-out test results

Sea Sand %	Slice No.	Average Wt. of the sample (gm)	Average Wt. of residue (gm)	% Wt. of sea sand	Total Weight of Sea Sand %
10%	1	0.256	0.000	0.000	9.046
	2	0.256	0.000	0.000	
	3	0.256	0.000	0.000	
	4	0.284	0.026	9.046	
20%	1	0.256	0.000	0.000	19.137
	2	0.256	0.000	0.000	
	3	0.274	0.019	6.934	
	4	0.295	0.036	12.203	
30%	1	0.256	0.000	0.000	29.370
	2	0.273	0.014	5.128	
	3	0.285	0.034	11.895	
	4	0.296	0.037	12.348	

Table 4.23 Weight method results

Sea Sand %	Slice No.	Average Wt. of the sample with sea sand (gm)	Average Wt. of Neat Epoxy (gm)	% Wt. of sea sand	Total Weight of Sea Sand %
10%	1	0.256	0.256	0.000	9.827
	2	0.256	0.256	0.000	
	3	0.256	0.256	0.000	
	4	0.284	0.256	9.827	
20%	1	0.256	0.256	0.000	19.819
	2	0.256	0.256	0.000	
	3	0.274	0.256	6.569	
	4	0.295	0.256	13.250	
30%	1	0.256	0.256	0.000	29.916
	2	0.273	0.256	6.227	
	3	0.285	0.256	10.175	
	4	0.296	0.256	13.514	

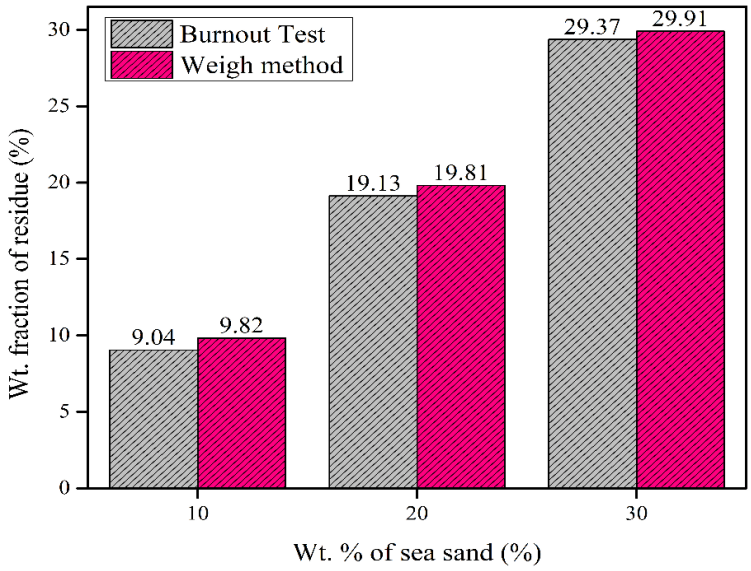

Figure 4.22 Comparison of sea sand content present in Burn-out and weight method

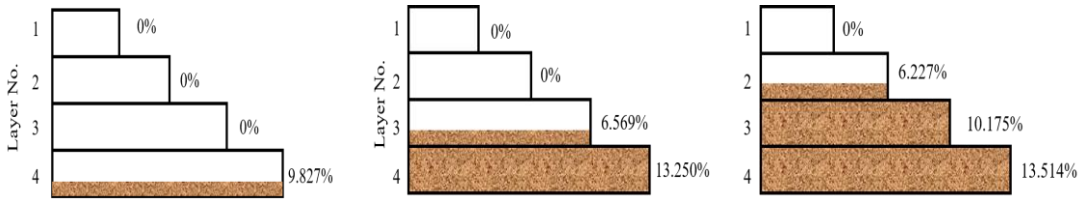

a) b) c)

Figure 4.23 Sea sand distribution in layers obtained from the weight method (a) 10%, (b) 20%, and (c) 30% composition

Tables 4.19 and 4.20 show that as the sea sand composition increases, the distribution occurs from the bottom of the layer and moves toward the top layers. Because of the higher density of sea sand than the epoxy, the sea sand moves towards the bottom of the layer, starting its settlement at layer four and moving towards the upper layers. Figure 4.22 illustrates both methods significantly matched each other. The loss of sand particles throughout the testing process could cause a slight deviation in burn-out method values. Figure 4.23 shows that the top layer is neat epoxy in all cases, and as the composition increases, the filling layers also increase from the bottom side. Figure 4.24 quantifies the degree of gradation in the processed FGPC samples.

Epoxy/ 30% sea sand composites were burnt to remove the epoxy, and the remaining residue of sea sand was collected from each layer, as seen in Figure 4.24. A quadratic equation may be used for curve fitting to model the variation of sea sand (30%) composition along the thickness of the sample. It was observed that the composite is a "quadratic functionally graded" composite; this means that the variation can be modeled mathematically by a quadratic functional equation.

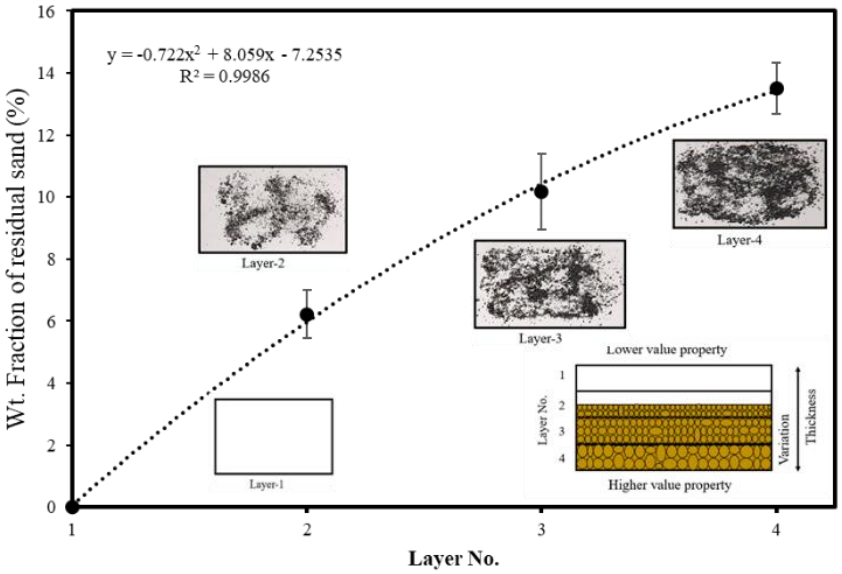

Figure 4.24 30% sea sand composition is burnt to remove the epoxy, and the remaining residue of sea sand was collected from each layer.

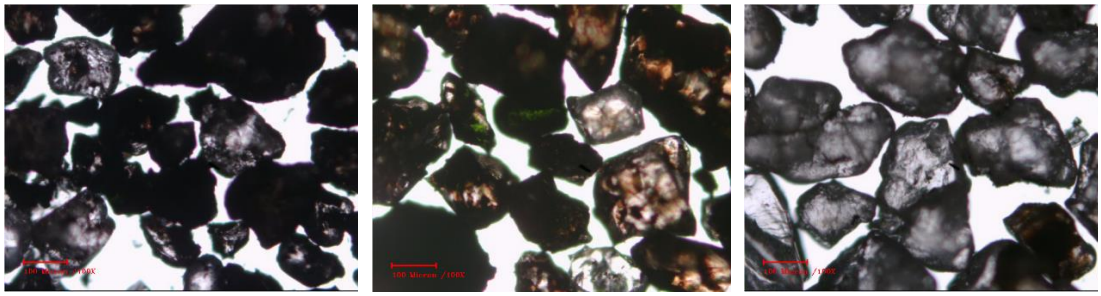

a) b) c)

Figure 4.25 Images of optical microscope showing residue of 30% sea sand composition after a burn-out test (a) layer2, (b) layer3, and (c) layer4

Figure 4.25 shows the Optical microscope images of the residue of 30%sea sand composition after the burn-out test (a) layer2, (b) layer3, and (c) layer4. The sea sand was divided into large, medium, and small-sized grains from all the layers from the optical microscope images. Using commercially available software, the average particle size is determined for each layer and found to be 149.79, 190.76, and 217.62 microns for layers 2, 3, and 4, respectively. From the figure, it is identified that as the layer of the slice increases from 2 to 4 layers, the particle size also increases, indicating

some particle gradation within the sample. This could be due to particle density, shape, or composition differences. Composite made with epoxy and sea sand particles, the concentration and size distribution of sea sand particles vary along the thickness of the composite, as shown in Figure 4.24. It was also observed that sea sand particles started to settle from the bottom during the curing, which led to a non-uniform distribution of particles along the thickness of the composite; this quantified the degree of gradation in processed FGPC samples

4.3.2 Physical properties FG cores and Skin

The amount of voids present in the composite significantly impacts its density. Equation (3) is used to determine the void content. Table 4.24 shows the sea sand-filled epoxy composite's density and void percentage. Epoxy/sea sand-filled composites have higher densities than neat epoxy, as observed. Results show that the density of the neat epoxy is lesser than the filler-added epoxy; it may be concluded that adding sea sand has increased the density of epoxy/sea sand composites. Table 4.24 also shows that for different compositions of sea sand, 0%, 10%, 20%, and 30% gives the void content of 0.182%, 0.414%, 0.420%, and 3.443%, respectively, for core materials, as shown in Figure 4.26. 30% sea sand composition gives the maximum percentage of porosity. As the sea sand composition increases to 30%, more room is created for voids, significantly increasing the void percentage.

Table 4.24 Density and Void percentage.

	Percentage of Filler composition	**Theoretical (kg/m^3)**	**Experimental**	**Void (%)**
Core	0%	1175.4	1173.26	0.182
	10%	1314.27	1308.83	0.414
	20%	1453.14	1447.03	0.420
	30%	1592.01	1557.2	3.443
Skin	JRJ (Jute-Rubber-Jute)	1054.48	986.93	6.406

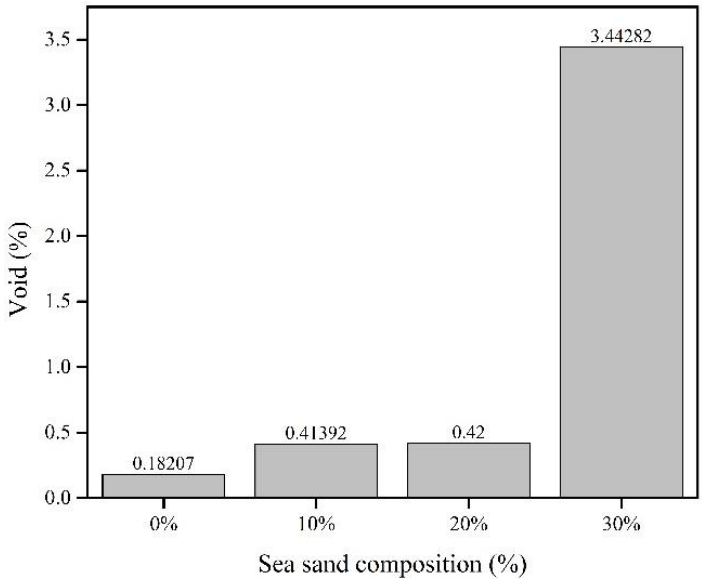

Figure 4.26 Void percentage for different compositions of sea sand

4.3.3 Mechanical properties FG cores and Skin

Shore D hardness was performed on neat epoxy, and sea sand was added as filler with different compositions like 10%,20%, and 30%. An average was calculated from five samples for each configuration to get more accurate results. Figure 4.27 shows the composites' hardness value and the impact of adding filler sea sand on the material hardness. The hardness of sea sand increases with an increase in composition. It could be because hardness is normally considered a surface property. The hardness improves as the volume fraction increases. Adding filler particles will increase the material's hardness since the material will be more resistant to plastic deformation (Bhagyashekar and Rao 2010). The hardness value of neat epoxy was 73 shores D, 79.2, 79.8, and 83.4 for 10%, 20%, and 30%, respectively. The hardness value of 30% composition of FGPC increases by 12.47% compared to neat epoxy. Table 4.25 shows the Shore D harness used to determine the hardness of core material and Shore A hardness used to find the hardness of natural rubber and flexible skin material.

Table 4.25 Hardness of Core and Skin materials

	Percentage of Filler composition	Hardness
Core (Shore D Hardness)	0%	73.00
	10%	79.20
	20%	79.80
	30%	83.40
Skin (Shore A hardness)	Natural Rubber	22.00
	JRJ (Jute-Rubber-Jute)	60.00

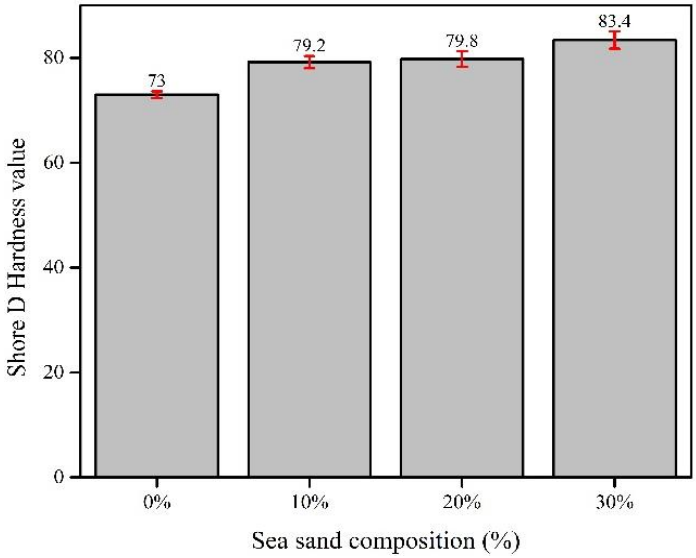

Figure 4.27 Shore D Hardness values for different compositions of sea sand

Results of Tensile testing

The specimens were prepared in accordance with ASTM standards; Table 4.26 shows the tensile test results, and Figure 4.28 shows the specific tensile strength for epoxy/sea sand composite for different compositions of sea sand. An average was calculated from five samples for each configuration to get more accurate results. As the filler percentage increased, it was found that the composite's tensile strength gradually decreased. Out of four compo\ites, neat epoxy has been found to have the highest

strength with 36.78 MPa, and epoxy with 30% sea sand shows less tensile strength with 15.24 MPa.

Table 4.26 Tensile properties

% of Filler composition	Ultimate stress (MPa)	Specific strength (kN-m)/kg	Ultimate Strain (%)	Modulus (MPa)
0%	36.78	31.34	3.00	991.21
10%	21.14	16.15	2.37	803.95
20%	15.42	10.66	2.08	786.10
30%	15.24	9.91	1.64	749.24
Skin	3.34	3.39	236.08	27.39

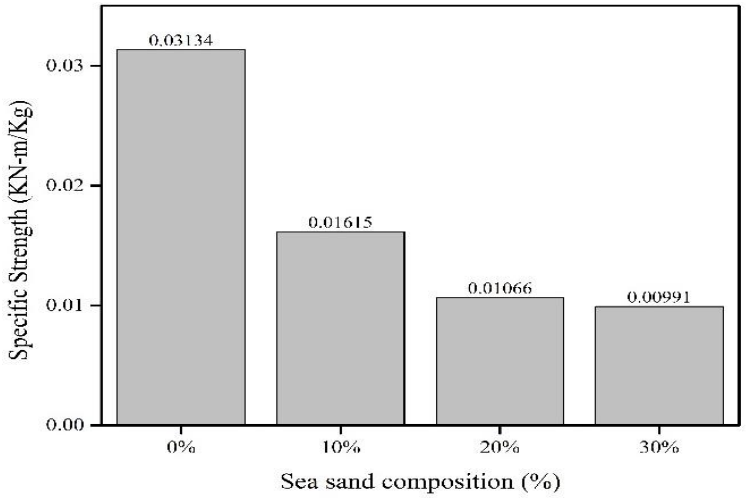

Figure 4.28 Specific strength for different compositions of sea sand

Figure 4.28 illustrates that as the composition of sea sand increased, both tensile strength and specific strength showed decremental values. It might be because of the development of agglomerates, and tensile strength decreased with increased filler loading. High filler loading enhanced filler particle agglomeration, which increased the brittleness. The hard fillers in the particle-filled composites are spread in a polymer matrix that is frequently brittle on its own; these fillers can cause discontinuity in the stress transmission across the polymer/filler interface. Sea sand acts as a stress raiser

that weakens the structure. The associated stress concentrations at the defect areas cause failure initiation. The increased filler composition makes these issues in such a composite worse. The tensile strength is quantitatively determined by the filler type, degree of load-sharing mechanisms, and bonding between matrix/fillers (Bhagyashekar and Rao 2010). The void may also be one reason for decreased tensile and specific strength; as the void increases, the tensile strength decreases.

Results of Flexural Test

The samples were prepared in accordance with ASTM standards; Table 4.27 and Figure 4.29 show the flexural test results for epoxy/sea sand composite for different compositions of sea sand. For testing, five samples were used, and an average was calculated. It was found that the composite's flexural strength gradually increases with the increase in sea sand percentage. Neat epoxy has been found to have the lowest flexural strength of 43.94 MPa, and epoxy with 30% sea sand shows maximum flexural strength of 60.97 MPa, loaded from composite side flexural strength increases by 27.93% compared to neat epoxy.

Table 4.27 Flexural Properties

	Percentage of Filler composition	**Ultimate stress (MPa)**
Flexural Properties	0%	43.94
	10%	46.94
	20%	48.84
	30%	60.97
	Skin	0.549

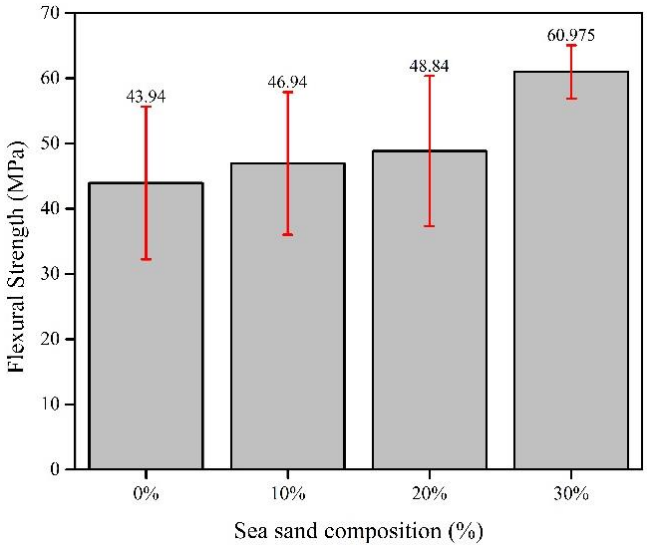

Figure 4.29 Flexural Strength for different compositions of sea sand

Figure 4.29 shows the increase in flexural strength in all the filled epoxy compared to plain epoxy; this might be because sea sand filler surfaces get direct transmission of the compressive load during the bending test and absorb greater bending load. The specimen's flexural strength is enhanced because the sea sand fillers absorb the greater bending load (Hegde et al. 2021). Hardness values confirmed that the surface of epoxy composite with sea sand is rougher than neat epoxy, indicating the filler's existence (Teh et al. 2004) and enabling additional load for fracture, contributing to the better flexural properties of all epoxy composites with sea sand.

Results of Impact testing

A Zwick Roell HIT 50P impact testing equipment with a striking pendulum velocity of 3.458 m/s and a nominal work capacity of 1 joule is used for the Izod impact test. Three samples were examined for each configuration, and an average was calculated. The FGPC impact strength is estimated using the energy absorbed, and it was found that the variation in impact strength for neat epoxy with epoxy /sea sand for different compositions like 10%, 20%, and 30%. The unnotched Izod impact strength of plain epoxy and epoxy/sea sand composite is illustrated in Figure 4.30. For skin material, the Charpy impact test uses an ISO179-1 standard with an impact velocity of

3.807m/s and an impact energy of 7.5 J. Due to the specimen's flexibility, there was no failure during the test. This suggests the ability to absorb more energy and has a higher impact strength.

Table 4.28 Impact strength of core and skin materials.

	Percentage of Filler composition	**Impact Strength**
Izod impact test (J/m)	0%	29.8
	10%	44.99
	20%	56.2
	30%	70.03
Charpy impact test (kJ/m^2)	JRJ (Jute-Rubber-Jute)	19.01

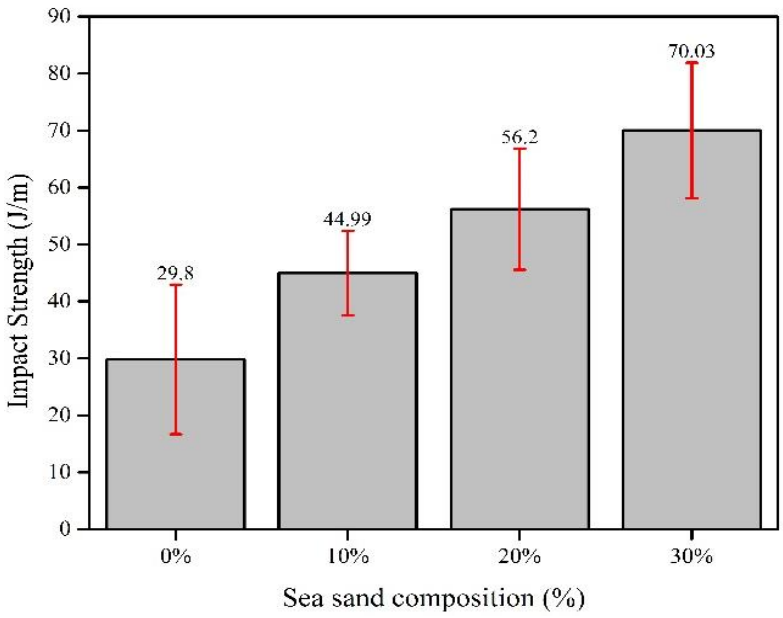

Figure 4.30 Impact Strength for different compositions of sea sand

Figure 4.30 shows that epoxy with 30% sea sand has the highest impact strength of 70.03 J/m, followed by 20%, 10%, and neat epoxy, which has an impact strength of 56.2 J/m and 44.99 J/m, respectively. The percentage of increase in impact strength

57.44%, 35.75%, and 19.74% is observed when compared with neat epoxy, which has a sea sand composition of 10%, 20%, and 30%. The filler's size, shape, and micro morphology are all factors that determine the impact strength. Impact strength is increased by the filler particle's lower aspect ratio and the polymer matrix's excellent particle dispersion. The inclusion of a small particle could strengthen the impact (. M. Riley, C. D. Paynter 1990; Bakar et al. 2010). Hardness values for filled epoxy show the existence of filler, and an increase in filler composition shows an increase in impact strength.

High Strain Rate Compression Test

Functionally graded epoxy/sea sand composite cylindrical specimens with 10mm diameter and 5mm thickness are placed between IB and TB. Compressive loading at high strain rates and gas gun pressures was tested at 2, 3, and 4 bars using SHPB to produce the loadings at different velocities. Samples were cut per the dimension shown in Figure 4.31 (a); at each pressure, three samples were taken for each test, and the average was determined. Stress-strain graphs were developed and analyzed from the initial pulse loading data, which provides the mechanical characteristics (Fan et al. 2015). Figure 4.31 (b) shows an example pulse signal received using strain gauges on IB TB and RB recorded during one of the tests with a high strain rate compression experiment. The engineering stress-strain graphs are obtained from the initial pulse impact using 1D stress wave theory, considering dynamic stress equilibrium in the test specimens under SHPB under compressive loading (Nie et al. 2018). The stress pulse (peak amplitude) attains the maximum strength; the sample can be fractured and lose its ability to carry the load, and small or no fracture is seen in the sample.

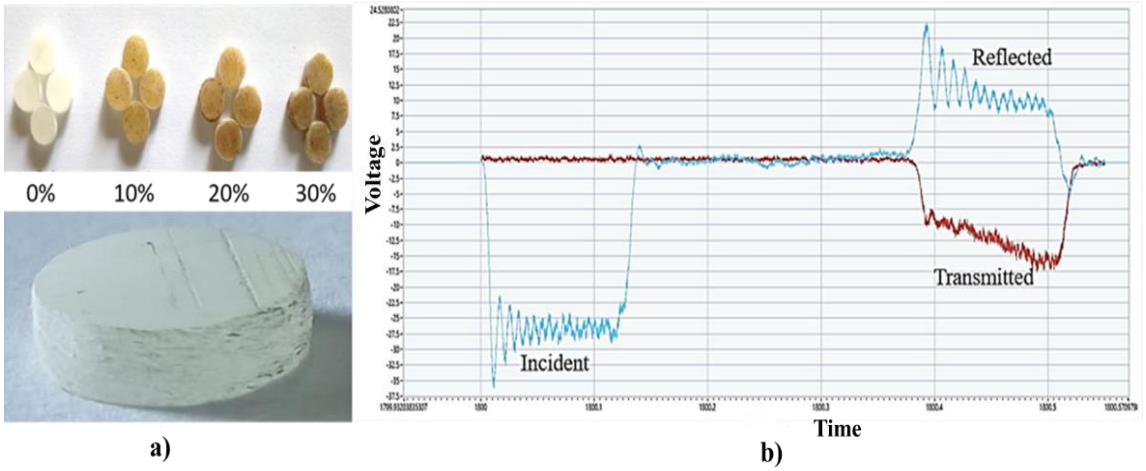

Figure 4.31 a) Sample prepared for SHPB test, b) SHPB test, Voltage vs. time (Reflected, transmitted, and Incident waves).

The TB and RB can be identified in the sample for neat epoxy, as shown in Figure 4.31 (b). By analyzing epoxy without filler and epoxy with filler composition of 30%, the dynamic signals indicated a dependence of the specimen's reflected signals on filler content. A slight difference can be seen in the waveforms of both TB and RB. The figure shows that the loading time of compression is lesser wave reflected through constant amplitude. This indicates an epoxy sample with an elastic response. As time increases, the development of plasticity behavior is seen in the sudden rise in the reflected signal. (Sassi et al., 2019).

Additionally, there is a clear distinction between the transmitted waveforms; the earlier exhibits a linearly elastic increment, while it exhibits a plastic reinforcing phase after the linearly elastic increment. The epoxy resin composite sample's plastic behavior is consistent with the unfractured samples. The reason for this is that adding fillers made the material more plastic.

For each loading condition, the three tests are carried out for epoxy and epoxy/sea-sand composite for different compositions of sea sand 10%, 20%, and 30% at different pressures 2, 3, and 4 bar. Table 4.29 lists the specifics of the experiments, including the specimen dimensions.

Table 4.29 List experimental parameters for high strain rate compression testing.

Pressure (bar)	Dimension (mm)		Velocity (m/sec)	Strain rate (/s)	σ_{max} (MPa)			
	Diameter	Height			0%	10%	20%	30%
2	10mm	5mm	~ 22	~870	103.94	105.01	106.77	107.21
3			~ 27	~1030	120.75	123.16	124.11	125.53
4			~ 30	~1183	137.68	137.85	138.44	138.48

Based on the stress-strain diagram illustrated in Figure 4.32 for an SHPB impact test, when the pressure increased from 2 bar to 4 bar, the strain also increased, indicating an increase in plastic deformation. This shows that the epoxy with sea sand specimens is more deformation-resistant when subjected to impact loading. After the maximum stress, a softening of the strain is also observed. It exhibits viscoelastic behavior, and the elastic behavior is linear, mainly in all phases; strain softening is seen after the yielding. Strain rate influences yield and subsequent behaviors; with increased strain rate, stress also increases.

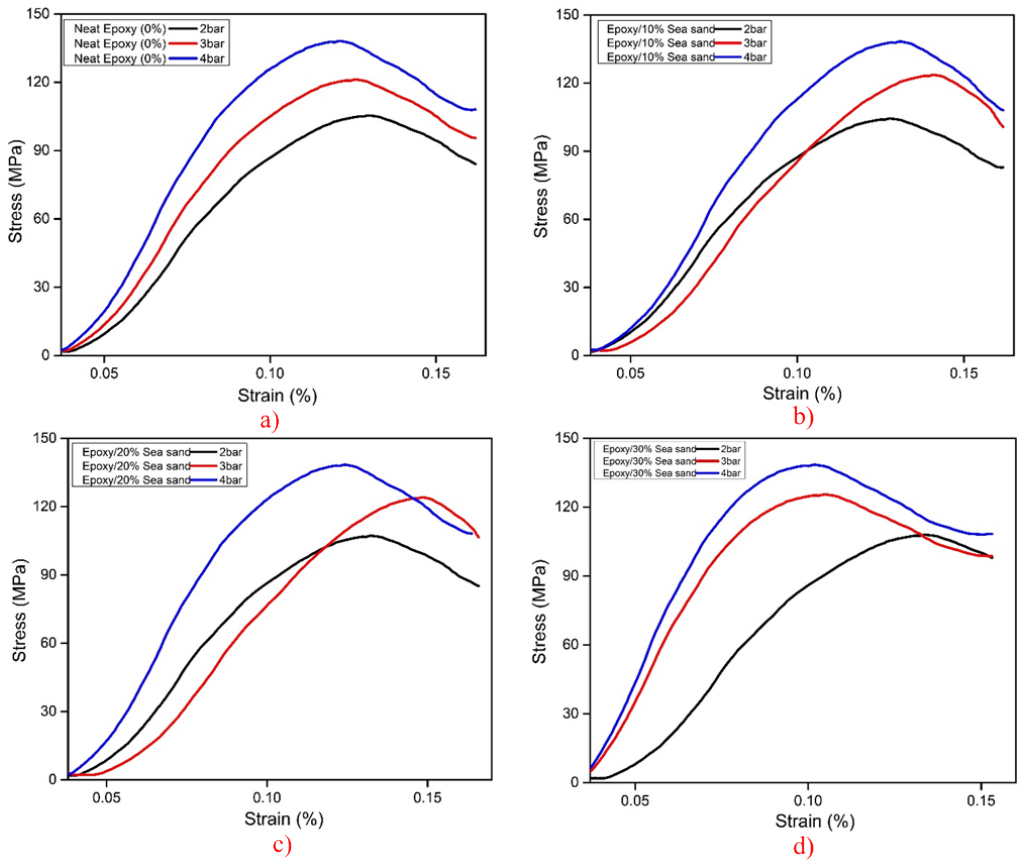

Figure 4.32 TB and RB for different pressures (a) epoxy without filler, b) Epoxy/10% sea sand, c) Epoxy/20% sea sand, d) Epoxy/30% sea sand.

The epoxy/sea sand composite's HSR compression properties are illustrated in Figure 4.32 at RT (room temperature). The typical characteristics of the stress-strain curves were a distinct non-linear deformation phase that manifested itself following an initial elastic portion, followed by a stress drop. The result indicated that the strain rate under compression responses significantly impacted the epoxy matrix composite's HSR compression characteristics. This was described by saying that at higher strain rates, damage cannot start and propagate in a timely manner. The damage initiation and development, in this instance, required additional effort. This would lead to an increase in compression strength and HSR. The increment in compression stress under HSR

loading is also caused by the viscoelastic characteristics of polymer matrix composites (Naik and Kavala 2008).

Figure 4.32 shows the sample stress-strain diagram for 0% and 30% sea sand composition. Figure 4.32 (a) illustrates the stress-strain curve of plain epoxy samples that were tested for SHPB under compression loading at 2 bar, 3 bar, and 4 bar, achieving velocities of approximately 21m/sec, 27m/sec, and 31m/sec, and strain rate of 856.34 s^{-1}, 1008.37 $s^{-1,}$ and 1181.94 s^{-1} respectively. Results from the graph indicate that neat epoxy's HSR compression strength and slope appeared to rise as strain rates increased. The maximum compressive strength with 30% filler composition is about 107.21 MPa, resulting in a 3.05% improvement over the neat epoxy for 2bar pressure. Similarly, maximum compressive strength with 30% filler composition is about 123.16 MPa and 137.68 MPa, resulting in a 3.80% and 0.57% improvement over the neat epoxy for 3bar and 4 bar pressure, respectively. As the percentage of the composition increases, a sudden drop in stress can be seen after reaching the ultimate stress, which causes the samples to lose their ability to carry the load. One essential aspect is how the sea sand is distributed inside the polymer matrix. Agglomeration of sea sand in polymers causes local stress concentration, which withdraws the matrix with the filler and decreases load transfer efficiency. It is challenging to fabricate composites, avoiding agglomeration and using standard mechanical mixing techniques. As a result, there is no noticeable increase in compressive strength between epoxy and filled epoxy.

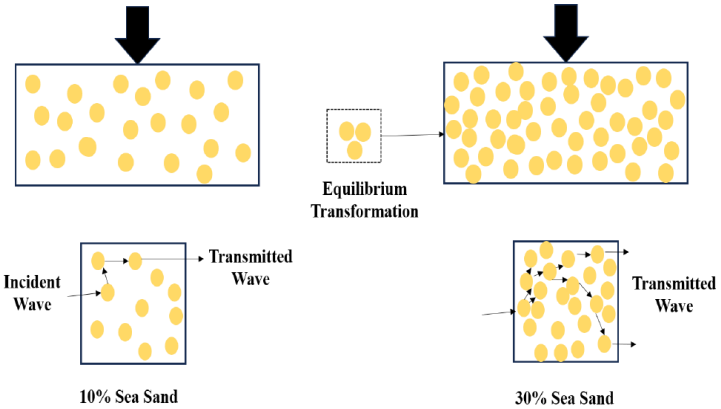

Figure 4.33 Mechanisms that influence dynamic compression using SHPB

Figure 4.33 shows the mechanisms that influence dynamic compression using SHPB. The mass fraction of sand particles significantly impacts the stress-strain relationship of composite foams. The mass fraction has no discernible effect on the critical stress between 10 and 30 wt%, but the plateau stress and densification strain are significantly altered. This can be because the microstructure of the composite, as specified by the nucleation amount, is unaffected by the mass fraction within the range. With a higher mass percentage, the incidence of local particle clusters rises, and more energy is lost by inter-particle interactions, determining the composite's densification strain and plateau stress. As the compressive strain increases, the discrete particles are pushed to aggregate and produce the cluster effect, which improves compressive resistance due to the composite's high strength and stiffness, as seen in Figure 4.33. The energy dissipation generated by inter-particle interactions results in an equilibrium state where the touched sand particles transition from one stable equilibrium to another. The cluster particles expand laterally in the second equilibrium stage. During compression, the base composite functions as a weak band, transferring compressive force to surrounding particles. Under the impact of high-strength sand particles, the stress-strain relationship without discontinuous compression response is mostly due to the equilibrium transformation expansion.

In SHPB testing, a compressive stress pulse is applied to the specimen through a striker bar, which generates compressive waves that propagate through the incident bar and into the specimen. The compressive waves cause deformation and compression of the material. As the compressive waves propagate through the sand-filled epoxy specimen, it undergoes deformation. The epoxy matrix deforms elastically, while the sand particles may experience both elastic and plastic deformation depending on the loading conditions and the characteristics of the sand particles. Under high compression rates, the sand particles may undergo fracture and crushing. The irregular shapes and sizes of the sand particles can lead to interparticle friction, which results in complex deformation behavior, including particle rearrangement, sliding, and crushing. As the compressive waves propagate through the specimen, there is a load transfer between

the epoxy matrix and the sand particles. Contact forces between the particles and the epoxy matrix influence the overall response of the material to compression. The presence of sand particles can contribute to energy dissipation mechanisms within the material. Frictional forces between the particles and between the particles and the epoxy matrix, as well as interparticle and matrix-particle contact forces, contribute to energy dissipation during deformation. SHPB testing is conducted at high strain rates, which can significantly influence the mechanical behavior of materials. At high strain rates, materials may exhibit different deformation mechanisms than static or quasi-static loading conditions.

The amount of sea sand added, the type and size of the sea sand particles, and the epoxy's curing conditions are some of the factors influencing the toughness of the epoxy. The addition of sea sand to epoxy enhances its toughness, wear, and impact resistance and reduces its cost. This is due to the fact that the sand particles can strengthen the epoxy and more evenly distribute stress throughout the material, minimizing cracking and other types of damage. It is important to remember that too much sand can make the epoxy extremely brittle or more challenging to work with. The epoxy and sand may not bond as well as they should, and the sand particles could leave voids or weaken the bond.

Furthermore, sea sand might include impurities that reduce the epoxy's strength and durability. The area under the curve (AUC) is commonly used to assess the toughness of polymer composite materials. In materials science, toughness denotes the material's capacity to absorb energy before fracturing. It is an important mechanical property of materials, particularly in applications where the material may be subject to impact or other forms of mechanical stress.

A stress-strain curve is generated through a mechanical test using the AUC method to determine the toughness of a polymer composite material. The AUC is then determined by integrating the area under the stress-strain curve until the fracture point. This measures the total energy the material absorbed during the test. Figure 4.34 shows that as the composition percentage increases, the toughness increases; similarly, as the

pressure or velocity increases, toughness also increases. It is also seen that compared to neat epoxy, there is a 15.12 % increase in the toughness for 30% composition of sea sand with epoxy for 2bar pressure; similarly, there is a 20.37% increase for 3 bar and 7.91% increase for 4 bar. From the result, it can be concluded that 3 bar pressure shows the maximum percentage of increase in toughness compared to 2 and 4 bar.

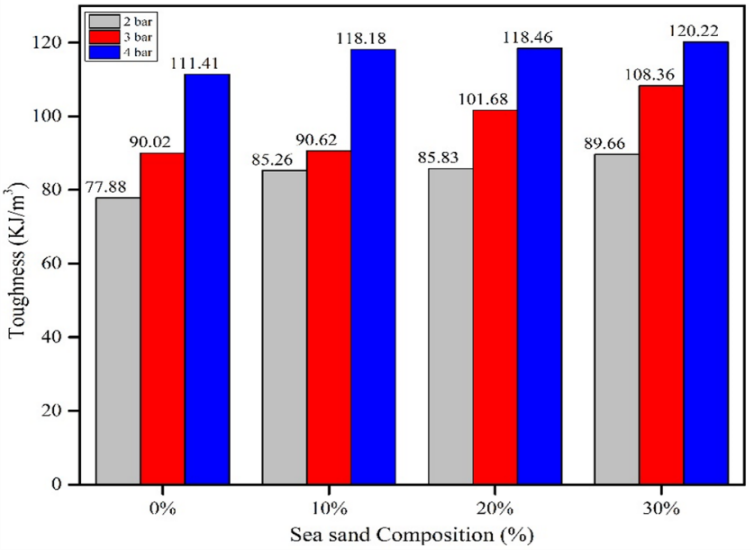

Figure 4.34 Toughness for different percentages of sea sand for different SHPB pressures.

Failure analysis of surfaces

The fracture sample surfaces of neat epoxy and filled composites containing varying weight percentages of sea sand (0%, 10%, 20%, and 30%) were evaluated using a Scanning Electron Microscope (SEM) EVO MA18 equipped with Oxford EDS(X-act). The magnification range used for the analysis was between 1x and 100,000x. To analyze the influence of sea sand morphological characteristics and weight percentage on the failure patterns of the FGPC composites. To avoid damage to the SEM equipment, the specimens were dusted by sputtering deposition rate with gold using sputtering equipment. Figure 4.35 shows the fractography of plain epoxy and epoxy composites; the plain epoxy fracture surface was relatively smooth, a characteristic of

brittle fracture (Voo et al. 2011). Based on these observations, neat epoxy is easily fractured under stress and has less resistance to crack propagation.

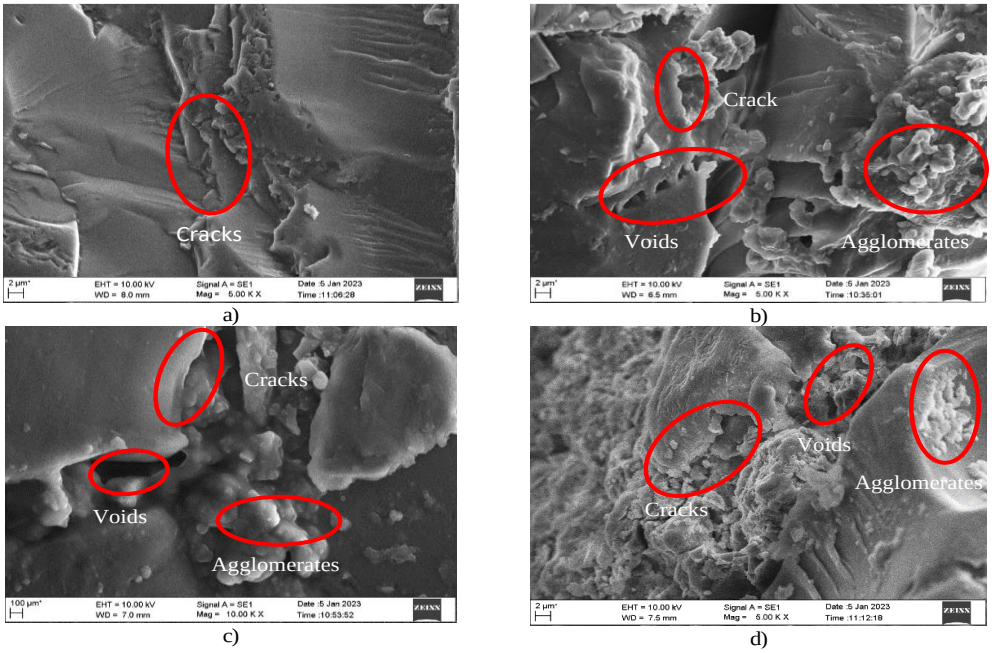

Figure 4.35 SEM images (a) Neat epoxy, (b) Epoxy/10% Sea sand, (c) Epoxy/20% Sea sand, and (d) Epoxy/30% Sea sand.

Figures 4.35 (b), (c), and (d) show that epoxy composites' fracture surfaces with 10%, 20%, and 30% sea sand have rough fracture surfaces and higher waves than neat epoxy. Higher crack resistance is shown by a rough fracture surface, indicating that crack propagation does not occur as rapidly as it would with neat epoxy. This shows the existence of sea sand, and the epoxy was strengthened by adding the sea sand filler. Therefore, more energy is needed for crack propagation (Wu et al. 2002). Increased crack deflection slows the propagation of crack by increasing the energy absorption caused by filler particles interacting with the crack growth. As the weight percentage of sea sand fillers increases, the actual number of particles present in the matrix also increases. When the crack propagates further, it interacts with a filler particle, which causes particle debonding, and then the matrix yields locally. The images show that the matrix with the sea sand is detached from the composite, which indicates better bonding. However, there is no evidence that the filler and matrix are debonding. Cracks, voids, and agglomerates are seen in the SEM images

and are marked with red circles; where agglomerates are formed may be because of parameters like larger surface area and physical entanglement (Ervina et al. 2016). Furthermore, voids may result from insufficient wetting caused by sea sand particles' weak interfacial contact with epoxy (Poh et al. 2014). The filler was drawn out when the force was applied because sea sand could not interact with the epoxy. Air bubble development while mixing contributes to the voids, as shown in Figures 4.34 (b), (c), and (d). Increased filler loading caused the mixture's viscosity to rise and led to the formation of voids, which are difficult to remove in the specimens.

4.4 Results of Low -Velocity Impact Test

The LVI tests were conducted at room temperature, and the impact energy was varied by changing the impactor's drop height. The impactor's potential energy increased with increasing drop height, which was then converted into kinetic energy upon release. Table 4.30 provides details of the testing conditions for all configurations.

Table 4.30 LVI Testing conditions

Height of the drop weight (m)	Initial velocity (m/sec)	Initial energy (J)
0.5	5.89	140.44
1	10.92	482.47
1.5	15.18	931.91

The suggested FGSC samples were tested to LVI at various impact energies of 140.44 J, 482.47J, and 931.91J, with initial velocities (5.89 m/s, 10.92 m/s, and 15.18m/s) with a drop height of 0.5m, 1m, and 1.5m. Where energy is absorbed (E_A), Energy residual/rebound (E_R), and Energy Initial/Impact (E_I). The EA ratio is the proportion of absorbed energy to the initial energy.

Table 4.31 LVI Properties

FGSC	Height of fall (m)	Energy (J)			Velocity (m/s)		CoR	E_A Ratio (ELP) (%)	Peak Force (N)	Depth of damage (mm)
		E_I	E_R	E_A	V_I	V_R				
SC0S	0.5	140.44	136.81	3.63	5.89	5.82	9.45	2.58	676.67	8.57
	1	482.47	448.35	34.12	10.92	10.53	11.89	7.07	7559.10	9.45
	1.5	931.91	750.30	181.62	15.18	13.62	7.19	19.49	15231.08	11.89
SC10S	0.5	140.44	135.46	4.98	5.89	5.79	9.10	3.54	1106.82	7.19
	1	482.47	428.41	54.06	10.92	10.29	11.22	11.20	8235.77	9.10
	1.5	931.91	749.73	182.18	15.18	13.61	3.92	19.55	15417.75	11.22
SC20S	0.5	140.44	131.12	9.32	5.89	5.69	7.10	6.63	1783.49	3.92
	1	482.47	404.44	78.03	10.92	10.00	11.40	16.17	8238.77	7.10
	1.5	931.91	721.56	210.35	15.18	13.36	2.55	22.57	15507.75	11.40
SC30S	0.5	140.44	129.36	11.08	5.89	5.66	4.85	7.89	2397.28	2.55
	1	482.47	338.63	143.84	10.92	9.15	9.10	29.81	13907.75	4.85
	1.5	931.91	647.80	284.12	15.18	12.65	0.83	30.49	15907.75	9.10

4.4.1 Force Vs. Time response of sandwich composites

The force-time trend of the proposed FGSC with an impact energy of 140.44 J is depicted in Figure 4.35. The behaviors for all proposed FGSC composites at different energy levels remain consistent with fluctuations in peak load, as shown in Table 4.31. Initially, during the impact event, the force exerted on the samples experiences a gradual increase. However, at a certain point, the force starts to decrease. This drop in force can be attributed to the potential failure of the composite material. The force on the specimen resumes an upward trend, gradually increasing until it reaches the peak force. After reaching the peak force, the force then begins to decrease. To minimize the influence of fluctuations and enhance clarity, a smoothing process has been applied to the force-time curve. The impact force initially exhibits a linear increase until a specific point is reached, wherein a sudden decrease in force is noticed. The reduction in force denotes the beginning of damage, which causes the composite material's stiffness to vary. This critical point, characterized by the reduction in force, is called the critical force ($P_{Critical}$). The $P_{Critical}$ value measures the composite's ability to withstand and resist damage (Caprino et al. 2015).

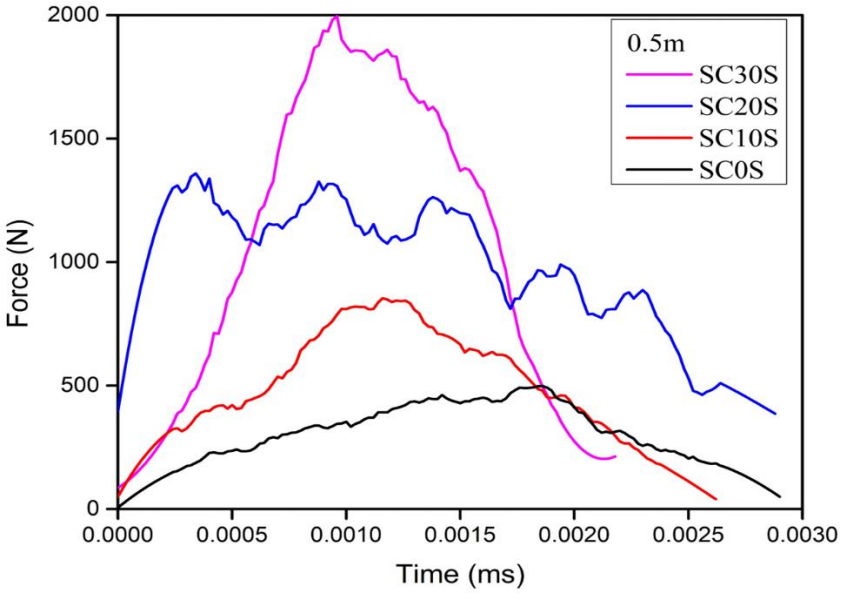

Figure 4.36 Force Vs. Time trend for 140.44J

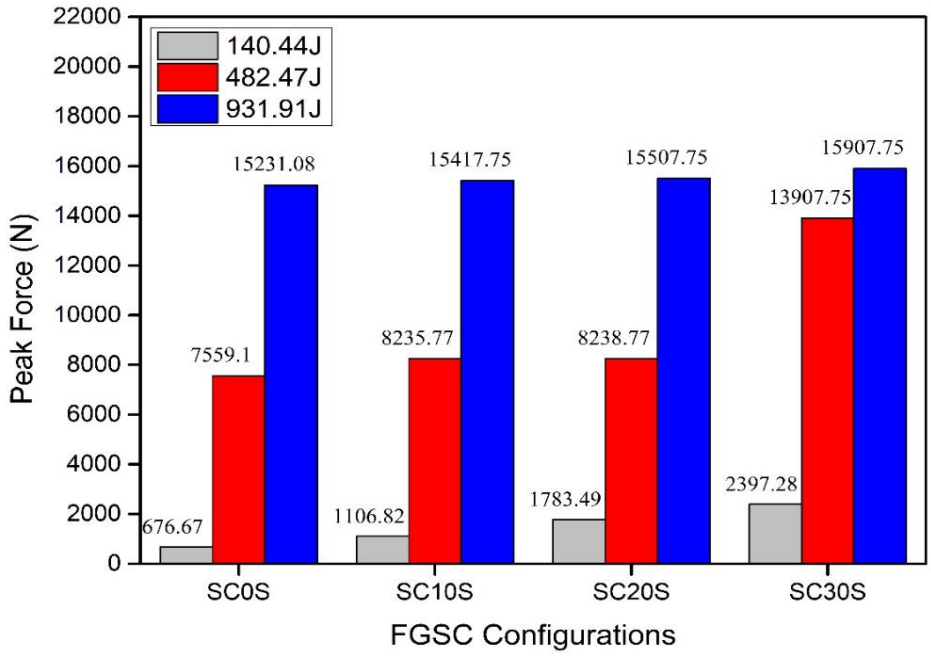

Figure 4.37 Peak force variation for different impact energies

After the critical force is reached, the behavior of the impact force can be linked to the progression of damage within the composite material. After the damage initiating force, there isn't any force disturbance. However, the force curve increases until it reaches its peak force. This is because the FGSC is unaffected by delamination. It's important to note that the suggested flexible skin material eliminates delamination, a common cause of failure in stiff composites (Tan et al. 2010). As given in Table 4.31, Peak force represents the material's load-bearing capacity. The variance in the peak force of the FGSC at various impacts is depicted in Figure 4.36.

It is observed that the peak force of SC30S shows a higher peak compared to SC0S, SC10S, and SC20S, indicating that the SC30S has a higher resistance to damage. The consistent rise in peak force with increasing impact energy indicates that peak force saturation still has not occurred. As a result, the proposed FGSC composites can withstand higher impact energy. The impactor's contact time with the sample remains constant for all three impact energies. This tendency is consistent with the findings in the study of Feraboli et al. (Feraboli and Kedward 2006). It is noted that the peak force

value of SC30S has been increased by 3.54% for 140.44J, 1.83% for 482.47J, and 1.04% for 931.91J compared to SC0S.

4.4.2 Energy Absorption

When the sample comes into contact with the impactor, a portion of the total energy is absorbed and dissipated. This absorbed energy represents the amount of energy converted into damage formation. From the time (t=0sec) of contact, KE (kinetic energy) is transferred from the projectile to the sample. Some of this energy is stored as elastic deformation inside the material, whereas the rest is mostly released when damage develops. Energy is also dispersed in negligible amounts by friction, heat, and sound. The projectile's KE is converted into elastic energy and stored within the sample once the impactor has delivered all of its KE to the sample (Kumbhare et al., 2022).

Regardless of the composition of filler used, Figure 4.37 (a) shows the susceptibility of the suggested FGSC to different compositions of sea sand filler. The observed energy absorption demonstrates the vulnerability of the composition to penetration, implying that the possibility of damage influences the performance of the composite. Furthermore, Figure 4.37 (a) shows residual energy degradation at higher impact energies, emphasizing the FGSC structure's reduced ability to store and recover energy. SC30S absorbs more energy than its other counterparts, which may be because of the energy absorption capability of sea sand. With increased E_I, the E_A ratio also increases. It is absorbed that the energy absorption value of SC30S has been increased by 3.05 times for 140.44J, 4.21 times for 482.47J, and 1.56 times for 931.91J compared to SC0S. Therefore, higher impact energies absorb more impact energy. SC30S E_A is greater than SC0S, SC10S, and SC20S. Compared to SC0S, SC10S, and SC20S, SC30S has lesser damage, which leads to more energy absorption, which can be related to this behavior. It is absorbed that the residual velocity of SC30S has been decreased by 2.74% for 140.44J, 13.10% for 482.47J, and 7.12% for 931.91J compared to SC0S. For FGSC, the input energy is 140.44 J. The Energy absorption of SC30S shows an increase of 55.05% compared to SC10S and 15.88% compared to SC20S. For Energy 482.47 J,

the Energy absorption of SC30S shows an increase of 62.41% compared to SC10S and 45.75% compared to SC20S. For Energy 931.91 J, the Energy absorption of SC30S shows an increase of 35.87% compared to SC10S and 25.96% compared to SC20S.

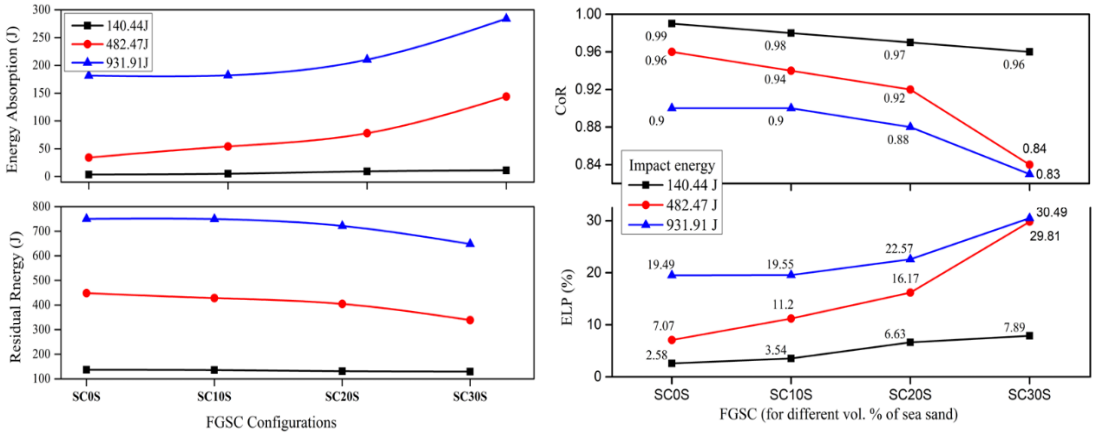

a) b)

Figure 4.38 a) Energy absorbed and Residual Energy, b) CoR and ELP For FGSC at various impact energies

4.4.3 Coefficient of restitution (CoR) and Energy loss percentage (ELP)

In the current study, the impactor is dropped from three heights (0.5m, 1m, and 1.5m) onto the proposed FGSC and strikes the composite at an initial velocity of V_I. Table 4.28 summarizes the calculated V_I, V_R, CoR, and ELP.

Figure 4.37 (b) depicts the CoR and ELP values for different energies of the FGSC. The CoR is observed to decrease as the impact energy increases. Thus, when the impact energy grows, the impactor's bouncing back is reduced since the target absorbs most energy due to damage initiation and propagation. The sea sand filler in the epoxy core is responsible for the decreased CoR seen for SC30S compared to SC0S. During an impact event, fillers like sea sand absorb and diffuse energy. This energy absorption causes the rebound velocity to decrease, which lowers the coefficient of restitution.

Similarly, SC30S limits the impactor's ability to bounce back to a greater degree, giving it greater absorbing energy and less damage resistance when the impact height increases. It is observed that the CoR value of SC30S has been decreased by 3.05% for 140.44J, 12.5% for 482.47J, and 7.77% for 931.91J compared to SC0S. Table 4.31 shows the peak force and energy absorption results that support this claim. A similar trend can be observed in ELP, as ELP is enhanced with the enhancement of impact energy. Therefore, ELP analysis shows that SC30S absorbs more energy than SC20S, SC10S, and SC0S. The E_A properties of the filler material can be used to explain why the ELP increased with the addition of sea sand.

The sea sand particles operate as energy sinks when the epoxy core packed with sea sand is impacted, absorbing and dispersing a significant amount of the KE. A larger ELP results from the sea sand particles absorbing more energy as the filler content rises. It is observed that the ELP of SC30S has been increased by 3.05 times for 140.44J, 4.21 times for 482.47J, and 1.56 times for 931.91J compared to SC0S. The sea sand filler in the epoxy core is responsible for the reduced CoR, increased ELP, and greater damage reduction for SC30S compared to SC0S. During LVI, fillers like sea sand typically absorb and diffuse energy and act as sinks. This energy absorption causes the rebound velocity to decrease. However, this lost kinetic energy is efficiently converted into absorbed energy by the SC30S composite, making it an excellent candidate for applications requiring superior energy absorption and damage resistance capabilities.

4.4.4 Results of FE analysis for LVI

Figure 4.38 compares the experimental and the FE concerning energy absorption. Figure 4.38 shows that the energy absorption FE value of SC30S has been increased by 3.14 times for 140.44J, 4.43 times for 482.47J, and 1.59 times for 931.91J compared to SC0S. The residual velocity of SC30S has decreased by 2.57% for 140.44J, 11.70% for 482.47J, and 6.06% for 931.91J compared to SC0S.

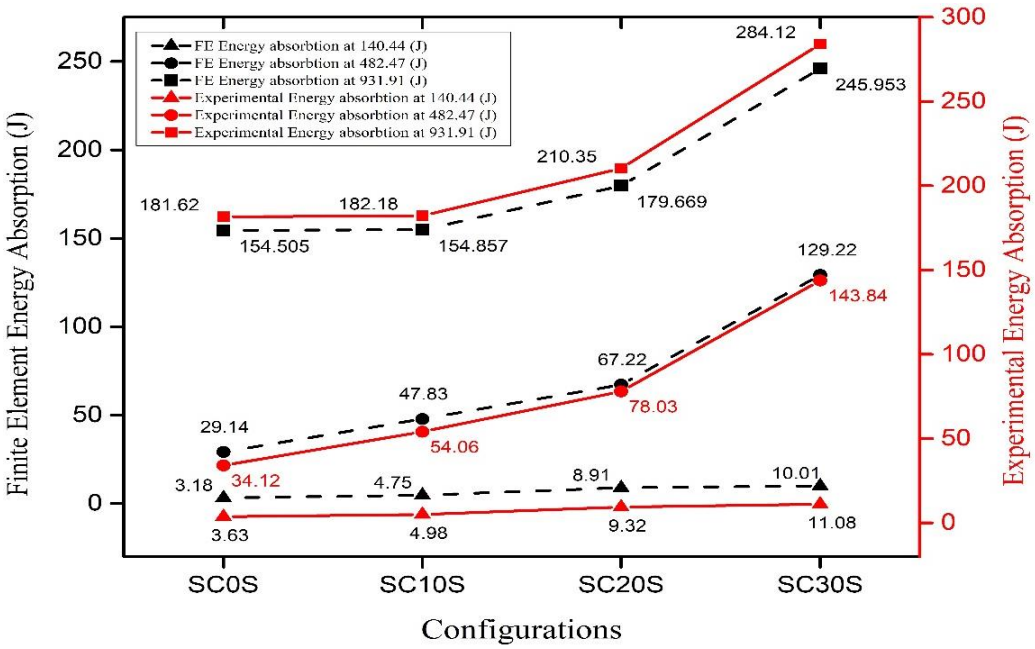

Figure 4.39 Comparison of experimental and FE results

4.4.5 FE and Experimental Damage assessment

4.4.5.1 Area of damage

In the current study, Image-J software performs damage analysis on samples evaluated employing the drop weight impact set-up at different impact energies. The impactor's high-impact energy causes significant damage to the sandwich structure. Figure 4.39 (a) depicts the damage caused to the skin (top face) of the proposed FGSC studied in this study at various impact energies. It shows the sample comparison between experimental damage samples and finite element (FE) analysis results for SC30S and a velocity of 15.84 m/s. A standard way of evaluating the accuracy of FE simulations is the area of damage. If minor variations exist between the experimental and FE results in the damage locations, the FE analysis can likely accurately predict the damage's extent. Figure 4.40 illustrates the damaged samples affected by a hemispherical impactor dropped from a height of 0.5m,1m, and 1.5m at 5.89, 10.92, and 15.185m/s impact velocities. From Figure 4.40, it is observed. The composites of

the figures are bent and indented, and neither the fiber and matrix of skin and core materials are torn or broken. Still, as the height of the impactor set-up is 1.5m and velocity 15.84m/sec, the indentation increases with damage to the core material, which is observed by visual inspection. It is also observed that when the hemispherical-shaped impactor hits the target, a blunt indentation is observed at the back surface of the FGSC composite, which is reduced as the impactor's velocity is reduced. It is usual practice to evaluate the accuracy of FE simulations by comparing the results of experimental and finite element (FE) analyses for damage samples based on the area of damage.

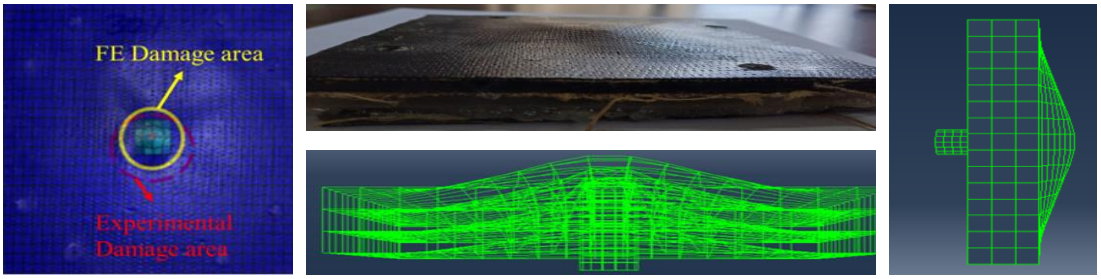

a) b)

Figure 4.40 Comparison of Experimental and FE damage samples (a) Damage area, (b) Back skin material bulging of the target because of the impact load for SC30S at 931.91J.

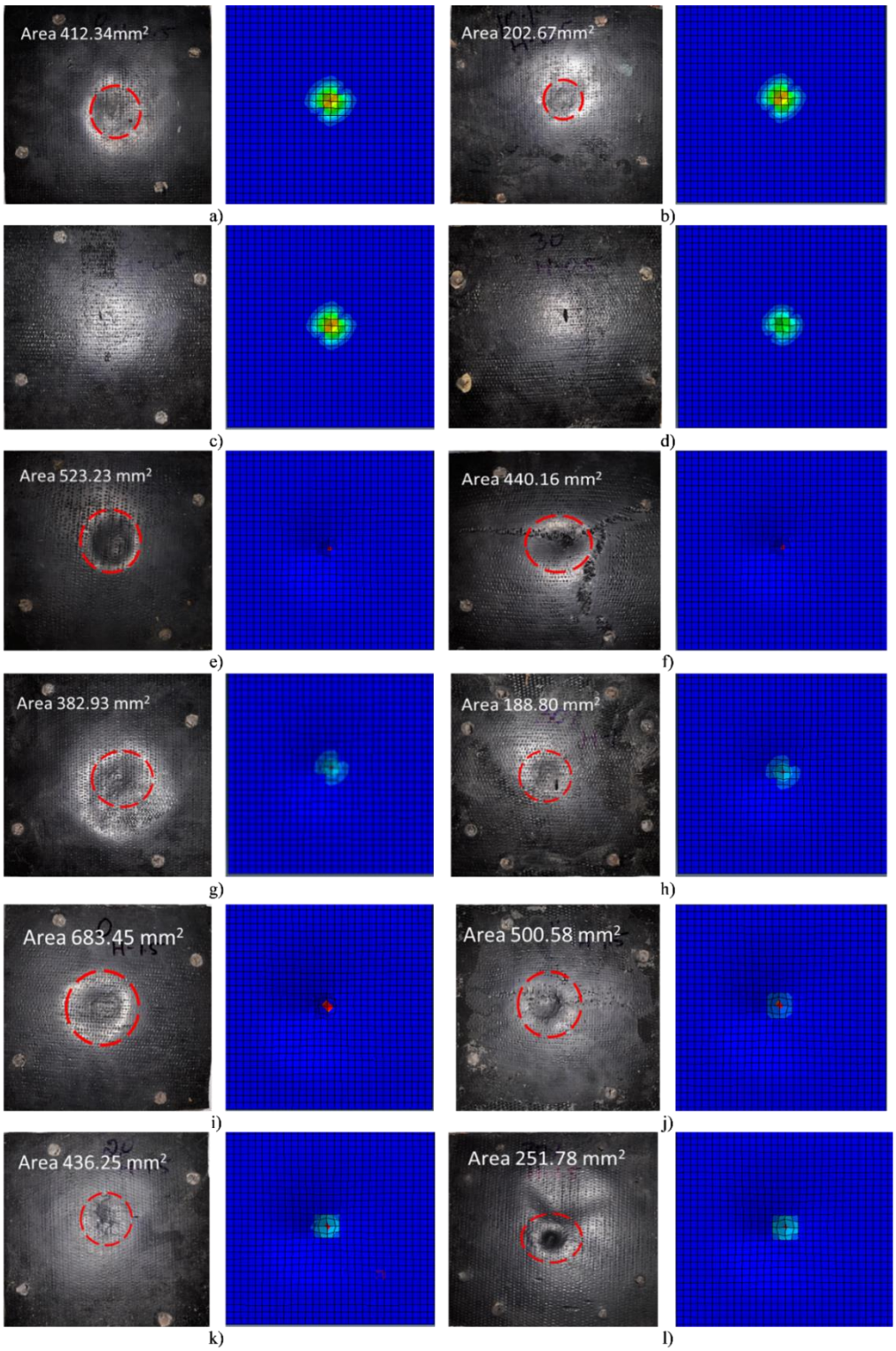
Area 412.34mm²
a)
Area 202.67mm²
b)
c)
d)
Area 523.23 mm²
e)
Area 440.16 mm²
f)
Area 382.93 mm²
g)
Area 188.80 mm²
h)
Area 683.45 mm²
i)
Area 500.58 mm²
j)
Area 436.25 mm²
k)
Area 251.78 mm²
l)

Figure 4.41 Damaged specimens of FGRPC sample a, b, c, d)0.5m height (5.89m/s) 0%,10%,20%,30% respectively, similarly e, f, g, h) 1m height (10.92m/s) and I, j, k, l)1.5m height (15.185m/s)

The addition of sea sand filler in epoxy composites at LVI (5.89, 10.92, and 15.84 m/s) leads to reduced damage compared to neat epoxy because the addition of sea sand filler can improve the energy dissipation capacity of the epoxy composite. Figure 4.39 shows that a higher peak force during LVI can indicate a higher level of energy absorption and damage resistance in an FGSC. The probability of material damage decreases when the peak force is higher, implying that the structure effectively absorbs and dissipates the impact energy. The maximum area of damage is observed for SC0S, and less damage is observed for SC30S for all three velocities. For velocity 5.89 m/sec for SC20S and SC30S, the addition of sea sand filler at these compositions significantly improves the impact resistance of the composite, and no damage is observed. An SC30S with a higher peak force is often associated with a more significant deformation and greater impact energy absorption. As a result of plastic deformation, the structure can absorb and distribute the energy across a large area. The core material (epoxy) absorbs and dissipates the impact energy.

Meanwhile, the skin layers work to stabilize and protect the core. As filler composition increases from 0% to 30%, the peak force increases, providing higher resistance to impact and damage. The area of damage develops with increasing impact energy, implying that higher impact energy causes more damage to the FGSC, indicating impacts with higher velocities have more kinetic energy, which causes the forces to be distributed more widely and intensely on the structure.

4.4.5.2 Depth of damage

Understanding the indentation behavior of a sandwich composite structure requires examining its response to indentation during loading, which involves the

deformation of the skin materials and crushing the core material. This interaction between skin deformation and core crushing can be complicated. However, analyzing indentation is more accessible in a sandwich beam configuration, and researchers have successfully developed theoretical contact laws that align well with experimental findings. In this study, the DoD (depth of the damage) caused by the impact is typically measured to assess the impact damage of functionally graded sandwich composites. To achieve this, the vernier is inserted into the impact damage and continues doing so until the material is undamaged. The length is then measured, and the DoD caused by the FGSC at various energy levels is noted in Table 4.31.

The observed values in Table 4.31 display the variation in the DoD for the suggested FGPC. Considering the identical energy level, SC30S absorbs more energy than SC20S, SC10S, and SC0S, suggesting that SC0S experiences more significant damage than SC20S, SC10S, and SC0S. This is confirmed by the degree of damage observed in the proposed FGSC at different impact energy levels. Because no substantial damage has been identified in any of the suggested sandwich structures at any impact energy levels, the FGSC demonstrates exceptional damage resistance. All configurations and energy levels were considered, and the back face of the proposed sandwich composite sustained no damage. Only bulging is observed at the rare face of the FGSC, with the core at 5.89 m/s and 10.92 m/s. No damage is observed at 15.84 m/s. Core crushing can be observed.

Most stiff composites evaluated by researchers (Majid et al. 2018; Ude et al. 2013) fail catastrophically within the selected impact velocity range. However, in the same impact velocity range, the FGSC presented in this study does not break catastrophically. It is noted that the DoD of SC30S has been decreased by 3.36 times for 140.44J, 1.94 times for 482.47J, and 1.30 times for 931.91J compared to SC0S. Because of the energy-absorbing characteristics of the filler, SC30S exhibits superior deformation resistance, whereas SC0S exhibits greater sensitivity to indentation since it lacks this energy-dissipating process. It is clear from Table 4.31 and the graphs that, when all configurations are considered, SC30S has a better energy absorption ratio and

a reduced DoD than the other configurations at any impact energy in the current investigation. The DoD develops as impact energy increases, implying that higher impact energy causes more damage to the FGSC. At higher impact energies than at lower impact energies, the sandwich structure absorbs maximum energy. This indicates that SC0S experiences more damage and minimal energy absorption than SC30S, releasing lesser elastic energy to the projectile. When CoR is considered, however, it can be shown that CoR decreases as DoD increases. According to Belingardi et al. (Belingardi and Vadori 2003), the E_A ratio is called the "Degree of Damage". The slope is larger after 5.89 m/s, showing that matrix cracking and fiber failure in skin and core crushing and cracking damage influence the damage at greater energy levels. The variance pattern remains the same for all FGSCs. Figure 4.36 (b) shows the target's back surface or back skin bulging because of the impact load. The composite's response to the applied force during the LVI event led to this bulging. Localized displacements and stress concentrations are caused on the rear surface due to the deformation, which happens as the panel absorbs and distributes the impact energy. It's crucial to remember that in some impact conditions, some bulging may be expected, especially if the material is intended to absorb energy or deform plastically to protect the structure from damage.

Figure 4.41 provides a graph of V_R and DoD with a schematic illustration of the relationship between V_R and the degree of damage sustained by the FGSC during an impact event. Because SC0S has more damage, elastic energy is returned to the impactor in more. The sea sand filler's influence on the epoxy core is essential in the increased damage resistance of SC30S compared to SC0S. Including fillers like sea sand in the context of Low-Velocity Impact (LVI) offers a large energy-absorbing component essential for the impact characteristics. The sea sand filler is an efficient energy absorber during the LVI event, absorbing and distributing impact energy inside the FGSC. As a result of this absorption, the rebound velocity decreases because a more significant percentage of the kinetic energy is lost rather than returned to the impactor.

As a result, SC30S significantly restricts the impactor's bounce-back behavior, which supports its improved energy-absorbing capacities.

The energy-dissipating characteristics of the sea sand filler in the core may be responsible for the decrease in damage for SC30S compared to SC0S. The addition of the sea sand filler may aid in more efficiently dispersing and distributing the impact energy throughout the composite, lowering stress concentrations and potential damage initiation sites. In addition, the filler effectively absorbs the lost kinetic energy, strengthening the material's resistance to impact forces and reducing the resulting damage. As a result, SC30S sustains less damage, making it an appropriate candidate for applications required for high energy absorption and resistance to damage-induced degradation.

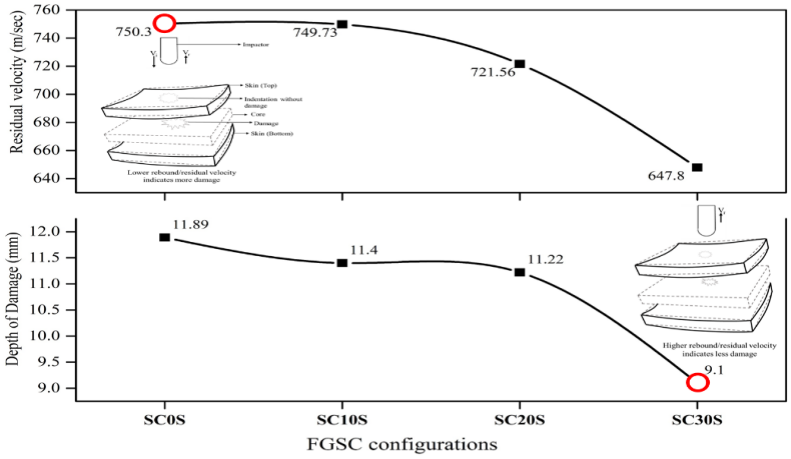

Figure 4.42 Relationship between rebound velocity and damage extent

4.5 Results of Ballistic Impact Test

4.5.1 FE Analysis

For the FE study, a 150 x 150 mm sandwich composite plate made of Face sheet Top/Bottom materials (Jute fiber-natural rubber-rubber based B-stage Pre-peg), Core material (epoxy/hardener, and sea sand as filler). Commercially available FE software

(ABAQUS dynamic explicit) is used to develop the FE model of the functionally graded sandwich composite plates. For FGSC, it has varied thicknesses of 10, 20, and 30 mm and a varied composition of 0%, 10%,20%, and 30%. FE analysis of the composite is performed at various speeds of 200, 275, and 350 m/s. Sandwich structures and bullets are considered deformable and rigid bodies, respectively. For analysis, a bullet with a diameter of 7.62 mm and a weight of 9.6g represents the bullet. Geometries for the sandwich composite and the projectile are developed, discretized, and then given material attributes. Following a mesh sensitivity analysis, converse meshing is used. The bullet is designed to strike the target normally.

The finite element analysis of the sandwich composite model made of an epoxy/sea sand core for different thicknesses and different % of sea sand with top and bottom skin materials made of Jute/rubber/Jute materials and subjected to an impact velocity (200, 275, and 350 m/sec) are conducted. At different velocities during impact loading, deformation and damage characteristics of the FGSC are observed. Kinetic energies (KE), V_R, E_A, and ballistic limit velocity are calculated and compared for various V_I.

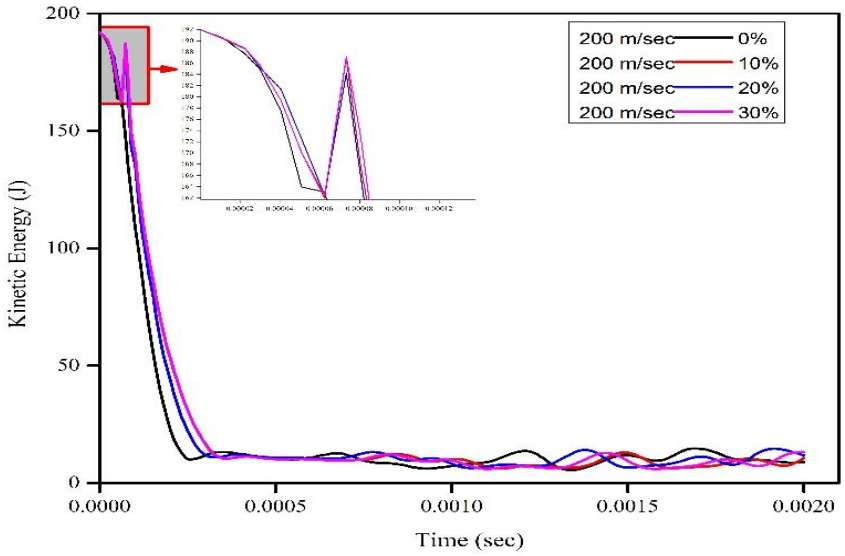

Figure 4.43 Variation in KE for different composition of filler composition for 10mm thickness core

Figure 4.42 shows the variation in kinetic energy (KE) with respect to the time of the impactor during an entire impact event. The information pertaining to the influence of flexible Facesheet and stiff core on the energy absorption behavior can be assessed. The impact conditions remain the same for all the configurations under consideration in the present study. The KE v/s time graph for the core with 10 mm thickness and sea sand of 0-30% composition when subjected to 200 m/s is shown. The trend remains the same for other configurations, too. From the FE approach, it is observed that a core of 10 mm thickness, when impacted with an impact velocity of 200 m/s, leads to less residual velocity for all the configurations under consideration, indicating more chances that the projectile gets arrested for all the cases. The rubber layer in the skin influences the stress wave propagation by reducing the rate of stress intensities transmitted to the core. Although less elastic than rubber, jute can still assist in energy absorption. The flexible skin (Jute/natural rubber/Jute) significantly contributes to the high energy absorption in FGCSC. The area marked in red shows initial expansion in the samples with different percentages of sea sand; the neat epoxy shows no initial excitation, indicating the absence of sea sand. After making contact with the target, the impactor's KE gradually decreases while the target's internal energy increases. When the impactor's KE is at its lowest, the target's internal energy reaches its maximum. After reducing to its absolute minimum, the impactor's KE begins to rise once more, and at some point, it stabilizes and remains constant. The impactor's residual energy is assumed to be this constant energy. Table 4.32 shows the FE results of energy absorption for different velocities, core thicknesses, and different compositions of sea sand with the core for FGSC.

Table 4.32 FE results for energy absorption and ballistic limit at different thicknesses and initial velocities

Core Thickness	**V_I (m/sec)**	**E_I (J)**	**E_A (J)**			
			0%	**10%**	**20%**	**30%**

10mm	200	192	185.7	185.85	186.08	186.57
	275	363	351.94	353.45	355.32	356.51
	350	588	572.14	579.36	580.63	582.63
20mm	200	192	192	192	192	192
	275	363	363	363	363	363
	350	588	575.57	579.55	581.77	583.13
30mm	200	192	192	192	192	192
	275	363	363	363	363	363
	350	588	588	588	588	588

The variation in energy absorption by the core of different thicknesses can be visualized in Figure 4.43.

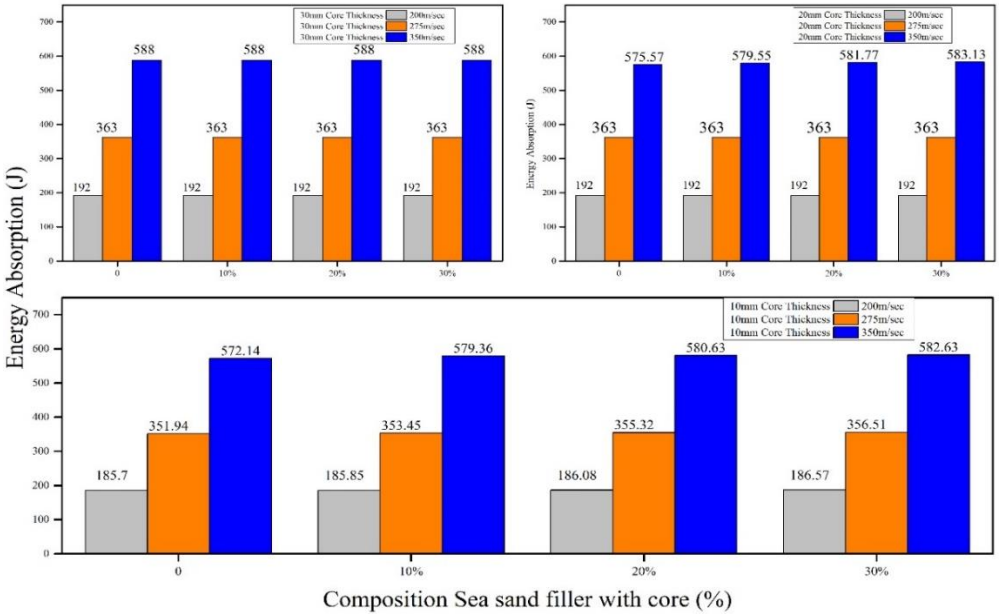

Figure 4.44 Energy absorption for different thicknesses of core and composition of sea sand and different velocities.

The energy absorption is highest for the core with 10 mm and 20 mm thickness when the sand with 30 vol% is reinforced in the epoxy matrix. This indicates a direct

correlation between the volume percentage of sea sand and energy absorption. Sand has inherent damping properties that help in dissipating energy. As the sand volume increases, more material is available to absorb and dissipate the energy from the impact, reducing the amount of energy transmitted through the material. With a higher sand volume, there is more interaction between the sand particles. These interactions increase friction and compaction, further contributing to impact energy's dissipation. The friction between sand particles converts kinetic energy into heat, absorbing more energy. Higher sand volume typically reduces the void spaces within the material. Reduced void spaces mean less air and more solid material to absorb the impact energy. This reduction in voids helps in creating a more uniform and continuous medium for energy absorption. However, for the core with 30 mm thickness, the energy absorption remains the same because the base material of the core might already possess a high level of energy absorption capacity, and the addition of sea sand within these percentages does not significantly enhance the overall energy absorption. The core material's inherent properties might dominate the energy absorption behavior. In a core of 30 mm thickness, the impact load might be distributed in such a way that the added sea sand does not influence the energy absorption significantly. The thickness might be sufficient to absorb the energy through the base material alone.

In a core with 10 mm thickness, the energy absorption increases marginally by 0.46 %, 1.3%, and 1.83% when impacted with the velocity of 200m/s, 275m/s, and 350m/s respectively, for the variation in sand volume percentage from 0%-30%. The marginal increases in energy absorption with increasing sand volume percentage and impact velocity can be attributed to the incremental contribution of sand to frictional interactions, compaction, and other energy dissipation mechanisms. These effects become more pronounced at higher velocities, leading to the observed increases of 0.46%, 1.3%, and 1.83% at 200 m/s, 275 m/s, and 350 m/s, respectively.

When the thickness of the core increased to 20 mm, it was found that the energy absorption at 200m/s and 275m/s remained the same for all the core configurations. But at 350 m/s, the energy absorption of the core filled with 30 vol % sand increases by

1.3% compared to the core without sand. This is due to the fact that at lower impact velocities (200 m/s and 275 m/s), the core material's inherent energy absorption capacity is sufficient, and the presence of sand does not significantly alter this capacity. However, at the higher impact velocity of 350 m/s, the additional energy absorption mechanisms activated by the presence of 30 vol% sand, such as increased friction, compaction, and particle interaction, contribute to a slight increase (1.3%) in energy absorption.

Further, when the core thickness is increased to 30 mm, all the configurations of the core exhibit contact energy absorption. The increase in core thickness to 30 mm enhances the overall energy absorption capacity due to the greater material volume, improved structural integrity, and more effective utilization of energy dissipation mechanisms. This results in all configurations of the core exhibiting contact energy absorption, as the thicker core can better accommodate and dissipate the impact energy.

Comparison of energy absorption by properties obtained by RoM and Experimental

In the FE analysis, mechanical and physical properties obtained from the RoM and experimental methods were used to study ballistic impact using Abaqus software. The main objective was to determine the energy absorption characteristics using 7.62mm bullets, as per NIJ standards, for different velocities of 200 m/sec, 275 m/sec, and 350 m/sec, percentages of sea sand (0%, 10%, 20%, and 30%) and core thicknesses (10mm, 20mm, and 30mm). Figure 4.44 shows the comparison between RoM and Experimental properties for energy absorption.

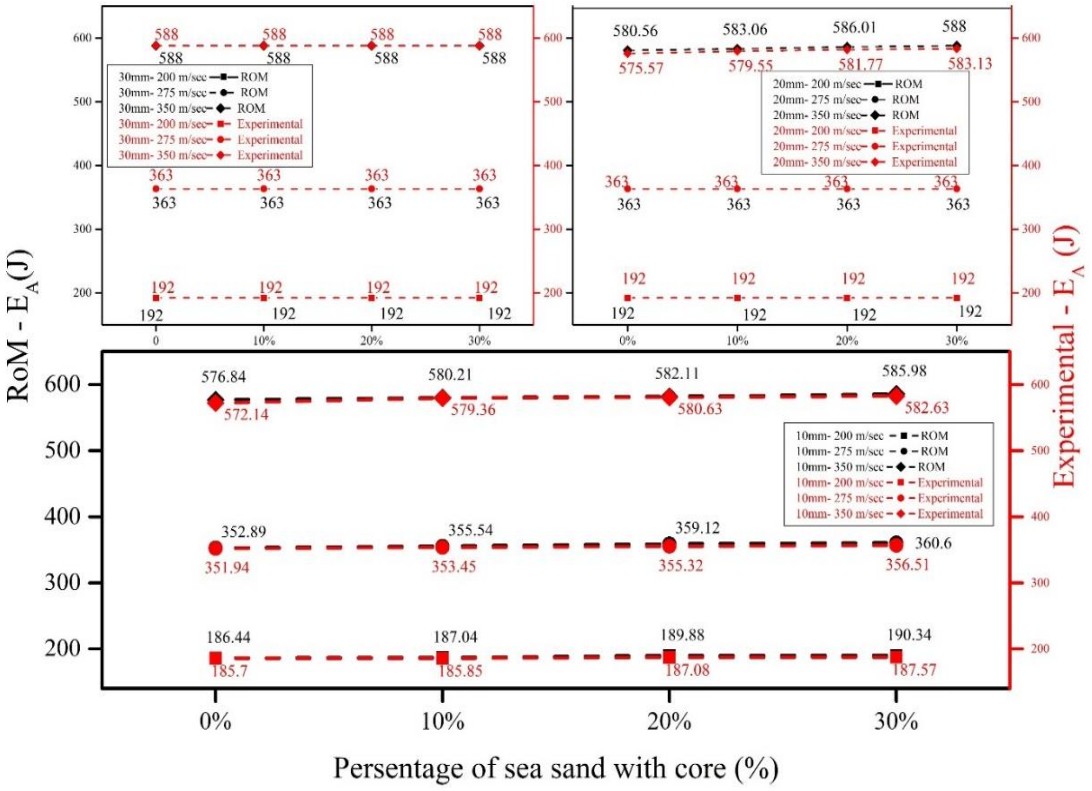

Figure 4.45 Comparison of RoM and Experimental Properties

Figure 4.44 shows the higher energy absorption from the properties obtained from RoM compared to experimental values, which can be attributed to several factors. The RoM frequently assumes the homogeneous distribution of reinforcements and ideal bonding between components. This might not be the case in actual materials, which could result in overestimating mechanical and physical properties and energy absorption. Actual materials have defects like inclusions, voids, and cracks that may significantly decrease their mechanical performance; these defects are usually not considered in the RoM. Furthermore, the RoM is based on the assumption that the material is homogeneous, although experimental samples may differ in their characteristics due to manufacturing procedures, which would result in reduced energy absorption.

The results show that as the sea sand percentage and the core thickness increased, the energy absorption capacity of the composite also increased in both cases.

Specifically, a core with a 10mm thickness was perforated at all tested velocities, indicating insufficient energy absorption capacity to stop the bullets. The comparison between the Rule of Mixture (ROM) and experimental values showed the percentage errors for 250 m/sec ranged from 0.40% to 1.50%, for 275 m/sec from 0.27% to 1.15%, and for 350 m/sec from 0.15% to 0.82%. However, when the core thickness was increased to 20mm, the composite successfully arrested bullets at velocities of 200 m/sec and 275 m/sec, showing enhanced energy absorption with the increased thickness. At the highest velocity of 350 m/sec, a 20mm thick core with a 30% sea sand composition was able to arrest the bullet according to RoM predictions, but this resulted in maximum back skin damage. In contrast, experimental results for the same configuration showed that the bullet perforated the composite without arrest, highlighting discrepancies between RoM and experimental. For the thickest core of 30mm, the sandwich composite could arrest the bullet for all the velocities. Even though the bullet was arrested, there was noticeable back skin damage for sea sand compositions of 0%, 10%, and 20%, indicating that the energy was absorbed but not completely dissipated without damaging the structure. Notably, the 30mm core composed of 30% sea sand could arrest the bullet without damaging the back skin, highlighting the effectiveness of this configuration in dissipating energy within the sandwich composite structure.

The optimal configuration observed from both analyses was a 30mm thick core with 30% sea sand, which provided maximum energy absorption while minimizing damage by arresting the bullet within the sandwich composite.

4.5.2 Experimental Analysis

The samples are prepared similarly to the samples prepared for LVI test. Table 4.33 shows the energy absorption details of cores with 10-30 mm thickness reinforced with 30 vol% of sea sand. From the FE analysis, it is found that the proposed cores, irrespective of their thickness, exhibit maximum energy absorption at 30 vol% of sea sand; hence, the experimental study is carried out for the core with 30 vol% of sea sand.

The energy absorption values obtained through the experimental and FE approach are presented in Table 4.33. The experimental results show that, irrespective of core thickness, energy absorption values increase as the impact velocity increases. Thicker cores have more material, leading to increased mass and volume. This means more energy can be absorbed before failure because more material can deform and dissipate energy. They also tend to be stiffer, which means they can resist higher loads before deforming. Thicker cores can distribute applied loads more effectively across their volume. This distribution reduces localized stresses and delays the onset of failure, allowing the core to absorb more energy over a larger area.

Table 4.33 Energy absorption, residual velocity obtained by FE and analytical methods

Thickness (mm)	**V_I (m/s)**	**FE**		**Experimental**	
		E_A (J)	**V_R (m/sec)**	**E_A (J)**	**V_R (m/sec)**
10	200	186.57	33.63	187.13	31.85
	275	356.51	36.77	357.64	33.42
	350	582.63	33.45	583.95	29.05
20	200	192	0	192	0
	275	363	0	363	0
	350	583.13	31.85	585.06	27.39
30	200	192	0	192	0
	275	363	0	363	0
	350	588	0	588	0

Core with 10 mm thickness, when impacted with 350 m/s, results in enhanced energy absorption of 3.12 times compared to an impact velocity of 200 m/s. At an impact velocity of 200 m/s, a core with 30 mm thickness exhibits energy absorption of 192 J, which is 2.6% more than that of a core of 10 mm thickness at the same velocity. Similarly, the energy absorption by a 30 mm core at 275 m/s is 363 J, which is 1.5 % more compared to a 10 mm core at the same impact velocity. However, the

enhancement in energy absorption by a 30 mm core is negligible compared to a 10 mm core when impacted at 350 m/s. This shows that with increased impact velocity, the effect of variation in the thickness of the core becomes negligible on the energy absorption behavior.

At lower impact velocities, the deformation and energy absorption are primarily influenced by the thickness of the core. A thicker core can absorb more energy due to increased mass, higher capacity for deformation, and improved load distribution, leading to a noticeable difference in energy absorption between 30 mm and 10 mm cores. As the impact velocity increases, the strain rate experienced by the material also increases. While the thicker core (30 mm) still absorbs more energy than the thinner core (10 mm), the difference in energy absorption becomes less pronounced. This can be due to the strain rate sensitivity of the materials involved. The material may exhibit different mechanical properties at higher strain rates, such as increased stiffness and reduced ductility, leading to less differentiation in energy absorption based on thickness alone. At very high impact velocities, the energy imparted by the impact is so high that the material and structural characteristics of the core reach their limits. Both the 30 mm and 10 mm cores may undergo catastrophic failure modes such as fragmentation or complete crushing, which diminish the effect of thickness on energy absorption. The core's ability to absorb energy becomes dominated by the failure mechanisms rather than progressive deformation, leading to negligible differences in energy absorption between different thicknesses.

As the impact velocity increases, the influence of core thickness on energy absorption diminishes because the deformation and failure mechanisms transition from being thickness-dependent to being dominated by high-rate dynamic effects and material limits.

The HVI performance of functionally graded core sandwich composites (FGCSC) with varying core thicknesses was investigated through finite element (FE) analysis and ballistic impact testing. The results are summarized in Table 4.34.

Table 4.34 Penetration of bullet for Fe and Experimental analysis

Thickness core (mm)	Total Thickness of FGSC (mm)	Remarks FE Analysis	Remarks (Ballistic Impact Testing)
10	30	Penetrated	Penetrated
20	40	Arrested (Penetrated at 350 m/sec)	Arrested (Penetrated at 350 m/sec)
30	50	Arrested	Arrested

The FGSC, with a 10 mm core and a total thickness of 30 mm, failed to arrest the projectile at the tested velocities, resulting in penetration. This indicates that the core's material volume and structural stiffness were insufficient to absorb and dissipate the kinetic energy of the impact effectively. The FGSC, with a 20 mm core and a total thickness of 40 mm, successfully arrested the projectile at lower impact velocities. However, at a high impact velocity of 350 m/s, both the FE analysis and ballistic impact testing showed penetration. This suggests a threshold impact velocity for this core thickness, beyond which the core's energy absorption capacity is exceeded. The FGSC, with a 30 mm core and a total thickness of 50 mm, demonstrated the highest resistance to HVI, successfully arresting the projectile in both FE analysis and ballistic testing at all tested velocities. This performance can be attributed to the increased material volume and enhanced energy dissipation mechanisms the thicker core provides.

The transition from penetration to arrest with increasing core thickness (10 mm to 30 mm) highlights material volumes and structural integrity's significant role in ballistic resistance. The 30 mm core's consistent ability to arrest projectiles underscores the importance of sufficient core thickness in FGCSC design for effective ballistic protection. The observed threshold velocity of 350 m/s for the 20 mm core indicates a critical point where the energy imparted by the projectile surpasses the core's capacity for energy absorption. This finding is crucial for understanding FGSC performance limits and designing composites that meet specific impact resistance requirements.

The alignment between FE analysis results and ballistic impact testing outcomes validates the accuracy and reliability of the FE model in predicting the ballistic performance of FGSC. This consistency supports using FE analysis as a predictive tool in designing and optimizing FGCSC for enhanced ballistic protection.

The study demonstrates that increasing the core thickness of FGSC significantly enhances their ballistic resistance by improving energy absorption and dissipation capabilities. The results indicate that while thinner cores (10 mm) are inadequate for arresting projectiles, thicker cores (20 mm and 30 mm) show progressively better performance, with the 30 mm core providing the most effective ballistic protection. These findings provide valuable insights for designing and developing FGCSC with optimized core thicknesses to meet specific ballistic protection requirements.

4.5.3 Cost Analysis

As observed, the 30mm core thickness has demonstrated the ability to arrest bullets across all configurations (0%, 10%, 20%, and 30% sea sand content). The reason for incorporating 30% sea sand into the epoxy core is to optimize the composite's mechanical properties, enhancing its ability to withstand and dissipate the energy of an impacting bullet more effectively than epoxy alone. This addition improves the HVI resistance and potentially offers cost benefits and environmental advantages by utilizing a readily available natural material. The cost analysis aims to analyze the cost implications of adding sea sand to epoxy cores used for HVI resistance. The analysis covers the material and processing costs associated with producing epoxy cores with and without sea sand, providing a comparative overview. The cost of epoxy is INR 445/kg, the hardener (10% of epoxy) INR 387/ 500 grams, and the cost of sea sand is zero as it is collected from the NITK beach Mangaluru, Karnataka, India.

Table 4.35 Cost analysis for the various cores developed in the present study

Mixture Composition	Requirement Epoxy + Hardner and Sea Sand (g)	Cost of Epoxy + Hardener (INR) and Sea Sand (INR)	Total Cost (INR)	Cost Reduction (%)
Neat epoxy (0% sand)	Epoxy - 729g Hardner - 64.40g Sea sand - 0g	Epoxy – 324.41 Hardner – 49.84 Sea sand - 0	374.25	0.00
10% Sea Sand	Epoxy - 656.1g Hardner - 57.96g Sea sand - 173.07g	Epoxy – 291.96 Hardner – 44.86 Sea sand - 0	336.82	8.90
20% Sea Sand	Epoxy - 583.2g Hardner - 51.52g Sea sand - 346.14g	Epoxy – 259.52 Hardner – 39.87 Sea sand - 0	299.40	19.53
30% Sea Sand	Epoxy - 510.3g Hardner - 45.08g Sea sand - 519.21g	Epoxy – 227.08 Hardner – 34.89 Sea sand - 0	261.97	32.47

Further, the cost of raw materials for producing a core of 150 X 150 mm and 30 mm thickness with 10%, 20%, and 30% sea sand is computed and presented in Table 4.35. The total volume of core produced is 6.75×10^{-4} m^3. To produce this volume of core, the amount of raw materials spent is found out, and the cost is calculated further. It was found that adding sea sand to the epoxy saved costs by 8.9% to 32.47%, resulting in the development of economic core material for HVI application and the conversion of waste resources into useful composite constituents for enhanced impact resistance.

The cost analysis indicates that incorporating sea sand into the epoxy core significantly reduces the total material cost. The pure epoxy core costs INR 374.25, while the composite core with 30% sea sand costs INR 261.97. This results in a cost reduction of 32.47%, highlighting the economic advantage of using sea sand in the composite core without compromising the material's integrity and high-velocity impact

resistance. The analysis covers the material costs associated with producing epoxy cores with and without sea sand, providing a comparative overview.

4.5.4 Damage assessment

Figure 4.45 shows the Penetration resistance of proposed sandwich composites with 10 and 30-mm core thicknesses at impact velocities of 200 m/s and 350 m/s.

Sandwich Composite	Impact Velocity	Penetration Behaviour
Sandwich with 0% sea sand reinforced core (10 mm thick core)	200 m/s	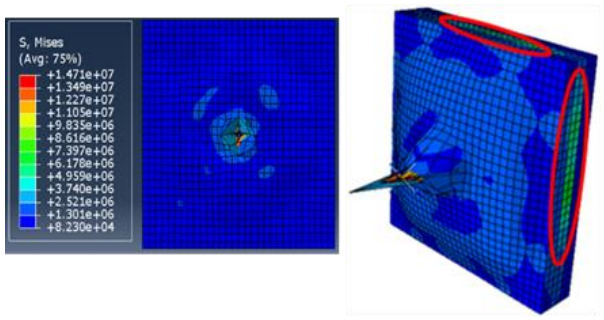
	350 m/s	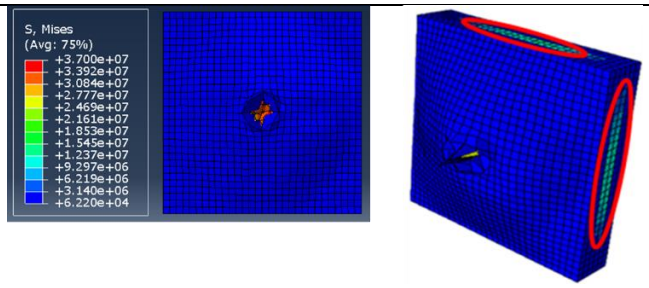
Sandwich with 0% sea sand reinforced core (30 mm thick core)	200 m/s	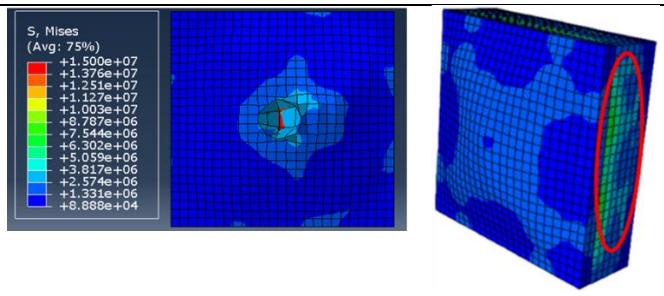

	350 m/s	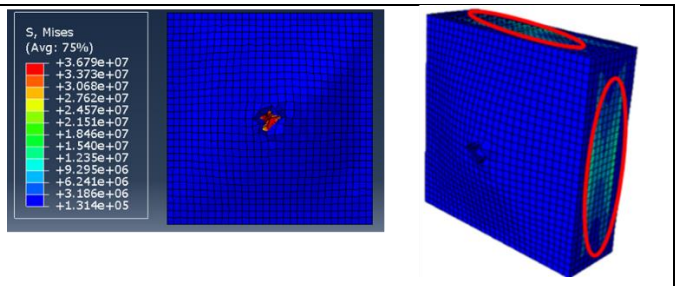
Sandwich with 30% sea sand reinforced core (10 mm thick core)	200 m/s	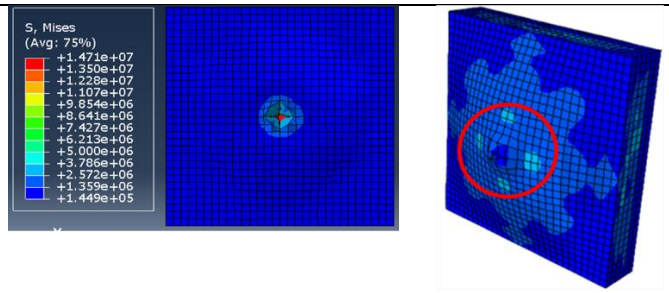
	350 m/s	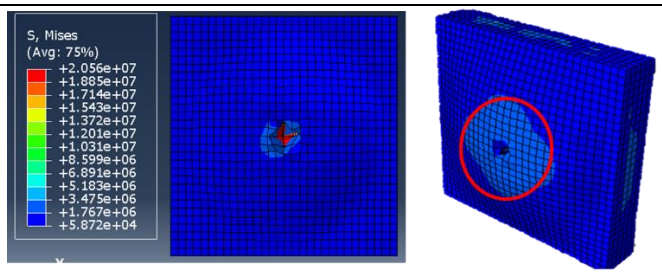
Sandwich with 30% sea sand reinforced core (30 mm thick core)	200 m/s	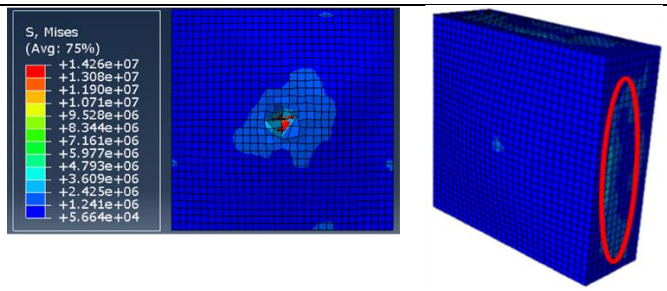
	350 m/s	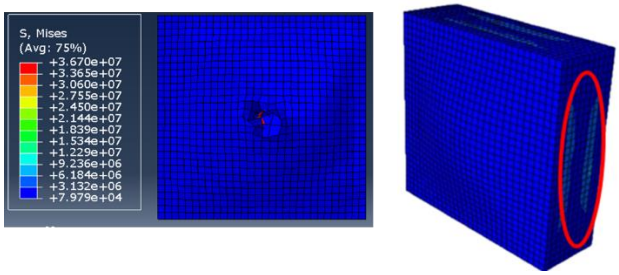

Figure 4.46 Penetration resistance of proposed sandwich composites with a core thickness of 10 and 30 mm at 200 m/s and 350 m/s.

From Figure 4.45, it can be seen that with an increase in the thickness of the sandwich composite, the resistance of the composite against penetration is increased. Flexible face sheets can bend and deform, which helps distribute the load over a larger area and reduces the impact force on any single point. Thicker composites can improve the overall structure's ability to resist penetration by enhancing this load distribution. A stiffer core can better absorb and distribute impact forces, reducing the likelihood of penetration. Increasing the core thickness enhances these properties, as the core can handle more load and dissipate energy more effectively. Thicker cores can dissipate more energy through compression and shear, providing greater resistance to penetration. The stiff core supports the flexible face sheets, preventing them from bending excessively and failing. The increased distance between the flexible face sheets due to a thicker core enhances the bending stiffness of the entire composite structure. This improved bending stiffness helps resist penetration by maintaining the integrity of the face sheets. However, the figure shows slight damage to the back skin for the 30 mm thick core with 0% sea sand. Increasing the sea sand composition to 30% with core epoxy results in the bullet being completely arrested within the composite. The area of damages, as depicted from FEA and experimentally tested samples of sandwich composite with a core thickness of 30 mm at different impact velocities of 200, 275, and 350 m/sec, is shown in Table 4.36.

Table 4.36 Area of damage sustained by the sandwich composite structure.

	Experiment		**FE Simulation**	
Damage area	Entry side damage (A_{EN})/mm^2	Exit side damage (A_{EX})/mm^2	Entry side damage (A_{EN})/mm^2	Exit side damage (A_{EX})/mm^2
S30C30S- 200 m/sec	957.61	Arrested	1078.40	Arrested
S30C30S- 350 m/sec	1366.74	Arrested	1591.13	Arrested

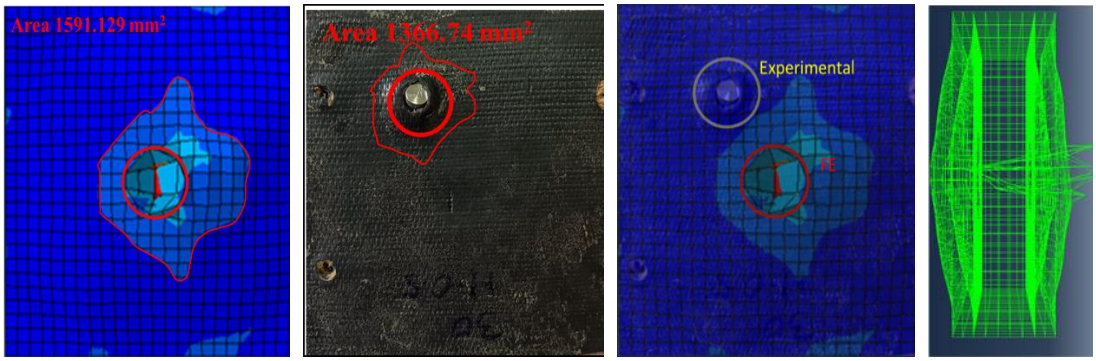

a) b) c) d)

Figure 4.47 Damage area representation in a) FEA model b) Experimental c) Comparison of FE and experimental d) Wire frame model

Figure 4.46 (a) depicts the entry damages (entry side) at 200 and 350 m/sec. It is observed that the projectile arrested within the sandwich composite for both the velocities and tensile forces at the exit and compressive stresses at the entry side may have increased the level of damage. The characteristic fractures predicted in FE for sandwiches, as illustrated in Figure 4.44, could be used to investigate this behavior. The projectile's interaction with a sandwich is plotted in Figure 4.46 after the impact. The projectile was arrested completely, as seen in the 30% sea sand composition and 30mm core thickness at 200m/sec and 350 m/sec. The projectile interaction with a sandwich structure consisting of a jute/rubber/jute flexible skin and an epoxy core filled with sea sand exhibits unique mechanical behaviors that improve its energy absorption capabilities. The jute mesh in the skin stretches upon impact. After the impact, the skin material undergoes significant elastic elongation, dissipating energy and delaying the onset of tearing through elastic yielding. This allows the core to initially experience compression, with the sea sand particles helping to distribute the load and reduce localized failure. The dominant failure mode observed is the ductile behavior of the rubber, which absorbs substantial energy and prolongs the core's ability to absorb impact through plastic deformation and microcracking. Combining these materials results in a synergistic effect that delays catastrophic failure, distributes energy more

evenly, and significantly improves the sandwich composite's overall impact resistance and durability.

Figure 4.46 (c) shows the damage that experimental damage resembles that found in the FEA model. Damage clears through holes produced by brittle fractures that cause material to be ejected as plugs. Before tearing and further damage, the sandwich displayed indications of skin spalling and elastic deformation of the rubber core.

The area of damage sustained by the sandwich composite structure was evaluated through both experimental testing and FE simulations. For the sandwich with a 30 mm core and 30 vol % of sea sand at 200 m/sec, the experimental entry side damage (A_{EN}) measured 957.61 mm², while the FE simulation results indicated 1078.40 mm², respectively. The percentage error between the experimental and FE simulation results for A_{EN} at 200 m/sec is approximately 12.61%. For 350 m/sec, the experimental A_{EN} was 1366.74 mm², whereas the FE simulation results showed 1591.13 mm², respectively. The exit side damage (AEX) indicates that the bullet is arrested within the composite. The results of FE and the experimental approach closely match with each other. The average depth measured in the sandwich for the targets was investigated. Both simulation and experiments revealed that the projectile was arrested by sandwich composite. The target's average depth is measured in the sandwich composite with a corresponding penetration depth below 42±5 mm. As shown in Figure 4.46 (d), the sandwich composite wireframe representation that stopped the bullet physically appeared to have penetrated more than halfway through its thickness (50 mm). It was discovered through simulation and experimentation that sandwich composite stopped the bullet.

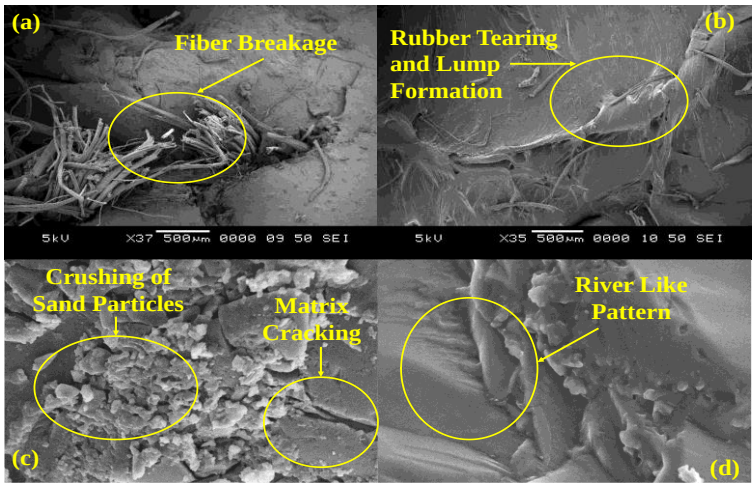

Figure 4.48 Damage mechanism involved in (a) fiber, (b) rubber layer, and (c&d) Core

The proposed flexible face sheet exhibits remarkably better ballistic behavior because of rubber's excellent damping properties. Pre-peg (B-stage cured rubber) improves fiber bonding, and rubber interleaving enables improved resistance against bullet movement. Additionally, it has been identified that the fundamental mechanisms of damage affecting flexible composites are fiber-breakage and tearing of rubber, which further contribute to the formation of lump and rubber detachment. The fiber-breakage mechanisms evident at the projectile's impact locations cause the fiber to fail when it achieves its maximum stress under the impact conditions. Rubber tearing happens when it is unable to further propagate. Therefore, it may be concluded that the pattern seen in the failed composite at higher impact velocities can be interpreted as the tearing of rubber.

It has been proposed that compression and bending cause the most damage to the jute-containing layer, which causes fiber-breaking and Pre-peg (B-stage cured rubber) tearing. Because the jute bonds to the compliant rubber, it eliminates the mechanism of fiber pull-out, which is observed in neat jute fabric. In the meantime, rubber tearing is the main cause of damage at the rubber-containing layer, where the compression of the rubber creates a resistance band. The rubber layer has the highest

energy absorption capacity and damage resistance. The jute layer, which provides less resistance to the bullet's movement and is damaged by fiber-breakage and prepreg (B-stage cured rubber) tearing, is encountered by the bullet as it hits the front face of the flexible sandwich composite structure. As the bullet continues its trajectory, it comes into contact with the natural rubber layer, providing the projectile with the greatest resistance because of its flexible behavior. Partial penetration occurs when the bullet's progress is stopped because the impact velocity is not high enough to overcome the resistive forces created by the suggested flexible composite. Nevertheless, the bullet completely penetrates the thickness of the suggested flexible face sheet when the impact velocity exceeds the resistive forces.

Since there is a rubber sheet and prepreg (B-stage cured rubber) present, there is compliance at the starting point of the rubber layer, which results in higher resistance forces. As the rubber in the flexible face sheet tears, this resistive force gradually decreases through the thickness of the rubber layer in the impact direction. The resistance provided by rubber to the bullet's movement at the point of entry is greater than that at the exit. The resistance that the rubber offers causes it to stretch along the bullet's path until the bullet's velocity surpasses the resistance that the rubber is offering. The fractography study of stiff core presented in Fig. 4.47 (c and d) reveals that failure mainly occurs due to the crushing of sand particles and matrix cracking. It also shows a river-like pattern, indicating brittle failure.

Damage to the sandwich composite is caused by matrix cracking when the bullet strikes the core. This decreases the composite's stiffness, exposing the way to other failure modes. Interlaminar stresses that occur at resin-rich locations cause delamination of the laminate, which primarily affects the composite's strength. In addition, the fillers absorb the load. The fillers partially withstand the bullet's penetration before crushing due to locally high stresses and indentation effects. Meanwhile, the matrix's fracture widens even deeper. The fillers resist the projectile's penetration to some extent, after which they crush because of locally higher stresses and the effect of indentation. In the meantime, the matrix crack starts to grow further.

CHAPTER 5

5 CONCLUSION

In the present study, the role of functionally graded core sandwich composite subjected to LVI and ballistic loading is studied using the FE and experimental approach. Based on the outcome, a comparative study of the stiff and flexible composites uses the FE approach. Various possible configurations of the jute/rubber/jute base flexible skin material and epoxy with the varied composition of sea sand (0%, 10%, 20%, 30%) and varied thickness (10mm, 20mm, 30mm) of the core sandwich composite are proposed for impact applications. These proposed configurations are studied for their ballistic impact response using FE simulation, and the best configurations are identified for further study. Further, their physical and mechanical properties characterize the selected functionally graded sandwich composite configurations. The impact behaviour of energy absorption and resistance to damage is studied for the proposed flexible sandwich composite. Based on these studies, the following conclusions are drawn:

- Statistical Six Sigma DMAIC methodology, incorporating qualitative (Pugh method) and quantitative (AHP) approaches, ensures a thorough and accurate material selection process. The choice of jute and rubber for skin material, paired with epoxy and sea sand for a core material in sandwich composite
- The energy absorption increases with an increase in filler composition from 0% to 30% at a low velocity of 10 m/sec, Intermediate velocity of 50 m/sec, high velocity of 100m/sec, and ballistic velocity of 350 m/sec. It is observed from the result that energy absorption increases with an increase in the thickness of the core material from 10mm to 30mm at 350 m/sec.
- The projectile with a conical shape absorbs the maximum energy, followed by hemispherical and flat-shaped projectiles. A flat projectile causes maximum damage, indicating that the larger the area of contact, the greater the composite damage. From the outcomes of the ANOVA, it is observed that the composition

of the filler is the most influencing parameter, followed by the thickness of the core and projectile shapes.

- The gradation test was performed to check the functional gradience using the burn-out test and weight method; the results of both methods significantly match each other.
- The void % in the composites is increasing as the filler composition. Specific tensile strength decreases with an increase in the filler composition. Hardness, Flexural strength, and impact strength increase as filler composition increases.
- For low-velocity impact testing, it is observed that a sandwich with 30% sea sand composition has superior damage resistance capabilities compared to its counterparts. The experimental and finite element (FE) analyses confirm increased energy absorption and decreased residual velocity at higher filler percentages. Notably, the sandwich with 30% sea sand composition demonstrates the lowest Depth of Damage and overall minimized damage across all impact energies, showcasing its exceptional damage resistance compared to other counterparts.
- Integrating computational and experimental methods has comprehensively understood functionally graded core sandwich composite's (FGSC) behavior under ballistic impact velocities of 200, 275, and 350 m/sec. Thicker cores correlated directly with better energy absorption, with a 30 mm thick core demonstrating the highest energy absorption capability compared to its counterparts. The study demonstrates that increasing the core thickness of FGCSC significantly enhances their high-velocity impact resistance by improving energy absorption and dissipation capabilities. The results indicate that while thinner cores (10 mm) are inadequate for arresting projectiles, thicker cores (20 mm and 30 mm) show progressively better performance, with the 30 mm core providing the most effective high-velocity impact protection. The cost analysis indicates that incorporating sea sand into the epoxy core significantly

reduces the total material cost. It was found that adding sea sand to the epoxy saved costs by 8.9% to 32.47%, resulting in the development of economic core material for high-velocity impact application and the conversion of waste resources into useful composite constituents for enhanced impact resistance. Damage area analysis showed a percentage error of approximately 12.61% between experimental and finite element simulation results for the entry area at 200 m/s. Fractography analysis reveals that face sheet damage is dominated by compression and bending, leading to fiber breakage and tearing of rubber, and the core failure mainly occurs due to the crushing of sand particles matrix cracking; it also shows a river-like pattern indicating brittle failure.

The jute/rubber/jute skin material effectively distributed impact energy and prevented penetration. At the same time, the epoxy/sea sand core played a crucial role in absorbing energy and maintaining structural integrity. The combination of these materials resulted in a sandwich composite with superior ballistic resistance, making it a promising candidate for use in advanced protective applications.

REFERENCES

M. Riley, C. D. Paynter, P. M. M. and J. M. A. (1990). “Factors Affecting the Impact Properties of Mineral Filled Polypropylene.” *Plast. Rubber Process. ing Appl.*, 14(2), 85–93.

Abbas, T., Ya, H. H., and Abdullah, M. Z. (2016). “Energy absorption capability of aluminium tube partially wrapped with glass/epoxy subjected to quasi-static loading.” *ARPN J. Eng. Appl. Sci.*, 11(24), 14313–14318.

Abrate, S. (n.d.). *Impact Engineering of composite structures*. (P. S. Udine, ed.), Springer Wien New york.

Abrate, S. (1991). “Materials on Laminated Composite Impact.” *Most*, 44(4).

Abrate, S. (1998). *Impact on Composite Structures*. Cambridge University Press, Melbourne.

Abtew, M. A., Boussu, F., Bruniaux, P., Loghin, C., and Cristian, I. (2019). “Ballistic impact mechanisms – A review on textiles and fibre-reinforced composites impact responses.” *Compos. Struct.*, 223(November 2018), 110966.

Afendi, M., Teramoto, T., and Bakri, H. Bin. (2011). “Strength prediction of epoxy adhesively bonded scarf joints of dissimilar adherends.” *Int. J. Adhes. Adhes.*, 31(6), 402–411.

Ahmad, M. R., Wan Ahmad, W. Y., Salleh, J., and Samsuri, A. (2007). “Performance of Natural Rubber Coated Fabrics under Ballistic Impact.” *Malaysian Polym. J.*, 2(1), 39–51.

Ahmadi, H., and Liaghat, G. (2019). “Analytical and experimental investigation of high-velocity impact on foam core sandwich panel.” *Polym. Compos.*, 40(6), 2258–2272.

Aized, T. (2012). *Total Quality Management And Six Sigma Edited by Tauseef Aized*.

Alam, S., and Khanal, D. (2020). “Impact analysis of honeycomb core sandwich panels.” *ASME Int. Mech. Eng. Congr. Expo. Proc.*, 12(2), 40–49.

Alemi-Ardakani, M., Milani, A. S., Yannacopoulos, S., and Shokouhi, G. (2016). “On the effect of subjective, objective and combinative weighting in multiple criteria decision making: A case study on impact optimization of composites.” *Expert Syst. Appl.*, 46, 426–438.

Ameen, W., Darwish, S. M., and Samhan, A. Al. (2015). “Towards enhancing peel strength of adhesively bonded joints.” *IOP Conf. Ser. Mater. Sci. Eng.*, 87(1).

Andrew, J. J., Srinivasan, S. M., Arockiarajan, A., and Dhakal, H. N. (2019). “Parameters influencing the impact response of fiber-reinforced polymer matrix composite materials: A critical review.” *Compos. Struct.*, 224, 111007.

Anish, Gupta, K. K., Kumar, A., Barnat-Hunek, D., and Andrzejuk, W. (2018). “Dynamic response with mass variation of laminated composite twisted plates.” *J. Mech. Sci. Technol.*, 32(9), 4145–4152.

Anojkumar, L., Ilangkumaran, M., and Vignesh, M. (2015). “A decision-making methodology for material selection in sugar industry using hybrid MCDM techniques.” *Int. J. Mater. Prod. Technol.*, 51(2), 102–126.

Ansari, M. M., and Chakrabarti, A. (2016). “Impact behavior of FRP composite plate under low to hypervelocity impact.” *Compos. Part B Eng.*, 95, 462–474.

Arbaoui, J., Schmitt, Y., Pierrot, J. L., and Royer, F. X. (2014). “Effect of core thickness and intermediate layers on mechanical properties of polypropylene honeycomb multi-layer sandwich structures.” *Arch. Metall. Mater.*, 59(1), 11–16.

Arya, P. K., Tupkari, S., Satish, K., Thakre, G. D., and Shukla, B. M. (2016). “DME blended LPG as a cooking fuel option for Indian household: A review.” *Renew. Sustain. Energy Rev.*, 53, 1591–1601.

Aryaei, A., Hashemnia, K., and Jafarpur, K. (2010). “Experimental and numerical study of ball size effect on restitution coefficient in low-velocity impacts.” *Int. J. Impact Eng.*, 37(10), 1037–1044.

Asim, M., Saba, N., Jawaid, M., and Nasir, M. (2018). “Potential of natural fiber/biomass filler-reinforced polymer composites in aerospace applications.” *Sustain. Compos. Aerosp. Appl.*, (June), 253–268.

ASTM D256-10e1. (2010). *Standard Test Methods for Determining the Izod Pendulum Impact Resistance of Plastics.*

Avery, J. G. (1981). *Design manual for impact damage tolerant aircraft structure*. *AGARDograph No 238*.

Bakar, M. B. A., Ishak, Z. A. M., Taib, R. M., Rozman, H. D., and Jani, S. M. (2010). “Flammability and Mechanical Properties of Wood Flour-Filled Polypropylene Composites.” (June).

Bandaru, A. K., Chavan, V. V., Ahmad, S., Alagirusamy, R., and Bhatnagar, N. (2016). “Ballistic impact response of Kevlar® reinforced thermoplastic composite armors.” *Int. J. Impact Eng.*, 89, 1–13.

Belingardi, G., and Vadori, R. (2003). “Influence of the laminate thickness in low-velocity impact behavior of composite material plate.” *Compos. Struct.*, 61(1–2), 27–38.

Belton, V. (1986). “A comparison of the analytic hierarchy process and a simple multi-attribute value function.” *Eur. J. Oper. Res.*, 26(1), 7–21.

Bernhard Pelzl, Rainerwolf, and KAUL, B. L. (2018). “Plastics, Additives.” *Ullmann’s Encycl. Ind. Chem.*, 1–57.

Bernier, H. (2005). “Scaling and Designing Large-Bore Two-Stage High Velocity Guns.” *High-Pressure Shock Compression Solids VIII*, 37–83.

Bhagyashekar, M. S., and Rao, R. M. V. G. K. (2010). “Characterization of mechanical behavior of metallic and non-metallic particulate filled epoxy matrix composites.” *J. Reinf. Plast. Compos.*, 29(1), 30–42.

Bhd, S. (1996). “Courses on Fibers Reinforced Composites Technology: Introduction to Materials, Processes and Applications.”

Birman, V., and Kardomateas, G. A. (2018). “Review of current trends in research and applications of sandwich structures.” *Compos. Part B Eng.*, 142(January), 221–240.

Bloch, R. (1976). “Viscoelastic behavior of filled and unfilled elastomers in moderately large deformations.” California Institute of Technology.

Cantwell, W. J., and Morton, J. (1991). “The impact resistance of composite materials - a review.” *Composites*, 22(5), 347–362.

Caprino, G., Carrino, L., Durante, M., Langella, A., and Lopresto, V. (2015). “Low impact behaviour of hemp fibre reinforced epoxy composites.” *Compos. Struct.*, 133, 892–901.

Célino, A., Fréour, S., Jacquemin, F., and Casari, P. (2014). “The hygroscopic behavior of plant fibers: A review.” *Front. Chem.*, 1(JAN), 1–12.

Ceresana. (2021). “Study on the Global Market for Fillers with Forecasts up to 2030.” *Mark. Study Fill. (6th Ed.*

Chang, C. W., Wu, C. R., Lin, C. T., and Chen, H. C. (2007). “An application of AHP

and sensitivity analysis for selecting the best slicing machine." *Comput. Ind. Eng.*, 52(2), 296–307.

Chatterjee, A. (1997). "Rigid body collisions: some general considerations, new collision laws, and some experimental data." *Thesis*.

Chatterjee, V. A., Verma, S. K., Bhattacharjee, D., Biswas, I., and Neogi, S. (2021). "Manufacturing of dilatant fluid embodied Kevlar-Glass-hybrid-3D-fabric sandwich composite panels for the enhancement of ballistic impact resistance." *Chem. Eng. J.*, 406(July 2020), 127102.

Chen, D. C. S. (2016). "Sand Absorbs High-Speed Ballistic Impact Better Than Steel." *NUS Res. team*.

Chen, S., Zang, M., Wang, D., Yoshimura, S., and Yamada, T. (2017). "Numerical analysis of impact failure of automotive laminated glass: A review." *Compos. Part B Eng.*, 122, 47–60.

Choqueuse, D., and Davies, P. (2008). "Ageing of composites in underwater applications." *Ageing Compos.*, 467–498.

Chotaliya, S., Chaudhari, S., Chauhan, T., Parmar, J., Pal, K., Chauhan, D., Professor, A., and Mahavir, B. (2020). "An Experimental Study on Different Properties of Sea Sand and River Sand." *Ijesc*, 8(3), 1085–1093.

Christensen, R. (1982). *Theory of Viscoelasticity An Introduction*. Academic Press Elsevier.

Christoforou, A. P., and Yigit, A. S. (1998). "Effect of flexibility on low-velocity impact response." *J. Sound Vib.*, 217(3), 563–578.

Colak, Ö. U., Bahlouli, N., Uzunsoy, D., and Francart, C. (2020). "High strain rate

behavior of graphene-epoxy nanocomposites." *Polym. Test.*, 81(July 2019).

Desai, S., Bidanda, B., and Lovell, M. R. (2012). "Material and process selection in product design using decision-making technique (AHP)." *Eur. J. Ind. Eng.*, 6(3), 322–346.

Dobyns, A. L. (1981). "Analysis of Simply-Supported Orthotropic Plates Subject to Static and Dynamic Loads." *AIAA J.*, 19(5), 642–650.

Doddamani, M. R., and Kulkarni, S. M. (2012a). "Instrumented ballistic performance of jute/epoxy sandwich with functionally graded rubber core." *Int. J. Mater. Eng. Innov.*, 3(2), 117–138.

Doddamani, M. R., and Kulkarni, S. M. (2012b). "Response of fly ash-reinforced functionally graded rubber composites subjected to mechanical loading." *Mech. Compos. Mater.*, 48(1), 89–100.

Doddamani, S., Kulkarni, S. M., Joladarashi, S., Kumar T S, M., and Gurjar, A. K. (2023a). "Analysis of lightweight natural fiber composites against ballistic impact: A Review." *Int. J. Light. Mater. Manuf.*

Doddamani, S., Kulkarni, S. M., Joladarashi, S., T S, M. K., and Gurjar, A. K. (2023b). "Analysis of lightweight natural fiber composites against ballistic impact: A review." *Int. J. Light. Mater. Manuf.*, 6(3), 450–468.

Elkington, M., Bloom, D., Ward, C., Chatzimichali, A., and Potter, K. (2015). "Hand layup: understanding the manual process." *Adv. Manuf. Polym. Compos. Sci.*, 1(3), 138–151.

Elmahdy, A., Zotti, A., Zuppolini, S., Zarrelli, M., Borriello, A., and Verleysen, P. (2021). "Effect of strain rate and silica filler content on the compressive behavior of rtm6 epoxy-based nanocomposites." *Polymers (Basel).*, 13(21), 1–20.

Ervina, J., Mariatti, M., and Hamdan, S. (2016). “Effect of Filler Loading on the Tensile Properties of Multi-walled Carbon Nanotube and Graphene Nanopowder filled Epoxy Composites.” *Procedia Chem.*, 19, 897–905.

Eshkoor, R. A., Ude, A. U., Oshkovr, S. A., Sulong, A. B., Zulkifli, R., Ariffin, A. K., and Azhari, C. H. (2014). “Failure mechanism of woven natural silk/epoxy rectangular composite tubes under axial quasi-static crushing test using trigger mechanism.” *Int. J. Impact Eng.*, 64, 53–61.

Evans, J. T. (1992). *Analysis and performance of fiber composites (second edition)*. *Mater. Sci. Eng. A*.

Fan, J. T., Weerheijm, J., and Sluys, L. J. (2015). “Dynamic compressive mechanical response of a soft polymer material.” *J. Mater.*, 79, 73–85.

Fawaz, Z., Zheng, W., and Behdinan, K. (2004). “Numerical simulation of normal and oblique ballistic impact on ceramic composite armours.” *Compos. Struct.*, 63(3–4), 387–395.

Feraboli, P., and Kedward, K. T. (2006). “A new composite structure impact performance assessment program.” *Compos. Sci. Technol.*, 66(10), 1336–1347.

Frey, D. D., Wijnia, Y., Katsikopoulos, K., Herder, P. M., Subrahmanian, E., and Clausing, D. P. (2008). “An evaluation of the Pugh controlled convergence method.” *2007 Proc. ASME Int. Des. Eng. Tech. Conf. Comput. Inf. Eng. Conf. DETC2007*, 3 PART A(January), 193–203.

Gangil, M., and Pradhan, M. K. (2018). “Optimization the machining parameters by using VIKOR Method during EDM process of Titanium alloy.” *Mater. Today Proc.*, 5(2), 7486–7495.

Garcia, C. D., Shahapurkar, K., Doddamani, M., Kumar, G. C. M., and Prabhakar, P.

(2018). “Effect of arctic environment on flexural behavior of fly ash cenosphere reinforced epoxy syntactic foams.” *Compos. Part B Eng.*, 151(April), 265–273.

Gardziella, A., and Mueller, R. (1990). “Phenolic Resins.” *Kunststoffe, Ger. Plast.*, 80(10), 66–68.

Garg, M., Sharma, S., and Mehta, R. (2015). “Pristine and amino-functionalized carbon nanotubes reinforced glass fiber epoxy composites.” *Compos. Part A Appl. Sci. Manuf.*, 76, 92–101.

Goldsmith, W., Wang, G. T., Li, K., and Crane, D. (1997). “Perforation of cellular sandwich plates.” *Int. J. Impact Eng.*, 19(5–6), 361–379.

Gopinath, G., Zheng, J. Q., and Batra, R. C. (2012). “Effect of matrix on ballistic performance of soft body armor.” *Compos. Struct.*, 94(9), 2690–2696.

Grujicic, M., Glomski, P. S., He, T., Arakere, G., Bell, W. C., and Cheeseman, B. A. (2009). “Material modeling and ballistic-resistance analysis of armor-grade composites reinforced with high-performance fibers.” *J. Mater. Eng. Perform.*, 18(9), 1169–1182.

Gunge, A., Koppad, P. G., Nagamadhu, M., Kivade, S. B., and Murthy, K. V. S. (2019). “Study on mechanical properties of alkali-treated plain woven banana fabric reinforced biodegradable composites.” *Compos. Commun.*, 13(December 2018), 47–51.

Gupta, N., and Woldesenbet, E. (2004). “Microballoon wall thickness effects on properties of syntactic foams.” *J. Cell. Plast.*, 40(6), 461–480.

Gupta, N., Woldesenbet, E., and Mensah, P. (2004). “Compression properties of syntactic foams: Effect of cenosphere radius ratio and specimen aspect ratio.” *Compos. Part A Appl. Sci. Manuf.*, 35(1), 103–111.

Gupta, N., Ye, R., and Porfiri, M. (2010). “Comparison of tensile and compressive

characteristics of vinyl ester/glass microballoon syntactic foams." *Compos. Part B Eng.*, 41(3), 236–245.

Gupta, N., Zeltmann, S. E., Shunmugasamy, V. C., and Pinisetty, D. (2014). "Applications of polymer matrix syntactic foams." *Jom*, 66(2), 245–254.

Haro, E. E., Szpunar, J. A., and Odeshi, A. G. (2018). "Dynamic and ballistic impact behavior of biocomposite armors made of HDPE reinforced with chonta palm wood (Bactris gasipaes) microparticles." *Def. Technol.*, 14(3), 238–249.

Harry S. Katz, J. V. M. (1978). *Handbook of fillers and reinforcements for plastics*. Van Nostrand Reinhold Company.

HARTNESS, P. O. S. A. J. T. T. M. C. (1988). "On Low-Velocity Impact Testing of Composite Materials." *J. Compos. Mater.*, 22(30).

Hegde, S., Padmaraj, N. H., Siddesh, V., Sunaya, T. S., Adithya Kini, K., and Sanil, V. K. (2021). "Experimental investigation of mechanical sustainability and acoustic performance of fly ash cenosphere/epoxy polymer composites." *J. King Saud Univ. - Eng. Sci.*, (xxxx).

Hirai, Y., Hamada, H., and Kim, J. K. (1998). "Impact response of woven glass-fabric composites - I. Effect of fibre surface treatment." *Compos. Sci. Technol.*, 58(1), 91–104.

Hongkarnjanakul, N., Bouvet, C., and Rivallant, S. (2013). "Validation of low-velocity impact modelling on different stacking sequences of CFRP laminates and influence of fibre failure." *Compos. Struct.*, 106, 549–559.

Huang, H., Liu, Z., Zhang, L., and Sutherland, J. W. (2009). "Materials selection for environmentally conscious design via a proposed life cycle environmental performance index." *Int. J. Adv. Manuf. Technol.*, 44(11–12), 1073–1082.

Iç, Y. T. (2012). “An experimental design approach using TOPSIS method for the selection of computer-integrated manufacturing technologies.” *Robot. Comput. Integr. Manuf.*, 28(2), 245–256.

Iqbal, M. A., Diwakar, A., Rajput, A., and Gupta, N. K. (2012). “Influence of projectile shape and incidence angle on the ballistic limit and failure mechanism of thick steel plates.” *Theor. Appl. Fract. Mech.*, 62(1), 40–53.

Ishai, O., and Cohen, L. J. (1967). “Elastic properties of filled and porous epoxy composites.” *Int. J. Mech. Sci.*, 9(8), 539–546.

Jamir, M. R. M., Majid, M. S. A., and Khasri, A. (2018). *Natural lightweight hybrid composites for aircraft structural applications. Sustain. Compos. Aerosp. Appl.*, Elsevier Ltd.

Jayaraman, T. (n.d.). “Natural Fibers in India.”

Jayavardhan, M. L., Bharath Kumar, B. R., Doddamani, M., Singh, A. K., Zeltmann, S. E., and Gupta, N. (2017). “Development of glass microballoon/HDPE syntactic foams by compression molding.” *Compos. Part B Eng.*, 130, 119–131.

Jin, N. J., Seung, I., Choi, Y. S., and Yeon, J. (2017). “Prediction of early-age compressive strength of epoxy resin concrete using the maturity method.” *Constr. Build. Mater.*, 152, 990–998.

Joshi, S. V., Drzal, L. T., Mohanty, A. K., and Arora, S. (2004). “Are natural fiber composites environmentally superior to glass fiber reinforced composites?” *Compos. Part A Appl. Sci. Manuf.*, 35(3), 371–376.

K. Ambika Devi, Bibin John, C. P. Reghunadhan Nair, K. N. N. (2007). “Syntactic Foam Composites of Epoxy-Allyl Phenol- Bismaleimide Ternary Blend—Processing and Properties.” *J. Appl. Polym. Sci.*, 105(5), 3715–3722.

Kabir, M. M., Wang, H., Aravinthan, T., Cardona, F., and Lau, K.-T. (2007a). “Effects of Natural Fibre Surface on Composite Properties : a Review.” *Energy, Environ. Sustain.*, (September 2016), 94–99.

Kabir, M. M., Wang, H., Aravinthan, T., Cardona, F., and Lau, K.-T. (2007b). “Effects of Natural Fibre Surface on Composite Properties : a Review.” *Energy, Environ. Sustain.*, 94–99.

Kärger, L., Baaran, J., Gunnion, A., and Thomson, R. (2009). “Evaluation of impact assessment methodologies. Part I: Applied methods.” *Compos. Part B Eng.*, 40(1), 65–70.

Kärger, L., Baaran, J., and Teßmer, J. (2008). “Efficient simulation of low-velocity impacts on composite sandwich panels.” *Comput. Struct.*, 86(9), 988–996.

Khodadadi, A., Liaghat, G., Ahmadi, H., Bahramian, A. R., and Razmkhah, O. (2019a). “Impact response of Kevlar/rubber composite.” *Compos. Sci. Technol.*, 184, 107880.

Khodadadi, A., Liaghat, G., Bahramian, A. R., Ahmadi, H., Anani, Y., Asemani, S., and Razmkhah, O. (2019b). “High-velocity impact behavior of Kevlar/rubber and Kevlar/epoxy composites: A comparative study.” *Compos. Struct.*, 216(February), 159–167.

Kishore, Shankar, R., and Sankaran, S. (2005). “Short-beam three-point bend tests in syntactic foams. Part I, II, III: Effect of microballoons content on shear strength.” *J. Appl. Polym. Sci.*, 98(2), 680–686.

Krupa, J., Bridges, D., and Hunter, R. (2015). “Guidebook to Decision-Making Methods DECISION-MAKING Developed for the Department of Energy.” (December).

Krzyzak, A., Mazur, M., Gajewski, M., Drozd, K., Komorek, A., and Przybyłek, P.

(2016). “Sandwich Structured Composites for Aeronautics: Methods of Manufacturing Affecting Some Mechanical Properties.” *Int. J. Aerosp. Eng.*, 2016.

Kumar, R., Kumar, K., Sahoo, P., and Bhowmik, S. (2014). “Study of Mechanical Properties of Wood Dust Reinforced Epoxy Composite.” *Procedia Mater. Sci.*, 6(Icmpc), 551–556.

Kumar, R., and Singal, S. K. (2015). “Penstock material selection in small hydropower plants using MADM methods.” *Renew. Sustain. Energy Rev.*, 52, 240–255.

Kumar, S., Durga Shankar Gupta, Singh, I., and Sharma, A. (2010). “Behavior of kevlar/epoxy composite plates under ballistic impact.” *J. Reinf. Plast. Compos.*, 29(13), 2048–2064.

Kumar, S., Patel, V. K., Mer, K. K. S., Fekete, G., Gangil, B., and Singh, T. (2018). “Influence of woven bast-leaf hybrid fiber on the physico-mechanical and sliding wear performance of epoxy-based polymer composites.” *Mater. Res. Express*, 5(10).

Kumar, V. (2019). “Application of ‘ Six Sigma -DMAIC Methodology ’ for the process improvement in a Rocker arm manufacturing company : A Case Study .” 2019, 217–224.

Kumbhare, K. S., Mahesh, V., Joladarashi, S., and Kulkarni, S. M. (2022). “Comparative study on low-velocity impact behavior of natural hybrid and non hybrid flexible thermoplastic-based composites.” *J. Thermoplast. Compos. Mater.*, 0(0), 1–18.

Lakshmi, L., and Nandakumar, C. G. (2016). “Investigations on the Performance of Metallic and Composite Body Armors.” *Procedia Technol.*, 25(Raerest), 170–177.

Lee, B. L., Walsh, T. F., Won, S. T., Patts, H. M., Song, J. W., and Mayer, A. H. (2001). “Penetration failure mechanisms of armor-grade fiber composites under impact.” *J. Compos. Mater.*, 35(18), 1605–1633.

Li, L., Wang, R., Zhao, H., Zhang, H., and Yan, R. (2021). “Combined effects of elevated temperatures and high strain rates on compressive performance of S30408 austenitic stainless steel.” *Structures*, 34(June), 1–9.

Liu, M. (2010). “Constitutive Equations for the Dynamic Response of Rubber.” *PhD Thesis*.

Liu, M., and Hoo Fatt, M. S. (2011). “A constitutive equation for filled rubber under cyclic loading.” *Int. J. Non. Linear. Mech.*, 46(2), 446–456.

Liu, P. F., Liao, B. B., Jia, L. Y., and Peng, X. Q. (2016). “Finite element analysis of dynamic progressive failure of carbon fiber composite laminates under low-velocity impact.” *Compos. Struct.*, 149, 408–422.

Liu, Y. J., Xia, C. Y., Ding, L., and Liu, C. H. (2013). “Influence of material on automotive crash-box crashworthiness subjected to low-velocity impact.” *Adv. Mater. Res.*, 655–657, 169–172.

M.R. Doddamani, S.M. Kulkarni, K. (2011). “Behavior of Sandwich Beams With Functionally Graded Rubber Core in Three-Point Bending.” *Polym. Compos.*, (1542).

Mahdi, E., Hamouda, A. S. M., and Sen, A. C. (2004). “Quasi-static crushing behaviour of hybrid and non-hybrid natural fibre composite solid cones.” *Compos. Struct.*, 66(1–4), 647–663.

Mahesh, V., Joladarashi, S., and Kulkarni, S. M. (2020). “A comprehensive review on material selection for polymer matrix composites subjected to impact load.” *Def. Technol.*, (xxxx).

Mahesh, V., Joladarashi, S., and Kulkarni, S. M. (2021a). “Development and mechanical characterization of novel polymer-based flexible composite and optimization of stacking sequences using VIKOR and PSI techniques.” *J. Thermoplast.*

Compos. Mater., 34(8), 1080–1102.

Mahesh, V., Joladarashi, S., and Kulkarni, S. M. (2021b). "A comprehensive review on material selection for polymer matrix composites subjected to impact load." *Def. Technol.*, 17(1), 257–277.

Majid, D. L., Mohd Jamal, Q., and Manan, N. H. (2018). "Low-velocity Impact Performance of Glass Fiber, Kenaf Fiber, and Hybrid Glass/Kenaf Fiber Reinforced Epoxy Composite Laminates." *BioResources*, 13(4), 8839–8852.

Maniya, K., and Bhatt, M. G. (2010). "A selection of material using a novel type decision-making method: Preference selection index method." *Mater. Des.*, 31(4), 1785–1789.

Mansor, M. R., Sapuan, S. M., Zainudin, E. S., Nuraini, A. A., and Hambali, A. (2013). "Hybrid natural and glass fibers reinforced polymer composites material selection using Analytical Hierarchy Process for automotive brake lever design." *Mater. Des.*, 51, 484–492.

Mardani, A., Jusoh, A., Nor, K. M. D., Khalifah, Z., Zakwan, N., and Valipour, A. (2015). "Multiple criteria decision-making techniques and their applications - A review of the literature from 2000 to 2014." *Econ. Res. Istraz.* , 28(1), 516–571.

Mastura, M. T., Sapuan, S. M., Mansor, M. R., and Nuraini, A. A. (2017). "Environmentally conscious hybrid bio-composite material selection for automotive anti-roll bar." *Int. J. Adv. Manuf. Technol.*, 89(5–8), 2203–2219.

Mateo, J. R. S. C. (2011). *Multi-Criteria Analysis in the Renewable Energy Industry*. Springer London.

Mathur, N. M., and Bairwa, K. (2017). "A literature review on Composite material and scope of Sugar cane Bagasse." *Int. J. Eng. Dev. Res.*, 5(4), 125–133.

Matveenko, V. P., Kosheleva, N. A., Shardakov, I. N., and Voronkov, A. A. (2018). “Temperature and strain registration by fibre-optic strain sensor in the polymer composite materials manufacturing.” *Int. J. Smart Nano Mater.*, 9(2), 99–110.

Mazumdar, S. (2002). *Composites Manufacturing Materials, Product, and Process Engineering*. CRC Press.

McKergow, M. (2014). “David Shaked: Strength-Based LEAN Six Sigma: Building positive and engaging business improvement.” *Interact. - J. Solut. Focus Organ.*, 6(1), 99–101.

Milani, A. S. S. M. G. (2012). “A Combined Finite Eiement-Muitipie Criteria Optimization Approach for Materiais Seiection of Gas Turbine Components.”

Minamoto, H., and Kawamura, S. (2009). “Effects of material strain rate sensitivity in low-speed impact between two identical spheres.” *Int. J. Impact Eng.*, 36(5), 680–686.

Mines, R. A. W., Roach, A. M., and Jones, N. (1999). “High-velocity perforation behaviour of polymer composite laminates.” *Int. J. Impact Eng.*, 22(6), 561–588.

Mitschang, P., and Hildebrandt, K. (2012). “Polymer and composite moulding technologies for automotive applications.” *Adv. Mater. Automot. Eng.*, 210–229.

Mohan Kumar T. S., Sharnappa Joladarashi, S. M. K., and Doddamani, S. (2023). “Experimental and numerical investigation on low-velocity impact response of sandwich structure with functionally graded core.” *Polym. Compos.*, online(online), 1–18.

Mohan Kumar, T. S., Joladarashi, S., Kulkarni, S. M., and Doddamani, S. (2022). “Optimization of process parameters for ballistic impact response of hybrid sandwich composites.” *Int. J. Interact. Des. Manuf.*

Mohan Kumar, T. S., Joladarashi, S., Kulkarni, S. M., and Doddamani, S. (2023). "Optimization of process parameters for ballistic impact response of hybrid sandwich composites." *Int. J. Interact. Des. Manuf.*, 17(3), 1099–1111.

Monteiro, S. N., Lopes, F. P. D., Ferreira, A. S., and Nascimento, D. C. O. (2009). "Natural-fiber polymer-matrix composites: Cheaper, tougher, and environmentally friendly." *Jom*, 61(1), 17–22.

Montgomery, D. C., and Woodall, W. H. (2008). "An overview of Six Sigma." *Int. Stat. Rev.*, 76(3), 329–346.

Morye, S. S., Hine, P. J., Duckett, R. A., Carr, D. J., and Ward, I. M. (2000). "Modelling of the energy absorption by polymer composites upon ballistic impact." *Compos. Sci. Technol.*, 60(14), 2631–2642.

Naik, N. K., and Doshi, A. V. (2008). "Ballistic impact behaviour of thick composites: Parametric studies." *Compos. Struct.*, 82(3), 447–464.

Naik, N. K., and Kavala, V. R. (2008). "High strain rate behavior of woven fabric composites under compressive loading." *Mater. Sci. Eng. A*, 474(1–2), 301–311.

Nalla Mohamed, M., Ananthapadmanaban, D., and Selvaraj, M. (2016). "Numerical Modeling of Energy Absorption Behaviour of Aluminium Foam Cored Sandwich Panels with Different Fibre Reinforced Polymer (FRP) Composite Facesheet Skins." *Appl. Mech. Mater.*, 852, 66–71.

Nash, N. H., Young, T. M., McGrail, P. T., and Stanley, W. F. (2015). "Inclusion of a thermoplastic phase to improve impact and post-impact performances of carbon fibre reinforced thermosetting composites - A review." *Mater. Des.*, 85, 582–597.

Nasir Hussain, N., Prakash Regalla, S., and Daseswara Rao, Y. V. (2017). "Low-velocity Impact Characterization of Glass Fiber Reinforced Plastics for Application of

Crash Box.” *Mater. Today Proc.*, 4(2), 3252–3262.

Nasirzadeh, R., and Sabet, A. R. (2014). “Study of foam density variations in composite sandwich panels under high-velocity impact loading.” *Int. J. Impact Eng.*, 63, 129–139.

Nie, H., Suo, T., Wu, B., Li, Y., and Zhao, H. (2018). “A versatile split Hopkinson pressure bar using electromagnetic loading.” *Int. J. Impact Eng.*, 116(February), 94–104.

Nikhil Gupta, E. W. (2002). “Microscopic Studies Of Syntactic Foams Tested Under Three-Point Bending Conditions.” *Proc. ETCE2002 ASME Eng. Technol. Conf. Energy Febr. 4-5, 2002, Houston, TX*, 1–6.

Norsuzila Ya’acob, M., Abdullah, M., Ismail, Medina, M., Talarico, T. L., Casas, I. A., Chung, T. C., Dobrogosz, W. J., Axelsson, L., Lindgren, S. E., Dobrogosz, W. J., Kerkeni, L., Ruano, P., Delgado, L. L., Picco, S., Villegas, L., Tonelli, F., Merlo, M., Rigau, J., Diaz, D., and Masuelli, M. (1989). “We are IntechOpen , the world’s leading publisher of Open Access books Built by scientists, for scientists TOP 1 %.” *Intech*, 32, 137–144.

Nurazzi, N. M., Khalina, A., Sapuan, S. M., Ilyas, R. A., Rafiqah, S. A., and Hanafee, Z. M. (2020). “Thermal properties of treated sugar palm yarn/glass fiber reinforced unsaturated polyester hybrid composites.” *J. Mater. Res. Technol.*, 9(2), 1606–1618.

Olsson, R. (1992). “Impact response of orthotropic composite plates predicted from a one-parameter differential equation.” *AIAA J.*, 30(6), 1587–1596.

Onut, S., Kara, S. S., and Mert, S. (2009). “Selecting the suitable material handling equipment in the presence of vagueness.” *Int. J. Adv. Manuf. Technol.*, 44(7–8), 818–828.

P. Breunig, V. Damodaran, K. Shahapurkar, S. Waddar, M. Doddamani, P. Jeyaraj, P.,

and Prabhakar. (2018). “Dynamic impact behavior of syntactic foam core sandwich composites.” *J. Compos. Mater.*, ...(...).

Palta, E., Fang, H., and Weggel, D. C. (2018a). “Finite element analysis of the Advanced Combat Helmet under various ballistic impacts.” *Int. J. Impact Eng.*, 112, 125–143.

Palta, E., Gutowski, M., and Fang, H. (2018b). “A numerical study of steel and hybrid armor plates under ballistic impacts.” *Int. J. Solids Struct.*, 136–137, 279–294.

Park, Y., Kim, Y. H., Baluch, A. H., and Kim, C. G. (2015). “Numerical simulation and empirical comparison of the high-velocity impact of STF impregnated Kevlar fabric using friction effects.” *Compos. Struct.*, 125, 520–529.

Patel, B. P., Bhola, S. K., Ganapathi, M., and Makhecha, D. P. (2004). “Penetration of projectiles in composite laminates.” *Def. Sci. J.*, 54(2), 151–159.

Patel, V. K., and Rawat, N. (2017). “Physico-mechanical properties of sustainable Sagwan-Teak Wood Flour/Polyester Composites with/without gum rosin.” *Sustain. Mater. Technol.*, 13(March), 1–8.

Phadnis, V. A., Pandya, K. S., Naik, N. K., Roy, A., and Silberschmidt, V. V. (2013). “Ballistic impact behaviour of woven fabric composite: Finite element analysis and experiments.” *J. Phys. Conf. Ser.*, 451(1).

Poh, C. L., Mariatti, M., Ahmad Fauzi, M. N., Ng, C. H., Chee, C. K., and Chuah, T. P. (2014). “Tensile, dielectric, and thermal properties of epoxy composites filled with silica, mica, and calcium carbonate.” *J. Mater. Sci. Mater. Electron.*, 25(5), 2111–2119.

Pugh, S. (1996). *Creating innovative products using total design.* Addison-Wesley Pub. Co.

Qi, C., Yang, S., Wang, D., and Yang, L. (2013). “Ballistic Resistance of Honeycomb Sandwich Panels under In-Plane High-Velocity Impact.” 2013.

Radzi Ali, M., Salit, M. S., Jawaid, M., Mansur, M. R., and Manap, M. F. A. (2017). *Polyurethane-Based Biocomposites*. *Polyurethane Polym. Compos. Nanocomposites*, Elsevier Inc.

Rahman, S., Odeyinka, H., Perera, S., and Bi, Y. (2012). “Product-cost modelling approach for the development of a decision support system for optimal roofing material selection.” *Expert Syst. Appl.*, 39(8), 6857–6871.

Rajesh Mathivanan, N., and Jerald, J. (2010). “Experimental investigation of low-velocity impact characteristics of woven glass fiber epoxy matrix composite laminates of EP3 grade.” *Mater. Des.*, 31(9), 4553–4560.

Rajole, S., Ravishankar, K. S., and Kulkarni, S. M. (2020). “Performance study of jute-epoxy composites/sandwiches under normal ballistic impact.” *Def. Technol.*, 16(4), 947–955.

Ramadhan, A. A., Abu Talib, A. R., Mohd Rafie, A. S., and Zahari, R. (2012). “The influence of impact on composite armour system kevlar-29/polyester- Al2O3.” *IOP Conf. Ser. Mater. Sci. Eng.*, 36(1).

Ramanathan, A., Krishnan, P. K., and Muraliraja, R. (2019). “A review on the production of metal matrix composites through stir casting – Furnace design, properties, challenges, and research opportunities.” *J. Manuf. Process.*, 42(September), 213–245.

Rao, R. V., and Davim, J. P. (2008). “A decision-making framework model for material selection using a combined multiple attribute decision-making method.” *Int. J. Adv. Manuf. Technol.*, 35(7–8), 751–760.

Razali, N., Sultan, M. T. H., Mustapha, F., Yidris, N., and Ishak, M. R. (2014). “Impact Damage on Composite Structures – A Review.” *Int. J. Eng. Sci.*, 3(7), 8–20.

Recht, R. F., and Ipson, T. W. (1960). “Ballistic perforation dynamics.” *J. Appl. Mech. Trans. ASME*, 30(3), 384–390.

Reddy, P. R. S., Reddy, T. S., Madhu, V., Gogia, A. K., and Rao, K. V. (2015). “Behavior of E-glass composite laminates under ballistic impact.” *Mater. Des.*, 84, 79–86.

Reyes, G., and Sharma, U. (2010). “Modeling and damage repair of woven thermoplastic composites subjected to low-velocity impact.” *Compos. Struct.*, 92(2), 523–531.

Roach, A. M., Jones, N., and Evans, K. E. (1998). “The penetration energy of sandwich panel elements under static and dynamic loading. Part II.” *Compos. Struct.*, 42(2), 135–152.

Rout, J., Misra, M., Tripathy, S. S., Nayak, S. K., and Mohanty, A. K. (2001). “The influence of fibre treatment of the performance of coir-polyester composites.” *Compos. Sci. Technol.*, 61(9), 1303–1310.

S.I. Ibekwe, P.F. Mensah, G. Li, and S. S. P. (2007). “Impact and post-impact response of laminated beams at low temperatures.” *Compos. Struct.*, 79(1), 12–17.

S.M.Kulkarni. (2002). “Processing, microstructural and mechanical behavioural aspects of fly ash-epoxy composites.” Indian Institute of Science.

Safri, S. N. A., Sultan, M. T. H., and Aminanda, Y. (2014a). “Impact characterisation of Glass Fibre Reinforced Polymer (GFRP) type C-600 and E-800 using a drop weight machine.” *Appl. Mech. Mater.*, 629(October), 461–466.

Safri, S. N. A., Sultan, M. T. H., and Cardona, F. (2015). “Impact damage evaluation of Glass-Fiber Reinforced Polymer (GFRP) using the drop test rig - An experimental based approach.” *ARPN J. Eng. Appl. Sci.*, 10(20), 9916–9928.

Safri, S. N. A., Sultan, M. T. H., Razali, N., Basri, S., Yidris, N., and Mustapha, F. (2014b). “The effect of layers and bullet type on impact properties of Glass Fibre Reinforced Polymer (GFRP) using a Single Stage Gas Gun (SSGG).” *Appl. Mech. Mater.*, 564(June), 428–433.

SANGAMESH. (2019a). “Development Of Sandwich Composites From Natural Materials For Bullet Proofing.” National Institute Of Technology Karnataka, Surathkal.

Sangamesh, Ravishankar, K. S., and Kulkarni, S. M. (2018). “Ballistic Impact Study on Jute-Epoxy and Natural Rubber Sandwich Composites.” *Mater. Today Proc.*, 5(2), 6916–6923.

Sanjay K, M. (2002). *Composites Manufacturing*. CRC Press.

Sassi, S., Tarfaoui, M., Nachtane, M., and Yahia, H. Ben. (2019). “Strain rate effects on the dynamic compressive response and the failure behavior of polyester matrix.” *Compos. Part B Eng.*, 174(March), 107040.

SCHAPERY, K. A. (1987). “On the characterization model of non-linear Viscoelastic materials.” *Polym. Test.*, 7(2), 137–147.

Sen, S., Jamal M, N. Bin, Shaw, A., and Deb, A. (2019). “Numerical investigation of ballistic performance of shear thickening fluid (STF)-Kevlar composite.” *Int. J. Mech. Sci.*, 164(March), 105174.

Shokrieh, M. M., and Javadpour, G. H. (2008). “Penetration analysis of a projectile in ceramic composite armor.” *Compos. Struct.*, 82(2), 269–276.

Shunmugasamy, V. C., Pinisetty, D., and Gupta, N. (2013). “Viscoelastic properties of hollow glass particle-filled vinyl ester matrix syntactic foams: Effect of temperature and loading frequency.” *J. Mater. Sci.*, 48(4), 1685–1701.

Siegfried, M., Tola, C., Claes, M., Lomov, S. V., Verpoest, I., and Gorbatikh, L. (2014). “Impact and residual after impact properties of carbon fiber/epoxy composites modified with carbon nanotubes.” *Compos. Struct.*, 111(1), 488–496.

Silva, R. V., Ueki, M. M., Spinelli, D., Bose Filho, W. W., and Tarpani, J. R. (2010). “Thermal, mechanical, and hygroscopic behavior of sisal fiber/polyurethane resin-based composites.” *J. Reinf. Plast. Compos.*, 29(9), 1399–1417.

Sreekantha Reddy, T., Rama Subba Reddy, P., and Madhu, V. (2019). “Low-velocity impact studies of E-glass/epoxy composite laminates at different thicknesses and temperatures.” *Def. Technol.*, 15(6), 897–904.

Sudhir Sastry, Y. B., Budarapu, P. R., Krishna, Y., and Devaraj, S. (2014). “Studies on ballistic impact of the composite panels.” *Theor. Appl. Fract. Mech.*, 72(1), 2–12.

Sunt, C. T., and Potti, S. V. (1996). “Velocities of Thick Composite Laminates Subjected To High-Velocity Impact.” *Int. J. Impact Eng.*, 18(3), 339–353.

Sy, B. L., Fawaz, Z., and Bougherara, H. (2019). “Numerical simulation correlating the low-velocity impact behaviour of flax/epoxy laminates.” *Compos. Part A Appl. Sci. Manuf.*, 126(January), 105582.

T. S. Mohan Kumar, Krishna, M., Joladarashi, S., and Kulkarni, S. M. (2020). “Alkali absorption and durability studies on CFRP laminated composites.” *AIP Conf. Proc.*, 2247(July).

Tagliavia, G., Porfiri, M., and Gupta, N. (2012). “Influence of moisture absorption on flexural properties of syntactic foams.” *Compos. Part B Eng.*, 43(2), 115–123.

Tan, K. T., Watanabe, N., and Iwahori, Y. (2010). “Effect of stitch density and stitch thread thickness on low-velocity impact damage of stitched composites.” *Compos. Part A Appl. Sci. Manuf.*, 41(12), 1857–1868.

Tan, V. B. C., Lim, C. T., and Cheong, C. H. (2003). “Perforation of high-strength fabric by projectiles of different geometry.” *Int. J. Impact Eng.*, 28(2), 207–222.

Teh, P. L., Ishak, Z. A. M., Hashim, A. S., Karger-Kocsis, J., and Ishiaku, U. S. (2004). “Effects of epoxidized natural rubber as a compatibilizer in melt compounded natural rubber-organoclay nanocomposites.” *Eur. Polym. J.*, 40(11), 2513–2521.

Teixeira de Freitas, S., Zarouchas, D., and Poulis, J. A. (2018). “The use of acoustic emission and composite peel tests to detect weak adhesion in composite structures.” *J. Adhes.*, 94(9), 743–766.

Ude, A. U., Ariffin, A. K., and Azhari, C. H. (2013). “Impact damage characteristics in reinforced woven natural silk/epoxy composite face-sheet and sandwich foam, coremat and honeycomb materials.” *Int. J. Impact Eng.*, 58, 31–38.

VanderKlok, A., Stamm, A., Dorer, J., Hu, E., Auvenshine, M., Pereira, J. M., and Xiao, X. (2018). “An experimental investigation into the high-velocity impact responses of S2-glass/SC15 epoxy composite panels with a gas gun.” *Int. J. Impact Eng.*, 111(May 2017), 244–254.

Vinay Kumar Patel, A. D. (2016). “Influence of CaCO3, Al2O3, and TiO2 microfillers on physico-mechanical properties of Luffa cylindrica/polyester composites.” *Eng. Sci. Technol. an Int. J.*, 19, 676–683.

Vishwas M. (2020). “Performance Evaluation Of Flexible Jute-Natural Rubber Composites For Impact Behaviour.” National Institute Of Technology Karnataka Surathkal.

Vishwas, M., Joladarashi, S., and Kulkarni, S. M. (2017). “Behaviour of Natural Rubber in Comparison with Structural Steel, Aluminium and Glass Epoxy Composite under Low Velocity Impact Loading.” *Mater. Today Proc.*, 4(10), 10721–10728.

Vishwas, M., Joladarashi, S., and Kulkarni, S. M. (2019). “Investigation on the effect of using rubber as core material in sandwich composite plate subjected to low-velocity normal and oblique impact loadings.” *Sci. Iran.*, 26(2), 897–907.

Voo, R., Mariatti, M., and Sim, L. C. (2011). “Properties of epoxy nanocomposite thin films prepared by spin coating technique.” *J. Plast. Film Sheeting*, 27(4), 331–346.

Vu-Quoc, L., Zhang, X., and Lesburg, L. (2001). “Normal and tangential force-displacement relations for frictional elastoplastic contact of spheres.” *Int. J. Solids Struct.*, 38(36–37), 6455–6489.

Wang, F., Drzal, L. T., Qin, Y., and Huang, Z. (2016). “Size effect of graphene nanoplatelets on the morphology and mechanical behavior of glass fiber/epoxy composites.” *J. Mater. Sci.*, 51(7), 3337–3348.

Wang, H., Hazell, P. J., Shankar, K., Morozov, E. V., and Escobedo, J. P. (2017). “Impact behaviour of Dyneema® fabric-reinforced composites with different resin matrices.” *Polym. Test.*, 61, 17–26.

Weir, G., and Tallon, S. (2005). “The coefficient of restitution for normal incident, low-velocity particle impacts.” *Chem. Eng. Sci.*, 60(13), 3637–3647.

Wen, H. M. (2000). “Predicting the penetration and perforation of FRP laminates struck normally by projectiles with different nose shapes.” *Compos. Struct.*, 49(3), 321–329.

Wen, H. M., Reddy, T. Y., Reid, S. R., and Soden, P. D. (1998). “Indentation, penetration and perforation of composite laminates and sandwich panels under quasi-static and projectile loading.” *Key Eng. Mater.*, 143(143 PART II), 501–552.

Wetzel, E. D., Wagner, P. N. J., and Lee, Y. S. (2004). “Protective Fabrics Utilizing Shear Thickening Fluids (STFs).” *4th Int. Conf. Saf. Prot. Fabr. Pittsburgh, PA*, (October), 1–23.

Wong, C. X., Daniel, M. C., and Rongong, J. A. (2009). “Energy dissipation prediction of particle dampers.” *J. Sound Vib.*, 319(1–2), 91–118.

Wong, K. W. Y., and Truss, R. W. (1994). “Effect of flyash content and coupling agent on the mechanical properties of flyash-filled polypropylene.” *Compos. Sci. Technol.*, 52(3), 361–368.

Wu, C. L., Zhang, M. Q., Rong, M. Z., and Friedrich, K. (2002). “Tensile performance improvement of low nanoparticles filled-polypropylene composites.” *Compos. Sci. Technol.*, 62(10–11), 1327–1340.

XIANGYANG QUAN. (1998). “An Engineering Approach to Modeling the Impact And Ballistic Response of Laminated Composite Structures.” (1050), 3–8.

Yan, L., Chouw, N., and Jayaraman, K. (2014). “Flax fibre and its composites - A review.” *Compos. Part B Eng.*, 56, 296–317.

Yap, J. W. H., Scott, M. L., Hachenberg, D., Baaran, J., and Rolfes, R. (2003). “Composite Stiffened Panel Impact Damage Simulations And Parametric Studies.” *10th Aust. Int. Aerosp. Congr.*, (1), 1–10.

Yogesha, M. R. S. J. J. V. R. N. Y. (2019). “TOPSIS method for selection of best composite laminate.” (2019).

Yung, K. C., Zhu, B. L., Yue, T. M., and Xie, C. S. (2009). “Preparation and properties of hollow glass microsphere-filled epoxy-matrix composites.” *Compos. Sci. Technol.*, 69(2), 260–264.

Yusof, N. S. B., Sapuan, S. M., Sultan, M. T. H., and Jawaid, M. (2020a). “Materials selection of ‘green’ natural fibers in polymer composite automotive crash box using DMAIC approach in Six Sigma method.” *J. Eng. Fiber. Fabr.*, 15(June).

Yusof, N. S. B., Sapuan, S. M., Sultan, M. T. H., and Jawaid, M. (2020b). “Materials selection of ‘green’ natural fibers in polymer composite automotive crash box using DMAIC approach in Six Sigma method.” *J. Eng. Fiber. Fabr.*, 15.

Zahid, S., Nasir, M. A., Nauman, S., Karahan, M., Nawab, Y., Ali, H. M., Khalid, Y., Nabeel, M., and Ullah, M. (2019). “Experimental analysis of ILSS of glass fibre reinforced thermoplastic and thermoset textile composites enhanced with multiwalled carbon nanotubes.” *J. Mech. Sci. Technol.*, 33(1), 197–204.

Zare, S., Shirvan, H. E., Hemmatjo, R., Faridan, M., Hajghani, M., and Dehaghi, B. F. (2018). “Using the analytic network process method for prioritizing and weighing shift work disorders among the personnel of hospitals of kerman university of Medical Sciences.” *J. Circadian Rhythms*, 16(1), 1–10.

Zhou, Z., and Qiao, P. (2018). “Bond behavior of epoxy-coated rebar in ultra-high performance concrete.” *Constr. Build. Mater.*, 182, 406–417.

Zhu, B., Wang, J., Wu, J., and Peng, D. (2012). “Thermal, dielectric and compressive properties of hollow glass microsphere filled epoxy-matrix composites.” *J. Reinf. Plast. Compos.*, 31(1311).

Žmindák, M., Pelagić, Z., Pastorek, P., Močilan, M., and Vybošťok, M. (2016). “Finite element modelling of high-velocity impact on plate structures.” *Procedia Eng.*, 136, 162–168.

Zukas, J. A. (1980). “Impact Dynamics: Theory and Experiment.” *US Army Armament Res. Dev. Command*, 1–66.

LIST OF PUBLICATIONS BASED ON PH.D. WORK

Sl. No.	Title of the paper	Authors	Journal Name, Year, Volume No., Issue, Pages)	Month, year of publication	Category*
1	Optimization of process parameters for ballistic impact response of hybrid sandwich composites	T. S. Mohan Kumar, Sharnappa Joladarashi, S. M. Kulkarni, Saleemsab Doddamani	International Journal on Interactive Design and Manufacturing (IJIDeM) 17:1099–1111	29 September 2022	1
2	Experimental and numerical investigation on low-velocity impact response of sandwich structure with functionally graded core	T. S. Mohan Kumar, Sharnappa Joladarashi, S. M. Kulkarni, Saleemsab Doddamani	Polymer Composites, Volume45, Issue 4, 10 March 2024, Pages 3225-3242	10 March 2024	1
3	Influence of sea sand reinforcement on the static and dynamic properties of functionally graded epoxy composites	T. S. Mohan Kumar, Sharnappa Joladarashi, S. M. Kulkarni, Saleemsab Doddamani	Iranian Polymer Science – https://doi.org/10.1007/s13726-024-01340-7 (In Press)	17 April 2024	1

4	Analysis of light Lightweight Natural Fiber Composites against Ballistic Impact: A Review	Saleemsab Doddamani, Satyabodh M. Kulkarni, Sharnappa Joladarashi, Mohan Kumar T S, Ashish Kumar Gurjar,	International Journal of Lightweight Materials and Manufacture, 6, 450-468, ISSN: 2588-8404	September 2023	1
5	Enhancing energy absorption in rubber–sand (Ru–San) composite blocks against ballistic impact: a multi-objective optimisation approach	Saleemsab Doddamani, Satyabodh M. Kulkarni, Sharnappa Joladarashi, Mohan Kumar T S, Ashish Kumar Gurjar,	Multiscale and Multidisciplinary Modeling, Experiments and Design https://doi.org/10.1007/s41939-024-00466-8	23 April 2024	1
6	Development of rubber-sand composite for enhanced impact resistance: Implications of vulcanization	Saleemsab Doddamani , Satyabodh M. Kulkarni, Sharnappa Joladarashi, Ashish Kumar Gurjar, Mohan Kumar T.S.	Engineering Science and Technology, an International Journal 51 (2024) 101631	2024	1

7	Comparative study on impact responses of sandwich composites with stiff and compliant core materials	T. S. Mohan Kumar, Sharnappa Joladarashi, S. M. Kulkarni	Mechanics of advanced materials and structures, Submitted to Journal (Accepted for Publication)	---	1
8	Review on Ballistic Crashworthiness of Natural Fiber Composites: Modeling and Material Selection	T. S. Mohan Kumar, Sharnappa Joladarashi, S. M. Kulkarni	Part C: Journal of Mechanical Engineering Science- (Under Review)	---	1
9	High Velocity Impact behavior of Sandwich Composite with Compliant Skin and Sea Sand Strengthened Functionally Graded Cores: Experimental and FE Approach	T. S. Mohan Kumar, Sharnappa Joladarashi, S. M. Kulkarni, Vishwas M	Journal of Sandwich Structures and Materials - (Under Review)	---	1
10	Influence of filler material on impact response of hybrid and green sandwich composites structures: FE study	T. S. Mohan Kumar, Sharnappa Joladarashi, S. M. Kulkarni,	International Conference on Sustainable Materials, Manufacturing & Industrial	---	3

			Engineering. ICSMMIE-2022, SIT, Tumakuru		
11	Effect of core thicknesses on ballistic behavior of sandwich composites: FE study	T. S. Mohan Kumar, Sharnappa Joladarashi, S. M. Kulkarni,	ICSMMIE-2022, SIT, Tumakuru	---	3

Category* 1: Journal paper, full paper reviewed 2: Journal paper, Abstract reviewed

3: Conference /Symposium paper, full paper reviewed 4: Conference /Symposium paper, Abstract reviewed

5: Others (including a paper in workshop, NITK Bulletin, short notes, etc.)

MOHAN KUMAR T S
Research Scholar

Dr. SHARNAPPA JOLADARASHI
Research Guide

22.10.2024
Dr. S M KULKARNI
Research Guide

BIO-DATA

1	Name	MOHAN KUMAR T S
2	Father's Name	N P Sadashivaiah
3	Date of Birth	December 14, 1985
4	Nationality	Indian
5	Permanent Address	#72, —Putteshwara Nilaya, Near Sri Ram Temple,1st Main Sri Ram Nagar, Tumakuru 572101, Karnataka, India
6	Office Adress	Assistant Professor, Dept. of Industrial Engineering and Management, Siddaganga Institute of Technology, Tumkur-572103
7	Mobile Number	+91-9964107757
8	Email-ID	mkmohants@gmail.com, mohankumarts@sit.ac.in

Educational Qualifications:

Sl No.	Qualification	University	College	Period	Performance
1.	Ph.D.	NITK, Surathkal	NITK, Surathkal	2021-2024	9.0 CGPA (Course Work)
2.	M.Tech, Computer Integrated Manufacturing	VTU, Belagavi	RVCE, Bengaluru	2008-2010	64.06 %
3.	B.E, Mechanical	VTU, Belagavi	HMSIT, Tumakuru	2003-2007	69.05 %

I declare that the above information is true and correct to the best of my knowledg**e.**

Mohan Kumar T S